HAL open science

Multiscale methods : non-intrusive implementation, advection-dominated problems and related topics

Rutger Biezemans

To cite this version:

Rutger Biezemans. Multiscale methods : non-intrusive implementation, advection-dominated problems and related topics. Analysis of PDEs [math.AP]. École des Ponts ParisTech, 2023. English. NNT : 2023ENPC0029 . tel-04481733

HAL Id: tel-04481733

https://pastel.hal.science/tel-04481733v1

Submitted on 28 Feb 2024

HAL is a multi-disciplinary open access archive for the deposit and dissemination of scientific research documents, whether they are published or not. The documents may come from teaching and research institutions in France or abroad, or from public or private research centers.

L'archive ouverte pluridisciplinaire **HAL**, est destinée au dépôt et à la diffusion de documents scientifiques de niveau recherche, publiés ou non, émanant des établissements d'enseignement et de recherche français ou étrangers, des laboratoires publics ou privés.

École des Ponts ParisTech

THÈSE DE DOCTORAT
de l'École des Ponts ParisTech

Multiscale methods: non-intrusive implementation, advection-dominated problems and related topics

École Doctorale 532 : Mathématiques et Sciences et Technologies de l'Information et de la Communication (MSTIC)

Spécialité : Mathématiques appliquées

préparée au sein de l'équipe MATHERIALS au laboratoire CERMICS de l'École des Ponts et à Inria Paris

soutenue le 21 septembre 2023, par
Rutger Adrianus Biezemans

devant le jury composé de :

Rémi Abgrall Professeur, University of Zürich	*Président*
Guillaume Enchéry Ingénieur de recherche, IFP Energies nouvelles	*Examinateur*
Claude Le Bris Chercheur, École des Ponts	*Directeur de thèse*
Frédéric Legoll Professeur, École des Ponts	*Co-encadrant*
Alexei Lozinski Professeur, Université de Franche-Comté	*Co-directeur de thèse*
Pascal Omnes Directeur de recherche, CEA	*Rapporteur*
Barbara Verfürth Professeure, University of Bonn	*Rapporteure*
Karen Veroy-Grepl Professeure, Eindhoven University of Technology	*Examinatrice*

MULTISCALE METHODS: NON-INTRUSIVE IMPLEMENTATION, ADVECTION-DOMINATED PROBLEMS AND RELATED TOPICS

RUTGER A. BIEZEMANS

THÈSE

pour obtenir le grade de

Docteur de l'École Nationale des Ponts et Chaussées

"Méthodes multi-échelles : approches non-intrusives, problèmes advection-dominés et questions reliées"

préparée au sein de l'équipe MATHERIALS
au laboratoire CERMICS de l'École des Ponts et à Inria Paris

soutenue le 21 septembre 2023, par

Rutger Adrianus Biezemans

devant le jury composé de :

Rémi Abgrall Professeur, University of Zurich	*Président*
Guillaume Enchéry Ingénieur de recherche, IFP Energies nouvelles	*Examinateur*
Claude Le Bris Chercheur, École des Ponts	*Directeur de thèse*
Frédéric Legoll Professeur, École des Ponts	*Co-encadrant*
Alexei Lozinski Professeur, Université de Franche-Comté	*Co-directeur de thèse*
Pascal Omnes Directeur de recherche, CEA	*Rapporteur*
Barbara Verfürth Professeure, University of Bonn	*Rapporteure*
Karen Veroy-Grepl Professeure, Eindhoven University of Technology	*Examinatrice*

THESIS

for the degree of

Docteur de l'École Nationale des Ponts et Chaussées

"Multiscale methods: non-intrusive implementation, advection-dominated problems and related topics"

prepared within the MATHERIALS team
at CERMICS (École des Ponts) and Inria Paris

defended on the 21st of September 2023 by

Rutger Adrianus Biezemans

before the doctorate committee consisting of:

Rémi Abgrall Professor, University of Zurich	*President*
Guillaume Enchéry Research engineer, IFP Energies nouvelles	*Voting member*
Claude Le Bris Researcher, École des Ponts	*Supervisor (directeur de thèse)*
Frédéric Legoll Professor, École des Ponts	*Supervisor (co-encadrant)*
Alexei Lozinski Professor, Université de Franche-Comté	*Supervisor (co-directeur de thèse)*
Pascal Omnes Research director, CEA	*Referee*
Barbara Verfürth Professor, University of Bonn	*Referee*
Karen Veroy-Grepl Professor, Eindhoven University of Technology	*Voting member*

Abstract

This thesis is concerned with computational methods for multiscale partial differential equations (PDEs), and in particular the multiscale finite element method (MsFEM). This is a finite element type method that performs a Galerkin approximation of the PDE on a problem-dependent basis. Three particular difficulties related to the method are addressed in this thesis. First, the intrusiveness of the MsFEM is considered. Since the MsFEM uses a problem-dependent basis, it cannot easily be implemented in generic industrial codes and this hinders its adoption beyond academic environments. A generic methodology is proposed to translate the MsFEM into an effective problem that can be solved by generic codes. It is shown by theoretical convergence estimates and numerical experiments that the new methodology is as accurate as the original MsFEM. Second, MsFEMs for advection-dominated problems are studied. These problems cause additional instabilities for naive discretizations. An explanation is found for the instability of previously proposed methods. Numerical experiments show the stability of an MsFEM with Crouzeix-Raviart type boundary conditions enriched with bubble functions. Third, a new convergence analysis for the MsFEM is presented that, for the first time, establishes convergence under minimal regularity hypotheses. This bridges an important gap between the theoretical understanding of the method and its field of application, where the usual regularity hypotheses are rarely satisfied.

Keywords: *Partial differential equations, numerical analysis, multiscale problems, MsFEM, non-intrusive methods, advection-dominated problems.*

Résumé

Cette thèse porte sur les méthodes numériques pour les équations aux dérivées partielles (EDP) multi-échelles, et en particulier sur la méthode dite des éléments finis multi-échelles (MsFEM). Celle-ci est une méthode de type éléments finis qui consiste en une approximation de Galerkin de l'EDP sur une base dépendant du problème. Trois difficultés particulières liées à cette méthode sont abordées dans cette thèse. Premièrement, puisque la MsFEM utilise une base dépendant du problème, la méthode ne peut être facilement implémentée dans des codes industriels génériques. Cela freine la diffusion de la MsFEM au-delà des environnements académiques. Une méthodologie générique est proposée pour convertir la MsFEM en un problème effectif qui peut être résolu par des codes génériques. Il est démontré par des résultats théoriques ainsi que des expériences numériques que la nouvelle méthodologie est aussi précise que la MsFEM originale. Deuxièmement, les MsFEM adaptées aux problèmes dominés par l'advection sont étudiées. Ce régime spécifique rend instables les discrétisations naïves. Une explication est trouvée pour l'instabilité de certaines méthodes proposées précédemment. Des expériences numériques montrent la stabilité d'une MsFEM avec des conditions aux limites de type Crouzeix-Raviart enrichie par des fonctions bulles. Troisièmement, une nouvelle analyse de convergence pour la MsFEM est présentée, permettant pour la première fois d'établir la convergence sous des hypothèses de régularité minimales. Cette démarche est importante pour réduire l'écart entre la théorie pour la MsFEM et son application en pratique, où les hypothèses de régularité habituelles sont rarement satisfaites.

Mots-clés : *Equations aux dérivées partielles, analyse numérique, problèmes multi-échelles, méthodes MsFEM, approches non intrusives, problèmes dominés par l'advection.*

Cadere non è inutile
Cadere è ritrovarsi,
ricordarsi di nuovo dell'essenziale invisibile

Diodato (2020)
Alveari – Che vita meravigliosa

To fall is not useless
To fall is to find oneself,
to remember again what's essential yet invisible

Voor mijn ouders,
Eric en Esther

Voor mijn broers,
Gregor, Jesper en Yvar

En ook
voor Laurie

Acknowledgements • Remerciements Dankwoord

Writing this thesis has been so much more than an opportunity to learn about numerical analysis and scientific computing. Eventhough I started my research during an international health crisis, I have had the opportunity to meet many interesting people to discuss science and to laugh with. Travelling and interacting with colleagues from all over the world has allowed me to challenge and to develop myself. To learn about myself. I want to thank everyone who made that possible.

Je voudrais d'abord remercier mes encadrants Claude Le Bris, Frédéric Legoll et Alexei Lozinski. Vous vous êtes montrés disponibles pendant trois ans pour m'inspirer, pour discuter et pour apporter votre enseignement. Votre aide a été essentielle pour faire de cette thèse ce qu'elle est aujourd'hui. Claude, merci d'avoir partagé tes points de vue sur l'activité du mathématicien numérique et tes connaissances des méthodes multi-échelles pendant nos nombreuses réunions. Merci Frédéric, pour ton intérêt pour les détails de mes recherches et pour toutes tes remarques qui m'ont permis d'améliorer la qualité des travaux dans cette thèse. Et je remercie Alexei de m'avoir transmis une partie de ton inépuisable enthousiasme pour la quête des "meilleures" méthodes numériques, pour tout ce que tu m'as appris en analyse numérique et pour un accueil très chaleureux à Besançon.

Je remercie également le DIM Math-Innov de la Région Île-de-France qui a soutenu mes recherches pendant trois ans.

I am grateful to Pascal Omnes and Barbara Verfürth for having accepted the role of *rapporteur* for this thesis. I would also like to thank the other members of the *jury*, Rémi Abgrall, Guillaume Enchéry and Karen Veroy, for your interest in my work shown by accepting the role of *examinateur*, and for your availability to attend my PhD defense in Champs-sur-Marne.

Il est aussi indispensable de remercier Isabelle Simunic, Stéphanie Bonnel et Julien Guieu pour tout leur support administratif lié à la thèse et aux missions que j'ai réalisées en France et à l'étranger. Ces voyages ont été enrichissants et formateurs tant sur le plan professionel que personnel, et ils ont largement contribué au plaisir que j'ai ressenti en faisant cette thèse.

Je tiens également à remercier Gabriel Stoltz et Frédéric Legoll pour l'opportunité d'enseigner les mathématiques appliquées aux élèves ingénieurs de l'École des Ponts dès ma première année en thèse. J'ai beaucoup apprécié les échanges avec les élèves et avec vous.

Quand j'étais penché sur mon bureau à me creuser la tête sur les méthodes des éléments finis, j'ai pu profiter de l'excellente ambiance au CERMICS. Merci Olga et Rémi pour vos conseils et votre accueil quand j'arrivais en thèse, Roberta pour ta gentillesse généreuse que tu partages avec tout le monde, Dylan, Gaspard, Laurent, Solal, Shiva, Éloïse pour

la joie que tu apportes au labo, Edoardo et Emanuele pour vos blagues aussi mauvaises qu'indispensables, Nerea, Jean, Régis pour l'organisation des JSJC, Giulia de m'avoir supporté pendant les dîners à Oslo et pendant l'école de recherche à Paris, Albéric, Simon, Amandine, évidemment l'équipe de la salle, Léo, Guillaume et Carlos, Étienne pour ton aide en informatique, en LaTeX et pour tes conseils en restaurants (aussi de la part de Laurie), Renato, Coco, Camila pour les thés partagés à Provins, Hélène, Vitor, Hervé, Julien, Fabian, Kacem, Léo, Noé, Luca, Andrea, Louis, Mathias, Guido, Épiphane, Alfred.

During the time that I lived at Cité Universitaire, I met many people with whom I have enjoyed life in Paris outside research hours. Je remercie Dylan pour tous les voyages que nous avons faits et les restaurants que nous avons testés. Merci à Sabrine, Dounia, Mouloud et Lina pour toutes nos sorties et soirées passées ensemble. Merci à Monica d'être mon amie depuis nos premiers cours à Orsay. I will always fondly remember musical moments with Bibi, Mehdi, Iris, Franca and Júlia. I am also grateful for many precious moments with Margherita, Lotte, Erika, Anissa, Aphrodite, Massi and Naomi, and with all those that I did not mention here. Ik wil in het bijzonder Charita, Nina en Alec bedanken voor jullie blijvende vriendschap na jullie vertrek uit Parijs.

Het is voor mij ook erg bijzonder dat oude vrienden uit Nederland al deze jaren in mijn leven zijn gebleven. Het contact is niet altijd even regelmatig gebleven, maar altijd even gezellig. Hiervoor bedank ik Steef, Willem, Dirk, Mike, Jasper, Jannes, Yoshi, Anouk, Martijn, Ruben, Steven, Matthijs, Abby, Christine.

Laurie, dankjewel voor alle dagen dat je me hebt geholpen om mijn werk te kunnen parkeren en ook voor alle dagen waarop je me juist alles uit handen hebt genomen, zodat ik al mijn tijd in mijn proefschrift kon steken. Meer nog wil ik je ervoor bedanken dat je elke dag een beetje leuker maakt. Ik hoop dat ik hetzelfde voor jou mag doen nu jouw avontuur net begonnen is.

Als laatste bedank ik mijn ouders. Ik schrijf deze woorden wanneer het precies vijf jaar geleden is dat jullie me naar het Collège néerlandais in Parijs gebracht hebben. Ik had toen nooit gedacht dat ik nu in Frankrijk mijn promotieonderzoek aan het afronden zou zijn. Ik ben dankbaar voor al het moois dat ik dankzij jullie steun heb kunnen beleven. Ik weet dat ik bij jullie altijd terecht kan voor leuke en ontspannen momenten, maar ook met mijn zorgen. Dat betekent alles voor mij. Dankjewel.

Noisy-le-Grand, France
1 September 2023

Table of Contents

List of Tables xx

List of Figures xxi

Publications based on the work in this thesis xxiii

Talks in conferences and seminars xxiv

1 Résumé étendu en français 1

1.1 Motivation . . . 1

1.2 Contexte . . . 2

1.3 Contributions de la thèse . . . 4

2 Introduction 11

2.1 Motivation . . . 11

2.2 Introduction to multiscale methods . . . 19

2.3 Contributions of the thesis . . . 31

I Non-intrusive Implementation of Multiscale Finite Element Methods

3 An illustrative example 47

3.1 Introduction . . . 47

3.2 Non-intrusive implementation of MsFEM: a simple case . . . 48

3.3 Comparison of Galerkin and Petrov-Galerkin MsFEM . . . 55

3.4 Concluding remarks on possible extensions . . . 58

4 The intrusive nature of the MsFEM 61

4.1 Discrete variational formulation . . . 62

4.2 A simple multiscale finite element method . . . 63

4.3 Intrusive workflow . . . 65

4.4 Effective problem on the macroscopic scale . . . 66

4.5 Non-intrusive workflow . . . 68

4.6 Interpretation of the non-intrusive MsFEM . . . 70

4.7 Relation to homogenization theory . . . 70

5 A general framework for multiscale finite element methods 73

5.1 Why develop a general framework? . . . 73

5.2 The continuous problem . . . 75

5.3 Piecewise affine structure . . . 77

5.4 Local problems . . . 79

5.5 The multiscale basis functions . . . 87
5.6 The global problem . . . 89

6 Non-intrusive MsFEM for the general framework 91
6.1 The Petrov-Galerkin MsFEM . . . 91
6.2 The non-intrusive Galerkin MsFEM . . . 94
6.3 Further extensions of the non-intrusive MsFEM . . . 96
6.4 Intrusiveness of other multiscale methods . . . 97

7 Comparison of the classical and non-intrusive MsFEM for diffusion problems 101
7.1 The general framework for diffusion problems . . . 101
7.2 Convergence results . . . 102
7.3 Convergence results in the periodic setting . . . 107
7.4 Numerical study of non-intrusive MsFEMs . . . 110

8 Some further considerations 115
8.1 Different oversampling techniques for the MsFEM-CR . . . 115
8.2 Non-intrusive implementation of a $\mathbb{P}_2$ MsFEM . . . 118

II Multiscale Finite Element Methods for Advection-Dominated Problems

9 Introduction and classical stabilization methods 129
9.1 Advection-dominated problems . . . 130
9.2 The multiscale setting . . . 131
9.3 Strongly consistent stabilization methods . . . 133
9.4 Variational stabilization methods . . . 134

10 Multiscale finite element methods for advection-diffusion problems 139
10.1 The multiscale finite element method . . . 139
10.2 A residual-free bubble point of view . . . 141
10.3 Enrichment by additional residual-free bubble functions . . . 144
10.4 Numerical experiment in 1D . . . 146
10.5 On the generalization to higher dimension . . . 148

11 An MsFEM with weak bubbles 151
11.1 The coarse scales . . . 152
11.2 Additional bubbles for the adv-MsFEM-CR . . . 154
11.3 A closer look at the bubbles . . . 155
11.4 Non-intrusive implementation . . . 158

12 Numerical results 165
12.1 First test case . . . 165
12.2 Second test case . . . 172

III Novel Convergence Analysis for Multiscale Finite Element Methods

13 A convergence theorem under minimal regularity hypotheses 177
13.1 Definition of the MsFEM framework . . . 178
13.2 Statement of the convergence results . . . 180

13.3 Auxiliary notions and results 181
13.4 Three central estimates 192
13.5 Proof of Theorem 13.1 199

Bibliography **203**

Detailed Table of Contents **213**

List of Tables

3.1 Errors between $u_H^{\varepsilon,G}$, $u_H^{\varepsilon,PG}$ and u_{ref} for several values of H (periodic case) . . . 58
3.2 Errors between $u_H^{\varepsilon,G}$, $u_H^{\varepsilon,PG}$ and u_{ref} for several values of H (locally periodic case) 59
3.3 Errors between $u_H^{\varepsilon,G}$, $u_H^{\varepsilon,PG}$ and u_{ref} for several values of H (non-periodic case) . 59

List of Figures

2.1 Basis functions $\phi_i^{\mathbb{P}_1}$ of the $\mathbb{P}_1$ Lagrange space in dimension 1 16

2.2 The difference between u_H^ε and the exact solution u^ε is large when the mesh size H does not resolve the microscale ε 16

2.3 Finite element approximations for the diffusion coefficient in (a) and three different mesh sizes 17

2.4 Example of a highly oscillatory coefficient A^ε and the associated multiscale basis functions in 1D 26

2.5 Example of (a) a $\mathbb{P}_1$ basis function and (b) a multiscale basis function in 2D . . 26

2.6 Errors of the $\mathbb{P}_1$ FEM and the MsFEM for a highly oscillatory diffusion coefficient in 1D 28

2.7 Comparison of the errors of three different FEMs applied to a highly oscillatory diffusion coefficient in 2D as the mesh size H varies 30

2.8 The multiscale basis function ϕ_i^ε can be written as the sum of a standard FEM basis function $\phi_i^{\mathbb{P}_1}$ and a linear combination of the numerical correctors $\chi_K^{\varepsilon,1}$ and $\chi_K^{\varepsilon,2}$ 32

2.9 Solution u to $-m\,u'' + u' = 1$ and its $\mathbb{P}_1$ approximation showing large spurious oscillations 36

2.10 Example of a multiscale basis function for the adv-MsFEM in 1D when the advection is strong 36

5.1 Oversampling patches for the MsFEM in 2D 79

5.2 Non-simplicial oversampling patches in 2D 80

7.1 Difference between the Galerkin MsFEM approximation and the non-intrusive Galerkin MsFEM approximation as the mesh size H varies 112

7.2 Comparison of the errors of the (intrusive) Galerkin MsFEM (5.15) and the (non-intrusive) Petrov-Galerkin MsFEM (6.1) as the mesh size H varies 114

8.1 Comparison of different oversampling strategies with weak, vanishing and affine boundary conditions for the MsFEM-CR as the mesh size H varies 119

10.1 Comparison of the exact solution u^ε of (9.3) and its approximation by the MsFEM-lin, the adv-MsFEM-lin and the adv-MsFEM-lin-B 144

10.2 Relative errors outside the boundary layer element between the reference solution u_h^ε and various numerical approximations u_H^ε as α varies 147

10.3 Fine-scale oscillations of the derivative of the reference solution u_h^ε and three stable (Ms)FEM approximations, for two different values of α 148

11.1 Comparison of a $\mathbb{P}_1$ CR basis function and an adv-MsFEM-CR basis function in the presence of a strong advection field 153

11.2 Bubble functions in dimension 1 158

11.3 Bubble functions for the adv-MsFEM-lin-B in dimension 2 158

12.1 Illustration of the first test case 166

12.2 The $\mathbb{P}_1$ part of various MsFEM approximations 167

12.3 Error measurement outside the boundary layer elements 168

12.4 Errors outside the boundary layer for $\mathbb{P}_1$ FEMs 168

12.5 Errors of various numerical approximations outside the boundary layer elements for varying α 169

12.6 Errors of various numerical approximations on the entire domain for varying α . 171

12.7 Comparison of some MsFEM variants in Galerkin and Petrov-Galerkin formulation for varying α 172

12.8 Errors of various numerical approximations outside the boundary layer elements for varying α 173

Publications based on the work in this thesis

The work of Part I of this thesis, with the exception of Chapter 8, has been communicated in the following two peer-reviewed publications.

[32] R. A. Biezemans, C. Le Bris, F. Legoll, and A. Lozinski. Non-intrusive implementation of Multiscale Finite Element Methods: An illustrative example. *Journal of Computational Physics*, 477:111914, 2023.

[31] R. A. Biezemans, C. Le Bris, F. Legoll, and A. Lozinski. Non-intrusive implementation of a wide variety of Multiscale Finite Element Methods. *Comptes Rendus. Mécanique, Online first*, 2023.

The results contained in Part II of this thesis are being prepared for publication as

[30] R. A. Biezemans, C. Le Bris, F. Legoll, and A. Lozinski. Multiscale Finite Element Methods and Bubble Functions for the Stable Approximation of Advection-Dominated Problems in Heterogeneous Media. In preparation.

Talks in conferences and seminars

During the preparation of this thesis, I have presented my research work in the following talks in conferences and seminars.

- *Some aspects of the analysis of MsFEM methods*,
  Congrès d'Analyse Numérique pour les Jeunes 2020, SMAI (online).
- *Introduction to multiscale finite element methods*,
  CERMICS Young Researchers Seminar (2021, online).
- *Multiscale finite element methods for advection-diffusion problems*,
  10ième Biennale Française des Mathématiques Appliquées et Industrielles,
  La Grande Motte, France (2021).
- *MsFEM for advection-diffusion problems*,
  Second French-German Workshop on Multiscale Problems, Besançon, France (2021).
- *Improved multiscale finite element methods for advection-diffusion problems*,
  CERMICS Young Researchers Seminar, Champs-sur-Marne, France (2022).
- *Improved multiscale finite element methods for advection-diffusion problems*,
  ECCOMAS Congress 2022, Oslo, Norway.
- *Non-intrusive implementation of multiscale finite element methods*,
  CANUM 2020(+2), Evian-les-Bains, France (2022).
- *Improved multiscale finite element methods for advection-diffusion problems*,
  SciCADE 2022, Reykjavík, Iceland.
- *Homogenization with FreeFEM*,
  Journées Scientifiques des Jeunes du CERMICS, Provins, France (2022).
- *Non-intrusive implementation of Multiscale Finite Element Methods*,
  CSE 2023, Amsterdam, The Netherlands.
- *Stabilization of advection-dominated problems in heterogeneous media: Multiscale Finite Element Methods & bubble functions*,
  CFC 2023, Cannes, France.

Chapter 1

Résumé étendu en français
Extended summary in French

Nous donnons ici un résumé des résultats contenus dans cette thèse en français, tous les autres chaptires étant rédigés en anglais. Nous renvoyons à l'Introduction pour une introduction plus élaborée.

1.1. Motivation

Dans cette thèse, nous nous intéressons à la résolution numérique d'équations aux dérivées partielles (EDP) multi-échelles, c'est-à-dire, à coefficients hautement oscillants. La dimension spatiale qui caractérise les oscillations est beaucoup plus petite que les dimensions de la taille du modèle global. Les modèles avec des propriétés multi-échelles apparaissent naturellement dans de nombreux domaines de la science et de l'ingénierie moderne. Dans le contexte des sciences des matériaux, on peut penser aux matériaux composites pour la conception des ailes d'avion, à l'étude de fibres qui sont elles-mêmes une collection de fibres plus fines, ou à l'utilisation du béton dans de nombreuses applications de génie civil. Nous mentionnons également la modélisation des écoulements souterrains, par exemple pour comprendre comment un polluant peut se propager à travers la surface de la terre, ou le flux d'air à travers une ville densément peuplée. Nous nous concentrons sur les propriétés multi-échelles en espace, et non en temps, ce qui nécessite des approches différentes en raison de la nature séquentielle du temps.

La simulation numérique d'un modèle multi-échelle basée sur la discrétisation complète de la micro-échelle conduit à un système linéaire énorme, dont la résolution peut prendre un temps de calcul considérable (voire prohibitif) ou peut être impossible en raison des contraintes de mémoire des outils de calcul disponibles. Or, souvent on ne s'intéresse pas aux fluctuations précises de la solution de l'EDP à l'échelle de ses variations les plus fines. Une connaissance beaucoup plus grossière, globale et macroscopique des propriétés des matériaux est suffisante dans ces cas, du moins dans un premier temps. On peut donc espérer qu'un modèle numérique qui lui aussi est grossier puisse fournir les informations désirées. Cependant, la microstructure du modèle contribue aux propriétés macroscopiques émergentes et ne peut être entièrement ignorée dans les simulations numériques. Des méthodes numériques *multi-échelles* ont été conçues pour incorporer la microstructure dans une approximation grossière.

Cette thèse se concentre principalement sur l'une de ces méthodes multi-échelles dite la *méthode des éléments finis multi-échelles*. Les sujets liés à cette méthode qui seront abordés sont les suivants.

Une partie importante de la thèse (la Partie I) traite de l'adaptation de la méthode des éléments finis multi-échelles de manière à ce qu'elle puisse être mise en œuvre à l'aide de grands logiciels existants actuellement utilisés dans l'industrie, sans avoir besoin de modifier ce logiciel, c'est-à-dire, sans être intrusif. Nous considérons cela comme une démarche essentielle pour toute méthode numérique afin de faciliter son utilisation pour des applications plus avancées.

Nous considérons dans la Partie II le développement des méthodes éléments finis multi-échelles pour les problèmes dominés par l'advection. Ce régime spécifique rend instables les discrétisations naïves. Malgré quelques résultats dans la littérature, aucune approche optimale n'a encore pu être identifiée. Nous donnerons quelques nouvelles perspectives.

La Partie III propose une nouvelle analyse de convergence de la méthode des éléments finis multi-échelles sous des hypothèses de régularité minimales sur les coefficients de l'EDP, là où les analyses existantes s'appuient sur des hypothèses de continuité qui sont rarement satisfaites dans les modèles visés par la méthode.

Les méthodes numériques proposées seront étudiées numériquement et comparées à d'autres méthodes numériques connues. Nos études seront également complétées par une analyse de convergence mathématique lorsque nous serons en mesure de l'établir.

1.2. Contexte

Nous étudierons dans cette thèse des méthodes de type éléments finis. Rappelons la méthode pour l'exemple d'une équation de diffusion. Soit Ω le domaine macroscopique du problème. Etant donnée une matrice de diffusion A^ε (où le symbole ε représente la taille de la microstructure), nous cherchons la fonction $u^\varepsilon \in H^1_0(\Omega)$ qui résout l'EDP

$$-\operatorname{div}(A^\varepsilon \nabla u^\varepsilon) = f \quad \text{dans } \Omega, \tag{1.1}$$

ou bien, de façon équivalente, la fonction u^ε est aussi l'unique solution du problème

$$\text{Trouver } u^\varepsilon \in H^1_0(\Omega) \text{ telle que} \quad \int_\Omega \nabla v \cdot A^\varepsilon \nabla u^\varepsilon = \int_\Omega f v \quad \text{pour tout } v \in H^1_0(\Omega), \tag{1.2}$$

communément appelée formulation variationnelle de l'EDP.

Nous introduisons ensuite un maillage du domaine Ω et un espace de dimension finie V_H tel que

(i) les fonctions de V_H sont polynomiales sur chaque maille, et
(ii) l'espace V_H admet une base de fonctions localisées sur un petit nombre de mailles.

La méthode des éléments finis (EF) consiste alors en la restriction du problème (1.2) à l'espace V_H:

$$\text{Trouver } u^\varepsilon_H \in V_H \text{ telle que} \quad \int_\Omega \nabla v_H \cdot A^\varepsilon \nabla u^\varepsilon_H = \int_\Omega f\, v_H \quad \text{pour tout } v_H \in V_H. \tag{1.3}$$

Ceci est appelé l'approximation de Galerkin du problème (1.2) sur l'espace V_H. Cet espace étant de dimension finie, ce problème se traduit en un système linéaire, et la méthode EF

consiste en la construction et la résolution de ce système.

Le point (i) ci-dessus est utile pour les propriétés d'approximation de V_H et simplifie le calcul des coefficients du système linéaire associé au problème discret (1.3). L'existence d'une base localisée est essentielle pour une construction efficace dudit système linéaire sur ordinateur et pour sa structure creuse.

Des méthodes EF ont été développées pour une grande variété de problèmes dans tous les domaines de la science et de l'ingénierie. Les principes décrits ci-dessus ont d'ailleurs facilité la conception de logiciels très généraux pour les EF. Cela a largement contribué au succès de la méthode dans les milieux académiques ainsi qu'industriels. Des traitements plus complets peuvent être lus dans [52, 73, 8, 37, 129].

Dans le contexte des problèmes multi-échelles, la méthode EF requiert un maillage au niveau de la plus fine micro-échelle. Quand la microstructure n'est pas résolue par le maillage, le résultat de la méthode est faux. Nous illustrerons ceci dans la Section 2.1.1 (voir en particulier les Figures 2.2, 2.3, 2.6 et 2.7). Il est important de noter que

non seulement les petites échelles de u^ε ne sont pas bien représentées par la méthode EF sur un maillage grossier, mais aussi les propriétés macroscopiques de l'approximation sont fausses si la microstructure n'est pas prise en compte.

En revanche, un maillage très fin donne lieu à un espace V_H de dimension très élevée et pour des modèles réels, la résolution sur ordinateur du système linéaire résultant est impossible.

Cette défaillance des méthodes standards a mené au développement de méthodes dédiées dites "multi-échelles" avec le but d'obtenir une approximation fiable de la solution de l'EDP sans la résolution d'un système linéaire immense. Ces méthodes s'éloignent de la grande généralité des méthodes EF, et construisent un modèle numérique grossier, dédié à l'approximation efficace d'une EDP donnée. Elles consistent généralement en deux étapes.

Pendant la première étape, dite l'étape *offline*, la microstructure est prétraitée numériquement d'une manière appropriée (voir ci-dessous pour l'exemple de la méthode des éléments finis multi-échelles). L'utilisation d'un maillage fin est inévitable pour cela. Typiquement, une stratégie de "diviser pour régner" est adoptée : le modèle global est divisé en plusieurs sous-domaines plus petits, qui sont tous traités séparément. Par conséquent, l'étape *offline* ne nécessite pas la résolution irréalisable d'un grand système linéaire tel que c'est le cas pour la résolution du problème original. L'étape *offline* est souvent adaptée au calcul parallèle, ce qui permet d'augmenter l'efficacité de cette étape.

Dans une deuxième étape, dite l'étape *online*, les résultats de tous les calculs locaux de l'étape *offline* sont combinés afin d'obtenir une approximation raisonnablement précise de u^ε sur un maillage grossier à un coût de calcul abordable.

Dans cette procédure, l'étape *offline* est coûteuse alors que le coût de calcul de l'étape *online* est largement réduit. Les méthodes multi-échelles sont donc efficaces quand un problème avec une microstructure fixée doit être résolu plusiers fois pour des conditions au bord ou des termes sources qui changent, par exemple. Dans ce cas, seule la méthode *online* est à répéter, et elle est beaucoup moins coûteuse que le calcul direct de la solution sur un maillage très fin. On peut penser, dans un milieu hétérogène donné, à la résolution de problèmes non-stationnaires, aux problèmes inverses, à la quantification d'incertitude, à l'évaluation des risques, au design, au contrôle et à l'optimisation, etc.

Des introductions générales aux méthodes multi-échelles sont disponibles dans [72, 15, 12]. Des références plus précises sont données dans la Section 2.2.2.

La méthode des éléments finis multi-échelles. Nous détaillons ici le principe de la méthode des éléments finis multi-échelles (méthode MsFEM pour l'anglais *multiscale finite element method*) qui a été introduite dans [98]. Soit $\mathscr{T}_H$ une triangulation conforme du domaine Ω, et pour chaque nœud interne x_i du maillage, soit $\phi_i^{\mathbb{P}_1}$ la fonction affine par morceaux qui vaut 1 en x_i et qui vaut 0 dans tous les autres nœuds. Nous remarquons au passage que ces fonctions forment une base pour la méthode EF classique $\mathbb{P}_1$ de Lagrange. Notons leur nombre par N.

Durant l'étape *offline* de la MsFEM, nous résolvons les problèmes suivants définissant les fonctions de base multi-échelles ϕ_i^ε, pour chaque $1 \leq i \leq N$,

$$\forall\, K \in \mathscr{T}_H, \quad \begin{cases} -\operatorname{div}(A^\varepsilon \nabla \phi_i^\varepsilon) = 0 & \text{dans } K, \\ \phi_i^\varepsilon = \phi_i^{\mathbb{P}_1} & \text{sur } \partial K. \end{cases} \tag{1.4}$$

L'étape *online* consiste ensuite à résoudre l'approximation de Galerkin du problème (1.2) sur l'espace V_H^ε engendré par les fonctions multi-échelles, c'est-à-dire,

$$\text{Trouver } u_H^\varepsilon \in V_H^\varepsilon \text{ telle que} \quad \int_\Omega \nabla v_H^\varepsilon \cdot A^\varepsilon \nabla u_H^\varepsilon = \int_\Omega f\, v_H^\varepsilon \quad \text{pour tout } v_H^\varepsilon \in V_H^\varepsilon. \tag{1.5}$$

La dimension de l'espace V_H^ε adapté au problème est identique à celle de l'espace V_H de la méthode EF $\mathbb{P}_1$. Il découle de (1.4) que le support de chaque fonction de base multi-échelle est égal au support de la fonction $\mathbb{P}_1$ $\phi_i^{\mathbb{P}_1}$ correspondante. La résolution du système linéaire associé à (1.5) a donc la même complexité que pour la méthode $\mathbb{P}_1$ standard sur le même maillage. A la différence des fonctions $\phi_i^{\mathbb{P}_1}$, les fonctions ϕ_i^ε 'connaissent' les oscillations de A^ε au sein de chaque maille du maillage. Nous pouvons donc espérer que la méthode MsFEM donne une approximation fiable de u^ε sur un maillage grossier alors que la méthode EF $\mathbb{P}_1$ n'en est pas capable. Ceci est effectivement le cas. Nous renvoyons à la Section 2.2.3 pour plus de détails.

Le défaut principal de la MsFEM comme elle est décrite ci-dessus est le choix des conditions affines aux bords de chaque maille K dans (1.4). Puisque les conditions au bord de u^ε ne sont connues que sur le bord du domaine global $\partial\Omega$, et que nous cherchons des fonctions de base avec un support restreint pour l'espace V_H^ε, il est nécessaire d'inventer des conditions au bord locales. Il est clair que le choix dans (1.4) ne reflète pas le caractère oscillant de u^ε. Des améliorations ont été proposées dans la littérature. Nous mentionnons la technique d'*oversampling* [98] et les conditions au bord locales de type Crouzeix-Raviart [112] (MsFEM-CR). La méthode MsFEM avec les conditions au bord locales comme dans (1.4) est appelée MsFEM-lin ici. Nous renvoyons encore à la Section 2.2.3 pour plus de détails.

1.3. Contributions de la thèse

1.3.1. Approches MsFEM non-intrusives. Nous avons vu dans la section précédente que la MsFEM remplace les fonctions de base *génériques, polynomiales* de la méthode EF $\mathbb{P}_1$ par des fonctions de base *dépendant du problème* ayant le même support afin de conserver les propriétés creuses de la méthode tout en augmentant sa performance pour une microstructure donnée. Nous considérons dans la Partie I de la thèse l'impact pratique de ce choix pour la mise en œuvre de la méthode.

Concentrons-nous ici sur la construction du système linéaire associé aux problèmes

discrets (1.3) et (1.5). Cela nécessite d'évaluer des intégrales des fonctions de base de l'espace discret V_H choisi. Pour les méthodes EF traditionnelles avec des fonctions de base polynomiales, cela peut être automatisé pour une grande variété de problèmes car les formules de quadrature standards peuvent facilement être évaluées sur chaque élément du maillage. Cette grande généralité des logiciels pour les méthodes EF est au cœur du large succès de la méthode en science mais aussi dans l'industrie. Le fait de changer les fonctions de base pour chaque problème individuel signifie que toutes ces routines dans les logiciels EF génériques doivent être adaptées. La MsFEM est donc intrusive. Ce caractère intrusif freine l'utilisation de la méthode dans des contextes industriels, où l'on ne souhaite pas ou l'on ne peut pas modifier un code qui est le fruit de plusieurs années de développement. Il semble essentiel qu'un code EF existant et optimisé puisse être utilisé avec le moins de modifications possible pour que la méthode MsFEM puisse être adoptée lorsqu'un code EF traditionnel est *déjà en utilisation*. À notre connaissance, la question de rendre les approches MsFEM moins intrusives n'avait pas été abordée dans la littérature avant les travaux de cette thèse.

La partie I de cette thèse propose une modification mineure de la MsFEM traditionnelle (la notion de 'mineur' sera précisée dans les Contributions 4, 5 et 6 ci-dessous), permettant une mise en œuvre de la méthode en utilisant un logiciel EF existant sans modifier aucune de ses routines internes. Cette approche est basée sur une ré-écriture des fonctions multi-échelles ϕ_i^ε définies dans (1.4), pour tout $1 \leq i \leq N$, sous la forme (voir l'Équation (4.10))

$$\forall\, K \in \mathscr{T}_H, \qquad \phi_i^\varepsilon = \phi_i^{\mathbb{P}_1} + \sum_{\alpha=1}^{d} \left(\partial_\alpha \phi_i^{\mathbb{P}_1}\right)\big|_K \, \chi_K^{\varepsilon,\alpha} \quad \text{dans } K,$$

où, pour chaque $K \in \mathscr{T}_H$ et chaque $1 \leq \alpha \leq d$, nous définissons la fonction $\chi_K^{\varepsilon,\alpha} \in H_0^1(K)$ appelée correcteur numérique comme l'unique solution au problème

$$\begin{cases} -\mathrm{div}(A^\varepsilon \nabla \chi_K^{\varepsilon,\alpha}) = \mathrm{div}(A^\varepsilon e_\alpha) & \text{dans } K, \\ \chi_K^{\varepsilon,\alpha} = 0 & \text{sur } \partial K. \end{cases} \tag{1.6}$$

La microstructure qui a été encodée dans les fonctions ϕ_i^ε est ainsi entièrement portée par les correcteurs numériques.

Ayant à notre disposition les correcteurs numériques, nous définissons un coefficient effectif, constant dans chaque maille grossière, par

$$\overline{A}\big|_K = \int_K \left(e_\beta + \nabla \chi_K^{\varepsilon,\beta}\right) \cdot A^\varepsilon \left(e_\alpha + \nabla \chi_K^{\varepsilon,\alpha}\right) \quad \text{pour chaque } K \in \mathscr{T}_H. \tag{1.7}$$

Nous démontrerons que le système linéaire associé à la méthode MsFEM (1.5) est *le même* que le système obtenu par une discrétisation par des EF $\mathbb{P}_1$ du problème effectif

$$\begin{cases} -\mathrm{div}\left(\overline{A}\,\nabla u\right) = f & \text{dans } \Omega, \\ u = 0 & \text{sur } \partial\Omega, \end{cases} \tag{1.8}$$

sur le maillage grossier $\mathscr{T}_H$. Le problème effectif peut être résolu par une méthode EF $\mathbb{P}_1$ standard car le coefficient effectif est constant par morceaux.

Ces observations ont mené à la première contribution de cette thèse qui est résumée

comme suit.

Contribution 1. *Approche MsFEM non-intrusive; voir l'Algorithme 4.1.*

→ *Dans l'étape offline, calculer les correcteurs numériques définis par* (1.6) *maille par maille. Utiliser ces correcteurs numériques pour calculer le coefficient effectif dans* (1.7).

→ *Dans l'étape online, résoudre l'EDP effective* (1.8) *avec un* ***logiciel EF existant****.*

→ *Nous introduirons une étape de post-processing afin d'obtenir l'approximation MsFEM de* u^ε *à partir de la solution du problème effectif et des correcteurs numériques calculés dans l'étape offline.*

Nous passons ensuite à la généralisation de cette approche non-intrusive à d'autres méthodes MsFEM. En effet, nous rappelons que différentes variantes existent en fonction du choix des conditions au bord locales dans la définition des fonctions multi-échelles. La méthode MsFEM peut également être adaptée à d'autres équations que celle de la diffusion pure (nous considérerons uniquement des dérivées spatiales dans cette thèse), donnant possiblement lieu à différentes EDP dans les problèmes locaux (1.4). Un exemple est donné dans la Section 1.3.2. Nous prenons en compte tous ces choix dans une formulation générale de la méthode MsFEM. Une motivation supplémentaire pour cette formulation générale était d'établir une analyse de convergence commune pour les méthodes MsFEM-lin et MsFEM-CR, dont un début est présenté dans la Partie III de la thèse.

Contribution 2. *Nous introduisons une formulation générale de la méthode MsFEM pour des EDP linéaires d'ordre 2, couvrant la MsFEM-lin, la MsFEM-CR, et une technique d'oversampling pour les deux variantes. La technique d'oversampling pour la MsFEM-CR est également une nouvelle contribution de la thèse. De plus, nous donnons une définition rigoureuse de la technique d'oversampling pour les mailles qui touchent la frontière* $\partial\Omega$ *du domaine global, ce qui est souvent incomplet dans la littérature. La formulation générale contient une généralisation de l'écriture* (1.6)*, qui est essentielle pour la contribution suivante.*

Contribution 3. *L'approche non-intrusive de la Contribution 1 est étendue à la formulation générale de la méthode MsFEM dans l'Algorithme 6.1. Le problème global effectif correspondant peut être résolu par un logiciel EF standard capable de traiter des EDP linéaires d'ordre 2 à coefficients constants par morceaux.*

La contribution suivante porte sur la différence entre la méthode MsFEM classique et la méthode obtenue en suivant l'approche non-intrusive. L'estimation suivante est établie dans la Section 6.2.

Contribution 4. *Reformulation du Théorème 6.3:*
Soit V_H^ε *l'espace engendré par les fonctions multi-échelles. Soit* a^ε*, resp.* F*, la forme bilinéaire, resp. la forme linéaire, correspondant à la formulation variationelle de l'EDP. (Nous considérons des variantes broken si la méthode est non-conforme.)*

L'approche non-intrusive de la méthode MsFEM

$$\textit{Trouver } u_H^\varepsilon \in V_H^\varepsilon \textit{ telle que} \quad a^\varepsilon(u_H^\varepsilon, v_H^\varepsilon) = F(v_H^\varepsilon) \quad \textit{pour tout } v_H^\varepsilon \in V_H^\varepsilon$$

correspond à trouver $u_H^\varepsilon \in V_H^\varepsilon$ *telle que*

$$a^\varepsilon(u_H^\varepsilon, \phi_i^\varepsilon) = F\big(\phi_i^{\mathbb{P}_1}\big) \quad \textit{pour tout } 1 \leq i \leq N,$$

où la fonction multi-échelle ϕ_i^ε *est définie à partir de la fonction de base standard* $\phi_i^{\mathbb{P}_1}$ *et des correcteurs numériques dans* (6.3).

Nous appliquerons également l'approche non-intrusive à une variante Petrov-Galerkin de la méthode MsFEM, où les fonctions test multi-échelles sont remplacées par les fonctions test de l'espace $\mathbb{P}_1$ standard. Nous trouverons que l'approche non-intrusive est équivalente à la méthode originale.

Contribution 5. *Reformulation du Théorème 6.2:*
Considérons la méthode MsFEM Petrov-Galerkin suivante:

$$\textit{Trouver } u_H^\varepsilon \in V_H^\varepsilon \textit{ telle que} \quad a^\varepsilon(u_H^\varepsilon, v_H) = F(v_H) \quad \textit{pour tout } v_H \in V_H^{\mathbb{P}_1},$$

où $V_H^{\mathbb{P}_1}$ *est l'espace* $\mathbb{P}_1$ *de Lagrange quand on considère la méthode MsFEM-lin, et* $V_H^{\mathbb{P}_1}$ *est l'espace* $\mathbb{P}_1$ *de Crouzeix-Raviart quand on considère la méthode MsFEM-CR. La solution de cette méthode est* ***identique*** *à la solution de la variante non-intrusive de la méthode.*

Dans quelques cas particuliers, on peut démontrer que l'approche non-intrusive pour la méthode MsFEM (Galerkin) est aussi identique à la méthode MsFEM Petrov-Galerkin introduite ci-dessus; voir le Lemme 6.4. Pour l'équation de la diffusion pure, nous établirons les résultats suivants.

Contribution 6. *Reformulation du Lemme 7.1 et du Théorème 7.10:*
Nous considérons l'équation de la diffusion pure. Soit 'MsFEM' la méthode MsFEM-lin ou la méthode MsFEM-CR, sans l'utilisation de la technique d'oversampling. Alors l'approche non-intrusive de la méthode MsFEM Galerkin coïncide avec la méthode MsFEM Petrov-Galerkin.
Soit $u_H^{\varepsilon,\mathsf{G}}$*, resp.* $u_H^{\varepsilon,\mathsf{PG}}$*, l'approximation de* u^ε *obtenue par la méthode MsFEM Galerkin, resp. la méthode MsFEM Petrov-Galerkin. Si* $f \in L^2(\Omega)$*, il existe une constante* $C > 0$ *indépendante de* ε*,* H *et* f *telle que*

$$\left\| u_H^{\varepsilon,\mathsf{G}} - u_H^{\varepsilon,\mathsf{PG}} \right\|_{H^1(\mathscr{T}_H)} \leq CH\|f\|_{L^2(\Omega)}.$$

La dernière contribution de la Partie I de la thèse est dédiée à l'implémentation de la méthode MsFEM en FreeFEM++ et les conclusions provenant des expérimentations numériques dans le cas de l'équation de la diffusion pure pour des coefficients de diffusion périodiques et non-périodiques.

Contribution 7. *Toutes les variantes de la méthode MsFEM couvertes par la formulation générale du Chapitre 5 de cette thèse, ont été implémentées en* FreeFEM++,

s'appuyant sur la structure commune entre ces méthodes qui a été identifiée grâce à la formulation générale de la Contribution 2. Le code correspondant est disponible à [29]. Les expérimentations numériques pour l'équation de la diffusion pure montrent que la méthode MsFEM Petrov-Galerkin, ainsi que la variante non-intrusive de la méthode MsFEM Galerkin, sont proches de la méthode MsFEM Galerkin originale. L'éventuelle erreur introduite par le passage à une approche non-intrusive est donc négligeable. De plus, cette observation est robuste par rapport à la périodicité ou non du coefficient de diffusion.

1.3.2. Méthodes MsFEM pour les problèmes avec advection dominante. Dans la partie II de la thèse, nous nous concentrerons sur l'équation d'advection-diffusion, c'est-à-dire que u^ε est la solution de l'équation suivante sur Ω :

$$-\operatorname{div}(A^\varepsilon \nabla u^\varepsilon) + b \cdot \nabla u^\varepsilon = f, \tag{1.9}$$

avec un champ d'advection $b \in L^\infty(\Omega)$ (et sous certaines hypothèses supplémentaires qui seront précisées dans le Chapitre 9). Nous considérons toujours un coefficient de diffusion hautement oscillant A^ε comme précédemment, et les problèmes associés à la méthode EF sur un maillage grossier persistent. Une autre difficulté pour l'approximation numérique de u^ε apparaît : nous nous intéressons particulièrement au cas où l'advection est dominante devant la diffusion. Nous étudierons des méthodes MsFEM qui visent à traiter les deux difficultés dans la Partie II.

Il est bien connu que, sous l'influence d'un champ d'advection dominant, la solution exacte u^ε peut développer des couches limites, où la solution est caractérisée par un fort gradient dans une petite partie du domaine. Il est également bien connu que les méthodes EF standards ne parviennent pas à capturer u^ε à moins que le maillage sous-jacent soit suffisamment fin pour prendre en compte ces couches limites. Sur un maillage grossier, l'approximation numérique montre de grandes oscillations qui peuvent se propager dans tout le domaine, alors que la solution exacte ne varie que lentement à l'extérieur de la couche limite. On dit que la méthode EF est instable dans le régime dominé par l'advection. Si la position de la couche limite est inconnue, une méthode EF standard nécessite donc un maillage très fin sur l'ensemble du domaine, ou des techniques d'adaptation de maillage itératives, qui peuvent toutes deux être coûteuses en termes de calcul. Des méthodes dites de stabilisation ont été développées pour obtenir une approximation adéquate sur un maillage grossier dans le cas des coefficients non-oscillants il y a plusieurs décennies. Ces méthodes introduisent toutes un paramètre de stabilisation et la qualité de l'approximation est sensible au choix de ce paramètre. En revanche, nous regarderons la stabilisation à travers les méthodes de type MsFEM dans cette thèse.

Il est clair que la méthode MsFEM définie par les fonctions multi-échelles dans (1.4) est instable aussi, car elle coïncide avec la méthode EF classique $\mathbb{P}_1$ quand A^ε est constante. Cette instabilité est illustrée par la Figure 10.1 du Chapitre 10. Cette méthode a été stabilisée par la méthode de stabilisation classique dite SUPG dans [114]. Nous nous concentrerons dans cette thèse sur une autre variante de la méthode MsFEM où les fonctions multi-échelles sont obtenues à partir de problèmes locaux contenant tous les termes de l'EDP (1.9), c'est-à-dire,

$$\forall K \in \mathscr{T}_H, \quad \begin{cases} -\operatorname{div}(A^\varepsilon \nabla \phi_i^{\varepsilon,\mathsf{adv}}) + b \cdot \nabla \phi_i^{\varepsilon,\mathsf{adv}} = 0 & \text{dans } K, \\ \phi_i^\varepsilon = \phi_i^{\mathbb{P}_1} & \text{sur } \partial K, \end{cases} \tag{1.10}$$

pour tout $1 \leq i \leq N$, que nous appelons la méthode adv-MsFEM-lin. Cette méthode a été étudiée dans [127, 128, 114, 119], mais toutes ses propriétés de stabilisation ne sont pas encore bien comprises. Les contributions à propos de cette méthode sont résumées ci-dessous.

Tout d'abord nous considérons la méthode adv-MsFEM-lin en dimension 1. Nous parlons de la méthode adv-MsFEM tout court, puisque le choix des conditions au bord dans les problèmes locaux (1.10) ne jouent un rôle qu'en dimension supérieure.

Contribution 8. *Reformulation du Théorème 10.4:*
En dimension 1, quand $f = 0$ et pour tout choix de conditions au bord sur $\partial\Omega$, l'approximation de la méthode adv-MsFEM est égale à la solution exacte de (2.27). Puisque les instabilités d'une méthode EF sont liées au choix des conditions de Dirichlet sur $\partial\Omega$ plutôt qu'au terme source f dans (1.9), nous en concluons que la méthode adv-MsFEM est stable. La stabilité pour f non-nulle est en effet observée numériquement.

Nous verrons aussi dans le Chapitre 10 que les fonctions multi-échelles $\phi_i^{\varepsilon,\mathsf{adv}}$ définies par (1.10) peuvent être fortement déformées sous l'influence du champ d'advection, et qu'elles ont dans ce cas des couches limites à l'intérieur de chaque maille. Voir la Figure 2.10. Cela rend la méthode inappropriée pour l'approximation de (1.9). Nous proposons de remédier à ce problème, tout en conservant la stabilité de la méthode, en ajoutant à l'espace d'approximation une bulle $B_K^{\varepsilon,\mathsf{adv}}$ sur chaque maille grossière $K \in \mathscr{T}_H$. Cette bulle est définie comme l'unique solution dans $H_0^1(K)$ du problème

$$-\operatorname{div}(A^\varepsilon \nabla B_K^{\varepsilon,\mathsf{adv}}) + b \cdot \nabla B_K^{\varepsilon,\mathsf{adv}} = 1 \quad \text{dans } K.$$

et mène à la méthode adv-MsFEM-lin-B (voir (2.30) pour la définition précise). Pour cette méthode, nous présenterons les résultats suivants dans cette thèse.

Contribution 9. *Si $A^\varepsilon = m\,\mathrm{Id}$ pour $m > 0$, et si b et f sont constants par morceaux, alors on peut associer à la méthode adv-MsFEM-lin-B un schéma effectif sur l'espace standard $\mathbb{P}_1$ de Lagrange qui coïncide avec la méthode classique des residual-free bubbles [41]. Ce schéma est le même que la formulation stabilisée SUPG avec un paramètre de stabilisation*

1) *qui a, en 1D, l'unique valeur pour laquelle le schéma effectif est exact aux nœuds (et la méthode adv-MsFEM-B est même exacte), mais*
2) *dont la valeur en dimension supérieure est trop petite pour assurer la stabilisation complète du schéma.*

Cette contribution explique donc l'instabilité de la méthode adv-MsFEM-lin en dimension 2 qui a été observée numériquement dans [114]. Pour la dimension 2, nous avons découvert la stabilité de la méthode adv-MsFEM-CR, où les fonctions multi-échelles $\phi_i^{\varepsilon,\mathsf{adv}}$ dans (1.9) sont définies avec des conditions de continuité faibles au bord de la maille K. Les conclusions des expérimentations numériques du Chapitre 12 sont les suivantes.

Contribution 10. *La méthode adv-MsFEM-CR est stable. Néanmoins, sa précision se dégrade dans le régime dominé par l'advection en raison de la forme inadéquate des fonctions multi-échelles, et l'ajout de fonctions bulles est nécessaire pour préserver la précision dans ce régime. L'erreur commise par la méthode adv-MsFEM-CR-B est*

robuste par rapport à l'importance relative de l'advection. La seule autre méthode étudiée ici ayant cette propriété est la méthode MsFEM-lin stabilisée par la technique SUPG. Contrairement à la méthode MsFEM-lin SUPG, la robustesse de la méthode adv-MsFEM-CR-B ne dépend pas d'un paramètre qui doit être correctement choisi. Enfin, nous introduirons une variante non-intrusive de la méthode adv-MsFEM-CR-B qui s'avère même légèrement plus précise que la méthode originale dans le régime dominé par l'advection.

1.3.3. Analyse de convergence de la MsFEM sous des hypothèses de régularité minimales. Des analyses de convergence pour diverses méthodes MsFEM sont disponibles dans la littérature. Elles estiment la différence $u^\varepsilon - u_H^\varepsilon$ avec une dépendance explicite en ε (la taille de la microstructure) et en H (la taille des mailles grossiers). Tous les résultats que nous connaissons considèrent le cas où $A^\varepsilon = A^{\mathsf{per}}(\cdot/\varepsilon)$ pour une matrice périodique A^{per} (voir [98, 99, 70, 100, 9, 112, 113, 94, 116, 114, 53]). Dans ce cadre, la théorie de l'homogénéisation montre que la suite des solutions $(u^\varepsilon)_{\varepsilon>0}$ tend vers une fonction $u^\star \in H_0^1(\Omega)$ lorsque $\varepsilon \to 0$, et l'hypothèse de périodicité permet d'établir un taux de convergence en ε (entre u^ε et une correction multi-échelle de $u^\star$) [28, 33]. Ce taux de convergence est essentiel dans une analyse de convergence.

A cette hypothèse de périodicité s'ajoutent des hypothèses de régularité pour A^{per} pour obtenir le taux de convergence évoqué ci-dessus. On suppose dans la littérature que A^{per} est höldérienne. Une telle hypothèse est très restrictive du point de vue de la modélisation car les matériaux multi-échelles sont typiquement caractérisés par des coefficients *discontinus*. Dans le Chapitre 13, nous démontrerons le théorème suivant, sans aucune hypothèse sur A^{per} à part celles qui assurent le caractère bien-posé de (1.1).

Contribution 11. *Reformulation du Théorème 13.1:*
Supposons que $A^\varepsilon = A^{\mathsf{per}}(\cdot/\varepsilon)$ pour une matrice périodique A^{per} qui n'est pas nécessairement höldérienne. Soit u_H^ε l'approximation numérique de u^ε par la méthode MsFEM-lin ou la méthode MsFEM-CR. Soit $(\mathscr{T}_H)_H$ une famille de triangulations régulière et quasi-uniforme. Supposons que $\varepsilon \leq H$ et que $u^\star \in H^2(\Omega)$. Alors

$$|u^\varepsilon - u_H^\varepsilon|_{H^1(\mathscr{T}_H)} \leq C \left(H|u^\star|_{H^2(\Omega)} + \sqrt{\frac{\varepsilon}{H}}\, |u^\star|_{H^1(\Omega)} \right).$$

Chapter 2

Introduction

This introduction provides the context and motivation of the research that is documented in this thesis, and it includes a summary of the main research contributions with an outlook on future research directions associated to each research topic. Parts I, II and III of the thesis each detail the contributions to one specific research area. The thesis is organized in such a way that these three parts can be read independently.

2.1. Motivation

This thesis is concerned with computational methods for partial differential equations in multiscale models. Models with multiscale properties naturally appear in many areas of modern science and engineering. In the context of materials science, one could think of composite materials for the design of aircraft wings, the study of fibers which are themselves a collection of many finer fibers, or the use of concrete in many civil-engineering applications. We also mention the modeling of sub-surface flow, for instance to understand how a pollutant may spread through the earth's surface, or the flow of the air through a dense city center. In this thesis, we consider multiscale properties in space, like in the above examples, and not in time, which require different approaches due to the sequential nature of time.

In many cases one wishes to perform numerical simulations, that is, to find an approximation of the unknown quantities of the model by executing some dedicated software on a computer, in order to understand the properties of the model. This can be the case when physical experiments are deemed too costly, take too much time, or when obtaining the desired information from an experimental setup is not even possible at all. Simulations can also be a solution when an approximate answer is needed within a limited amount of time that does not allow for elaborate experiments, or if the model is to be studied for a large variation of different parameter values in the early stages of a design process. All these various needs have led to the development of a plethora of computational techniques (and the development of the associated hardware and software) over the past seven decades.

The above examples of multiscale models are all characterized by variations on a scale that is much smaller than the global dimension of the system. The numerical simulation of a multiscale model based on the complete discretization of the microscale then leads to an enormous linear system, the resolution of which may take a considerable

(possibly prohibitively large) amount of computational time, or may be impossible due to memory constraints of the available computer architecture. Direct numerical simulation is therefore often unfeasible.

In many applications, one is not actually interested in the precise fluctuations of the solution of the model at the scale of its finest variations. Much coarser, global, macroscopic knowledge of material properties is often sufficient, at least as a first step. One may thus hope that a corresponding coarse numerical model can provide the desired information. However, the microstructure of the model does have a large impact on the emergent macroscopic properties, and it cannot be entirely discarded in numerical simulations. In Section 2.1.1 we will show for the explicit example of the *finite element method* (one particularly successful computational technique) that a reliable solution cannot be obtained if the small variations of the model are ignored.

The above considerations have motivated the development of multiscale computational techniques, which have known a particular interest during the past three decades. The goal of such techniques is to preprocess the microstructure in such a way that, once the preprocessing step has been completed, a coarse numerical model is available that provides a reasonably accurate approximation of the global properties of the system of interest at a low computation cost. Note that the preprocessing step is unavoidably computationally expensive since it has to process the microstructure properly. However, it typically follows a 'divide and conquer' strategy and does not require equally extensive computational resources as the resolution of the original problem, at least when the space dimension is not too large (e.g. in dimension 2 or 3). It is also usually suited for parallel computation. A multiscale approach is therefore advantageous when similar problems are to be solved many times, in which case the expensive preprocessing step has to be performed only once. Since the global numerical model is coarse, it can be solved rapidly, yielding a significant computational gain compared to the repeated direct simulation of the complete microstructure. Nonetheless, when the problem at hand is to be solved only once, multiscale approaches may still be beneficial if the global problem cannot be treated directly. One may also consider iterative methods, that share some ideas with multiscale methodes, on which we comment in Section 2.2.2.

This thesis mainly focuses on one such multiscale method known as the *multiscale finite element method*. We cannot treat all applications mentioned above within the scope of the present thesis. We rather consider somewhat abstract models that are a building block for the resolution of many of the above-mentioned applications. The focus is on settings for which, in spite of some research efforts in the past, a definite best approach has not yet been identified. A considerable part of the thesis also investigates the adaptation of the multiscale finite element method in such a way that it can be implemented by the use of large, existing software packages that are currently used in industry, without the need to modify this software. That is, without being *intrusive*. We consider this an essential feature of any computational technique in order to facilitate its use for more advanced applications, and have accordingly included the mention of 'non-intrusive methods' in the title of the thesis. The proposed numerical methods are studied numerically and compared to other known numerical models. This is complemented by a mathematical convergence analysis when we are able to conduct it.

In the rest of this introduction, we motivate the advent of multiscale computational techniques during the past decades and give an overview of key contributions in the field. Then we give a more detailed description of the research contributions of the thesis that are presented in Parts I, II and III.

2.1.1. The finite element method. We consider numerical methods of finite element type in this thesis. Let us recall the principle of the finite element method on the example of a simple diffusion equation. We fix a domain $\Omega \subset \mathbb{R}^d$ and we consider the partial differential equation (PDE)

$$-\operatorname{div}(A\nabla u) = f \quad \text{in } \Omega, \tag{2.1}$$

subject to the boundary condition $u = 0$ on the boundary $\partial\Omega$ of the domain. This equation appears in the modeling of thermal or electric conductivity, for instance, in which case u is the (unknown) temperature or electric potential, respectively, and the matrix A is a $d \times d$ matrix that characterizes the conductivity of the medium at any point of the domain Ω. The equation also appears in more complicated models arising from physics, engineering, biology, etc. It is also a building block for the discretization of many more involved (non-linear, non-stationary) models.

For the purpose of designing a finite element method (FEM) for the PDE (2.1), the PDE is written in a weak formulation, also called variational formulation. For simplicity, we suppose that $f \in L^2(\Omega)$. Then the variational formulation of (2.1) is as follows: find $u \in H_0^1(\Omega)$ such that, for all $v \in H_0^1(\Omega)$, it holds

$$\int_\Omega \nabla v \cdot A\nabla u = \int_\Omega fv. \tag{2.2}$$

It is a classical result that u solves the weak form (2.2) if and only if it satisfies the strong form (2.1) in the sense of distributions. Moreover, when the matrix A is elliptic (that is, $\xi \cdot A\xi \geq m\|\xi\|^2$ for all $\xi \in \mathbb{R}^d$ and for some $m > 0$) and bounded, one can show well-posedness of (2.1) by the classical Lax-Milgram Theorem. We refer e.g. to [129, Chapter 3] for details.

A classical idea in the approximation of variational problems is to solve the problem obtained when $H_0^1(\Omega)$ is replaced by a finite-dimensional subspace V_H. We can then define the numerical approximation $u_H \in V_H$ as the unique solution to

$$\int_\Omega \nabla v_H \cdot A\nabla u_H = \int_\Omega f\, v_H \quad \text{for all } v_H \in V_H. \tag{2.3}$$

This is called a Galerkin approximation of (2.2). Clearly, there exists great flexibility in the design of Galerkin approximations based on the choice of the subspace V_H. Once V_H is fixed and a basis has been chosen, the problem (2.3) is equivalent to a linear system whose number of unknowns equals $\dim(V_H)$ and which consists of the same number of equations, obtained upon choosing for v_H in (2.3) the basis functions of V_H. We also say that (2.3) is *tested* against the basis of V_H. Under the same conditions as for the continuous problem (2.2), the discrete problem (2.3) has a unique solution.

Finite element methods correspond to choosing a subspace V_H in the Galerkin approximation (2.3) with certain characteristic, advantageous properties. In short, for a classical FEM, the space V_H

(i) is constructed on a mesh of the domain Ω,
(ii) consists of functions that are polynomial on each mesh element,
(iii) has a basis of functions that are localized on a small number of mesh elements as much as possible.

The piecewise polynomial character of the space V_H (throughout this thesis, 'piecewise'

means that the property is true on every mesh element) ensures useful approximation properties of the space V_H, and it guarantees that the coefficients of the linear system resulting from (2.3) are easy to compute. The localization of the basis functions is essential for an efficient computation of these coefficients on a computer, and for a sparse structure of the linear system. The dimension of V_H is also called the number of degrees of freedom of the FEM.

For the second property above, the description 'functions that are close to polynomials' would in fact be more appropriate (albeit rather vague), in order not to neglect the possibility of isoparametric finite elements. We do not consider such methods in this thesis.

Many spaces with the above properties have been developed for various applications. An overview is beyond the scope of this introduction. Thorough introductions to finite element methods can be found in many textbooks. We cite [73, 8, 37, 129]. We also mention the classical monograph [52]. An interesting historical account of the birth of finite element methods can be found in [80], and a brief account of the development of the method during the 20th century in [126].

The FEM has had huge success in scientific computing for almost any branch of science and engineering. It is nowadays widespread due to its established performance for a wide range of applications. It can be used for the approximation of symmetric and nonsymmetric problems, for non-linear problems and eigenvalue problems. The popularity of the FEM is also due to the fact that general-purpose software can be written for large classes of FEMs with relative ease due to the above three characteristic principles. Moreover, the FEM enjoys an elaborate and well-understood mathematical framework to study its performance (e.g., convergence upon mesh refinement and increase of the polynomial degree), the foundations of which were laid in the 1970s.

Before investigating the FEM for multiscale problems specifically, let us comment on some liberty in defining FEMs that is not contained in the succinct presentation above. In particular, the concepts of Petrov-Galerkin methods and of non-conforming methods shall play a role in this thesis.

In the linear system corresponding to (2.3), the unknowns are the coefficients of u_H in the basis of V_H. The equations are obtained upon testing (2.3) against the basis functions of V_H. However, in principle, a linear system can be obtained upon testing (2.3) against different functions that *do not belong to* V_H. An FEM then takes the form: find $u_H \in V_H$ such that

$$\int_\Omega \nabla w_H \cdot A \nabla u_H = \int_\Omega f\, w_H \quad \text{for all } w_H \in W_H, \tag{2.4}$$

where W_H can, in principle, be any finite-dimensional space with the same dimension as V_H. We call V_H the trial space (or approximation space), and W_H the test space. When the test and trial spaces are different, we speak of a Petrov-Galerkin approximation of (2.2). The freedom in the choice of test space can be used to improve the stability properties of the FEM. We cite [58]: "...in designing Petrov-Galerkin methods, while we must choose trial spaces with good approximation properties, we may design test spaces solely to obtain good stability properties." This has further been explored in the series of works [59, 60, 135]. The use of Petrov-Galerkin approximations long predates these relatively recent works, and is as old as the finite element method itself. In the context of advection-dominated problems, which we will consider in more detail in Part II of the thesis, the benefit of Petrov-Galerkin formulations was also investigated, e.g., in [43, 122, 77].

The use of Petrov-Galerkin approximations may also be advantageous for the implementation of an FEM. This point of view is extensively discussed for multiscale methods in Part I of the thesis. We also refer to [71].

We further mention that, in fact, the trial and test spaces need not be subspaces of $H^1_0(\Omega)$ to design effective FEMs. There is indeed a huge variety of such *non-conforming* finite element methods, as they are called. In this thesis, we will consider variants of the classical finite element introduced in [56] by Crouzeix and Raviart, which now carries their names. In particular, this finite element is not continuous (but continuous only in a weak sense). One can even go further in this direction and employ Discontinuous Galerkin methods. We refer to [61] for an introduction.

2.1.2. The finite element method applied to multiscale problems. Somewhat contrary to the many successes of the FEM that were underlined above, we will now show that the direct use of FEMs, at least in their classical form, is not efficient for the resolution of multiscale problems. This has led to the development of dedicated multiscale approaches, which we review in Section 2.2. We restrict ourselves here to the example of the diffusion equation.

Let us introduce a strongly heterogeneous diffusion coefficient A^ε, a $d \times d$ matrix satisfying the same ellipticity property as above. We use the superscript ε throughout to remind the reader of the presence of a small scale, the scale of the heterogeneities of the medium that is modeled by A^ε, which is much smaller than the typical dimensions of the domain Ω. Correspondingly, we denote by $u^\varepsilon \in H^1_0(\Omega)$ the solution to (2.1) when A is replaced by A^ε, which equivalently solves

$$\int_\Omega \nabla v \cdot A^\varepsilon \nabla u^\varepsilon = \int_\Omega f v \quad \text{for all } v \in H^1_0(\Omega). \tag{2.5}$$

We now recall the classical Lagrange FEM of order 1. It is based on continuous piecewise polynomials of degree 1 for the trial space V_H. More precisely, let $\mathscr{T}_H$ be a conformal simplicial mesh (often called a triangulation) of Ω. For detailed definitions we refer to [129] in order to keep the presentation concise. Here, H denotes the size of the mesh elements, typically defined as $H = \max_{K \in \mathscr{T}_H} \operatorname{diam}(K)$. For simplicity, we suppose that Ω is a polyhedron, so that $\overline{\Omega} = \bigcup_{K \in \mathscr{T}_H} \overline{K}$. Now V_H is the $\mathbb{P}_1$ Lagrange space

$$V_H^{\mathbb{P}_1} = \left\{ v \in \mathscr{C}^0(\Omega) \,|\, v = 0 \text{ on } \partial\Omega \text{ and } \forall\, K \in \mathscr{T}_H,\ v|_K \in \mathbb{P}_1(K) \right\},$$

where $\mathbb{P}_1(K)$ denotes the space of all polynomials on K of total degree at most 1. The notation $V_H^{\mathbb{P}_1}$ may also be used to indicate other spaces of piecewise affine functions later on in this introduction. The standard basis of this space in the case of a one-dimensional domain $\Omega = (0,1)$ is shown in Figure 2.1. The basis functions clearly satisfy the locality property required above.

The space $V_H^{\mathbb{P}_1}$ is a subspace of $H^1_0(\Omega)$. We can thus define the $\mathbb{P}_1$ FEM approximation $u_H^\varepsilon \in V_H^{\mathbb{P}_1}$ as the unique solution in $V_H^{\mathbb{P}_1}$ to the problem

$$\int_\Omega \nabla v_H \cdot A^\varepsilon \nabla u_H^\varepsilon = \int_\Omega f\, v_H \quad \text{for all } v_H \in V_H^{\mathbb{P}_1}. \tag{2.6}$$

Convergence of u_H^ε towards u^ε is guaranteed (under certain regularity properties of the

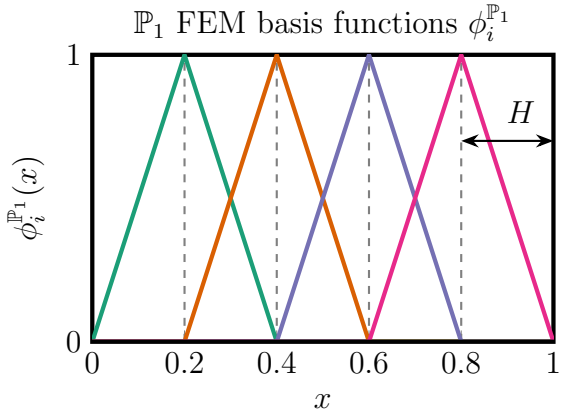

Figure 2.1: *Basis functions $\phi_i^{\mathbb{P}_1}$ of the $\mathbb{P}_1$ Lagrange space $V_H^{\mathbb{P}_1}$ in dimension 1.*

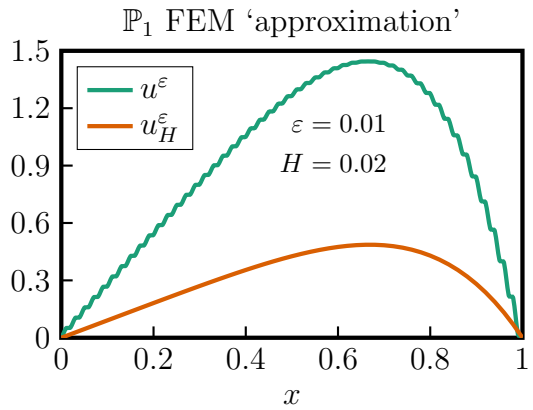

Figure 2.2: *For the diffusion coefficient (2.8), the difference between u_H^ε and the exact solution u^ε is large when the mesh size H does not resolve the microscale ε.*

mesh for which we refer to the Bibliography) as $H \to 0$. See, for instance, Theorem 3.16 of [73], which gives the following order of convergence:

$$\|u^\varepsilon - u_H^\varepsilon\|_{H^1(\Omega)} \leq CH|u^\varepsilon|_{H^2(\Omega)}. \tag{2.7}$$

(Here, $|\cdot|_{H^2(\Omega)}$ denotes the H^2-semi-norm; one can show that u^ε belongs to $H^2(\Omega)$ if we assume that Ω is convex, see [85, Theorem 3.2.1.2].)

The multiscale character of the diffusion coefficient A^ε requires that the mesh size H properly resolves the heterogeneities of the problem at the microscopic scale ε in order to reach the convergence (2.7). In this case, the dimension of the space $V_H^{\mathbb{P}_1}$ is huge, and accordingly, the linear system corresponding to (2.6) will be large. The resolution of the linear system becomes numerically intractable for many relevant applications.

Figure 2.2 shows an illustration in the one-dimensional case. For the diffusion coefficient

$$A^\varepsilon(x) = \begin{cases} 1 \text{ if } \lfloor x/\epsilon \rfloor \text{ is even,} \\ 10 \text{ if } \lfloor x/\epsilon \rfloor \text{ is odd,} \end{cases} \tag{2.8}$$

and the right-hand side $f(x) = 100x^3$, we show the exact solution u^ε and the $\mathbb{P}_1$ FEM approximation u_H^ε defined by (2.6). The mesh size used is $H = 2\varepsilon$. Note that, even though $H > \varepsilon$, this is still small if one considers that ε is a microscopically small length scale. Yet the numerical approximation u_H^ε fails to approximate the solution anywhere on Ω. Here, we must distinguish two different properties of the approximation u_H^ε:

1. The microscopic oscillations of u^ε are not captured by u_H^ε. This is obviously impossible when the approximation space $V_H^{\mathbb{P}_1}$ does not contain any oscillations at this length scale.
2. The *macroscopic* profile of u^ε is not captured by u_H^ε. This is a shortcoming of the FEM methodology itself rather than the approximation space, because one easily imagines a piecewise affine function being much closer to u^ε than the "approximation" of Figure 2.2.

The same phenomenon persists for higher-dimensional problems. We show a two-dimensional example in Figure 2.3 for the PDE $-\operatorname{div}(A^\varepsilon \nabla u^\varepsilon) = 500$, which illustrates the

vast number of degrees of freedom that is required to obtain a satisfactory approximation with the $\mathbb{P}_1$ FEM. To properly resolve a diffusion coefficient with only 25 heterogeneities in an otherwise homogeneous medium, even a naive $\mathbb{P}_1$ approximation with more than 1500 degrees of freedom looses a considerable amount of information about the global profile of u^ε. One readily understands that the requried number of degrees of freedom explodes for real-sized three-dimensional systems with hundreds of heterogeneities. We summarize the above observations as follows:

The $\mathbb{P}_1$ FEM cannot be used to compute an approximation of u^ε if the mesh is coarse. All macroscopic properties are lost if the microstructure is ignored.

This conclusion remains true for higher-order FEMs when the mesh does not resolve the microstructure.

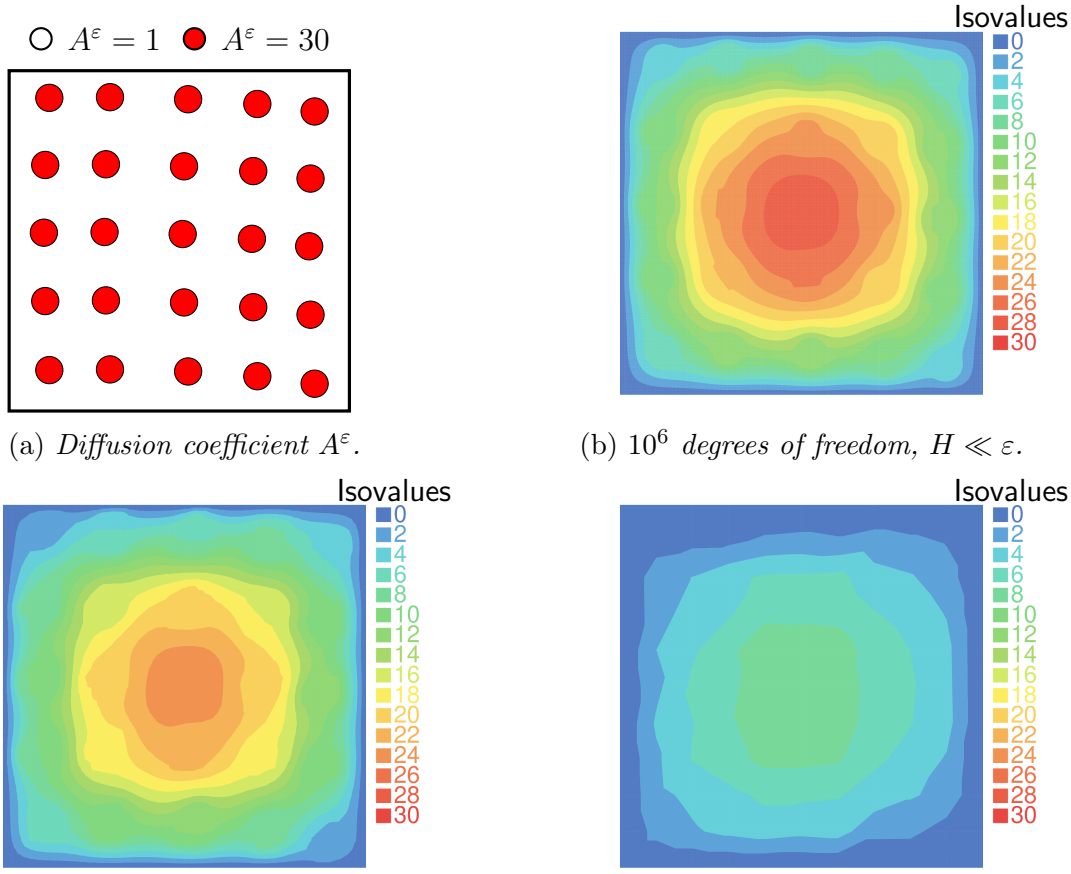

(a) *Diffusion coefficient A^ε.*

(b) 10^6 *degrees of freedom, $H \ll \varepsilon$.*

(c) *1521 degrees of freedom, $H \sim \varepsilon$.*

(d) *81 degrees of freedom, $H \gg \varepsilon$.*

Figure 2.3: *Finite element approximations for the diffusion coefficient in (a) and three different mesh sizes H. The maximum of the solution drops rapidly when the mesh does not sufficiently accurately resolve the heterogeneities.*

Let us now give some explanation for the inability of the FEM to capture even the global properties of u^ε if the mesh is too coarse. In the Galerkin approximation (2.6), note that the gradients ∇v_H and ∇u_H^ε are constant inside each element of the mesh. We

can thus rewrite the left-hand side as

$$\int_\Omega \nabla v_H \cdot A^\varepsilon \nabla u_H^\varepsilon = \sum_{K\in\mathscr{T}_H} \nabla v_H|_K \cdot \left(\int_K A^\varepsilon\right) \nabla u_H^\varepsilon|_K = \int_\Omega \nabla v_H \cdot A^{\mathsf{av}} \nabla u_H^\varepsilon, \tag{2.9}$$

where A^{av} is a matrix that is constant in each mesh element and is defined by the averages

$$A^{\mathsf{av}}|_K = \frac{1}{|K|}\int_K A^\varepsilon \quad \text{for all } K \in \mathscr{T}_H. \tag{2.10}$$

Thus, for all matrices that have the same piecewise average as A^ε, the $\mathbb{P}_1$ Lagrange FEM gives the same approximation. This is not a problem as long as the diffusion matrix varies mildly around its average inside each element of the mesh $\mathscr{T}_H$, which would be the case if we could afford to use a sufficiently fine mesh. When the diffusion matrix varies rapidly inside the element, Figures 2.2 and 2.3 show that the effective behaviour of the solution u^ε is quite different from the properties predicted by the FEM, which only sees A^{av}. In particular, it was shown in [21] that coefficients can be constructed for which the $\mathbb{P}_1$ FEM converges arbitrarily slowly on a uniform mesh in 1D.

To understand why replacing A^ε by A^{av}, as happens implicitly in the FEM, is illegitimate, it is instructive to focus on a one-dimensional example. In the one-dimensional case, say on the domain $\Omega = (0,1)$, the problem reduces to the ordinary differential equation $-(A^\varepsilon(u^\varepsilon)')' = f$ with homogeneous Dirichlet boundary conditions. The equation can be integrated directly; this yields

$$u^\varepsilon(x) = -\int_0^x \frac{C^\varepsilon + F(t)}{A^\varepsilon(t)}\,\mathrm{d}t \quad \text{with } C^\varepsilon = -\frac{\displaystyle\int_0^1 F(t)/A^\varepsilon(t)\,\mathrm{d}t}{\displaystyle\int_0^1 1/A^\varepsilon(t)\,\mathrm{d}t},$$

and where F is a primitive of f. When, for instance, $A^\varepsilon = A^{\mathsf{per}}(\cdot/\varepsilon)$ where A^{per} is periodic with period 1, it is easy to show that, for any integrable function g,

$$\int_0^1 \frac{g(t)}{A^\varepsilon(t)}\,\mathrm{d}t \to \int_0^1 \frac{1}{A^\star}\,g(t)\,\mathrm{d}t \quad \text{as } \varepsilon \to 0,$$

where

$$A^\star = \left(\int_0^1 \frac{1}{A^{\mathsf{per}}}\right)^{-1} \tag{2.11}$$

is the harmonic average of A^{per}. Consequently, C^ε converges to the constant $C^\star$ defined as

$$C^\star = -A^\star \int_0^1 \frac{1}{A^\star}\,F(t)\,\mathrm{d}t,$$

and u^ε converges (pointwise) to the function $u^\star$ that is given by

$$u^\star(x) = -\int_0^x \frac{1}{A^\star}\,(C^\star + F(t))\,\mathrm{d}t.$$

One immediately sees that $u^\star$ is a solution to the differential equation $-(A^\star(u^\varepsilon)')' = f$ with the constant diffusion coefficient $A^\star$. However, $A^\star$ is the *harmonic average* of A^{per}, and not the *arithmetic* average (2.10) that is encoded in the FEM through (2.9).

We point the reader towards [33, Section 2.1] for interesting and more general considerations regarding these simple computations. For the purposes of this introduction, the conclusion for a periodic diffusion coefficient is twofold:

1. The solution u^ε is, at least when ε is small (and in a sense that can be made precise) close to $u^\star$, which is the solution to a differential equation with a *constant* coefficient, but
2. this coefficient is not equal to, and is in general *very different* from the averaged coefficient A^{av} from (2.10) that is seen by the $\mathbb{P}_1$ FEM.

Let us give an optimistic interpretation of these observations: for a multiscale problem, there may exist a piecewise constant, 'effective' diffusion coefficient, which describes the macroscopic behaviour of u^ε more accurately than A^{av}. In the context of the mathematical theory of homogenization, this may be formalized in the limit that the microscopic parameter tends to 0. The existence of effective coefficients is a commonly used principle in materials science, and they can be characterized by physical measurements, for instance. In order to use the FEM for simulations in the multiscale context, it must be adapted such that, either implicitly or explicitly, the effective properties of the problem are captured. This is the goal of the multiscale methods that we describe in the next section. We will also see that homogenization theory justifies many of the above remarks in a general setting.

To conclude this section about the finite element method in general, let us comment on the convergence (2.7) of the FEM. We now know that a small value of the mesh size H does not necessarily mean that the error $u^\varepsilon - u^\varepsilon_H$ is small when the coefficient A^ε is strongly heterogeneous. We also understand that the error does not decrease upon mesh refinement as long as the resulting mesh is too coarse to resolve the microstructure of A^ε, because the FEM approximation is still based on the erroneous average A^{av}. Is there a contradiction? The answer is, of course, no. When A^ε is highly oscillatory, with oscillations at the scale ε, the second derivatives of u^ε are of the order of ε^{-1}. The error in (2.7) may thus be large when H/ε is large, i.e., when the microstructure is not properly resolved. The classical error estimate remains valid, but becomes meaningless in the multiscale context.

2.2. Introduction to multiscale methods

We start this section with a theoretical approach rather than a numerical one: a short description of the mathematical theory of homogenization. We will also explain why the direct use of this theory is rather limited in practice, and then move on to numerical approaches for multiscale problems.

2.2.1. Homogenization theory. In the mathematical theory of homogenization, a sequence of diffusion coefficients A^ε indexed by $\varepsilon \to 0$ is considered along with the corresponding solutions u^ε to (2.5). One aims to study the existence of a limit u^ε as $\varepsilon \to 0$, and the properties of this limit function when it exists.

One of the most general notions in homogenization theory is that of H-convergence. For all $0 < m \leq M$ we introduce the space of (bounded, invertible) matrices

$$\mathscr{M}_{m,M} = \left\{ A \in \mathbb{R}^{d\times d} \,|\, \forall\, \xi \in \mathbb{R}^d : \xi \cdot A\xi \geq m\|\xi\|^2,\, \xi \cdot A^{-1}\xi \geq M^{-1}\|\xi\|^2 \right\}.$$

A sequence of matrices A^ε in $L^\infty(\Omega, \mathscr{M}_{m,M})$ is said to H-converge to $A^\star \in L^\infty(\Omega, \mathscr{M}_{m,M})$ (called homogenized limit, or H-limit) if, for any $f \in H^{-1}(\Omega)$ the sequence of solutions u^ε to (2.5) satisfies

$$\begin{cases} u^\varepsilon \rightharpoonup u^\star \text{ weakly in } H^1_0(\Omega), \\ A^\varepsilon \nabla u^\varepsilon \rightharpoonup A^\star \nabla u^\star \text{ weakly in } L^2(\Omega)^d \text{ as } \varepsilon \to 0, \end{cases}$$

where $u^\star \in H^1_0(\Omega)$ is the solution to

$$\int_\Omega \nabla v \cdot A^\star \nabla u^\star = \langle f, v \rangle_{H^{-1}(\Omega), H^1_0(\Omega)} \quad \text{for all } v \in H^1_0(\Omega), \tag{2.12}$$

or equivalently, $u^\star$ solves to the so-called homogenized equation $-\operatorname{div}(A^\star \nabla u^\star) = f$. An important (compactness) result is that any sequence of matrices in $L^\infty(\Omega, \mathscr{M}_{m,M})$ has an H-converging subsequence. For this result and those below and their and proofs, we refer to [7, Chapter 1]. It also contains an account of other ideas in homogenization (the theory of Γ-convergence, the probabilistic theory of homogenization, physical approaches to averaging) with many references. Among the vast literature regarding H-convergence, let us mention [124, 134, 133, 33]. The theory of homogenization also goes beyond the study of the pure diffusion equation. In this regard one may consult [33, Chapter 6], for instance.

For our purposes, let us rephrase the above as follows: if we suppose that we are along a subsequence such that A^ε H-converges towards $A^\star$, the function u^ε is, when ε is small enough, close to $u^\star$, which is characterized by $A^\star$. The matrix $A^\star$ does not depend on the microscopic parameter ε. If $A^\star$ varies slowly (we will see below that $A^\star$ is constant when A^ε is the rescaling of a fixed periodic matrix), the FEM can provide us with an approximation of $u^\star$, and thus of u^ε. All these approximate ideas can be made precise in particular situations for a more rigorous convergence analysis. We recall the one-dimensional periodic setting considered above in which we found $A^\star$ to be the harmonic average (2.11), which is in fact constant throughout Ω.

The homogenized matrix $A^\star$ can be characterized as follows. For $\alpha = 1, \dots, d$, let e_α be the α-th canonical basis vector of $\mathbb{R}^d$ and x^α the α-th coordinate function. Then, denoting the limit in the sense of distributions by $\mathscr{D}'(\Omega)\text{-}\lim$,

$$A^\star e_\alpha = \mathscr{D}'(\Omega)\text{-}\lim_{\varepsilon \to 0} A^\varepsilon \nabla v^\varepsilon_\alpha,$$

where $(v^\varepsilon_\alpha)_\varepsilon$ is a sequence in $H^1(\Omega)$ of so-called oscillating test functions, satisfying

$$\begin{cases} v^\varepsilon_\alpha \rightharpoonup x_\alpha \text{ weakly in } H^1(\Omega), \\ -\operatorname{div}(A^\varepsilon \nabla v^\varepsilon_\alpha) \to -\operatorname{div}(A^\star e_\alpha) \text{ strongly in } H^{-1}(\Omega) \text{ as } \varepsilon \to 0. \end{cases} \tag{2.13}$$

We note that this characterization is not explicit, since the sequence of oscillating test functions depends on $A^\star$. Moreover, the oscillating test functions are not defined uniquely, since an arbitrary sequence of functions that converges to 0 strongly in $H^1_0(\Omega)$ can be added to any such sequence. This characterization does confirm, however, that the arithmetic average (2.9) encoded in the standard $\mathbb{P}_1$ FEM is much too naive a notion of averaging to treat the microscale ε properly.

The above characterization can be made explicit in some cases when the matrices of

the sequence $(A^\varepsilon)_\varepsilon$ have a specific structure. Let us consider the periodic case, where $A^\varepsilon = A^{\mathsf{per}}(\cdot/\varepsilon)$ for a Q-periodic function A^{per}. Here Q denotes the unit cube of $\mathbb{R}^d$. A detailed account of homogenization theory in this setting can be found in [28]. The oscillating test functions can now be defined explicitly as

$$v_\alpha^\varepsilon = x_\alpha + \varepsilon\, w_\alpha^{\mathsf{per}}(\cdot/\varepsilon), \quad \alpha = 1, \dots, d, \tag{2.14}$$

where the corrector function w_α^{per} is defined as the periodic solution in $H^1(Q)$ to

$$-\operatorname{div}(A^{\mathsf{per}}(\nabla w_\alpha^{\mathsf{per}} + e_\alpha)) = 0, \tag{2.15}$$

which is unique up to an irrelevant additive constant. The homogenized limit of A^ε is then given by

$$A^\star e_\alpha = \int_Q A^{\mathsf{per}}(\nabla w_\alpha^{\mathsf{per}} + e_\alpha), \quad 1 \le \alpha \le d, \tag{2.16}$$

and it is constant. Upon introducing $A^{\mathsf{per,av}} = \displaystyle\int_Q A^{\mathsf{per}}$, we can rewrite this expression as

$$A^\star e_\alpha = A^{\mathsf{per,av}} e_\alpha + \int_Q A^{\mathsf{per}}(\nabla w_\alpha^{\mathsf{per}}), \quad 1 \le \alpha \le d, \tag{2.17}$$

that is, the homogenized matrix $A^\star$ equals the arithmetic average of A^{per}, which is correctly approximated by (2.10) seen in the $\mathbb{P}_1$ FEM, plus a *correction* term that depends, through the corrector functions w_α^{per}, on A^{per} in a non-linear way. Note that the expression for $A^\star$ is no longer the harmonic mean of A^{per} as was the case in the one-dimensional setting. Let us also mention that the corrector function can be used to build an approximation of u^ε in the H^1-norm (as opposed to the weak convergence in (2.13) obtained for $u^\star$). This is made precise in Section 4.7.

In summary, the notion of averaging encoded in a standard FEM should be corrected when the underlying mesh does not resolve the microstructure. In view of the intricate, non-linear dependence between A^ε and $A^\star$, it seems impossible to propose a *generic* FEM that incorporates the suitable correction for any microstructure. In the periodic case, however, the following *problem-dependent* computational strategy can be deduced from the above for a known microstructure A^{per}:

1. For $\alpha = 1, \dots, d$, we use an FEM on Q to solve (2.15) for w_α^{per}.
2. We compute $A^\star$ from (2.16).
3. Since $A^\star$ is constant, the $\mathbb{P}_1$ FEM can now be used to compute an approximation of $u^\star$ from (2.12) on a coarse mesh.
4. An approximation of u^ε can now be constructed from $u^\star$ and a linear combination of the corrector functions $w_1^{\mathsf{per}}, \dots, w_d^{\mathsf{per}}$.

This procedure, and its approximation qualities, are extensively discussed in [33, Sections 5.1.2-5.1.3]. It results in a tremendous computational gain, since none of the finite element approximations above has to resolve the microscale ε. Hence, a microscopically fine mesh for the entire domain Ω is never used. However, to put this method into practice, it is essential that A^ε be the rescaling of a fixed, known, periodic matrix A^{per}.

Explicit descriptions of the corrector functions and the homogenized matrix are also available for some perturbations of the periodic setting. We refer to [33, Chapter 4]

and [83]. In [33, Section 5.1.4], the implications of such perturbations for the above approach are detailed. We summarize two factors that complicate the computational procedure outlined above for the periodic setting. First, the corrector equation (2.15) is, in general, not posed on a bounded domain, but on the entire space $\mathbb{R}^d$. Second, the homogenized matrix may no longer be given by an average as in (2.16), but as the asymptotic limit of the average over large volumes. The above procedure may be adapted to such settings, and it may still be advantageous to put the approach into practice if the problem (2.5) has to be solved many times for different right-hand sides. Indeed, the homogenized matrix $A^\star$ only has to be computed once, and once it has been computed, the resolution of the homogenized equation (2.12) is extremely fast compared to the full resolution of (2.5) on a fine mesh.

Even beyond these complications, it may be the case that no theoretical framework is known for the specific microstructure at hand, and that no explicit description of the corrector functions w_α^ε and the homogenized matrix $A^\star$ are available. One might even wonder if, given a single real-life microstructure A^ε, it can be embedded in a sequence of diffusion coefficients so that the limit of u^ε as $\varepsilon \to 0$ can be studied. This is often far from trivial, for instance if the microstructure is obtained from measurements on the system under consideration.

Different numerical techniques are thus required to treat more general problems than those accessible through homogenization theory. The theory that is briefly outlined in this section, albeit well-developed theoretically, can only serve as a guideline for the design of such techniques. Nevertheless, we would like to mention that homogenization theory still plays a key role in the convergence theory of many such multiscale computational methods.

2.2.2. Multiscale computational methods; numerical homogenization. Here we give a general overview of various *multiscale computational approaches* of finite element type that aim to include the microscopic information of the model, while solving global problems such as (2.6) only on a low-dimensional space such as V_H. The numerical methods that are studied in the rest of the thesis fall under this category of computational approaches. Contrary to the homogenization theory recalled above, these do not rely on an asymptotic study of the microstructure in order to formulate a problem on a coarse space. This implies that multiscale approaches generally consist of two steps. A first *offline stage* during which the microstructure is processed in some appropriate way (see below for examples). Since this stage is to be performed numerically, the use of a fine mesh is unavoidable. Typically, a 'divide and conquer' strategy is adopted: the global model is divided into several smaller subdomains that are processed separately. This way, the offline stage does not lead to numerically intractable problems such as the resolution of the original model on a fine mesh. It is often amenable to parallel computing, allowing to increase the computational efficiency of the procedure. In a second step, the *online stage*, the results of all local computations are combined in order to obtain a reasonably accurate approximation of u^ε on a coarse mesh at an affordable computational cost.

Since the microstructure is processed numerically rather than analytically to replace the averaged coefficient from (2.10) by a more appropriate 'effective model', in the spirit of the homogenized coefficient in (2.12), this field of scientific computing is also called *numerical homogenization*. See [72, 15, 12] for more detailed reviews of the field.

Obvious ways to include the fine-scale information of A^ε in the approximation space V_H may be through the computation of eigenfunctions of the associated differential opera-

tor, or by the computation (on a fine mesh) of the inverse image of a small number of selected simple functions. Such functions are in general *global*. Hence, one may not be able to actually compute them. There is also a more fundamental problem. Recall property (iii) on page 13 that underlies the efficiency of the FEM: its basis functions are *local*. Therefore, and we quote [12], "The true art in numerical homogenization is to identify a localized basis of the generalized finite element space to preserve the favourable sparsity and complexity properties of standard FEMs without affecting the universal accuracy."

We emphasize that the goal of numerical homogenization is not to obtain the same accuracy as would be obtained if one were capable of solving the large-scale linear system associated to an FEM resolving the entire microstructure. If this is what one wishes to achieve, iterative methods such as domain decomposition methods and the multigrid method could be considered. These are general-purpose methods to accelerate the resolution of generic FEMs (and other discretization techniques). Such methods iterate between the resolution of local and (coarse) global problems until a convergence criterion is met. Multiscale methods are one-shot, bottom-up methods, and our goal is to design a single coarse problem that provides sufficient accuracy under this constraint, specifically adapted to the PDE and its coefficients at hand. On the other hand, ideas of the multiscale methods we discuss below can also be used to build efficient preconditioners for iterative methods applied to multiscale problems. We refer to [1, 84, 36]. An introduction to iterative methods that does right to the field is beyond the scope of this text. We mention the introductory texts [42, 63].

Numerical homogenization techniques are mainly of interest under two conditions:

1. A coarse approximation of the solution u^ε is sufficient, so a microscopic discretization is not required by the problem specifications.
2. The same microstructure has to be processed many times. One can think of non-stationary problems, inverse problems, uncertainty quantification, risk assessment, design loops, control and optimization problems, etc.

Let us detail the second point. We have explained so far that the FEM is a *generic* method, but that it suffers from a great loss of accuracy when applied to multiscale problems with a coarse mesh. However, if the problem is to be solved only once, it is best to resort to available standard techniques to solve the problem on a fine mesh whenever possible. If, on the other hand, a problem with the same microstructure is to be solved multiple times, for instance because the right-hand side f in (2.5) changes, or different boundary conditions are imposed, the computational cost accumulates and becomes so large that one might consider resorting to more specialized techniques. Numerical homogenization approaches design a coarse, *problem-dependent* model for the online stage which is cheap to solve. The expensive part of the strategy, the offline stage, is only executed once. The computational gain with respect to a classical FEM on a coarse mesh thus increases each time the problem is solved again. By giving up the generality of classical FEMs, we improve the performance of the method for the problem at hand. We consider the impact of this choice on the implementation of the method in Section 2.3.1 and more elaborately in Part I of the thesis.

We now mention a few concrete examples of numerical homogenization techniques. The *Heterogeneous Multiscale Method* (HMM) was introduced in [67]. It was classified in [12] as a homogenization-based method. The method supposes that an effective model for the PDE under consideration exists and that its form is known. The effective coefficients of the model are then estimated in the quadrature points of an FEM on a coarse

mesh. The estimation is carried out by the resolution of a subscale problem inspired by homogenization theory (such as the corrector problem (2.15)) in small cells around each quadrature point. These cells must be large enough to be representative of the local microstructure. The computation of these effective coefficients constitutes the offline stage of the method. The online stage then consists in solving a standard FEM approximation of the effective model on the aforementioned coarse mesh. We refer to [5] for a detailed review of the method, its analysis and the many applications of the HMM framework.

Another class of multiscale methods identified in [12] is that of variational approaches. Contrary to the HMM, all these approaches aim to correct the Galerkin approximation (2.6) through the use of all the scales that cannot be resolved by the coarse mesh, and not just in small representative elements around a small number of points throughout the domain. We introduce the ideas behind the *Multiscale Finite Element Method* (MsFEM) and the *Localized Orthogonal Decomposition* (LOD).

The MsFEM [98] performs a Galerkin approximation of (2.5) on a low-dimensional, problem-dependent space. This idea originally dates back to [20, 18]. The basis functions of this space are computed (numerically) during the offline stage. They are defined as the solution to a PDE like (2.15). This PDE has to be localized (since we want to keep the local character of standard finite element functions) by a choice of boundary conditions on each mesh element. This has led to the definition of numerous MsFEM variants that are revisited in more detail in the next section. The online stage consists in performing a Galerkin approximation on the pre-computed space.

The convergence analysis of the MsFEM is carried out under periodicity assumptions and relies on available results from homogenization theory, exploiting the fact that the problem-dependent basis functions solve a PDE similar to the corrector equation (2.15). See, for instance, [70, 99, 9, 112]. This is also the case for the HMM. It is important to note that such assumptions are not required to put the approach into practice on a specific problem.

The MsFEM can also be related to the general framework of the Variational Multiscale Method (VMM) [101] based on local Green's functions of the differential operator inside each mesh element, and the equivalent concept of residual-free bubbles [38]; this relationship is given in (2.22) below. Nonetheless, the presentation of the MsFEM is classically closer to the interpretation based on homogenization theory. The contributions of this thesis reveal that the link with the VMM can be useful for both the implementation of the method and the understanding of some of its stabilizing properties. See, in particular, Equation (2.22) and Contributions 1, 3 and 9 in Section 2.3 below.

The more general VMM framework of [102] introduces global corrector Green's functions, and defines problem-dependent basis functions that are globally supported. Therefore, these ideal basis functions (ideal from an approximation point of view) are not suitable for the use in an FEM. When the coarse space is defined as the image of an appropriate projection operator, it was observed that the basis functions decay exponentially. This was first proved for elliptic problems in [120]. A modified localization strategy for these functions was used to introduce in [93] what is now known as the LOD. Yet another variant with basis functions that decay even faster was recently proposed in [90]. The offline and online stages of the LOD are thus similar in nature to those of the MsFEM and consist in the computation of a low-dimensional problem-dependent discretization space on which a subsequent Galerkin approximation is performed. An additional parameter in the definition of the LOD is the width of the patches to which the basis functions are localized. These have to be taken larger than the support of the classical $\mathbb{P}_1$ Lagrange

basis functions, unlike the MsFEM basis functions, which have exactly the same support as the $\mathbb{P}_1$ basis functions.

The exponential decay of the ideal basis functions and the convergence of the LOD can be shown without any assumptions on the microstructure. A general framework for the LOD is described in [12]. We also refer the reader to the monograph [121].

One may draw parallels between the techniques described above and the field of model order reduction for parameterized PDEs [55, 27], and especially localized model order reduction [44]. Indeed, the problem-dependent spaces above can be seen as reduced-order subspaces of the finite element space that fully resolves the microstructure, and both methods rely on (local) solves of the model to construct a suitable low-dimensional space that approximates the solution of the global problem. We do not, however, consider a parameterized family of PDEs, but a single fixed microstructure that is encoded in a dedicated approximation space. A more detailed review of model order reduction is beyond the scope of this thesis and we refer to the above references.

Finally, let us mention one particular topic that we consider particularly important for multiscale methods. In Section 2.3.1, we discuss the problem of intrusiveness, which is central to Part I of the thesis. It considers the question of how to adapt existing FEM software to a multiscale approach. In the next section, we review the MsFEM in more detail, which is the approach on which this thesis focuses. Some more details on the HMM and the LOD, with a focus on the related intrusiveness, can be found in Section 6.4.

2.2.3. The multiscale finite element method. The MsFEM was described above as an FEM that performs a Galerkin approximation of (2.5) on a problem-dependent space. The original space proposed in [98] is defined as follows. Consider a (coarse) mesh $\mathscr{T}_H$ and the $\mathbb{P}_1$ Lagrange space $V_H^{\mathbb{P}_1}$ associated to this mesh. We denote the interior vertices of the mesh (those that do not lie on $\partial\Omega$) by $x_1, \dots, x_N$. Let $\phi_1^{\mathbb{P}_1}, \dots, \phi_N^{\mathbb{P}_1}$ be the standard basis of V_H defined by the property $\phi_i^{\mathbb{P}_1}(x_j) = \delta_{i,j}$ for all $1 \leq i, j \leq N$. See Figure 2.1 for an illustration in dimension 1. Then for all $1 \leq i \leq N$, we define a *multiscale basis function* ϕ_i^ε as the unique solution to

$$\forall\, K \in \mathscr{T}_H, \quad \begin{cases} -\operatorname{div}(A^\varepsilon \nabla \phi_i^\varepsilon) = 0 & \text{in } K, \\ \phi_i^\varepsilon = \phi_i^{\mathbb{P}_1} & \text{on } \partial K. \end{cases} \tag{2.18}$$

We show an example of such multiscale basis functions in Figure 2.4 in dimension 1. We give an example of a $\mathbb{P}_1$ basis function and a multiscale basis function in dimension 2 in Figure 2.5.

For any interface of the mesh, the local boundary conditions for a multiscale basis function ϕ_i^ε are the same on both sides of the interface. Therefore, each basis function ϕ_i^ε is continuous and it belongs to $H_0^1(\Omega)$. Consequently, the multiscale space

$$V_H^\varepsilon = \operatorname{span}\{\phi_i^\varepsilon \mid 1 \leq i \leq N\}$$

is a subspace of $H_0^1(\Omega)$. The Galerkin projection

$$\text{Find } u_H^\varepsilon \in V_H^\varepsilon \text{ such that} \quad \int_\Omega \nabla v_H^\varepsilon \cdot A^\varepsilon \nabla u_H^\varepsilon = \int_\Omega f\, v_H^\varepsilon \quad \text{for all } v_H^\varepsilon \in V_H^\varepsilon \tag{2.19}$$

thus has a unique solution, like the continuous problem (2.5). This is called the MsFEM approximation of u^ε.

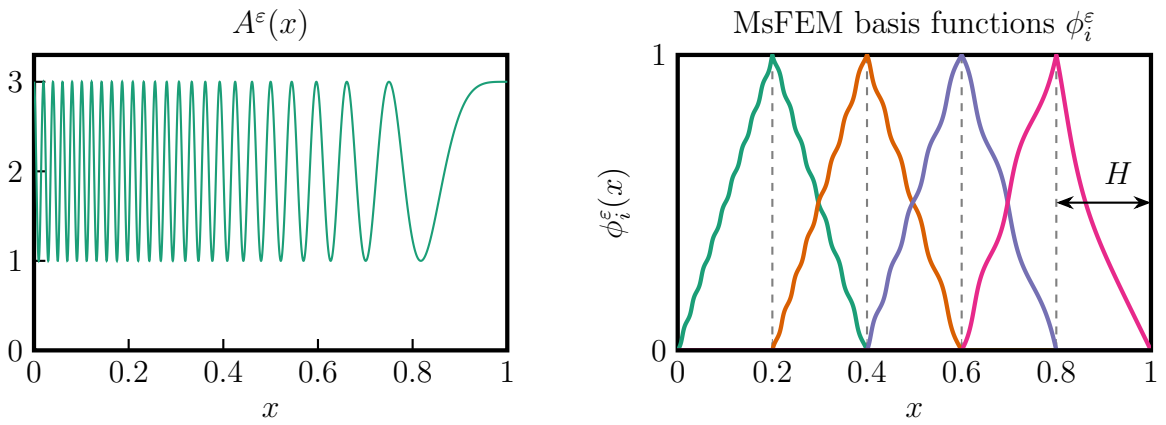

Figure 2.4: *Example of a highly oscillatory coefficient A^ε and the associated multiscale basis functions in 1D.*

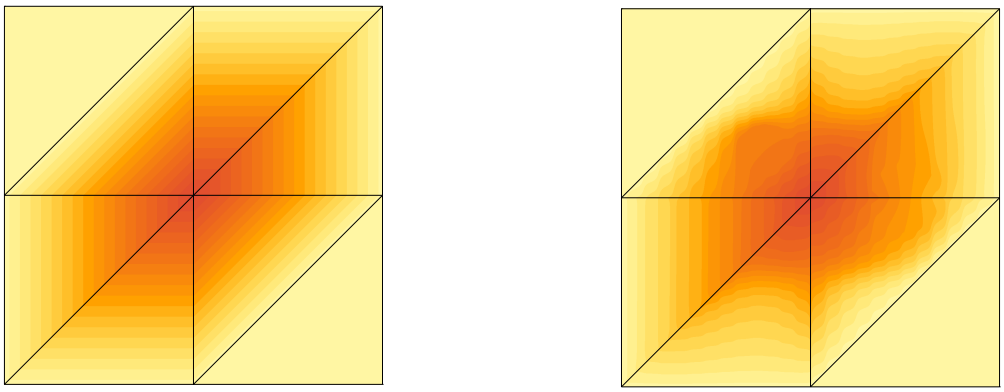

(a) $\phi_i^{\mathbb{P}_1}$ (b) ϕ_i^ε

Figure 2.5: *Example of (a) a $\mathbb{P}_1$ basis function and (b) a multiscale basis function associated to the same vertex in 2D.*

In practice, no analytical expression for the basis functions ϕ_i^ε is known beyond the one-dimensional situation. They have to be approximated numerically. To this end, a fine mesh that resolves the microstructure of A^ε is used for each $K \in \mathscr{T}_H$, and (2.18) can be approximated by, e.g., a standard $\mathbb{P}_1$ FEM on this mesh. Since the problems on all mesh elements are independent, these computations can moreover be executed in parallel. This is the offline stage of the MsFEM. The resolution of (2.19), once the basis multiscale basis functions have been computed, constitutes the online stage. This comprises the construction of the linear system associated to (2.19) and its resolution. Note that the matrix of this linear system only depends on the multiscale basis functions, and not on the right-hand side, and can therefore also be computed once and for all during the offline stage of the MsFEM. In what follows, we omit the explicit reference to the numerical approximations of the ϕ_i^ε that are used in practice for ease of exposition. The statements below can be generalized to the situation where this fine-scale discretization is taken into account. The associated additional numerical error can be supposed small since the fine mesh resolves the microstrucure. This error can be studied explicitly (as is done in [9], for instance), but will be neglected in this thesis, as is also common in the MsFEM literature.

The MsFEM in dimension 1. Let us now consider the performance of the MsFEM. We first give some elements applicable to the one-dimensional situation. It is easy to show that the MsFEM is exact at the vertices of the mesh in dimension 1, i.e., $u_H^\varepsilon(x_i) = u^\varepsilon(x_i)$ for all vertices x_i of the mesh, regardless of the mesh size used. This is a well-known property of FEMs in dimension 1 with test functions that solve locally the adjoint problem to the PDE under consideration. Since the problem (2.5) is self-adjoint (in dimension 1, A^ε is a scalar, so we do not need to assume that it is symmetric here), the MsFEM satisfies the exactness property. We observe a radical difference with respect to the situation of the classical $\mathbb{P}_1$ FEM, for which we have seen that, with the same number of degrees of freedom, it fails to even find an approximate value of u^ε at the vertices of the mesh; see Figure 2.2.

A rate of convergence can also be established by relatively elementary arguments. If we consider an interval Ω divided into a number of subintervals all of equal length H, it is shown in [33, Section 5.2.1.2] that

$$\|u^\varepsilon - u_H^\varepsilon\|_{H^1(\Omega)} \leq CH\|f\|_{L^2(\Omega)}, \tag{2.20}$$

whenever $m \leq a^\varepsilon(x) \leq M$ for almost all $x \in \Omega$ and with a constant C that does not depend on ε. (The estimate from [33, Section 5.2.1.2] only has the L^2-norm of $(u^\varepsilon - u_H^\varepsilon)'$ on the left-hand side; by the Poincaré inequality on $H_0^1(\Omega)$, the two norms are equivalent.) The key point here is that the right-hand side f is independent of the microstructure, in sharp contrast to the error bound in (2.7). The MsFEM estimate (2.20) is thus meaningful in all regimes of H and ε, while we have seen that the bound (2.7) for the classical $\mathbb{P}_1$ FEM may be large when H/ε is large.

The above properties provide a solid theoretical motivation, at least in dimension 1, for the introduction of the MsFEM (and for the LOD, which coincides with the MsFEM in dimension 1). Numerical results confirm the superior quality of the MsFEM. In Figure 2.6 we show the relative errors $\|u_h^\varepsilon - u_H^\varepsilon\|_{L^2(\Omega)}/\|u_h^\varepsilon\|_{L^2(\Omega)}$ and $\|(u_h^\varepsilon - u_H^\varepsilon)'\|_{L^2(\Omega)}/\|(u_h^\varepsilon)'\|_{L^2(\Omega)}$ with respect to a numerically computed reference solution u_h^ε as the mesh size H varies. The diffusion coefficient for these computations is $A^\varepsilon(x) = 2 + \cos\left(\dfrac{2\pi x}{\varepsilon}\right)$ and the right-hand side is $f(x) = x^3$. We used $\varepsilon = 2^{-9} \approx 0.002$ and computed the basis functions of the MsFEM on a uniform fine mesh of size $h = 2^{-14} = \varepsilon/32$. The reference solution is computed by a $\mathbb{P}_1$ FEM on the same mesh. The $\mathbb{P}_1$ FEM error displays a plateau when $H > \varepsilon$. This can be explained by our findings in (2.9). Even if we refine the mesh size, the FEM continues to compute an approximation to a PDE with an incorrect effective diffusion coefficient (the arithmetic average of A^ε, while the harmonic average corresponds to the homogenized limit and would yield a much better approximation). The error of the MsFEM, on the other hand, decreases with the precise convergence rate predicted above, and is in the asymptotic regime of convergence even when $H \gg \varepsilon$.

It is also noteworthy that the error analysis in 1D is carried out *without any assumptions on the structure of* A^ε except that it is bounded from above and from below. In particular, no arguments of homogenization theory are necessary to establish the rate of convergence. The critical point in the analysis is that the error between u^ε and its nodal interpolant in the MsFEM space V_H^ε vanishes at the nodes and is therefore *completely localized*. It can thus be estimated by integrations by parts and Poincaré inequalities. This argument is intrinsically restricted to the one-dimensional situation.

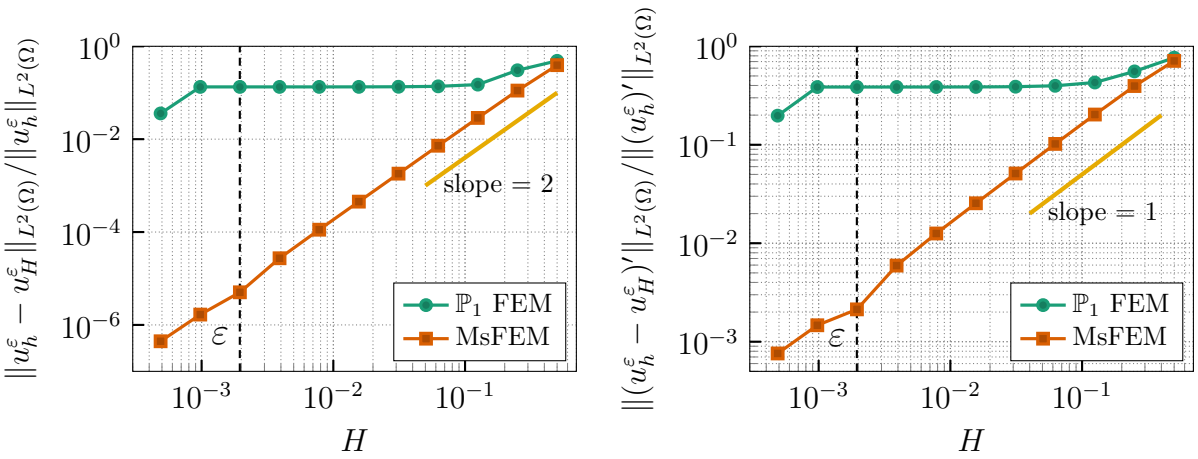

Figure 2.6: *Errors of the $\mathbb{P}_1$ FEM and the MsFEM in the L^2-norm and the semi-H^1-norm for a highly oscillatory diffusion coefficient in 1D.*

The MsFEM in higher dimension. The automatic localization of the error, as we just found in dimension 1, does not carry over to the higher-dimensional situation. As we quoted from [12] before, localization is the essence of the design of a numerical homogenization technique. It is only in the higher-dimensional case that different localization choices come into play.

For the MsFEM methodology, the localization is maximal, since the problems (2.18) are entirely localized to a single mesh element K, and the MsFEM basis functions enjoy the same favourable localization properties as those of the $\mathbb{P}_1$ FEM. This comes at the cost of placing rather *arbitrary* boundary conditions on ∂K for each local problem. Optimal boundary conditions would reflect the oscillatory behaviour of u^ε over the mesh interfaces. On the contrary, the piecewise affine boundary conditions used in (2.18) discard all oscillations around the mesh interfaces. The difference with respect to the one-dimensional case is that, in the latter, the boundary conditions are set at the endpoints of an interval, hence the space of possible boundary conditions for u^ε only has dimension 2. As soon as we are in a higher-dimensional case, the dimension of possible boundary conditions at the boundary of a mesh element is infinite.

The design of improved multiscale finite element methods since its original introduction can, at least for pure diffusion problems, be characterized as the quest for improved boundary conditions for the multiscale basis functions. The choice of affine conditions in (2.18) was already realized to be suboptimal at the time of their introduction in [98] and in the same work, an oversampling variant was proposed. In this case, the local problems (2.18) are posed on a simplex larger than K, again with affine boundary conditions. The restriction to K of the solutions to these problems, which are now oscillatory on ∂K, are used to construct the multiscale basis functions. This MsFEM variant is described in detail in Chapter 5 of the thesis. Another approach is the MsFEM with Crouzeix-Raviart type boundary conditions proposed in [112]. It does not prescribe Dirichlet boundary conditions in the local problems, but only sets the average over each interface (and a constant flux, see Example 5.13). The resulting basis functions are only weakly continuous in the sense that the average jump over each interface is zero. This MsFEM approach was found to be particularly useful when combined with bubble functions and applied to the case of perforated domains [113]. Note that, in order to introduce more flexible local boundary conditions, both of the above MsFEM approaches use non-conforming

approximation spaces (i.e., the basis functions described above do not belong to $H_0^1(\Omega)$ due to jumps over element interfaces). A different path was followed in [9, 94], where higher-order variants of the MsFEM are proposed. (Indeed, note that the MsFEM with basis functions as in (2.18) reduces to the standard $\mathbb{P}_1$ FEM if A^ε is constant. Hence, it can be considered an MsFEM of order 1.) We also mention the work [53] that proposes a high-order method for general polytopal meshes.

Let us now explain the impact of the localization of the MsFEM basis functions on the convergence analysis of the MsFEM in higher dimension. In contrast to the one-dimensional case, the convergence analysis can no longer be carried out without any additional assumptions on the structure of A^ε. All analyses of the MsFEM and its variations that we are aware of (see [98, 99, 70, 100, 9, 112, 113, 94, 116, 114, 53]) assume that $A^\varepsilon = A^{\mathsf{per}}(\cdot/\varepsilon)$ is the rescaling of a periodic matrix A^{per}. In that case, explicit results known from homogenization theory allow to obtain a precise rate of convergence of the error in terms of H and ε around the interfaces of the mesh, where boundary layers are formed due to the choice of artificial boundary conditions in the local problems (2.18). We emphasize that the assumption of periodicity is not needed for the actual application of the MsFEM. The typical error estimate obtained for an MsFEM (of order 1 on the coarse mesh) is of the form

$$\|u^\varepsilon - u_H^\varepsilon\|_{H^1(\Omega)} \leq CH\|u^\star\|_{H^2(\Omega)} + C\left(\sqrt{\varepsilon} + H + \sqrt{\frac{\varepsilon}{H}}\right)\|\nabla u^\star\|_{W^{1,\infty}(\Omega)}, \tag{2.21}$$

where $u^\star$ is the homogenized limit of u^ε (see (2.12)). It is assumed that A^{per} and $u^\star$ are sufficiently regular. We extensively discuss regularity in Section 2.3.3, where we introduce a new analysis of MsFEMs that does not require such additional regularity hypotheses.

In the regime where H is larger than ε but not that much larger, the error bound (2.21) *grows* when H decreases. This is known as the *resonance effect* in the literature, interrupting convergence of the MsFEM when the mesh size H is close to the typical size of the microscopic variations of A^ε. Convergence is then only resumed when $H < \varepsilon$, when the microstructure is resolved by the mesh and the MsFEM is close to the $\mathbb{P}_1$ FEM.

The oversampling variant of the MsFEM studied in [70] allows to replace the factor $\sqrt{\varepsilon/H}$ by ε/H, and the Petrov-Galerkin variant (with $\mathbb{P}_1$ Lagrange test functions) of [100] by just ε, by assuming a large (possibly prohibitively large) oversampling ratio. The higher-order methods [9, 94, 53] replace the factor H by H^k if the approximation space is sufficiently large and the homogenized solution $u^\star$ belongs to $H^{k+1}(\Omega)$.

The resonance effect is not only an artefact of the numerical analysis, but also appears in practice. In Figure 2.7 we show the errors as the mesh size H varies for the $\mathbb{P}_1$ FEM, the MsFEM using the basis functions (2.18) (referred to as MsFEM-lin here, because of the affine boundary conditions) and the MsFEM variant with oversampling from [98] using a so-called homothety ratio of 3 (MsFEM-OS(3); see Definition 5.7 for details). The computations are performed on the domain Ω and the coarse mesh is a uniform $1/H \times 1/H$ triangulation of Ω. We consider the diffusion coefficient

$$A^{\varepsilon,\mathsf{per}}(x) = \nu^\varepsilon(x)\,\mathrm{Id}, \quad \nu^\varepsilon(x_1, x_2) = 1 + 100\,\cos^2(\pi\, x_1/\varepsilon)\sin^2(\pi\, x_2/\varepsilon),$$

with $\varepsilon = \pi/150 \approx 0.02$ and the right-hand side $f(x_1, x_2) = \sin(x_1)\sin(x_2)$. The MsFEM approximations are compared to a reference solution u_h^ε computed by a $\mathbb{P}_1$ Lagrange FEM on a uniform 1024×1024 triangulation of Ω. The same fine mesh is used for the computation of the MsFEM basis functions. All computations are executed with

FreeFEM++ [91] and the associated scripts are available at [29].

Figure 2.7 shows that the $\mathbb{P}_1$ FEM error is again stuck at a high error plateau in the regime $H > \varepsilon$. The MsFEMs perform significantly better, even though the MsFEM-lin suffers from the resonance error for rather large values of H and its performance is comparable to the $\mathbb{P}_1$ FEM when $H \approx \varepsilon$. The oversampling strategy clearly shows an improvement of the error and the resonance effect appears for smaller values of H than for the MsFEM-lin.

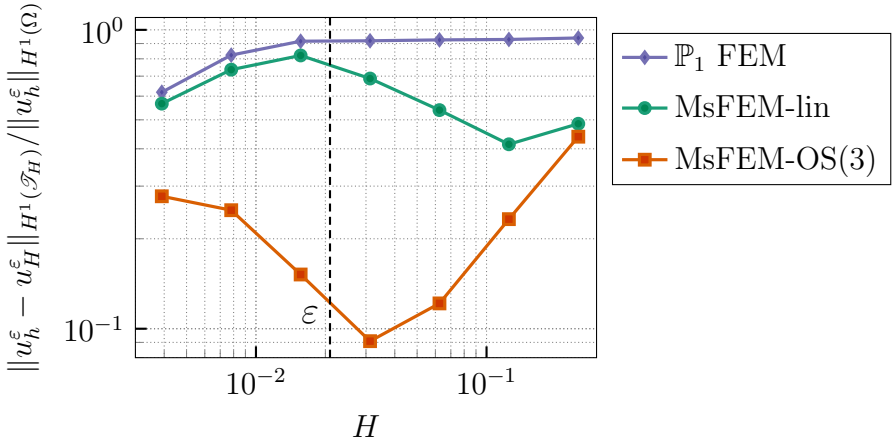

Figure 2.7: *Comparison of the errors of three different FEMs applied to a highly oscillatory diffusion coefficient in 2D as the mesh size H varies.*

Other improvements of the MsFEM have been proposed that rely on the resolution of local *spectral* problems. Different ideas to use spectral problems in the construction of a finite element approach were proposed and analysed in [19, 96, 95]. Local spectral problems to enrich MsFEM type methods were introduced in [68, 97]. These enrichment strategies consider fine-scale finite element spaces of harmonic functions with non-zero boundary conditions on each coarse mesh element. Spectral problems are solved in these spaces to select relevant modes for the enrichment of an MsFEM space like those described above. However, these spectral problems are posed in high-dimensional spaces that can be thought of as parameterized by all possible boundary conditions on the fine mesh. In order to identify the relevant modes more efficiently, ideas from localized model order reduction can be used, in particular, random techniques to reduce the dimension of the spectral problems. We refer to [89, 45], and to [47, 62] for examples of randomized techniques for MsFEM type methods. They were also used for efficient sampling of high-dimensional spaces in the LOD proposed in [90]. A different type of enrichment of classical MsFEM spaces, which is polynomial-based rather than spectral-based, can be found in [117] for the MsFEM-lin, and in [74] for the MsFEM-CR applied to Stokes flows. For the work of this thesis, however, we study the use and design of the lowest-dimensional MsFEM spaces without any of the above-mentioned enrichment strategies. The topics of this thesis (intrusivenss in Part I, instabilities due to advective effects in Part II) are relevant for all MsFEM variants, and it seems necessary to draw conclusions for the most basic MsFEM variants first.

Remark 2.1. The localization strategy for the LOD is quite different from the MsFEM. The LOD first proposes an exact decomposition of the solution on a discrete space of globally supported multiscale basis functions and a space of unresolved features, which

corresponds to the kernel of a quasi-interpolation operator. It then approximates the multiscale basis functions by localization on patches of mesh elements around the original support of the $\mathbb{P}_1$ basis function. The error analysis of this procedure, which can be carried out without any periodicity assumptions and assumptions on the regularity of the coefficient A^ε, shows that the common convergence rates of the FEM with respect to H are preserved if the thickness δ of the patches satisfies $\delta \geq CH \log(H^{-1})$ [93]. In this thesis we focus on methods of MsFEM type in order to keep the same sparsity properties as those of classical FEMs.

2.3. Contributions of the thesis

Here we give a detailed summary of the research contributions of Parts I, II and III of the thesis. We also mention some directions for future research.

2.3.1. Non-intrusive implementation of the MsFEM. We have emphasized above that the MsFEM replaces the classical $\mathbb{P}_1$ FEM basis functions by problem-dependent basis functions with the same support to maintain favourable sparsity properties of the FEM while making the method more efficient for a given microstructure. We did not discuss the practical impact of replacing *generic, polynomial* basis functions by *multiscale* basis functions on the implementation of the method. Let us do so here. We focus on the construction of the linear system that corresponds to the discrete problem (2.6) or (2.19). This requires integrations of the basis functions of the discrete space. For traditional FEMs with polynomial basis functions, this can be automated for a large variety of problems because standard quadrature formulas can easily be evaluated on each mesh element. The large generality of FEM software is at the core of its wide success in science but also in industry. Changing the basis functions means that all such highly efficient routines in generic FEM software should be adapted for each individual problem. The MsFEM is thus intrusive. For more details, see Section 4.3.

The implementation of an MsFEM is rightfully considered relatively easy in comparison to the full implementation from scratch of a traditional FEM [69, 125]. Nevertheless, the intrusive character of the MsFEM hinders the use of the method in industrial contexts, because there is a huge reluctance to modify a legacy code that has been developed over the time of several years, if this is even possible at all. It thus seems essential that an existing, optimized FEM code can be used with as little modifications as possible for the MsFEM to be adopted when such a traditional FEM legacy code is *already in use*. To the best of our knowledge, the question of how to make MsFEM approaches less intrusive had not been addressed in the literature before the work of this thesis.

Part I of this thesis proposes a minor modification of the MsFEM, commonly presented as (2.19), that allows for an MsFEM implementation using existing FEM software without changing any of its internal routines. The notion of 'minor' modifications here will be specified in Contributions 4, 5 and 6 below. We outline the new implementation here.

The intrusiveness of the MsFEM is due to the following fact: the microstructure is preprocessed through the computation of specialized basis functions in (2.18), thereby coupling the microstructure explicitly to the global numerical model. We observe in Equation (4.10) that, for each $1 \leq i \leq N$, the multiscale basis functions can also be

written as

$$\forall\, K \in \mathscr{T}_H, \qquad \phi_i^\varepsilon = \phi_i^{\mathbb{P}_1} + \sum_{\alpha=1}^{d} \left(\partial_\alpha \phi_i^{\mathbb{P}_1}\right)\big|_K \, \chi_K^{\varepsilon,\alpha} \quad \text{in } K, \tag{2.22}$$

where for each $K \in \mathscr{T}_H$ and all $1 \leq \alpha \leq d$, we define the function $\chi_K^{\varepsilon,\alpha} \in H_0^1(K)$ as the unique solution to

$$\begin{cases} -\mathrm{div}(A^\varepsilon \nabla \chi_K^{\varepsilon,\alpha}) = \mathrm{div}(A^\varepsilon e_\alpha) & \text{in } K, \\ \chi_K^{\varepsilon,\alpha} = 0 & \text{on } \partial K. \end{cases} \tag{2.23}$$

We note in passing that these functions correspond to the residual-free bubbles of [38], even though this work did not introduce them for the purpose of numerical homogenization. The microstructure that is encoded in the MsFEM is fully captured by the functions $\chi_K^{\varepsilon,\alpha}$, which can be computed separately on each mesh element and independently of the basis functions $\phi_i^{\mathbb{P}_1}$, contrary to the formulation of ϕ_i^ε in (2.18). These functions are illustrated in Figure 2.8. Each multiscale basis function is thus rewritten as the sum of a standard $\mathbb{P}_1$ basis function and a linear combination of the functions $\chi_K^{\varepsilon,\alpha}$.

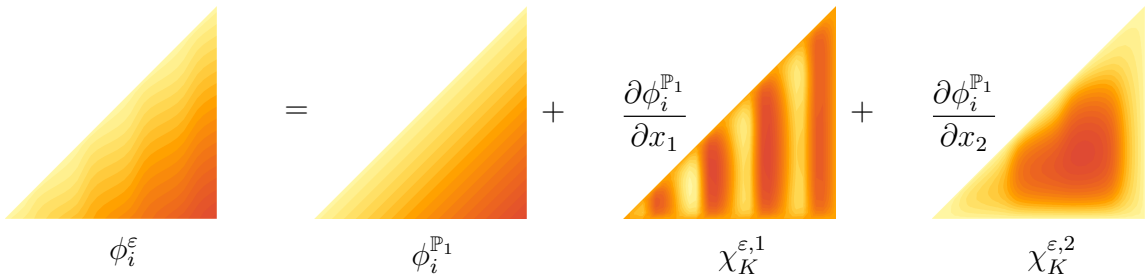

Figure 2.8: *The multiscale basis function ϕ_i^ε can be written as the sum of a standard FEM basis function $\phi_i^{\mathbb{P}_1}$ and a linear combination of the numerical correctors $\chi_K^{\varepsilon,1}$ and $\chi_K^{\varepsilon,2}$. We show a single mesh element K in 2D and the basis function associated to the bottom right vertex of K.*

Note that the gradients of the $\mathbb{P}_1$ basis functions in (2.22) are constant on each mesh element K. Combining this with linearity of the problem, we show in (4.13) that, for all $1 \leq i, j \leq N$,

$$\int_\Omega \nabla \phi_j^\varepsilon \, A^\varepsilon \, \nabla \phi_i^\varepsilon = \int_\Omega \nabla \phi_j^{\mathbb{P}_1} \, \overline{A} \, \nabla \phi_i^{\mathbb{P}_1}, \tag{2.24}$$

such that the entries of the linear system of the MsFEM are entirely expressed in terms of the standard $\mathbb{P}_1$ basis functions $\phi_i^{\mathbb{P}_1}$ and the piecewise constant matrix $\overline{A}$ defined as

$$\overline{A}\big|_K = \int_K \left(e_\beta + \nabla \chi_K^{\varepsilon,\beta}\right) \cdot A^\varepsilon \left(e_\alpha + \nabla \chi_K^{\varepsilon,\alpha}\right) \quad \text{for all } K \in \mathscr{T}_H. \tag{2.25}$$

The right-hand side of (2.24) corresponds exactly to the coefficients of the linear system associated to the $\mathbb{P}_1$ FEM approximation of

$$\begin{cases} -\mathrm{div}\left(\overline{A} \, \nabla u\right) = f & \text{in } \Omega, \\ u = 0 & \text{on } \partial\Omega. \end{cases} \tag{2.26}$$

Since $\overline{A}$ is piecewise constant, this problem can be solved by a standard FEM on a coarse

mesh.

In the spirit of (2.17), we can rewrite the expression for $\overline{A}$ as A^{av} defined in (2.10) plus a certain correction. Therefore, the functions $\chi_K^{\varepsilon,\alpha}$ are called *numerical correctors*, and $\overline{A}$ the *effective diffusion coefficient* associated to the MsFEM.

The above considerations have led to the introduction of the MsFEM Algorithm 4.1, summarized as the *non-intrusive MsFEM workflow* below. It decouples processing the microstructure in the offline stage from the resolution of a global finite element problem in the online stage thanks to the numerical correctors and the effective coefficient. This allows to solve the global FEM problem with an existing legacy code for $\mathbb{P}_1$ finite elements after computing the numerical correctors and the effective diffusion coefficient. The code for the latter can be developed separately, without modifying the legacy code. We comment on the difference with respect to the original MsFEM below in Contributions 4 and 6.

Contribution 1. *Non-intrusive MsFEM workflow; for details see Algorithm 4.1.*

→ *In the offline stage, compute numerical correctors in each mesh element from (2.23). Use the numerical correctors to average the microstructure in the form of the effective, piecewise constant coefficient in (2.25).*

→ *In the online stage, solve the effective PDE (2.26) by a standard FEM* ***with a legacy code****.*

→ *We introduce a post-processing stage to restore microscopic features in the macroscopic FEM result from the online stage with the help of the numerical correctors computed in the offline stage.*

We recognize in the non-intrusive MsFEM workflow all the same steps as in the computational strategy for periodic homogenization that was derived in Section 2.2.1. However, in contrast to this computational strategy, the numerical corrector and effective quantities we introduce here for the MsFEM need to be computed on every mesh element, and are in general different from one mesh element to the other (and this remains true even if the coefficient A^ε is periodic).

We next consider the generalization of the approach to other MsFEMs. It was explained in Section 2.2.3 that different boundary conditions can be considered than those in (2.18), which we call the MsFEM-lin. We recall the MsFEM-OS (oversampling) and the MsFEM-CR (Crouzeix-Raviart). Moreover, the MsFEM definition may be adapted to different PDEs (we exclusively consider PDEs with spatial derivatives in this thesis), possibly changing both the global PDE and the PDE defining the multiscale basis functions and hence the numerical correctors. We refer to Section 5.1 for details. (See also Section 2.3.2 for some examples.) In order to study the extension of the non-intrusive MsFEM workflow to different MsFEMs, we formulate a general framework to define MsFEMs for linear second-order PDEs in Chapter 5 of the thesis. A key element of this framework is that the MsFEM basis functions are defined by a generalization of (2.22) where the $\mathbb{P}_1$ function $\phi_i^{\mathbb{P}_1}$ can either belong to the $\mathbb{P}_1$ Lagrange or the $\mathbb{P}_1$ Crouzeix-Raviart space. In the general framework, we also extend the oversampling technique described for the MsFEM-lin above to the MsFEM-CR variant. An additional motivation for this general framework has been to establish a common convergence analysis for the MsFEM-lin and the MsFEM-CR, a start of which is presented in Part III of this thesis.

Contribution 2. *We propose a general framework for the formulation of MsFEMs for linear second-order PDEs, covering the MsFEM-lin and MsFEM-CR variants as well as two different oversampling techniques for both of them. The oversampling technique for the MsFEM-CR is another contribution of the thesis. Furthermore, we give a rigorous definition of the oversampling procedure near the boundary $\partial\Omega$ of the global domain, which is often missing in the literature. Within the full generality of our framework, the equivalence of definitions of the multiscale basis functions as solutions to local PDEs and as a sum of a $\mathbb{P}_1$ basis function and a linear combination of locally defined numerical correctors is established in Lemmas 5.22 and 5.23.*

Contribution 3. *The non-intrusive MsFEM of Contribution 1 is generalized to our general MsFEM framework in Algorithm 6.1. The global effective problem of the online stage can be solved by any legacy FEM software for general linear second-order PDEs with piecewise constant coefficients.*

Let us now comment on the relation between the traditional MsFEM and the method obtained following our non-intrusive workflow. In Section 6.2 we establish the following.

Contribution 4. *Rephrasing Theorem 6.3:*
Let V_H^ε be the MsFEM space under consideration, and let a^ε, respectively F, be the bilinear form, resp. the linear form, of the variational formulation of the global PDE on Ω, broken over the mesh elements if the MsFEM is non-conforming. Then the non-intrusive variant of the MsFEM

$$\text{Find } u_H^\varepsilon \in V_H^\varepsilon \text{ such that} \quad a^\varepsilon(u_H^\varepsilon, v_H^\varepsilon) = F(v_H^\varepsilon) \quad \text{for all } v_H^\varepsilon \in V_H^\varepsilon$$

corresponds to finding $u_H^\varepsilon \in V_H^\varepsilon$ such that

$$a^\varepsilon(u_H^\varepsilon, \phi_i^\varepsilon) = F\big(\phi_i^{\mathbb{P}_1}\big) \quad \text{for all } 1 \le i \le N,$$

where the multiscale basis function ϕ_i^ε is defined in terms of the $\mathbb{P}_1$ basis function $\phi_i^{\mathbb{P}_1}$ and the appropriate numerical correctors in (6.3).

This is easily understood on the example detailed above. Indeed, Equation (2.24) shows that the matrix of the linear system related to the MsFEM, and thus the left-hand side of the discrete variational formulation, is unchanged upon introducing the non-intrusive variant. The above result states that the same holds true within the general framework. On the contrary, the right-hand side of the non-intrusive MsFEM is obtained upon discretizing (2.26) by a standard $\mathbb{P}_1$ FEM, so the right-hand side is tested against $\mathbb{P}_1$ basis functions rather than multiscale basis functions. Following the same reasoning for a Petrov-Galerkin MsFEM in Section 6.1, we obtain the following property.

Contribution 5. *Rephrasing Theorem 6.2:*
Conisder the Petrov-Galerkin MsFEM

$$\text{Find } u_H^\varepsilon \in V_H^\varepsilon \text{ such that} \quad a^\varepsilon(u_H^\varepsilon, v_H) = F(v_H) \quad \text{for all } v_H \in V_H^{\mathbb{P}_1},$$

where $V_H^{\mathbb{P}_1}$ is the $\mathbb{P}_1$ Lagrange space for MsFEM-lin variants, and the $\mathbb{P}_1$ Crouzeix-Raviart space for MsFEM-CR variants. The solution obtained with this MsFEM is

identical *to the solution of its non-intrusive implementation.*

In some particular cases, the non-intrusive implementation of the (Galerkin) MsFEM coincides with the Petrov-Galerkin MsFEM; see Lemma 6.4. In the particular case of pure diffusion problems, we have the following comparison of the Galerkin and Petrov-Galerkin MsFEM.

Contribution 6. *Rephrasing Lemma 7.1 and Theorem 7.10:*
We consider a pure diffusion problem. Let 'MsFEM' refer to the MsFEM-lin or the MsFEM-CR, both without oversampling. Then the non-intrusive variant of the Galerkin MsFEM coincides with the Petrov-Galerkin MsFEM.
Let $u_H^{\varepsilon,\mathsf{G}}$*, respectively* $u_H^{\varepsilon,\mathsf{PG}}$*, denote the approximation of* u^ε *provided by the Galerkin MsFEM, resp. the Petrov-Galerkin MsFEM. When* $f \in L^2(\Omega)$*, there exists a constant* $C > 0$ *independent of* ε*,* H *and* f *such that*

$$\left\| u_H^{\varepsilon,\mathsf{G}} - u_H^{\varepsilon,\mathsf{PG}} \right\|_{H^1(\mathscr{T}_H)} \leq CH\|f\|_{L^2(\Omega)}.$$

Additional estimates are established in Chapter 7 under additional structural assumptions on the diffusion coefficient.

The final contributions of Part I of the thesis are concerned with the implementation of the MsFEM in FreeFEM++ and some of the conclusions that are drawn from numerical experiments for pure diffusion problems both with periodic and non-periodic diffusion coefficients.

Contribution 7. *All MsFEM variants described by the common framework of Chapter 5 are implemented in* FreeFEM++*, taking advantage of the common structure that is identified in the general MsFEM framework. The corresponding scripts are available at [29]. Numerical experiments for pure diffusion problems show that the Petrov-Galerkin MsFEM as well as the non-intrusive variant of the Galerkin MsFEM is close to the original Galerkin MsFEM. Any possible additional error introduced by making the MsFEM non-intrusive is thus negligible. These observations are robust with respect to (non-)periodicity of the diffusion coefficient.*

Outlook. The development of the non-intrusive MsFEM framework of Part I relies to a great extent on the relation (2.22) without any higher-order derivatives of $\phi_i^{\mathbb{P}_1}$, i.e., it relies on the fact that $\phi_i^{\mathbb{P}_1}$ is piecewise affine. For the high-order MsFEMs proposed in [9, 94], similar expressions can be derived for the multiscale basis functions, but piecewise $\mathbb{P}_k$ functions are required in such expansions. In Section 8.2 we propose a generalization of the non-intrusive approach on the example of the $\mathbb{P}_2$ MsFEM of [9]. The effective coefficients are given by up to fourth order tensors and the effective PDE becomes a fourth-order PDE if the original problem was a second-order PDE. The expressions obtained are considerably more involved than for the MsFEMs that are covered by our general framework. It does not seem obvious to easily implement this 'non-intrusive' approach.

Let us also mention that the various improvements of the MsFEM that proceed by enriching the MsFEM space, briefly described at the end of Section 2.2.3, are not covered by our general framework. Additional or different ideas may be required to propose efficient non-intrusive implementations of such MsFEMs.

Finally, it is appropriate to say that our general framework does not set the boundaries as to what might be considered a '$\mathbb{P}_1$ MsFEM'. We have aimed to identify a common structure among those MsFEMs we are aware of, and exploited this structure to define a non-intrusive implementation for all of them. Other ideas to improve the boundary conditions of the local problems in the MsFEM may still be found, and we hope that our considerations will also be valuable for new variants. In this regard, we mention the work of [3, 4], where insights into parabolic cell problems are used to obtain an exponentially converging resonance error for the HMM. These ideas may also be explored to further improve the oversampling strategy for the MsFEM.

2.3.2. MsFEMs for the stabilization of advection-dominated problems. In Part II of this thesis we focus explicitly on the advection-diffusion equation, i.e., u^ε is the solution to

$$-\operatorname{div}(A^\varepsilon \nabla u^\varepsilon) + b \cdot \nabla u^\varepsilon = f, \tag{2.27}$$

with an advection field $b \in L^\infty(\Omega)$ (and under some more hypotheses that are specified in Chapter 9). We still consider a strongly heterogeneous diffusion coefficient A^ε as above, and the related problems for an FEM on a coarse mesh remain. Another difficulty for the numerical approximation of u^ε is added: we are particularly interested in the case when the advective effects dominate the diffusive effects. We shall consider multiscale methods that aim to handle both difficulties in Part II.

It is well-known that, under the influence of a dominating advection field, the exact solution u^ε can develop sharp boundary layers, where the solution has a strong gradient in a small part of the domain. It is also well-known that standard FEMs fail to capture u^ε unless the underlying mesh is sufficiently fine to resolve the boundary layers. When this is not the case, its numerical approximation suffers from large oscillations that can propagate through the entire domain, while the exact solution only varies slowly outside the boundary layer. This is illustrated in Figure 2.9. It is said that the FEM is unstable in the advection-dominated regime. We recall this phenomenon in more detail in Chapter 9. If the position of the boundary layer is unknown, a standard FEM thus requires a fine mesh over the entire domain, or iterative mesh adaptation techniques, both of which can be costly computationally.

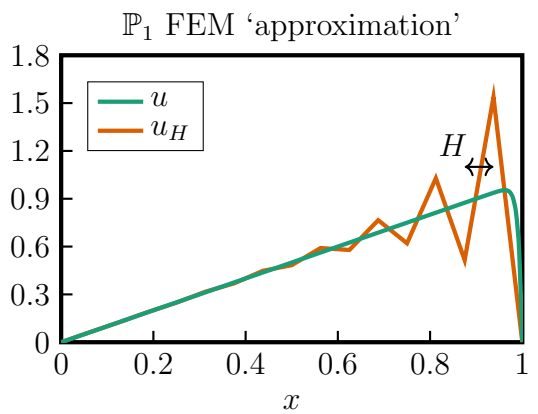

Figure 2.9: *Solution u to $-m\,u'' + u' = 1$ and its $\mathbb{P}_1$ approximation for $m = 2^{-7}$ and $H = 2^{-4}$, showing large spurious oscillations.*

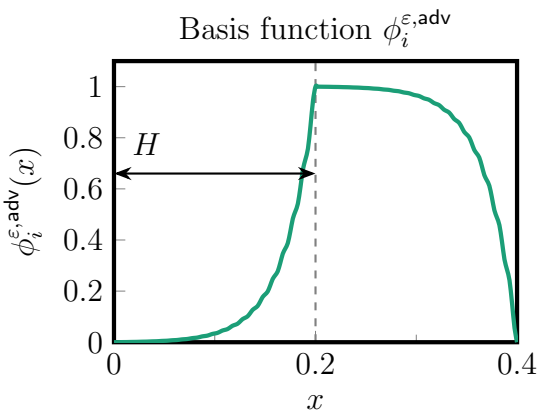

Figure 2.10: *Example of a multiscale basis function for the adv-MsFEM solving (2.28) in 1D when the advection is strong.*

In the context of slowly-varying diffusion coefficients, the question of removing the above-mentioned spurious oscillations from the numerical approximation has been investigated since long and has lead to multiple efficient so-called stabilization techniques such as the SUPG method from [43] or the methods developed in [103, 104]. A general exposition of such techniques can be found in the textbooks [131, 129]. These techniques are highly sensitive to the correct choice of certain stabilization parameters. (See [107] for a review of proposed choices and their motivation.) Although useful guidelines are available in the literature, for which improved convergence results can be established, these only provide an order of magnitude depending on the constants that appear in inverse inequalities. For such results we refer again to the aforementioned textbooks. The question of how to determine an 'optimal' stabilization parameter in dimension higher than 1 is still unsolved.

We observe the following similarities between multiscale problems as described in Section 2.2 and single-scale advection-dominated problems: both can be solved by an FEM on a sufficiently fine mesh, both lead to macroscopically incorrect results when the small-scale phenomena are not resolved due to a mesh that is too coarse, and adapted FEMs have been designed to capture the macroscopic scales for both problems on a coarse mesh. In particular, the above-mentioned stabilization techniques and the numerical homogenization approaches that were mentioned in the previous sections all bear similarities with the general VMM mentioned in Section 2.2.2. The aforementioned multiscale approaches have also been used to include stabilizing effects for advection-dominated problems. The LOD was used to this end when the diffusion coefficient is constant in [118, 34]. An HMM for steady advection-diffusion problems is presented and analysed in [6], and for unsteady advection-diffusion problems it can be found in [92]. In Part II of this thesis we only study MsFEM type methods for the steady advection-diffusion equation.

Let us discuss the development of MsFEMs for advection-diffusion problems in some more detail. At the time of the introduction of the method in [98], it was proposed to encode only the leading order elliptic operator of the PDE in these basis functions. The MsFEM basis functions are then defined by (2.18) (but possibly with a different choice of local boundary conditions), also for a non-zero advection field b in (2.27). Evidently, this method can have no stabilizing properties for advection-dominated problems since it coincides with the $\mathbb{P}_1$ FEM if A^ε is constant, irrespectively of the size of b. This is illustrated in Figure 10.1 in Chapter 10. This variant of the MsFEM was investigated in [114] for advection-dominated problems, where the combination with the classical SUPG stabilization was proposed and was found to achieve the required stability in the advection-dominated regime.

Another MsFEM may be proposed by changing the PDE solved locally by the multiscale basis functions in order to also encode the advective effects in the approximation space. One can hope that this also encodes stabilizing properties in the approximation space. To this end, we introduce the basis functions $\phi_i^{\varepsilon,\mathsf{adv}}$, for $1 \leq i \leq N$, as the solution to

$$\forall\, K \in \mathscr{T}_H, \quad \begin{cases} -\operatorname{div}(A^\varepsilon \nabla \phi_i^{\varepsilon,\mathsf{adv}}) + b \cdot \nabla \phi_i^{\varepsilon,\mathsf{adv}} = 0 & \text{in } K, \\ \phi_i^\varepsilon = \phi_i^{\mathbb{P}_1} & \text{on } \partial K. \end{cases} \tag{2.28}$$

See Figure 2.10. We refer by 'adv-MsFEM-lin' to the MsFEM that corresponds to the Galerkin approximation on the space spanned by the basis functions $\phi_i^{\varepsilon,\mathsf{adv}}$. Such an MsFEM was first investigated in [127, 128] for both steady and unsteady problems. However, there is not yet a general understanding of the stabilizing properties of this MsFEM

variant, even for a constant advection field. This has motivated the investigation of adv-MsFEM approaches that is reported in Part II of the thesis. Let us also mention the work [10], which combines the MsFEM proposed in [9] with the method of characteristics to obtain a stable approximation of non-stationary advection-diffusion problems.

A convergence analysis for the adv-MsFEM-lin variant was given in dimension 1 in [114, 119], but the method was found to be unstable in higher dimension. In Chapter 10 we provide new insights into the stability of the adv-MsFEM-lin in dimension 1 and the lack of stability in higher dimension. The first contribution is the following. Note that in 1D, all choices for the local boundary conditions coincide, and we refer to the adv-MsFEM-lin simply by adv-MsFEM in the following.

Contribution 8. *Rephrasing Theorem 10.4:*
In dimension 1, when $f = 0$ and for any choice of boundary conditions on $\partial\Omega$, the adv-MsFEM approximation equals the exact solution to (2.27). Since instabilities are due to the Dirichlet boundary conditions rather than the source term f, we conclude that the adv-MsFEM is stable. Stability for non-zero f is indeed observed numerically.

We also observe in Chapter 10 that the adv-MsFEM-lin basis functions can be strongly deformed under the influence of the advection field, and display boundary layers inside each mesh element. This can clearly be seen on the example in Figure 2.10. Such basis functions are not suitable for an accurate representation of the exact solution u^ε, which only develops a boundary layer near the boundary of the global domain. To overcome this problem, while preserving the stability of the adv-MsFEM-lin (that is, in dimension 1), we propose the addition of bubble functions to the approximation space. These are defined, for all $K \in \mathscr{T}_H$, as the unique solution $B_K^{\varepsilon,\mathsf{adv}} \in H_0^1(K)$ to

$$-\operatorname{div}(A^\varepsilon \nabla B_K^{\varepsilon,\mathsf{adv}}) + b \cdot \nabla B_K^{\varepsilon,\mathsf{adv}} = 1 \quad \text{in } K. \tag{2.29}$$

We define the adv-MsFEM-lin-B as the following multiscale finite element method. Let $V_{H,B}^{\varepsilon,\mathsf{adv}}$ be the multiscale space

$$V_{H,B}^{\varepsilon,\mathsf{adv}} = \operatorname{span}\left\{ \phi_i^{\varepsilon,\mathsf{adv}} \,\middle|\, 1 \le i \le N \right\} \bigoplus \operatorname{span}\left\{ B_K^{\varepsilon,\mathsf{adv}} \,\middle|\, K \in \mathscr{T}_H \right\}.$$

The adv-MsFEM-lin-B approximation of u^ε is the unique function $u_{H,B}^{\varepsilon,\mathsf{adv}} \in V_{H,B}^{\varepsilon,\mathsf{adv}}$ such that

$$\int_\Omega \nabla v_{H,B}^{\varepsilon,\mathsf{adv}} \cdot A^\varepsilon \nabla u_{H,B}^{\varepsilon,\mathsf{adv}} + v_{H,B}^{\varepsilon,\mathsf{adv}}\, b \cdot \nabla u_{H,B}^{\varepsilon,\mathsf{adv}} = \int_\Omega f\, v_{H,B}^{\varepsilon,\mathsf{adv}} \quad \text{for all } v_{H,B}^{\varepsilon,\mathsf{adv}} \in V_{H,B}^{\varepsilon,\mathsf{adv}}. \tag{2.30}$$

This is simply a Galerkin approximation of the variational formulation of (2.27) on the space $V_{H,B}^{\varepsilon,\mathsf{adv}}$. To understand the stabilizing properties of the adv-MsFEM-lin-B, we use a characterization like (2.22) that is established in the general framework of Part I, and combine it with the residual-free bubble method of [41]. There exist numerical correctors $\chi_K^{\varepsilon,\mathsf{adv},1}, \dots, \chi_K^{\varepsilon,\mathsf{adv},d}$ such that

$$\forall\, K \in \mathscr{T}_H, \quad u_{H,B}^{\varepsilon,\mathsf{adv}} = u_H + \sum_{\alpha=1}^{d} \partial_\alpha \Big(u_H^{\varepsilon,\mathsf{adv}} \Big|_K \Big) \chi_K^{\varepsilon,\mathsf{adv},\alpha} + \beta_K B_K^{\varepsilon,\mathsf{adv}} \quad \text{on } K, \tag{2.31}$$

for some $u_H \in V_H^{\mathbb{P}_1}$ that is called the underlying $\mathbb{P}_1$ part of the solution, and for some

constants $\beta_K \in \mathbb{R}$. Inserting this in (2.30), it is possible to derive an effective scheme only for u_H (by a method known as static condensation). This allows to make an interesting link with the classical stabilization literature, and the conclusions that can be drawn are contained in the next contribution.

Contribution 9. *When $A^\varepsilon = m\,\mathrm{Id}$ with $m > 0$, and when b and f are piecewise constant, the effective scheme for the underlying $\mathbb{P}_1$ part u_H resulting from the adv-MsFEM-lin-B coincides with the scheme obtained with the residual-free bubble method. Classical results show that the effective scheme coincides with the SUPG scheme with a specific value of the stabilization parameter. Moreover, it is known that*

1) in 1D, this stabilization parameter has the unique value for which nodal exactness is obtained (the adv-MsFEM-B is even exact in this case), but

2) this stabilization parameter is too small to achieve full stabilization for higher-dimensional problems.

In view of Contribution 9, the final contributions of the thesis focus on the design of a stable MsFEM in dimension higher than 1. Here we exploit the fact that the local boundary conditions in (2.28) are to be invented. This gives us some freedom that may have an impact on the stabilizing effects encoded in the MsFEM. We present in Chapter 11 the adv-MsFEM-CR and the adv-MsFEM-CR-B, using basis functions that are only weakly continuous across the interfaces of the mesh, and possibly adding bubble functions, which only vanish weakly (in the sense of the average) on the interfaces. See (11.1) and (11.5) for precise definitions. Contrary to the adv-MsFEM-lin or the MsFEM-CR basis functions, we cannot establish well-posedness of the adv-MsFEM-CR basis functions. We observed that the fine mesh used during the offline stage should be taken sufficiently fine to ensure an accurate computation of these basis functions. The conclusions from our numerical experiments with this method are summarized as follows.

Contribution 10. *The adv-MsFEM-CR is stable, in the sense that the underlying $\mathbb{P}_1$ part of the solution is free from unphysical oscillations. Its accuracy degrades in the advection-dominated regime due to the inadequate shape of the basis functions, and the addition of bubble functions is required to preserve accuracy in this regime. The error committed by the adv-MsFEM-CR-B is found to be robust with respect to the relative effect of the advection. The only other method in our study with this property is the MsFEM-lin with SUPG stabilization. Contrary to the MsFEM-lin SUPG, the robustness of the adv-MsFEM-CR-B does not depend on a parameter that has to be properly adjusted. Finally, we introduce a non-intrusive variant of the adv-MsFEM-CR-B that turns out to be slightly more accurate than the original method in the advection-dominated regime.*

A final observation about the bubble functions is important to understand the efficiency of the MsFEM variant with bubbles. We show in Section 11.3 that the coefficient β_K in (2.31) is (both for the adv-MsFEM-lin-B and the adv-MsFEM-CR-B) given by

$$\beta_K = \frac{\displaystyle\int_K f B_K^{\varepsilon,\mathsf{adv}}}{\displaystyle\int_K B_K^{\varepsilon,\mathsf{adv}}}. \tag{2.32}$$

Thus, the number of unknowns to be computed by the resolution of a linear system is the same for the adv-MsFEM-(lin/CR)-B as for the adv-MsFEM-(lin/CR) *without bubble functions.* In other words, the linear system to be solved in the online stage has the same size for both variants and the computational cost of the online stage does not increase significantly upon adding bubble functions. The only increase of the computational cost is in the offline stage, because one additional bubble function has to be computed per mesh element. The non-intrusive approximation of the adv-MsFEM-(lin/CR)-B consists in applying the techniques of Part I, along with replacing (2.32) by

$$\beta_K = \frac{1}{|K|} \int_K f.$$

This way, the coefficient β_K can be computed by single-scale finite element software operating on a coarse mesh that does not have access to numerical quadrature rules on the fine mesh on which the bubble function $B_K^{\varepsilon,\mathsf{adv}}$ is defined.

Outlook. There is an important drawback of the adv-MsFEM-CR-B (the method that we discovered to be stable in this thesis): the basis functions encoding the stabilizing properties depend on the advection field b. They should in principle be recomputed when the advection field changes, which is the case in many non-stationary equations, optimization problems, etc. This is unfeasible in practice, since it requires that the expensive offline stage of the MsFEM be executed for each iteration – it is no longer offline. For the adv-MsFEM-CR-B to be efficient for such problems, it should be combined with other model-order reduction techniques. One may explore, for instance, the reduced basis method, as is done in [35] in the context of the LOD. See [130] for a comprehensive introduction to reduced bases.

At the same time, our numerical observation that the adv-MsFEM-CR-B is stable in the advection-dominated regime motivates the pursuit of more theoretical studies. It might be insightful to know if the method can, for constant coefficients, be interpreted as a stabilized variant of a standard Crouzeix-Raviart discretization (just like we found for the adv-MsFEM-lin-B in Contribution 9 in relation to the residual-free bubble method). The works [108, 110, 17, 64] focus on the stabilization of non-conforming FEMs for problems with slowly-varying coefficients, but a link with the adv-MsFEM-CR-B has not yet been found. This seems a preliminary step to a rigorous analysis of the more challenging multiscale setting. It may also lead to new ideas for the stabilization of non-conforming FEMs for single-scale problems.

2.3.3. Convergence analysis of the MsFEM under minimal regularity hypothes. We stated in Section 2.2.3 that the error estimate (2.21), and its variations for different MsFEMs, are obtained, for all analyses that we are aware of, under the assumption of a rescaled periodic diffusion coefficient, i.e., $A^\varepsilon = A^{\mathsf{per}}(\cdot/\varepsilon)$. Moreover, and this is the part of the analysis that we aim to improve, it is assumed that A^{per} is Hölder continuous and that the homogenized limit $u^\star$ belongs to $W^{2,\infty}(\Omega)$. However, for well-posedness of (2.5), it suffices to assume that A^{per} is elliptic and uniformly bounded, without any additional regularity hypotheses. Such regularity assumptions are extremely restrictive from a modelling point of view, because real multiscale materials such as composite materials are typically characterized by *discontinuous coefficients.* In Chapter 13, we propose a new convergence analysis of the MsFEM that shows an error bound similar to (2.21),

merely assuming that A^{per} is bounded. We also weaken the required regularity of $u^\star$, only assuming that $u^\star \in H^2(\Omega)$. We summarize the main ideas behind our analysis below.

Let us first explain the role of the periodicity assumption in the analysis. The definition of the MsFEM basis functions in (2.18) combines the oscillatory behaviour of A^ε inside a mesh element K with non-oscillatory local boundary conditions on ∂K. These local boundary conditions are not satisfied by u^ε (except on the global boundary $\partial\Omega$) and induce oscillatory boundary layers in the error $u^\varepsilon - u^\varepsilon_H$ around ∂K. This is explained by the expression (2.35) below. The size of these boundary layers has to be characterized in terms of H and ε. To this end, a more detailed description of u^ε is used, based on some arguments that we outline below. Although different local boundary conditions are imposed for different MsFEM variants, the principle generalizes since no MsFEM can prescribe the exact oscillatory behaviour of u^ε on ∂K.

If A^ε is embedded in a sequence of matrices for $\varepsilon \to 0$, and if the sequence H-converges to a matrix $A^\star$ (which is true up to taking a subsequence), we know that u^ε converges to $u^\star$ solution to (2.12). However, according to the definition of H-convergence, the convergence is only weak in $H^1_0(\Omega)$ (and strong in $L^2(\Omega)$ by the Rellich Theorem [7, Lemma 1.2.6]). Strong convergence of the gradient can be obtained with the help of corrector results. Using the oscillating test functions v^ε_α defined in (2.13), we have

$$u^\varepsilon(x) \approx u^{\varepsilon,1}(x) \coloneqq u^\star(x) + \sum_{\alpha=1}^{d} \partial_\alpha u^\star(x)\,(v^\varepsilon_\alpha(x) - x_\alpha),$$

and $\nabla(u^\varepsilon - u^{\varepsilon,1})$ converges to zero strongly in $L^1_{loc}(\Omega)$. The function $u^{\varepsilon,1}$ is called the first-order two-scale expansion of u^ε. See, e.g., [7, Section 1.3.6].

The above framework for the first-order two-scale expansion is too general to obtain a *rate of convergence* with respect to ε. (We recall that an explicit characterization of v^ε_α is not even available.) This is why additional structural properties for A^ε are assumed in the literature. When $A^\varepsilon = A^{\mathsf{per}}(\cdot/\varepsilon)$, by (2.14), we have

$$u^\varepsilon(x) \approx u^{\varepsilon,1}(x) = u^\star(x) + \varepsilon \sum_{\alpha=1}^{d} \partial_\alpha u^\star(x)\, w^{\mathsf{per}}_\alpha\left(\frac{x}{\varepsilon}\right). \tag{2.33}$$

The fact that w^{per}_α solves (2.15) in a suitable functional space does allow to establish a rate of convergence for $u^\varepsilon - u^{\varepsilon,1}$ in the periodic setting. A classical result of periodic homogenization (see, e.g., [112, Proposition 3.1] and [134, p. 28]) shows that if, for all $1 \le \alpha \le d$, $w^{\mathsf{per}}_\alpha \in W^{1,\infty}(Q)$ and if $u^\star \in W^{2,\infty}(\Omega)$, there exists a constant $C > 0$ that does not depend on ε such that

$$\|u^\varepsilon - u^{\varepsilon,1}\|_{H^1(\Omega)} \le C\sqrt{\varepsilon}\|\nabla u^\star\|_{W^{1,\infty}(\Omega)}. \tag{2.34}$$

The regularity assumption for A^{per} originates at this point: if A^{per} is Hölder continuous, the functions w^{per}_α are indeed in $W^{1,\infty}(Q)$. (See [33, Theorem A.12].)

A similar expansion holds for the MsFEM solution u^ε_H. Since each multiscale basis function ϕ^ε_i solves (2.18) on all mesh elements K, and since $A^\star$ is constant in the periodic setting, one can show that the homogenized limit of ϕ^ε_i is $\phi^{\mathbb{P}_1}_i$ for all $1 \le i \le N$.

Consequently, the MsFEM solution u_H^ε satisfies, on all $K \in \mathscr{T}_H$,

$$u_H^\varepsilon \approx u_H^{\varepsilon,1} := u_H^\star + \varepsilon \sum_{\alpha=1}^{d} \partial_\alpha (u_H^\star|_K)\, w_\alpha^{\mathsf{per}}\left(\frac{x}{\varepsilon}\right) \quad \text{on } K, \tag{2.35}$$

where $u_H^\star \in V_H^{\mathbb{P}_1}$ is defined by the property $u_H^\star(x_i) = u_H^\varepsilon(x_i)$ for all $1 \le i \le N$. The difference $u_H^\varepsilon - u_H^{\varepsilon,1}$ can be bounded on each K using a localized variant of (2.34). See [9, Lemma 2.13], for instance. Note that $u_H^\varepsilon - u_H^{\varepsilon,1}$ has an oscillatory boundary layer around the interfaces ∂K, since the functions $w_\alpha^{\mathsf{per}}\left(\frac{\cdot}{\varepsilon}\right)$ oscillate on ∂K but the functions u_H^ε and $u_H^\star$ do not. Also note that $\nabla u_H^\star$ is piecewise constant.

Schematically, the MsFEM analyses in the literature rely on writing the error of the MsFEM as

$$u^\varepsilon - u_H^\varepsilon = \left(u^\varepsilon - u^{\varepsilon,1}\right) + \left(u^{\varepsilon,1} - u_H^{\varepsilon,1}\right) + \left(u_H^{\varepsilon,1} - u_H^\varepsilon\right).$$

The first and last term are estimated using the homogenization properties (2.33) and (2.35), and contribute to an order $\sqrt{\varepsilon}$ and $\sqrt{\varepsilon/H}$ in the error bound (2.21). The second term is essentially a difference between $u^\star$ and a function from the standard $\mathbb{P}_1$ space $V_H^{\mathbb{P}_1}$, which is estimated using standard interpolation arguments from finite element analysis and contributes to an order H in the error bound (2.21).

While the above sketch of an MsFEM convergence proof does, of course, have to be complemented by a rigorous study of all approximations that are used, it is sufficient to introduce the ideas behind our new convergence analysis. First one may note that the boundary layer around $\partial\Omega$ is estimated twice: once when estimating $u^\varepsilon - u^{\varepsilon,1}$ on Ω and a second time when estimating $u_H^{\varepsilon,1} - u_H^\varepsilon$ on those mesh elements K that touch $\partial\Omega$. Also note that u^ε and u_H^ε in fact satisfy *the same Dirichlet condition* on $\partial\Omega$, and there is no oscillatory boundary layer in the error here. It is introduced in the analysis by the choice of looking at the intermediate quantity $u^\varepsilon - u^{\varepsilon,1}$. Thus, it seems that the estimate (2.34) may be improved if we do not use $u^{\varepsilon,1}$ in the analysis.

In the convergence proof of Chapter 13, we follow this line of thought. We show in Lemma 13.12 an interpolation result for $u^\varepsilon - u_H^{\varepsilon,1}$ directly, and show that the error is bounded by the difference $u^\star - u_H^\star$, which can be estimated using classical interpolation results. (To be more precise, in Lemma 13.12, we show an interpolation estimate for an arbitrary element $v_H \in V_H^{\mathbb{P}_1}$ instead of $u_H^\star$, which is later combined with the Céa or Strang Lemma, and we include an estimate of the boundary layer.) This results in Corollary 13.14, which provides an interpolation estimate for u^ε by the multiscale space V_H^ε in terms of the interpolation error of $u^\star$ by the standard $\mathbb{P}_1$ space $V_H^{\mathbb{P}_1}$.

The main advantage of this analysis is the following. Estimates for the oscillatory boundary layer need never be applied to $u^{\varepsilon,1}$ as in (2.34), but only to functions like $u_H^{\varepsilon,1}$ of the form (2.35) with $u_H^\star \in V_H^{\mathbb{P}_1}$. The difference with $u^{\varepsilon,1}$ from (2.33) is that $u_H^\star$ is *piecewise affine* and we can use the fact that all Sobolev norms are equivalent on the finite-dimensional space $V_H^{\mathbb{P}_1}$. Such regularity is not known for $u^\star$ a priori. As a consequence, we will see that we can establish our central homogenization property of Lemma 13.11 without assuming any regularity on A^ε and $u^\star$. This is in sharp contrast to the classical analyses that rely on (2.34).

Additionally, we point out the similarities between the definition of a multiscale basis function ϕ_i^ε in (2.22) and the two-scale expansion $u_H^{\varepsilon,1}$ in (2.35). The generalization of (2.22) in the MsFEM framework of Contribution 2 helped us realize that the central role of $u_H^{\varepsilon,1}$ in our analysis can be used in the analysis of the MsFEM-lin as well as the

MsFEM-CR. Part III of this thesis presents for the first time a unifying convergence proof for both MsFEM variants. We note, however, that the MsFEM-CR requires some additional arguments due to its non-conforming character.

The above considerations have led to the following result that is proved in Chapter 13.

Contribution 11. *Rephrasing Theorem 13.1:*
Suppose that $A^\varepsilon = A^{\mathsf{per}}(\cdot/\varepsilon)$, where A^{per} is periodic, but not necessarily Hölder continuous. Let u_H^ε be the MsFEM-lin or MsFEM-CR approximation of u^ε. Suppose that $(\mathscr{T}_H)_H$ is a regular family of simplicial meshes and that it is quasi-uniform, that $\varepsilon \leq H$, and that $u^\star \in H^2(\Omega)$. Then

$$|u^\varepsilon - u_H^\varepsilon|_{H^1(\mathscr{T}_H)} \leq C \left(H|u^\star|_{H^2(\Omega)} + \sqrt{\frac{\varepsilon}{H}}\, |u^\star|_{H^1(\Omega)} \right).$$

Contrary to the previously available analyses, no additional regularity is required for A^ε besides its coercivity and boundedness. We also note that the term with the prefactor $\sqrt{\varepsilon}$ is no longer present, making our estimate sharper than (2.21). This is due to the fact that we no longer use the estimate (2.34) in the analysis. Regarding the regularity assumed for the homogenized solution $u^\star$, the condition $u^\star \in H^2(\Omega)$ is unavoidable since even the standard $\mathbb{P}_1$ FEM requires the same regularity for the solution in order to establish convergence at the rate H; see (2.7). Hence, our convergence analysis for the MsFEM is carried out under minimal regularity hypotheses. Finally, Contribution 6 shows that the same rate of convergence is obtained for the Petrov-Galerkin variant of the MsFEM with test function in the standard $\mathbb{P}_1$ space.

Outlook. Let us outline a few research directions that could be pursued to further improve the convergence analysis in the MsFEM literature. Contribution 11 states a convergence result for the MsFEM-lin and the MsFEM-CR. Oversampling variants are not considered. For the MsFEM-lin with oversampling, convergence proofs can be found in [70, 100]. It may be interesting to extend the proof under minimal regularity hypotheses to this setting, and to one of the oversampling variants of the MsFEM-CR proposed in this thesis.

Another possible extension concerns the high-order MsFEMs as proposed in [9, 94]. We recall that one of the main novelties in our analysis is that we no longer introduce $u^{\varepsilon,1}$ from (2.33) but rather compare u^ε directly to $u_H^{\varepsilon,1}$ defined in (2.35). Then we exploit that $u_H^\star$ is piecewise smooth (since it belongs to the standard finite element space $V_H^{\mathbb{P}_1}$) while this is not known for $u^\star$. This still holds true when $V_H^{\mathbb{P}_1}$ is replaced by a space of piecewise higher-order polynomials. Inverse inequalities can be applied to obtain estimates in any desired Sobolev norm. Using these observations, it may be possible to generalize the analysis of Part III to high-order MsFEMs.

A final future research direction could be to weaken the structural hypotheses on A^ε. We worked with the periodicity hypothesis, like all other analyses we are of, in order to have a rate of convergence for the approximations in (2.33) and (2.35). Rates of convergence for the corrector results have also been established for certain perturbations of the periodic setting. We refer to [33, 83]. Such results may be useful to prove convergence of the MsFEM in perturbations of the periodic setting as well.

Part I

Non-intrusive Implementation of Multiscale Finite Element Methods

Chapter 3

An illustrative example

In Section 2.3.1 of the general Introduction, we introduced the question of designing non-intrusive MsFEMs in order to ease the adoption of the method in situations where a large legacy code for traditional FEMs is already in use. Our first work on this topic was published in [32]. The contents of the article are reproduced in this chapter in its entirety because of its concise and pedagogical character. It can be read independently of the rest of the thesis. Minor modifications to the text of [32] have been made only for the purpose of coherence with the rest of the thesis. The other chapters of Part I of the thesis (Chapters 4 to 8) address the design of non-intrusive MsFEMs in a more general setting.

3.1. Introduction

We consider the highly oscillatory diffusion problem

$$-\operatorname{div}(A^\varepsilon \nabla u^\varepsilon) = f \quad \text{in } \Omega, \qquad u^\varepsilon = 0 \quad \text{on } \partial\Omega, \tag{3.1}$$

in a bounded domain $\Omega \subset \mathbb{R}^d$, where the diffusion coefficient A^ε is assumed to oscillate on a typical length scale of size ε much smaller than the diameter of Ω, and to satisfy the usual ellipticity assumptions (see Section 3.2 below for details). The reason for considering (3.1) is two-fold: first, this problem is ubiquitous in scientific computing; second, we see it as a template to develop new ideas that we will next extend to other problems.

We seek a numerical approximation of (3.1) by applying a Galerkin approach. It is well-known that standard finite element methods yield an approximation of poor accuracy, as a consequence of the highly oscillatory nature of the problem, unless a prohibitively expensive fine mesh is employed. Dedicated multiscale approaches have thus been introduced, which provide a reasonably accurate approximation of (3.1) for a limited computational cost. Among the many multiscale approaches that have been proposed in the literature, we mention the *Heterogeneous Multiscale Method* (henceforth abbreviated as HMM) [5], the *Localized Orthogonal Decomposition* method (LOD) [12], and the *Multiscale Finite Element Method* (MsFEM) on which we focus here (see [98, 69, 111] for a comprehensive exposition).

Specifically, the MsFEM method is a finite element type method, which consists of two steps:

- an "offline" stage, where highly oscillatory, problem-dependent (but right-hand side independent) basis functions are numerically computed as solutions to local problems (that mimick the reference problem on a subdomain);
- an "online" stage, where a Galerkin approximation of (3.1), performed in the finite-dimensional space generated by the basis functions computed in the offline stage, is solved. This provides a numerical solution that, in the $H^1(\Omega)$ norm, approximates the solution u^ε to the highly oscillatory problem (3.1).

The MsFEM approach is particularly interesting in multi-query contexts, where (3.1) is to be repeatedly solved for multiple right-hand sides f (think e.g. of optimization problems, or of time-dependent problems where (3.1) would be the typical equation to solve to advance from one time step to the next). In this case, the offline stage is only performed once and a significant computational gain is thus achieved.

Several MsFEM variants exist, depending on the specific definition of the basis functions. Although their implementation is rightfully considered to be relatively easy (see e.g. [69, 125]), they are all definitely intrusive. They indeed require to change the finite element basis set and adjust it to the problem at hand. Our aim in this chapter is to investigate how these approaches can be adapted (possibly at the price of a marginal loss in their efficiency) so that they become as little intrusive as possible, thereby allowing to use only a *legacy*, single-scale software (based on standard finite elements) to recover an accurate approximation of (3.1). We believe that such an endeavor will eventually facilitate the dissemination of MsFEM methods within industrial, non-academic codes.

This chapter is organized as follows. In Section 3.2, on the example of the diffusion problem (3.1), we introduce the simplest MsFEM approach (namely the so-called linear MsFEM) in a Galerkin setting (see Algorithm 3.1), and present its non-intrusive variant, namely Algorithm 3.2. We also outline the relation between this variant and a Petrov-Galerkin variant of the MsFEM. Some elements of numerical analysis (along with an illustrative numerical result) are provided in Section 3.3, to estimate the additional error introduced by the non-intrusive implementation of the method. It is well-known that the linear MsFEM variant considered in Sections 3.2 and 3.3 is outperformed by several MsFEM variants. For pedagogical purposes, we have deliberately chosen to present our ideas on this simple variant and to collect in Section 3.4 some concluding remarks on the many possible extensions of our methodology to design non-intrusive implementations of existing approaches.

We have implemented the two algorithms we describe below in the finite element software FreeFEM++ [91], and the corresponding scripts can be found at [29]. Note that the non-intrusive variant (i.e., Algorithm 3.2) is easy to implement in any finite element software, since it is designed to be used in any legacy code.

A comprehensive presentation of our procedure, with applications to several MsFEM variants, several equations and various boundary conditions, is the subject of ongoing investigations (see the remainder of Part I of the thesis).

3.2. Non-intrusive implementation of MsFEM: a simple case

We provide problem (3.1) with all the usual assumptions that make it well-posed at the continuous level and amenable to a classical Galerkin approximation. In particular, we

assume that $A^\varepsilon \in L^\infty(\Omega, \mathbb{R}^{d\times d})$ satisfies the bounds

$$\begin{aligned} &\forall \xi \in \mathbb{R}^d, \quad m\,|\xi|^2 \le \xi \cdot A^\varepsilon(x)\xi \quad \text{a.e. in } \Omega \\ \text{and} \qquad &\forall \xi, \eta \in \mathbb{R}^d, \quad |\eta \cdot A^\varepsilon(x)\xi| \le M\,|\xi|\,|\eta| \quad \text{a.e. in } \Omega, \end{aligned} \tag{3.2}$$

for some $M \ge m > 0$ independent of ε, and that f *does not oscillate* on the microscopic scale ε. Note that no further structural assumptions on A^ε are made (in particular, A^ε need not be of the form $A(\cdot/\varepsilon)$ for a fixed rescaled function A). We respectively denote by

$$a^\varepsilon(u,v) = \int_\Omega \nabla v \cdot A^\varepsilon \nabla u \qquad \text{and} \qquad F(v) = \int_\Omega f v \tag{3.3}$$

the bilinear and linear forms associated to the variational formulation of (3.1). We seek a numerical approximation of (3.1) by applying an MsFEM type Galerkin approach. To this end, we introduce a conformal simplicial mesh $\mathscr{T}_H$ of Ω (i.e., made of triangles if $d = 2$, tetrahedra if $d = 3$) and denote by V_H the usual conformal $\mathbb{P}_1$ approximation space on $\mathscr{T}_H$. For any $u, v \in H^1(K)$, we also define $a^\varepsilon_K(u,v) = \displaystyle\int_K \nabla v \cdot A^\varepsilon \nabla u$ and $F_K(v) = \displaystyle\int_K f v$.

3.2.1. The Multiscale Finite Element Method. The MsFEM is a Galerkin approximation that adapts the finite-dimensional approximation space in order to obtain a satisfactory accuracy even on a coarse mesh. Let $x_1, \dots, x_{N_v}$ be the interior vertices (i.e., the N_v vertices that do not lie on $\partial\Omega$) of $\mathscr{T}_H$, and let $\phi_i^{\mathbb{P}_1}$ be the unique element of V_H such that $\phi_i^{\mathbb{P}_1}(x_j) = \delta_{i,j}$ for all $1 \le j \le N_v$. For any $1 \le i \le N_v$, we define the *multiscale basis function* $\phi_i^\varepsilon \in H^1_0(\Omega)$, which is supported by the exact same mesh elements as $\phi_i^{\mathbb{P}_1}$, by

$$\forall K \in \mathscr{T}_H, \qquad -\operatorname{div}(A^\varepsilon \nabla \phi_i^\varepsilon) = 0 \ \text{ in } K \quad \text{and} \quad \phi_i^\varepsilon = \phi_i^{\mathbb{P}_1} \ \text{ on } \partial K. \tag{3.4}$$

The multiscale approximation space is defined as

$$V_H^\varepsilon = \operatorname{span}\{\phi_i^\varepsilon,\ 1 \le i \le N_v\},$$

and it has the same dimension as V_H. The MsFEM approach then consists in computing the approximation $u_H^\varepsilon \in V_H^\varepsilon$ defined by the problem

$$\forall v_H^\varepsilon \in V_H^\varepsilon, \qquad a^\varepsilon(u_H^\varepsilon, v_H^\varepsilon) = F(v_H^\varepsilon). \tag{3.5}$$

Since the space V_H^ε is problem-dependent, we can hope (and this is indeed the case) the approximation (3.5) to capture the exact solution much better than a $\mathbb{P}_1$ approximation on the same mesh (even on a mesh of size H of the order of ε).

The computation of $\{\phi_i^\varepsilon\}_{1\le i\le N_v}$ is called the *offline stage* of the MsFEM. All the problems (3.4) on different mesh elements are independent of each other, and can thus be solved in parallel. On the other hand, the term *online stage* is used for the resolution of the global problem (3.5), where the number of degrees of freedom is the same as in a standard $\mathbb{P}_1$ approximation on V_H.

Remark 3.1 (Fine-scale discretization)**.** In practice, the local problems (3.4) need to be approximated, for instance using a standard $\mathbb{P}_1$ approximation on a fine mesh (of $K \in \mathscr{T}_H$) of mesh size $h \le \varepsilon$ which resolves the oscillations of A^ε. We omit here this additional discretization. All that follows can readily be extended to the case when only

some numerical approximation of ϕ_i^ε is available.

The MsFEM approach can schematically be presented as Algorithm 3.1. Lines 1–11 (resp. 12–16) constitute the offline (resp. online) stage.

Algorithm 3.1 MsFEM approach for Problem (3.1) (see comments in the text)

1: Construct a mesh $\mathscr{T}_H$ of Ω, denote N_v the number of internal vertices and $\mathscr{N}(n, K)$ the global index of the vertex of $K \in \mathscr{T}_H$ that has local index $1 \leq n \leq d+1$ in K

2: **for** $1 \leq i \leq N_v$ **do**
3: Solve for ϕ_i^ε in (3.4)
4: **end for**

5: Set $\mathbb{A}^\varepsilon := 0$ and $\mathbb{F}^\varepsilon := 0$
6: **for all** $K \in \mathscr{T}_H$ **do**
7: **for** $1 \leq m \leq d+1$ **do**
8: Set $j := \mathscr{N}(m, K)$
9: **for** $1 \leq n \leq d+1$ **do**
10: Set $i := \mathscr{N}(n, K)$ and $\mathbb{A}^\varepsilon_{j,i} \mathrel{+}= a_K^\varepsilon\left(\phi_i^\varepsilon, \phi_j^\varepsilon\right)$
11: **end for**
12: Set $\mathbb{F}^\varepsilon_j \mathrel{+}= F_K\left(\phi_j^\varepsilon\right)$
13: **end for**
14: **end for**

15: Solve the linear system $\mathbb{A}^\varepsilon U^\varepsilon = \mathbb{F}^\varepsilon$

16: Obtain the MsFEM approximation $u_H^\varepsilon = \displaystyle\sum_{i=1}^{N_v} U_i^\varepsilon \phi_i^\varepsilon$

Implementing Algorithm 3.1 in an industrial code is challenging. Indeed, the practical implementation of any finite element method relies on (i) the construction of a mesh, (ii) the construction of the linear system associated to the discrete variational formulation and (iii) the resolution of the linear system. An efficient implementation of the second step heavily relies on the choice of the discretization space. Regarding the construction of the linear system (performed in line 10 of Algorithm 3.1), it is by no means obvious to adapt existing finite element codes based on generic spaces like V_H to a different, problem-dependent choice of space such as V_H^ε. No analytic expressions for the basis functions ϕ_i^ε are available (and thus a fine mesh should be used to approximate them), the computation of $a_K^\varepsilon\left(\phi_i^\varepsilon, \phi_j^\varepsilon\right)$ and $F_K\left(\phi_j^\varepsilon\right)$ should be performed by quadrature rules on the fine mesh because the integrands are highly oscillatory, one should have at hand the correspondence between element and vertex indices in the coarse mesh, the assembly of the global stiffness matrix $\left\{\mathbb{A}^\varepsilon_{j,i}\right\}_{1\leq i,j\leq N_v}$ should be manually performed, etc. To alleviate these obstacles, we shall next introduce a way of implementing MsFEM that capitalizes on an existing code for solving (3.1) by a $\mathbb{P}_1$ approximation on $\mathscr{T}_H$ in the case of slowly-varying diffusion coefficients.

To the best of our knowledge, the question of how to make MsFEM approaches less intrusive has not been studied in the literature, and this work (that will be complemented in the remainder of Part I) is a first step in that direction. On the other hand, for some other multiscale approaches (including HMM and LOD), this question has been (at least partially) addressed. By construction, HMM methods are less invasive, since

they primarily aim at approximating u^ε on the *coarse scales*. The first step of these methods somewhat consists in building an effective, slowly-varying diffusion coefficient (which plays the role of the matrix $\overline{A}$ introduced in (3.11) below), which can next be used in any single-scale solver. The LOD approach, which, similarly to MsFEM, aims at approximating u^ε on *the coarse and the fine scales*, is also invasive in general, since it also introduces adapted basis functions. As shown in [79], the LOD can be recast as a $\mathbb{P}_1$ discretization of an appropriate single-scale problem, an observation which opens the way to non-intrusive implementations. Note however that, despite its current intrusiveness, MsFEM has its own advantages over other multiscale approaches: it directly aims at approximating the oscillatory solution u^ε (*including* its fine-scale details), and makes use of *fully localized* basis functions to do so.

3.2.2. Equivalent problem on the macroscopic scale. Our starting point for reducing intrusiveness in the above MsFEM implementation is the following key observation. On any $K \in \mathscr{T}_H$, by linearity of the definition (3.4) of ϕ_i^ε in terms of $\phi_i^{\mathbb{P}_1}$, and because the finite element space V_H consists of functions that are piecewise affine (that is to say, $\nabla\phi_i^{\mathbb{P}_1}$ is constant in each K), we have the expansion

$$\phi_i^\varepsilon(x)|_K = \phi_i^{\mathbb{P}_1}(x) + \sum_{\alpha=1}^d (\partial_\alpha \phi_i^{\mathbb{P}_1})|_K \; \chi_K^{\varepsilon,\alpha}(x), \tag{3.6}$$

for any basis function ϕ_i^ε of V_H^ε. Here, $\chi_K^{\varepsilon,\alpha} \in H_0^1(K)$ is defined as the solution to the local problem

$$-\operatorname{div}(A^\varepsilon \nabla \chi_K^{\varepsilon,\alpha}) = \operatorname{div}(A^\varepsilon e_\alpha) \quad \text{in } K, \qquad \chi_K^{\varepsilon,\alpha} = 0 \quad \text{on } \partial K, \tag{3.7}$$

where e_α denotes the α-th canonical unit vector of $\mathbb{R}^d$. Considering indeed the right-hand side of (3.6), we compute that its gradient in K is $\sum_{\alpha=1}^d (\partial_\alpha \phi_i^{\mathbb{P}_1})|_K \; (e_\alpha + \nabla\chi_K^{\varepsilon,\alpha}(x))$. In view of (3.7), we obtain

$$-\operatorname{div} A^\varepsilon \left[\sum_{\alpha=1}^d (\partial_\alpha \phi_i^{\mathbb{P}_1})|_K \; (e_\alpha + \nabla\chi_K^{\varepsilon,\alpha}) \right] = 0 \quad \text{in } K.$$

The right-hand side of (3.6) therefore satisfies the PDE in (3.4). It also satisfies the boundary conditions in (3.4), in view of the boundary conditions in (3.7). Since the solution to (3.4) is unique, we deduce the identity (3.6).

For each $K \in \mathscr{T}_H$ and each $1 \le \alpha \le d$, we extend $\chi_K^{\varepsilon,\alpha}$ by 0 outside K, thereby obtaining a function $\chi_K^{\varepsilon,\alpha} \in H_0^1(\Omega)$. We then deduce from (3.6) that there is a one-to-one correspondence between functions in V_H^ε and functions in V_H. More precisely, for any $v_H^\varepsilon \in V_H^\varepsilon$, there exists a unique $v_H \in V_H$ such that

$$v_H^\varepsilon = v_H + \sum_{K \in \mathscr{T}_H} \sum_{\alpha=1}^d (\partial_\alpha v_H)|_K \; \chi_K^{\varepsilon,\alpha}, \tag{3.8}$$

and conversely, for any $v_H \in V_H$, we have $v_H + \sum_{K \in \mathscr{T}_H} \sum_{\alpha=1}^d (\partial_\alpha v_H)|_K \; \chi_K^{\varepsilon,\alpha} \in V_H^\varepsilon$. In particular, the function associated to $\phi_i^\varepsilon \in V_H^\varepsilon$ is $\phi_i^{\mathbb{P}_1} \in V_H$.

We now consider the linear system associated to (3.5) and insert therein the expansion (3.8) for the multiscale basis functions. The solution to (3.5) reads $u_H^\varepsilon = \sum_{i=1}^{N_v} U_i^\varepsilon \, \phi_i^\varepsilon$, where $U^\varepsilon = \left(U_1^\varepsilon, \ldots, U_{N_v}^\varepsilon\right)^T$ is the solution to

$$\mathbb{A}^\varepsilon \, U^\varepsilon = \mathbb{F}^\varepsilon, \tag{3.9}$$

where, for all $1 \leq i, j \leq N_v$, we define $\mathbb{A}_{j,i}^\varepsilon = a^\varepsilon\left(\phi_i^\varepsilon, \phi_j^\varepsilon\right)$ and $\mathbb{F}_j^\varepsilon = F\left(\phi_j^\varepsilon\right)$.

Taking $v_H^\varepsilon = \phi_i^\varepsilon$ (and thus $v_H = \phi_i^{\mathbb{P}_1}$) in (3.8) and using that $\nabla \phi_i^{\mathbb{P}_1}$ is piecewise constant, we write

$$\nabla \phi_i^\varepsilon = \sum_{K \in \mathscr{T}_H} \sum_{\alpha=1}^{d} (\partial_\alpha \phi_i^{\mathbb{P}_1})|_K \; \left(e_\alpha + \nabla \chi_K^{\varepsilon,\alpha}\right).$$

Inserting this relation in the definition of the matrix elements $\mathbb{A}_{j,i}^\varepsilon$, we obtain

$$\begin{aligned}
\mathbb{A}_{j,i}^\varepsilon &= \int_\Omega \nabla \phi_j^\varepsilon \cdot A^\varepsilon \nabla \phi_i^\varepsilon \\
&= \sum_{K \in \mathscr{T}_H} \sum_{\alpha,\beta=1}^{d} (\partial_\beta \phi_j^{\mathbb{P}_1})|_K \; \left(\int_K \left(e_\beta + \nabla \chi_K^{\varepsilon,\beta}\right) \cdot A^\varepsilon \left(e_\alpha + \nabla \chi_K^{\varepsilon,\alpha}\right)\right) \; (\partial_\alpha \phi_i^{\mathbb{P}_1})|_K \\
&= \sum_{K \in \mathscr{T}_H} \sum_{\alpha,\beta=1}^{d} (\partial_\beta \phi_j^{\mathbb{P}_1})|_K \; a_K^\varepsilon \left(x^\alpha + \chi_K^{\varepsilon,\alpha}, x^\beta + \chi_K^{\varepsilon,\beta}\right) \; (\partial_\alpha \phi_i^{\mathbb{P}_1})|_K,
\end{aligned} \tag{3.10}$$

where $x^\alpha = x \cdot e_\alpha$ is the α-th coordinate function. We now define the piecewise constant matrix-valued field $\overline{A} \in \mathbb{P}_0(\mathscr{T}_H, \mathbb{R}^{d \times d})$ by

$$\overline{A}_{\beta,\alpha}\big|_K = \frac{1}{|K|} \, a_K^\varepsilon \left(x^\alpha + \chi_K^{\varepsilon,\alpha}, x^\beta + \chi_K^{\varepsilon,\beta}\right) \quad \text{for each } K \in \mathscr{T}_H \text{ and } 1 \leq \alpha, \beta \leq d, \tag{3.11}$$

where $|K|$ denotes the area or volume of the mesh element K. Using (3.7) and the bounds (3.2) satisfied by A^ε, it is easy to show (see Lemma 7.2 for the lower bound; the upper bound can be shown by similar arguments) that $\overline{A}$ satisfies the following uniform lower and upper bounds: for any ξ and η in $\mathbb{R}^d$,

$$m \, |\xi|^2 \leq \xi \cdot \overline{A}(x) \xi \qquad \text{and} \qquad \left|\eta \cdot \overline{A}(x) \xi\right| \leq M \left(1 + \frac{M}{m}\right) |\xi| \, |\eta| \;\; \text{a.e. in } \Omega. \tag{3.12}$$

Motivated by (3.10) and (3.11), we introduce the coarse-scale problem

$$-\operatorname{div}\left(\overline{A} \, \nabla u\right) = f \;\; \text{in } \Omega, \qquad u = 0 \;\; \text{on } \partial\Omega, \tag{3.13}$$

and its $\mathbb{P}_1$ Galerkin discretization: find $u_H \in V_H$ such that

$$\forall \, v_H \in V_H, \qquad a^{\overline{A}}(u_H, v_H) = F(v_H), \tag{3.14}$$

where the linear form F is defined by (3.3) and the bilinear form $a^{\overline{A}}$ is defined by

$$\forall \, u, v \in H_0^1(\Omega), \qquad a^{\overline{A}}(u, v) = \sum_{K \in \mathscr{T}_H} a_K^{\overline{A}}(u, v) \quad \text{with} \quad a_K^{\overline{A}}(u, v) = \int_K \nabla v \cdot \overline{A} \nabla u.$$

Problem (3.14) equivalently writes

$$\mathbb{A}^{\mathbb{P}_1} U^{\mathbb{P}_1} = \mathbb{F}^{\mathbb{P}_1}, \tag{3.15}$$

with

$$\forall 1 \leq i, j \leq N_v, \qquad \mathbb{A}^{\mathbb{P}_1}_{j,i} = a^{\overline{A}}\left(\phi_i^{\mathbb{P}_1}, \phi_j^{\mathbb{P}_1}\right), \qquad \mathbb{F}^{\mathbb{P}_1}_j = F\left(\phi_j^{\mathbb{P}_1}\right). \tag{3.16}$$

We then deduce from (3.10) that

$$\mathbb{A}^{\varepsilon}_{j,i} = \int_\Omega \nabla\phi_j^{\mathbb{P}_1} \cdot \overline{A}\nabla\phi_i^{\mathbb{P}_1} = \mathbb{A}^{\mathbb{P}_1}_{j,i}, \tag{3.17}$$

where we recall that the piecewise constant matrix $\overline{A}$ given by (3.11), and therefore the stiffness matrix $\mathbb{A}^{\mathbb{P}_1}$, depends on the fine-scale oscillations of A^ε. The above calculations yield the following result.

Lemma 3.2. *The stiffness matrix $\mathbb{A}^\varepsilon$ in (3.9) of the MsFEM problem (3.5) is identical to the stiffness matrix $\mathbb{A}^{\mathbb{P}_1}$ in (3.15) of the $\mathbb{P}_1$ problem (3.14).*

We note that the right-hand side vector $\mathbb{F}^\varepsilon$ in (3.9) is in general different from the right-hand side vector $\mathbb{F}^{\mathbb{P}_1}$ in (3.15), since we integrate f against highly oscillatory basis functions in the former problem and against $\mathbb{P}_1$ basis functions in the latter. The solutions U^ε and $U^{\mathbb{P}_1}$ to (3.9) and (3.15), respectively, are thus a priori different.

The above observations suggest using the identity (3.17) of the stiffness matrices to replace the MsFEM discrete problem (3.9) by the discrete problem (3.15) stemming from the $\mathbb{P}_1$ Galerkin approximation of the *single scale* problem (3.13), which itself may be easily implemented in legacy codes. This results in our non-intrusive MsFEM strategy presented in Algorithm 3.2. We can distinguish there the *offline stage* (in lines 1–14) and the *online stage* (in lines 15–20). The few lines that differ between Algorithm 3.2 and a standard $\mathbb{P}_1$ algorithm are highlighted in blue. The lines in black are already present in standard codes and are written in Algorithm 3.2 for the sake of completeness.

The superiority of Algorithm 3.2 over the classical MsFEM Algorithm 3.1 is that the global problem of the online stage (including its right-hand side) can be completely constructed and solved using a pre-existing $\mathbb{P}_1$ PDE solver. The only requirements in the legacy code are the ability to provide piecewise constant diffusion coefficients to the solver and the existence of a procedure which provides the value of the solution at any point in Ω. The part of the offline stage which manipulates fine meshes (in lines 3-6) and the post-processing step (in line 20) can, on the other hand, be developed independently. The requirement for these fine-scale solvers is that they have access to the coarse mesh $\mathscr{T}_H$ of the global solver and that they can evaluate u_H anywhere in Ω (which is useful in line 20). Note also that the fine-scale problem (3.7) is only indexed by the coarse mesh element K, in contrast to the fine-scale problem (3.4), which is indexed both by the coarse mesh element K and the vertex index i. In the latter case, one has to know, for each element K, the global number of the element vertices, a piece of information which may be difficult to access in a legacy code. In the former case, this correspondence is not needed to compute $\overline{A}$ and $\overline{u}^\varepsilon_H$, which are entirely defined element-wise.

Remark 3.3 (Link with homogenization theory)**.** The above non-intrusive implementation involves quantities which are of course reminiscent of standard quantities intro-

Algorithm 3.2 Non-intrusive MsFEM approach for Problem (3.1) (see comments in the text)

Construct a mesh $\mathscr{T}_H$ of Ω, denote N_v the number of internal vertices and $\mathscr{N}(n,K)$ the global index of the vertex of $K \in \mathscr{T}_H$ that has local index $1 \leq n \leq d+1$ in K

for all $K \in \mathscr{T}_H$ **do**
  for $1 \leq \alpha \leq d$ **do**
    Solve for $\chi_K^{\varepsilon,\alpha}$ defined by (3.7)
  end for
  Compute $\overline{A}|_K$ defined by (3.11)
end for

Set $\mathbb{A}^{\mathbb{P}_1} := 0$ and $\mathbb{F}^{\mathbb{P}_1} := 0$
for all $K \in \mathscr{T}_H$ **do**
  for $1 \leq m \leq d+1$ **do**
    Set $j := \mathscr{N}(m,K)$
    for $1 \leq n \leq d+1$ **do**
      Set $i := \mathscr{N}(n,K)$ and $\mathbb{A}^{\mathbb{P}_1}_{j,i} \mathrel{+}= a_K^{\overline{A}}\left(\phi_i^{\mathbb{P}_1}, \phi_j^{\mathbb{P}_1}\right)$
    end for
    Compute $\mathbb{F}^{\mathbb{P}_1}_j \mathrel{+}= F_K\left(\phi_j^{\mathbb{P}_1}\right)$
  end for
end for

Solve the linear system $\mathbb{A}^{\mathbb{P}_1} U^{\mathbb{P}_1} = \mathbb{F}^{\mathbb{P}_1}$

Obtain the coarse approximation $u_H = \displaystyle\sum_{i=1}^{N_v} U_i^{\mathbb{P}_1}\, \phi_i^{\mathbb{P}_1}$

Obtain the MsFEM approximation given in K by $\overline{u}_H^\varepsilon = u_H + \displaystyle\sum_{\alpha=1}^{d} (\partial_\alpha u_H)|_K\, \chi_K^{\varepsilon,\alpha}$

duced in homogenization. The problem (3.7), the effective diffusion matrix (3.11), the single-scale problem (3.13) and the expansion (3.8) resemble the corrector problem, the homogenized matrix, the homogenized problem and the two-scale expansion of the oscillatory solution, respectively. In the same spirit, in the case when A^ε is the rescaling of some periodic matrix, it can be shown (see Lemma 7.11) that the effective diffusion matrix $\overline{A}$ converges to the homogenized matrix when $\varepsilon \to 0$.

As shown by (3.17), the matrix $\mathbb{A}^{\mathbb{P}_1}$ in (3.15) is identical to the matrix $\mathbb{A}^\varepsilon$ in (3.9). However, in general, the right-hand sides $\mathbb{F}^\varepsilon$ in (3.9) and $\mathbb{F}^{\mathbb{P}_1}$ in (3.15) are different. This motivates the introduction of the following Petrov-Galerkin variant of the MsFEM: find $u_H^{\varepsilon,PG} \in V_H^\varepsilon$ such that

$$\forall\, v_H \in V_H, \qquad a^\varepsilon\left(u_H^{\varepsilon,PG}, v_H\right) = F(v_H). \tag{3.18}$$

Note that, in contrast to (3.5), we take the test functions in the $\mathbb{P}_1$ space V_H rather than in the multiscale space V_H^ε. We denote $\mathbb{A}^{\varepsilon,PG}_{j,i} = a^\varepsilon\left(\phi_i^\varepsilon, \phi_j^{\mathbb{P}_1}\right)$ the stiffness matrix of the resulting linear system. Of course, the right-hand side vector of this linear system is equal to $\mathbb{F}^{\mathbb{P}_1}$ defined by (3.16).

Lemma 3.4. *The stiffness matrices $\mathbb{A}^\varepsilon$ and $\mathbb{A}^{\varepsilon,PG}$ of the problems (3.5) and (3.18) are identical (and thus identical to $\mathbb{A}^{\mathbb{P}_1}$). The right-hand side vector of (3.18) is identical to the right-hand side vector $\mathbb{F}^{\mathbb{P}_1}$ of the problem (3.14). The solution $u_H^{\varepsilon,PG}$ to the Petrov-Galerkin MsFEM (3.18) thus coincides with the function $\overline{u}_H^\varepsilon$ computed by Algorithm 3.2.*

Proof. To prove this lemma, it is enough to show that the stiffness matrices of (3.5) and (3.18) are equal. Using an integration by parts, we compute

$$\begin{aligned} a^\varepsilon\left(\phi_i^\varepsilon, \phi_j^\varepsilon - \phi_j^{\mathbb{P}_1}\right) &= \sum_{K\in\mathscr{T}_H} \int_K \nabla\left(\phi_j^\varepsilon - \phi_j^{\mathbb{P}_1}\right)\cdot A^\varepsilon \nabla\phi_i^\varepsilon \\ &= \sum_{K\in\mathscr{T}_H} \int_{\partial K} \left(\phi_j^\varepsilon - \phi_j^{\mathbb{P}_1}\right) n\cdot A^\varepsilon\nabla\phi_i^\varepsilon - \int_K \left(\phi_j^\varepsilon - \phi_j^{\mathbb{P}_1}\right) \operatorname{div}\left(A^\varepsilon\nabla\phi_i^\varepsilon\right), \end{aligned} \tag{3.19}$$

where n is the unit outward normal vector on ∂K. The two terms above vanish in view of (3.4). This implies the identity of the stiffness matrices of (3.5) and (3.18) and the well-posedness of the Petrov-Galerkin approximation (3.18). ■

To summarize, the above procedure to go from the MsFEM problem (3.5) to its non-intrusive implementation described in Algorithm 3.2 is based on the following steps:

1. we use the linearity of the problem and the fact that gradients of $\mathbb{P}_1$ basis functions are constant in each mesh element to establish the identity (3.6);
2. we can then recast the MsFEM stiffness matrix $\mathbb{A}^\varepsilon$ as the stiffness matrix $\mathbb{A}^{\mathbb{P}_1}$ of the $\mathbb{P}_1$ discretization of an appropriate problem;
3. we approximate the right-hand side $\mathbb{F}^\varepsilon$ of the MsFEM problem by a right-hand side $\mathbb{F}^{\mathbb{P}_1}$ which can be computed in a manner consistent with a $\mathbb{P}_1$ discretization;
4. we postprocess the $\mathbb{P}_1$ solution to obtain an approximation of the reference solution.

We nowhere use in these steps that the discrete problem we are actually solving (here (3.15)) in fact corresponds to some discretization (here, a Petrov-Galerkin discretization) of the reference problem. This correspondence is useful to estimate the error introduced by the non-intrusive implementation (a task we perform in Section 3.3 below), but it does not necessarily hold for other variants of MsFEM (e.g. the oversampling variant briefly mentioned in Section 3.4 below) and it is not required to put the non-intrusive approach in action.

We expect the computational cost of Algorithm 3.2 to be smaller than that of Algorithm 3.1, since $\mathbb{F}^{\mathbb{P}_1}$ is cheaper to compute than $\mathbb{F}^\varepsilon$ (we do not need to use a quadrature rule on the fine mesh). On the other hand, Algorithm 3.2 (and non-intrusive implementations in general) may introduce additional numerical errors. We estimate these in Section 3.3.

3.3. Comparison of Galerkin and Petrov-Galerkin MsFEM

3.3.1. Theoretical results. In this section, we estimate the difference between the solutions to the Galerkin and the Petrov-Galerkin approximations (3.5) and (3.18). We first recall that, for any $v_H^\varepsilon \in V_H^\varepsilon$, there exists a unique $v_H \in V_H$ such that (3.8) holds. We now establish a variational relation between v_H^ε and v_H.

Lemma 3.5. *Let $v_H^\varepsilon \in V_H^\varepsilon$. There exists a unique $v_H \in V_H$ such that (3.8) holds, and v_H is the unique solution in V_H to the problem*

$$\forall\, w_H \in V_H, \quad a^{\overline{A}}(v_H, w_H) = a^\varepsilon(v_H^\varepsilon, w_H), \tag{3.20}$$

where $\overline{A}$ is defined by (3.11). In addition, we have $\|\nabla v_H\|_{L^2(\Omega)} \leq \dfrac{M}{m}\, \|\nabla v_H^\varepsilon\|_{L^2(\Omega)}$.

Proof. We take some $v_H^\varepsilon \in V_H^\varepsilon$ and expand it following (3.8): we thus write $v_H^\varepsilon = v_H + \sum_{K\in\mathscr{T}_H} \sum_{\alpha=1}^{d} (\partial_\alpha v_H)|_K\, \chi_K^{\varepsilon,\alpha}$ for some $v_H \in V_H$. Consider now some $w_H \in V_H$. Using (3.7), (3.11) and that ∇w_H and ∇v_H are piecewise constant, we compute that

$$a^\varepsilon(v_H^\varepsilon, w_H) = \sum_{K\in\mathscr{T}_H} \sum_{\alpha,\beta=1}^{d} (\partial_\beta w_H)|_K \left(\int_K e_\beta \cdot A^\varepsilon \left(e_\alpha + \nabla\chi_K^{\varepsilon,\alpha}\right)\right) (\partial_\alpha v_H)|_K = a^{\overline{A}}(v_H, w_H).$$

We thus observe that v_H satisfies (3.20). In addition, the equation (3.20) completely characterizes v_H, since $a^{\overline{A}}$ is coercive on $H_0^1(\Omega)$ in view of (3.12). The estimate for v_H directly follows by taking $w_H = v_H$ in (3.20) and using the coercivity of $\overline{A}$ and the upper bound on A^ε. ■

We now proceed with the following error estimate.

Lemma 3.6. *Let $u_H^{\varepsilon,G}$ denote the solution to the approximation (3.5) (provided by Algorithm 3.1), where we have added the superscript G to emphasize that (3.5) is a* Galerkin *approximation. Let $u_H^{\varepsilon,PG}$ be the solution to the Petrov-Galerkin approximation (3.18) (provided by Algorithm 3.2). Assume that $f \in L^2(\Omega)$. There exists a constant C independent of ε, H and f such that*

$$\left\| u_H^{\varepsilon,G} - u_H^{\varepsilon,PG} \right\|_{H^1(\Omega)} \leq C\, H\, \|f\|_{L^2(\Omega)}.$$

The classical error estimate for the Galerkin MsFEM approach (3.5) is obtained in the literature under the assumption that A^ε is actually the rescaling of a given periodic matrix. The bound on $\|u_H^{\varepsilon,G} - u^\varepsilon\|_{H^1(\Omega)}$ in this estimate reads $C\,(H + \sqrt{\varepsilon} + \sqrt{\varepsilon/H})$ for some C independent of ε and H (see e.g. [69]). Lemma 3.6 and a triangle inequality show that the same convergence rate holds for the Petrov-Galerkin MsFEM approach (3.18), of course under the same periodicity assumption.

Proof. Let $e_H^\varepsilon = u_H^{\varepsilon,G} - u_H^{\varepsilon,PG}$. Since the numerical approximations $u_H^{\varepsilon,G}$ and $u_H^{\varepsilon,PG}$ both belong to V_H^ε, we are in position to use (3.8) for $e_H^\varepsilon \in V_H^\varepsilon$: there thus exists $e_H^{\mathbb{P}_1} \in V_H$ such that

$$e_H^\varepsilon = e_H^{\mathbb{P}_1} + e_H^{\text{osc}} \qquad \text{with} \qquad e_H^{\text{osc}} = \sum_{K\in\mathscr{T}_H} \sum_{\alpha=1}^{d} (\partial_\alpha e_H^{\mathbb{P}_1})|_K\, \chi_K^{\varepsilon,\alpha}. \tag{3.21}$$

We can thus write

$$a^\varepsilon(e_H^\varepsilon, e_H^\varepsilon) = a^\varepsilon\left(u_H^{\varepsilon,G}, e_H^\varepsilon\right) - a^\varepsilon\left(u_H^{\varepsilon,PG}, e_H^{\mathbb{P}_1}\right) - a^\varepsilon\left(u_H^{\varepsilon,PG}, e_H^{\text{osc}}\right).$$

Since e_H^ε can be used as a test function in (3.5) and $e_H^{\mathbb{P}_1}$ in (3.18), this implies

$$a^\varepsilon(e_H^\varepsilon, e_H^\varepsilon) = (f, e_H^\varepsilon)_{L^2(\Omega)} - (f, e_H^{\mathbb{P}_1})_{L^2(\Omega)} - a^\varepsilon(u_H^{\varepsilon,PG}, e_H^{\mathrm{osc}}) = (f, e_H^{\mathrm{osc}})_{L^2(\Omega)} - a^\varepsilon(u_H^{\varepsilon,PG}, e_H^{\mathrm{osc}}).$$

Using that e_H^{osc} vanishes on all the edges of the coarse mesh (because of the boundary conditions satisfied by $\chi_K^{\varepsilon,\alpha}$), the same integration by parts that led to (3.19) shows that $a^\varepsilon\left(u_H^{\varepsilon,PG}, e_H^{\mathrm{osc}}\right) = 0$. We therefore infer from the above equation and the Cauchy-Schwarz inequality that

$$a^\varepsilon(e_H^\varepsilon, e_H^\varepsilon) \leq \|f\|_{L^2(\Omega)} \, \|e_H^{\mathrm{osc}}\|_{L^2(\Omega)} \,. \tag{3.22}$$

We proceed by bounding $\|e_H^{\mathrm{osc}}\|_{L^2(\Omega)}$ from above in terms of $\|\nabla e_H^\varepsilon\|_{L^2(\Omega)}$ in the right-hand side of (3.22). The Poincaré inequality in each K implies that there exists a constant C, independent of H but dependent on the regularity of the mesh, such that, for any $K \in \mathscr{T}_H$,

$$\|e_H^{\mathrm{osc}}\|_{L^2(K)} \leq C\, H \, \|\nabla e_H^{\mathrm{osc}}\|_{L^2(K)} \,. \tag{3.23}$$

Using the problem (3.7) satisfied by each $\chi_K^{\varepsilon,\alpha}$, the identity (3.21) and the fact that $\partial_\alpha e_H^{\mathbb{P}_1}$ is constant in each K, we observe that e_H^{osc} satisfies the following variational formulation in each $K \in \mathscr{T}_H$:

$$\forall\, v \in H_0^1(K), \qquad a_K^\varepsilon\left(e_H^{\mathrm{osc}}, v\right) = -\sum_{\alpha=1}^{d} (\partial_\alpha e_H^{\mathbb{P}_1})|_K \; a_K^\varepsilon\left(x^\alpha, v\right) = -a_K^\varepsilon\left(e_H^{\mathbb{P}_1}, v\right).$$

Upon testing against $v = e_H^{\mathrm{osc}} \in H_0^1(K)$ and using the bounds (3.2), it follows that $\|\nabla e_H^{\mathrm{osc}}\|_{L^2(K)} \leq \dfrac{M}{m} \left\|\nabla e_H^{\mathbb{P}_1}\right\|_{L^2(K)}$. We thus deduce from (3.23) that

$$\|e_H^{\mathrm{osc}}\|_{L^2(\Omega)} \leq C\, H \, \frac{M}{m} \left\|\nabla e_H^{\mathbb{P}_1}\right\|_{L^2(\Omega)} \,. \tag{3.24}$$

In order to estimate $\nabla e_H^{\mathbb{P}_1}$ in terms of e_H^ε, we apply Lemma 3.5 to $v_H^\varepsilon = e_H^\varepsilon \in V_H^\varepsilon$ and obtain that $\left\|\nabla e_H^{\mathbb{P}_1}\right\|_{L^2(\Omega)} \leq \dfrac{M}{m} \|\nabla e_H^\varepsilon\|_{L^2(\Omega)}$. Upon inserting this estimate and (3.24) in the right-hand side of (3.22), and using the lower bound (3.2) on A^ε in the left-hand side of (3.22), it follows that $\|\nabla e_H^\varepsilon\|_{L^2(\Omega)} \leq C\, H \, \|f\|_{L^2(\Omega)}$. We conclude the proof by the application of a Poincaré inequality in Ω. ■

3.3.2. Numerical results. We now present some numerical examples to illustrate the above result. We take $\Omega = (0,1)^2$, $A^\varepsilon(x) = a_{\mathrm{per}}^\varepsilon(x)\,\mathrm{Id}$ with

$$a_{\mathrm{per}}^\varepsilon(x) = 1 + 100\, \cos^2(\pi\, x_1/\varepsilon)\, \sin^2(\pi\, x_2/\varepsilon), \tag{3.25}$$

which is ε-periodic, and $f(x) = \sin(x_1)\,\sin(x_2)$. For $\varepsilon = \pi/150 \approx 0.02$, we consider the reference solution u_{ref} (computed in practice on a fine mesh of size $h = 1/1024$), and, for various values of H (ranging from $1/4$ to $1/256$), the solution $u_H^{\varepsilon,G}$ to the Galerkin approximation (3.5) and the solution $u_H^{\varepsilon,PG}$ to the Petrov-Galerkin approximation (3.18). In Table 3.1, we show the error $\left\|u_H^{\varepsilon,G} - u_{\mathrm{ref}}\right\|_{H^1(\Omega)}$ and the difference $\left\|u_H^{\varepsilon,G} - u_H^{\varepsilon,PG}\right\|_{H^1(\Omega)}$. As expected from Lemma 3.6, we observe that the difference $u_H^{\varepsilon,G} - u_H^{\varepsilon,PG}$ is extremely small (here by a factor of at least 300) in comparison to the error $u_H^{\varepsilon,G} - u_{\mathrm{ref}}$. The intrusive

and the non-intrusive MsFEMs thus share the same accuracy.

Table 3.1: *Errors between $u_H^{\varepsilon,G}$, $u_H^{\varepsilon,PG}$ and $u_{\rm ref}$ for several values of H (periodic case).*

H/ε	$\left\|u_H^{\varepsilon,G} - u_{\rm ref}\right\|_{H^1(\Omega)}$	$\left\|u_H^{\varepsilon,G} - u_H^{\varepsilon,PG}\right\|_{H^1(\Omega)}$
11.94	5.64×10^{-3}	1.55×10^{-5}
5.97	4.81×10^{-3}	1.29×10^{-5}
2.98	6.26×10^{-3}	8.51×10^{-6}
1.49	7.99×10^{-3}	1.08×10^{-5}
0.75	9.54×10^{-3}	9.93×10^{-6}
0.37	8.56×10^{-3}	6.65×10^{-6}
0.19	6.58×10^{-3}	3.53×10^{-6}

To demonstrate the robustness of our conclusions with respect to the choice of A^ε, we next consider two other cases, a locally-periodic example and a fully non-periodic one. Recall that the purpose of MsFEM approaches is to address general multiscale settings. In contrast to quantitative homogenization theory, their implementation does not rely on any geometric assumption on the microstructure, such as periodicity.

In the first situation, we set $A^\varepsilon(x) = \left(1 + \cos^2(2\pi x_1)\right) a^\varepsilon_{\rm per}(x)\,{\rm Id}$ where $a^\varepsilon_{\rm per}$ is defined by (3.25). We therefore have $A^\varepsilon(x) = A_{\rm loc-per}\left(x, \dfrac{x}{\varepsilon}\right)$ Id, where, for any fixed $x \in \Omega$, the function $y \in \mathbb{R}^d \to A_{\rm loc-per}(x, y)$ is $\mathbb{Z}^d$-periodic. In the second situation, we take

$$A^\varepsilon(x) = 1 + \left(1 + 100\cos^2(\pi x_1/\varepsilon)\sin^2(\pi x_2/\varepsilon)\right)\cos^2\left(\frac{x_1^2 + x_2^2}{\varepsilon}\right).$$

All the other parameters are identical to those of the periodic test case. In Tables 3.2 and 3.3, we show the error $\left\|u_H^{\varepsilon,G} - u_{\rm ref}\right\|_{H^1(\Omega)}$ and the difference $\left\|u_H^{\varepsilon,G} - u_H^{\varepsilon,PG}\right\|_{H^1(\Omega)}$ for various values of H. As in the periodic case, we again observe that the difference $u_H^{\varepsilon,G} - u_H^{\varepsilon,PG}$ is extremely small (by a factor of at least 50 in the locally periodic case and at least 200 in the fully non-periodic case) in comparison to the error $u_H^{\varepsilon,G} - u_{\rm ref}$. Again, the intrusive and the non-intrusive MsFEMs share the same accuracy.

3.4. Concluding remarks on possible extensions

Despite the fact that it significantly improves upon the classical FEM approach, the MsFEM approach using the basis functions ϕ_i^ε defined by (3.4) suffers from a well-known shortcoming, due to the fact that *affine* boundary conditions are imposed for ϕ_i^ε. The method cannot yield an accurate approximation of the reference solution u^ε near the edges of the coarse mesh elements, since the exact solution oscillates along the edges while the numerical approximation does not. To overcome this drawback, several alternative definitions of the multiscale basis functions have been proposed, leading to different MsFEM variants, including the oversampling variant, introduced in [98] and nowadays considered to be a reference MsFEM variant. We investigate in the remainder of Part I how the non-intrusive implementation procedure presented here can be extended to that case. We

Table 3.2: *Errors between $u_H^{\varepsilon,G}$, $u_H^{\varepsilon,PG}$ and u_{ref} for several values of H (locally periodic case).*

H/ε	$\left\|u_H^{\varepsilon,G} - u_{\mathrm{ref}}\right\|_{H^1(\Omega)}$	$\left\|u_H^{\varepsilon,G} - u_H^{\varepsilon,PG}\right\|_{H^1(\Omega)}$
11.94	3.65×10^{-3}	7.17×10^{-5}
5.97	3.17×10^{-3}	1.95×10^{-5}
2.98	4.14×10^{-3}	6.62×10^{-6}
1.49	5.33×10^{-3}	7.93×10^{-6}
0.75	6.36×10^{-3}	7.13×10^{-6}
0.37	5.71×10^{-3}	4.77×10^{-6}
0.19	4.39×10^{-3}	2.55×10^{-6}

Table 3.3: *Errors between $u_H^{\varepsilon,G}$, $u_H^{\varepsilon,PG}$ and u_{ref} for several values of H (non-periodic case).*

H/ε	$\left\|u_H^{\varepsilon,G} - u_{\mathrm{ref}}\right\|_{H^1(\Omega)}$	$\left\|u_H^{\varepsilon,G} - u_H^{\varepsilon,PG}\right\|_{H^1(\Omega)}$
11.94	8.69×10^{-3}	2.32×10^{-5}
5.97	7.11×10^{-3}	3.22×10^{-5}
2.98	8.81×10^{-3}	2.59×10^{-5}
1.49	1.12×10^{-2}	2.51×10^{-5}
0.75	1.30×10^{-2}	1.53×10^{-5}
0.37	1.07×10^{-2}	9.85×10^{-6}
0.19	7.55×10^{-3}	4.00×10^{-6}

note that oversampling multiscale basis functions are again defined in terms of $\phi_i^{\mathbb{P}_1}$ in a *linear* manner, which allows to obtain a formula analogous to (3.6). The stiffness matrices of the Galerkin and the Petrov-Galerkin approximations are in general different (in contrast to the case studied here, see Lemma 3.4), but the two of them can be expressed as the stiffness matrix obtained using a standard $\mathbb{P}_1$ approximation of the single-scale problem (3.13), for a suitably defined piecewise constant effective matrix $\overline{A}$. For the sake of conciseness of the present chapter, we postpone the presentation of all the details of these extensions to the next chapters.

To outline the versatility of the above procedure leading to a non-intrusive implementation, we eventually make a few remarks on the advection-diffusion problem

$$-\operatorname{div}(A^\varepsilon \nabla u^\varepsilon) + b \cdot \nabla u^\varepsilon = f \quad \text{in } \Omega, \qquad u^\varepsilon = 0 \quad \text{on } \partial\Omega.$$

The MsFEM basis functions may be defined by (3.4) or by a similar equation including the advection term (see e.g. [114] and Part II of this thesis). Oversampling may also be used. In all cases, for the same reasons as above, an identity of the type (3.6) holds, which allows to express the stiffness matrix of the approach as the stiffness matrix obtained using a standard $\mathbb{P}_1$ finite element approximation of a single-scale problem containing diffusion and advection terms, with appropriate definitions of a diffusion matrix $\overline{A}$ and an advection field $\overline{b}$ that are both piecewise constant. This is detailed in the remainder of Part I.

Chapter 4

The intrusive nature of the MsFEM

Chapters 4 to 7 discuss non-intrusive implementation strategies of MsFEMs, possibly after small modifications of the method. The contents of these chapters have been published in [31]. The non-intrusive approach of Chapter 3 is generalized here to a wide variety of (previously known and some unknown) MsFEMs. We focus on MsFEMs with an 'underlying $\mathbb{P}_1$ space' (to be defined in Chapter 5). In Chapter 8, we briefly consider the extension of the non-intrusive implementation strategy to higher-order MsFEMs on one particular example (in Section 8.2), and we propose different oversampling strategies for the MsFEM-CR than those proposed in [31].

In the present chapter, we recall the basic principles of the FEM and the MsFEM and we illustrate the intrusive character of the MsFEM. We also recall the non-intrusive MsFEM approach that was proposed in Chapter 3 for the simplest MsFEM variant on the example of a diffusion problem. We highlight a link between the non-intrusive MsFEM approach and classical homogenization here. Then we summarize in Chapter 5 which properties of the MsFEM are essential for the non-intrusive workflow, and show that all these properties can be found within a general framework covering a wide variety of MsFEMs. We extend the non-intrusive MsFEM approach to this general MsFEM framework in Chapter 6. In Chapter 3 we saw that the non-intrusive MsFEM approach is equivalent to a Petrov-Galerkin MsFEM (with $\mathbb{P}_1$ test functions). This is no longer true for all MsFEMs covered by our general framework, and we obtain two non-intrusive MsFEMs: the Petrov-Galerkin MsFEM, which is completely equivalent to its non-intrusive implementation, and an approximate version of the Galerkin MsFEM that can be implemented in a non-intrusive way. The three essential formulas for the formulation of the non-intrusive MsFEM can easily be compared across these chapters, since they are highlighted in special blue boxes in Chapter 4 for the diffusion setting and in Chapters 5 and 6 for the general framework. We study the difference between the original and non-intrusive MsFEM more closely in Chapter 7 for the general MsFEM framework in the setting of diffusion problems. We obtain a number of convergence results for the difference between the intrusive and non-intrusive MsFEM approximations. The different MsFEM approaches introduced in this part of the thesis are compared numerically in Section 7.4. We shall assess the efficiency of our approaches for diffusion problems with coefficients that are not covered by the convergence results of Chapter 7. Our results show that the Petrov-Galerkin MsFEM as well as the non-intrusive approximation of the Galerkin MsFEM are close to the original Galerkin MsFEM. Any possible additional error introduced by making the

MsFEM non-intrusive is thus negligible.

Notation. Let us introduce some notation that will be used in the remaining chapters of Part I. We adopt standard notation for Sobolev spaces. In particular, $H^1(\Omega)$ denotes the space of functions $u \in L^2(\Omega)$ whose first derivatives (in the sense of distributions) belong to $L^2(\Omega)$ and $H^1_0(\Omega)$ its subspace of functions with vanishing trace on the boundary of Ω. The dual space of $H^1_0(\Omega)$ is denoted $H^{-1}(\Omega)$. The space $W^{1,\infty}(\Omega)$ is the space of almost everywhere bounded functions whose derivatives are also bounded almost everywhere. Further, for a given simplicial mesh $\mathscr{T}_H$ of Ω, we use the notation $H^1(\mathscr{T}_H)$ to denote the broken Sobolev space

$$H^1(\mathscr{T}_H) = \left\{ u \in L^2(\Omega) \;\middle|\; u|_K \in H^1(K) \text{ for all mesh elements } K \in \mathscr{T}_H \right\}.$$

The standard norm for the space $H^1(\Omega)$ is $\|u\|_{H^1(\Omega)} = \sqrt{\|u\|^2_{L^2(\Omega)} + \|\nabla u\|^2_{L^2(\Omega)}}$ and the corresponding broken norm is $\|u\|_{H^1(\mathscr{T}_H)} = \sqrt{\sum_{K\in\mathscr{T}_H} \|u\|^2_{H^1(K)}}$. The space of functions whose restriction to each element of $\mathscr{T}_H$ is a polynomial of degree k is denoted $\mathbb{P}_k(\mathscr{T}_H)$.

4.1. Discrete variational formulation

Let $d \geq 1$ denote the space dimension of interest and let $\Omega \subset \mathbb{R}^d$ be a bounded polytope (e.g. a polygon in dimension $d = 2$, a polyhedron in dimension $d = 3$). Convexity of Ω can be assumed for elliptic regularity results to hold, for which we refer to [85]. This technical assumption is not necessary for the algorithmic aspects of the MsFEM that are the main focus of Part I of this thesis.

By way of example, we consider first the diffusion equation with homogeneous Dirichlet boundary conditions. In a second step, from Section 5.1.3 onwards, we will also consider more general problems, and we will mention other types of boundary conditions in Section 6.3. More precisely, we focus here on the boundary value problem

$$\begin{cases} -\mathrm{div}(A^\varepsilon \nabla u^\varepsilon) = f & \text{in } \Omega, \\ u^\varepsilon = 0 & \text{on } \partial\Omega, \end{cases} \tag{4.1}$$

where the diffusion tensor $A^\varepsilon \in L^\infty(\Omega,\ \mathbb{R}^{d\times d})$ satisfies the uniform bounds

$$\begin{aligned} &\forall\, \xi \in \mathbb{R}^d, \quad m|\xi|^2 \leq \xi \cdot A^\varepsilon(x)\, \xi \quad \text{a.e. in } \Omega, \\ \text{and} \quad &\forall\, \xi, \eta \in \mathbb{R}^d, \quad |\eta \cdot A^\varepsilon(x)\xi| \leq M\, |\xi|\, |\eta| \quad \text{a.e. in } \Omega, \end{aligned} \tag{4.2}$$

for some $M \geq m > 0$ independent of ε. The right-hand side f does not vary on the microscopic scale ε. We denote the diffusion tensor with a superscript ε to keep in mind that A^ε might be highly oscillatory on a typical length scale of size ε much smaller than the diameter of Ω (assumed to be of order 1). No further structural assumptions on A^ε are made. In particular, A^ε need not be the rescaling of a fixed periodic matrix of the form $A^\varepsilon(x) = A(x/\varepsilon)$. We will specialize to this periodic setting in Section 7.3 only to obtain convergence results, but this assumption is of no relevance for the practical implementation of the MsFEM. Let us also mention that none of the considerations in

Chapters 4 to 8 require symmetry of the diffusion tensor. Our development of non-intrusive MsFEMs also generalizes to linear *systems* of PDEs. The analysis we provide is also expected to extend to e.g. the system of linear elasticity up to some technicalities that we do not consider here.

For simplicity of exposition, we assume that $f \in L^2(\Omega)$ (rather than $f \in H^{-1}(\Omega)$, for which the problem (4.1) is in fact well-posed). We do so to avoid unnecessary technicalities. Our proposed non-intrusive MsFEM carries over to the more general case. For some convergence results, the condition $f \in L^2(\Omega)$ cannot be relaxed. In this case, this is also explicitly stated.

Problem (4.1) admits a unique solution in the space $H^1_0(\Omega)$. This solution is also characterized by the variational formulation

$$\begin{cases} \text{Find } u^\varepsilon \in H^1_0(\Omega) \text{ such that} \\ \quad a^{\varepsilon,\mathsf{diff}}(u^\varepsilon, v) = F(v) \qquad \text{for all } v \in H^1_0(\Omega), \end{cases} \tag{4.3}$$

where the bilinear form $a^{\varepsilon,\mathsf{diff}}$ and the linear form F are defined, for any $u, v \in H^1_0(\Omega)$, by

$$a^{\varepsilon,\mathsf{diff}}(u, v) = \int_\Omega \nabla v \cdot A^\varepsilon \nabla u, \qquad F(v) = \int_\Omega f v. \tag{4.4}$$

The coercivity hypothesis in (4.2) ensures that the bilinear form $a^{\varepsilon,\mathsf{diff}}$ is coercive on the space $H^1_0(\Omega)$. Then the Lax-Milgram Theorem [81, Theorem 5.8] shows that (4.3) is indeed well-posed.

The numerical approximation of (4.3) with a finite element method starts by the introduction of a mesh $\mathscr{T}_H$ for Ω. The subscript H denotes the typical size of the mesh elements. We assume $\mathscr{T}_H$ to be a simplicial, conformal mesh. For some convergence results, we shall assume quasi-uniformity. These assumptions are standard in finite element analysis. We refer, e.g., to [129, 52, 73] for a general exposition and various examples. Again, these regularity properties of the mesh do not have any impact on the implementation of the MsFEM on a given mesh. The regularity plays a role only to obtain convergence results.

A finite element method for (4.1) is obtained by restricting the equivalent formulation (4.3) to a finite-dimensional subspace of $H^1_0(\Omega)$, typically consisting of functions that are piecewise polynomial on the mesh $\mathscr{T}_H$. We suppose that we are in the regime where H is larger than or comparable to the microscale ε. In this case, it is well known that a Galerkin approximation of (4.3) on, say, the standard (conforming) Lagrange $\mathbb{P}_1$ space on $\mathscr{T}_H$ provides only a poor, not to say an incorrect approximation of u^ε. See Section 2.1.2 and [12, Example 1.1], for instance, for explicit examples where the $\mathbb{P}_1$ approximation on a coarse mesh fails. At the same time, the use of a finite element method on a fine mesh of size $H \ll \varepsilon$ might be unfeasible from a computational point of view because of its prohibitive computational cost. To remedy this issue, we shall next introduce the *multiscale finite element method* (MsFEM) [98, 69].

4.2. A simple multiscale finite element method

The MsFEM is a Galerkin approximation of (4.3) for which the approximation space is adapted in order to achieve satisfactory accuracy even on a coarse mesh. The correct choice of approximation space yields a numerical approximation that is much closer to

u^ε than a standard $\mathbb{P}_1$-approximation when ε is smaller than H, and especially when ε becomes asymptotically small. To begin with, we introduce here the simplest variant of the MsFEM, which originally appeared in [98], before moving on to other MsFEM variants in Section 5.1.3.

Let $x_1, \ldots, x_{N_0}$ be an enumeration of the interior vertices of the mesh $\mathscr{T}_H$, i.e., the vertices that do not lie on $\partial\Omega$. We denote by $\phi_i^{\mathbb{P}_1}$ the unique piecewise $\mathbb{P}_1$ function such that $\phi_i^{\mathbb{P}_1}(x_j) = \delta_{i,j}$ for all $1 \le j \le N_0$. (These are the basis functions for the standard $\mathbb{P}_1$ Lagrange finite element.) We define the *multiscale basis functions* ϕ_i^ε (for $1 \le i \le N_0$) by

$$\forall\, K \in \mathscr{T}_H, \quad \begin{cases} -\mathrm{div}(A^\varepsilon \nabla \phi_i^\varepsilon) = 0 & \text{in } K, \\ \phi_i^\varepsilon = \phi_i^{\mathbb{P}_1} & \text{on } \partial K. \end{cases} \tag{4.5}$$

All these problems, on each mesh element K, are again well-posed by coercivity of A^ε and the Lax-Milgram Theorem. The functions ϕ_i^ε so defined belong to the global space $H_0^1(\Omega)$ because the local boundary conditions on ∂K imply continuity across all mesh elements K. It is also immediately seen that ϕ_i^ε is supported by exactly the same mesh elements as $\phi_i^{\mathbb{P}_1}$.

Remark 4.1. On each mesh element K, problem (4.5) defines at most $d+1$ non-trivial basis functions. Let $i_1, \ldots, i_{d+1}$ be the indices of the vertices of K. It is easily inferred from (4.5) that $\phi_{i_{d+1}}^\varepsilon\Big|_K = 1 - \sum_{j=1}^{d} \phi_{i_j}^\varepsilon\Big|_K$. Thus, one only has to compute d basis functions by the resolution of the PDE (4.5) on K.

The multiscale approximation space is defined as $V_{H,0}^\varepsilon = \mathrm{span}\{\phi_i^\varepsilon \mid 1 \le i \le N_0\}$. This is a finite-dimensional space of the same dimension as the one used for a $\mathbb{P}_1$ Lagrange finite element approximation on the mesh $\mathscr{T}_H$. The MsFEM consists in computing the approximation $u_H^\varepsilon \in V_{H,0}^\varepsilon$ defined by the problem

$$\forall\, v_H^\varepsilon \in V_{H,0}^\varepsilon, \qquad a^{\varepsilon,\mathsf{diff}}(u_H^\varepsilon, v_H^\varepsilon) = F(v_H^\varepsilon)\,. \tag{4.6}$$

Since $V_{H,0}^\varepsilon$ is a subspace of $H_0^1(\Omega)$, the bilinear form $a^{\varepsilon,\mathsf{diff}}$ is coercive on $V_{H,0}^\varepsilon$ and the discrete problem (4.6) is again well-posed by virtue of the Lax-Milgram Theorem.

The computation of the multiscale basis functions ϕ_i^ε is called the *offline stage* of the MsFEM and only has to be carried out once if (4.1) has to be solved multiple times for different right-hand sides. Also note that all problems (4.5) are independent of each other, and can thus be solved in parallel. Once all basis functions are known, one can compute the stiffness matrix of the MsFEM (see Section 4.3 for more details), which is also part of the offline stage. In practice, the ϕ_i^ε are approximated numerically on a fine mesh of $K \in \mathscr{T}_H$ of mesh size $h \le \varepsilon$ that resolves the oscillations of A^ε. We omit these details here because they have no importance for the non-intrusive strategy that we shall propose below.

The resolution of the global problem (4.6), each time the right-hand side F changes, is called the *online stage*. The computational cost for this problem is the same as for a standard $\mathbb{P}_1$ approximation on the same mesh. A further discussion of the practical implementation of the MsFEM is provided in Section 4.3. This discussion partially reproduces some elements of Chapter 3. We include it here to clarify and motivate the developments in the sequel.

4.3. Intrusive workflow

The practical resolution of the global problem (4.6) consists in the construction and resolution of the following linear system:

$$\mathbb{A}^{\varepsilon} U^{\varepsilon} = \mathbb{F}^{\varepsilon}, \tag{4.7}$$

with the stiffness matrix $\mathbb{A}^{\varepsilon}$ and the right-hand side $\mathbb{F}^{\varepsilon}$ of the linear system given by

$$\forall\, 1 \leq i,\, j \leq N_0, \quad \mathbb{A}^{\varepsilon}_{j,i} = a^{\varepsilon,\mathsf{diff}}\left(\phi^{\varepsilon}_i,\, \phi^{\varepsilon}_j\right), \quad \mathbb{F}^{\varepsilon}_j = F\left(\phi^{\varepsilon}_j\right), \tag{4.8}$$

where we recall that N_0 denotes the number of interior vertices of $\mathscr{T}_H$. The MsFEM approximation u^{ε}_H is given by $u^{\varepsilon}_H = \sum_{i=1}^{N_0} U^{\varepsilon}_i \phi^{\varepsilon}_i$. The MsFEM can then be written (as it is traditionally presented) as in Algorithm 4.1. We use the notation $a^{\varepsilon,\mathsf{diff}}_K(u,v) = \int_K \nabla v \cdot A^{\varepsilon} \nabla u$ for all $u, v \in H^1(K)$ and we write $F_K(v) = \int_K fv$ for any $v \in L^2(K)$.

Algorithm 4.1 MsFEM approach for problem (4.1) (see comments in the text)

1: Construct a mesh $\mathscr{T}_H$ of Ω, denote N_0 the number of internal vertices and $\mathscr{N}(n,K)$ the global index of the vertex of $K \in \mathscr{T}_H$ that has local index $1 \leq n \leq d+1$ in K
2: Set $\mathbb{A}^{\varepsilon} := 0$ and $\mathbb{F}^{\varepsilon} := 0$
3: **for all** $K \in \mathscr{T}_H$ **do**
4: **for** $1 \leq n \leq d+1$ **do**
5: Set $i := \mathscr{N}(n,K)$
6: Solve for $\phi^{\varepsilon}_i|_K$ in (4.5)
7: **end for**
8: **for** $1 \leq l \leq d+1$ **do**
9: Set $j := \mathscr{N}(l,K)$
10: **for** $1 \leq n \leq d+1$ **do**
11: Set $i := \mathscr{N}(n,K)$ and $\mathbb{A}^{\varepsilon}_{j,i} \mathrel{+}= a^{\varepsilon,\mathsf{diff}}_K(\phi^{\varepsilon}_i,\, \phi^{\varepsilon}_j)$
12: **end for**
13: Set $\mathbb{F}^{\varepsilon}_j \mathrel{+}= F_K(\phi^{\varepsilon}_j)$
14: **end for**
15: **end for**
16: Solve the linear system $\mathbb{A}^{\varepsilon} U^{\varepsilon} = \mathbb{F}^{\varepsilon}$
17: Obtain the MsFEM approximation $u^{\varepsilon}_H = \sum_{i=1}^{N_0} U^{\varepsilon}_i \phi^{\varepsilon}_i$

Lines 1-12 of Algorithm 4.1 (resp. 13-17) constitute the offline (resp. online) stage of the MsFEM. Note that the computation of the stiffness matrix $\mathbb{A}^{\varepsilon}$ in line 11 only depends on the multiscale basis functions (and not on the right-hand side f) and can therefore be carried out once and for all in the offline stage. Also note that, for an efficient computation of the ϕ^{ε}_i in line 6, one should apply Remark 4.1. Only the online stage is to be repeated when problem (4.1) is to be solved multiple times for various right-hand sides f.

Implementing Algorithm 4.1 in an industrial code is challenging. Indeed, the practical implementation of any finite element method relies on (i) the construction of a mesh, (ii)

the construction of the linear system associated to the discrete variational formulation and (iii) the resolution of the linear system. An efficient implementation of the second step heavily relies on the choice of the discretization space.

Regarding the construction of the linear system (performed in line 11 of Algorithm 4.1), it is by no means obvious to adapt existing finite element codes based on generic approximation spaces (for instance spaces of piecewise polynomial functions, such as the piecewise affine functions that we will introduce in Definition 5.4 below) to a different, problem-dependent choice of space such as V_H^ε. No analytic expressions for the basis functions ϕ_i^ε are available (and thus a fine mesh should be used to approximate them), the computation of $a_K^\varepsilon(\phi_i^\varepsilon, \phi_j^\varepsilon)$ should be performed by quadrature rules on the fine mesh because the integrands are highly oscillatory, one should have at hand the correspondence between element and vertex indices of the coarse mesh ($\mathscr{N}(n, K)$ in Algorithm 4.1), the assembly of the global stiffness matrix $\{\mathbb{A}_{j,i}^\varepsilon\}_{1\le i,j\le N_0}$ should be executed by a dedicated new piece of software, etc. To alleviate these obstacles, we introduce below a way of implementing the MsFEM that capitalizes on an existing code for solving (4.1) by a $\mathbb{P}_1$ approximation on $\mathscr{T}_H$ in the case of slowly varying diffusion coefficients. The three central identities for our approach that we aim to generalize in the remainder of Part I are framed in distinctive blue boxes.

4.4. Effective problem on the macroscopic scale

Let us consider the construction of the stiffness matrix of the MsFEM in more detail. The stiffness matrix defined in (4.8) requires the computation of the quantities

$$\mathbb{A}_{j,i}^\varepsilon = a^{\varepsilon,\mathsf{diff}}(\phi_i^\varepsilon, \phi_j^\varepsilon) = \sum_{K\in\mathscr{T}_H} \int_K \nabla\phi_j^\varepsilon \cdot A^\varepsilon \nabla\phi_i^\varepsilon, \tag{4.9}$$

for all $1 \le i, j \le N_0$.

Following Chapter 3, we rewrite the multiscale basis functions as

$$\boxed{\forall\, K \in \mathscr{T}_H, \qquad \phi_i^\varepsilon = \phi_i^{\mathbb{P}_1} + \sum_{\alpha=1}^d \left(\partial_\alpha \phi_i^{\mathbb{P}_1}\right)\big|_K \chi_K^{\varepsilon,\alpha} \quad \text{in } K,} \tag{4.10}$$

for all $1 \le i \le N_0$, where, for each mesh element K, we define the numerical corrector $\chi_K^{\varepsilon,\alpha} \in H_0^1(\Omega)$ $(1 \le \alpha \le d)$ as the function supported by K that is the unique solution to the local problem

$$\boxed{\begin{cases} -\mathrm{div}(A^\varepsilon \nabla \chi_K^{\varepsilon,\alpha}) = \mathrm{div}(A^\varepsilon e_\alpha) & \text{in } K, \\ \chi_K^{\varepsilon,\alpha} = 0 & \text{on } \partial K. \end{cases}} \tag{4.11}$$

Here, e_α denotes the α-th canonical unit vector of $\mathbb{R}^d$. The expansion (4.10) is obtained upon rewriting (4.5) as a PDE for $\phi_i^\varepsilon - \phi_i^{\mathbb{P}_1}$, and then using linearity of the PDE and the fact that $\nabla\phi_i^{\mathbb{P}_1}$ is constant in K to show that $\sum_{\alpha=1}^d \left(\partial_\alpha \phi_i^{\mathbb{P}_1}\right)\big|_K \chi_K^{\varepsilon,\alpha}$ is indeed the unique solution to this PDE.

Inserting (4.10) for the trial and test functions in (4.9) and again exploiting the fact that all $\phi_i^{\mathbb{P}_1}$ have piecewise constant gradients, we obtain

$$\begin{aligned}\mathbb{A}^{\varepsilon}_{j,i} &= \sum_{K\in\mathscr{T}_H}\sum_{\alpha,\beta=1}^{d} \left(\partial_\beta\phi_j^{\mathbb{P}_1}\right)\big|_K \left(\int_K \left(e_\beta + \nabla\chi_K^{\varepsilon,\beta}\right)\cdot A^\varepsilon\left(e_\alpha + \nabla\chi_K^{\varepsilon,\alpha}\right)\right)\left(\partial_\alpha\phi_i^{\mathbb{P}_1}\right)\big|_K \\ &= \sum_{K\in\mathscr{T}_H}\sum_{\alpha,\beta=1}^{d} \left(\partial_\beta\phi_j^{\mathbb{P}_1}\right)\big|_K\, a_K^{\varepsilon,\mathsf{diff}}\left(x^\alpha + \chi_K^{\varepsilon,\alpha}, x^\beta + \chi_K^{\varepsilon,\beta}\right)\left(\partial_\alpha\phi_i^{\mathbb{P}_1}\right)\big|_K .\end{aligned}$$

Next we define the piecewise constant effective diffusion tensor $\overline{A}\in\mathbb{P}_0(\mathscr{T}_H,\,\mathbb{R}^{d\times d})$ by

$$\overline{A}_{\beta,\alpha}\big|_K = \frac{1}{|K|}a_K^{\varepsilon,\mathsf{diff}}\left(x^\alpha + \chi_K^{\varepsilon,\alpha},\, x^\beta + \chi_K^{\varepsilon,\beta}\right), \tag{4.12}$$

for each $K\in\mathscr{T}_H$ and all $1\le\alpha,\beta\le d$, and where $|K|$ denotes the measure of the mesh element K. Then (4.9) can be written as

$$\boxed{\mathbb{A}^{\varepsilon}_{j,i} = \int_\Omega \nabla\phi_j^{\mathbb{P}_1}\cdot\overline{A}\,\nabla\phi_i^{\mathbb{P}_1}.} \tag{4.13}$$

Motivated by (4.13), we introduce the coarse-scale problem

$$\begin{cases} -\mathrm{div}\left(\overline{A}\,\nabla u\right) = f & \text{in } \Omega, \\ \qquad\qquad\quad u = 0 & \text{on } \partial\Omega, \end{cases} \tag{4.14}$$

and its Galerkin discretization with $\mathbb{P}_1$ Lagrange elements: with

$$V_{H,0} = \mathrm{span}\left\{\phi_i^{\mathbb{P}_1} \mid 1\le i\le N_0\right\}$$

(note that the definition of $V_{H,0}$ will be generalized in Definition 5.5), find $u_{H,0}\in V_{H,0}$ such that

$$\forall\, v_H\in V_{H,0},\quad \overline{a}^{\mathsf{diff}}(u_H, v_H) = F(v_H), \tag{4.15}$$

where the linear form F is defined in (4.3) and the bilinear form $\overline{a}^{\mathsf{diff}}$ is defined as

$$\forall\, u,v\in H_0^1(\Omega),\quad \overline{a}^{\mathsf{diff}}(u,v) = \int_\Omega \nabla v\cdot\overline{A}\,\nabla u. \tag{4.16}$$

Problem (4.15) equivalently writes

$$\mathbb{A}^{\mathbb{P}_1}\,U^{\mathbb{P}_1} = \mathbb{F}^{\mathbb{P}_1}, \tag{4.17}$$

with

$$\forall\, 1\le i,j\le N_0,\quad \mathbb{A}^{\mathbb{P}_1}_{j,i} = \overline{a}^{\mathsf{diff}}\left(\phi_i^{\mathbb{P}_1},\phi_j^{\mathbb{P}_1}\right),\quad \mathbb{F}^{\mathbb{P}_1}_j = F\left(\phi_j^{\mathbb{P}_1}\right). \tag{4.18}$$

Comparing the expressions (4.13) and (4.18), we deduce that $\mathbb{A}^{\varepsilon} = \mathbb{A}^{\mathbb{P}_1}$. In other words:

Lemma 4.2. *The stiffness matrix of the MsFEM problem (4.6) is identical to the stiffness matrix of the $\mathbb{P}_1$ problem (4.15).*

This lemma immediately implies that the $\mathbb{P}_1$ problem (4.15) is well-posed, since the MsFEM (4.6) itself is well-posed.

Let us point out that problems (4.14) and (4.15) are defined entirely in terms of quantities that vary only on the macroscopic scale H. The finite element problem (4.15) can thus be solved using a legacy code that is designed for standard FEMs. Lemma 4.2 then suggests including the $\mathbb{P}_1$ approximation (4.15) of the effective, coarse-scale problem (4.14) as an integral part of the MsFEM approach. We do so in Algorithm 4.2 below.

The right-hand side vector $\mathbb{F}^\varepsilon$ in (4.8) is, in general, different from $\mathbb{F}^{\mathbb{P}_1}$ in (4.18). Indeed, we integrate the product of f with highly oscillatory basis functions in the former problem and with $\mathbb{P}_1$ basis functions in the latter. The solutions U^ε and $U^{\mathbb{P}_1}$ to (4.7) and (4.17), respectively, are thus different a priori.

4.5. Non-intrusive workflow

We propose the following non-intrusive MsFEM variant:

$$\begin{aligned} &\text{Set } u_H^\varepsilon = u_H + \sum_{K\in\mathscr{T}_H} (\partial_\alpha u_H)|_K\, \chi_K^{\varepsilon,\alpha} \in V_{H,0}^\varepsilon, \\ &\text{where } u_H \in V_{H,0} \text{ is the unique solution to (4.15).} \end{aligned} \tag{4.19}$$

The MsFEM approximation u_H^ε is well-defined, since we have seen above that problem (4.15) is well-posed.

Note that the symbol u_H^ε shall be used here and in the sequel for the solution to various MsFEMs variants to alleviate the notation. The exact MsFEM will be specified by the context. We will use distinct notation for different MsFEM variants when required for clarity.

The most efficient way to compute u_H^ε from u_H is not as stated here, however. The *evaluation* of $u_H(x)$ may require the determination of the degrees of freedom associated to the simplex K to which x belongs. This demands the use of the internal mechanisms of the legacy code that is used to compute u_H. The use of the legacy code can be avoided by expanding u_H as follows. For any affine function φ on K, we have

$$\varphi(x) = \varphi\left(x_{c,K}\right) + \sum_{\alpha=1}^{d} \partial_\alpha\varphi\,\left(x^\alpha - x_{c,K}^\alpha\right) \quad \text{on } K, \tag{4.20}$$

where x^α denotes the function that to a point $x \in \Omega$ associates its α-th coordinate, and $x_{c,K} = (x_{c,K}^1, \ldots, x_{c,K}^d)$ is the centroid of K. If one uses the legacy code to store the values of $u_H(x_{c,K})$ and $\partial_\alpha u_H$ element by element at the end of the online stage, then u_H^ε defined in (4.19) can be computed element by element according to

$$\forall\, K \in \mathscr{T}_H, \quad u_H^\varepsilon(x) = u_H(x_{c,K}) + \sum_{\alpha=1}^{d} (\partial_\alpha u_H)|_K \left(x^\alpha - x_{c,K}^\alpha + \chi_K^{\varepsilon,\alpha}(x)\right) \quad \text{on } K, \tag{4.21}$$

without using the legacy code.

The above observations culminate in the computational approach presented in Algorithm 4.2. We can distinguish

(1) the offline stage consisting of lines 1-7,

(2) the online stage being executed entirely in line 8,

(3) a post-processing step in line 9.

Algorithm 4.2 Non-intrusive MsFEM approach for problem (4.1)

1: Let $\mathscr{T}_H$ be the mesh used by the legacy code
2: **for all** $K \in \mathscr{T}_H$ **do**
3: **for** $1 \leq \alpha \leq d$ **do**
4: Solve for $\chi_K^{\varepsilon,\alpha}$ defined by (4.11)
5: **end for**
6: Compute $\overline{A}|_K$ defined by (4.12)
7: **end for**
8: Use the legacy code to solve for u_H defined by (4.15) and to save $\{u_H(x_{c,K})\}_{K\in\mathscr{T}_H}$ and $\{(\partial_\alpha u_H)|_K\}_{K\in\mathscr{T}_H,\,1\leq\alpha\leq d}$
9: Obtain the MsFEM approximation u_H^ε by (4.21)

The superiority of Algorithm 4.2 over the classical MsFEM Algorithm 4.1 is that the global problem of the online stage can completely be constructed and solved by the use of a pre-existing $\mathbb{P}_1$ PDE solver. The only requirements for the legacy code are the functionality to provide piecewise constant diffusion coefficients to the solver and the existence of a procedure to store the value of the $\mathbb{P}_1$ solution and its gradient at the centroids of the mesh. An additional advantage in the online stage is that the construction of the right-hand side $\mathbb{F}^{\mathbb{P}_1}$ (see (4.18)) for the global problem only requires a numerical quadrature on the coarse mesh and is therefore cheaper than the construction of $\mathbb{F}^\varepsilon$ (see (4.8)), involving the multiscale basis functions and requiring numerical quadratures at the microscale.

The part of the offline stage that manipulates fine meshes (lines 2-7) and the post-processing step can be developed independently of the legacy code used in line 8. The requirement for these fine-scale solvers is that they have access to the coarse mesh $\mathscr{T}_H$ used by the global solver. Note also that the local problem (4.11) is only indexed by the coarse mesh element K, in contrast to the local problem (4.5) that is indexed both by the coarse mesh element K and the vertex index i. For the latter problems, one has to know, for each element K, the global index that corresponds to the vertices of K, a piece of information that may be difficult to access in a legacy code. For the problems (4.11), this correspondence is not needed to compute $\overline{A}$, nor for the computation of the fine-scale solution u_H^ε in (4.21), both of which are entirely defined element-wise.

Remark 4.3 (Quantities of interest)**.** In the post-processing step of Algorithm 4.2, it is easy to compute pointwise values of the approximation u_H^ε by (4.21) and to use these for further computational steps, such as the evaluation of the energy or other quantities of interest. This task can be carried out element wise, hence Equation (4.21) can easily be used. (See also Remark 7.13.)

Remark 4.4 (Visualization)**.** We focus our attention here on the visualization of the MsFEM approximation u_H^ε, which can be an important tool in engineering practices. Visualization requires the combination of information on neighbouring mesh elements, and this can in general not be carried out by the legacy code since it does not have access to the fine meshes used to compute the numerical correctors. Even if this were the case,

the fine meshes may not yield a globally conformal mesh when combined. The question of a global visualization then becomes a complex one that requires innovations beyond the contributions of this thesis. Instead, we propose the following two-step visualization approach:

- One can visualize the coarse part u_H of the MsFEM approximation for a global view of the solution with the tools provided by the legacy code that is used to compute u_H;
- The fine scale details of u_H^ε in regions of interest can be studied through zooms inside mesh elements, using the code that is used for computations at the microscale.

4.6. Interpretation of the non-intrusive MsFEM

We emphasized above that the right-hand sides of the linear system for the MsFEM in (4.8) and the linear system solved for the non-intrusive MsFEM in (4.18) are different in general. This motivates the comparison of the non-intrusive MsFEM approach (4.19) to the following Petrov-Galerkin MsFEM:

$$\text{Find } u_H^\varepsilon \in V_{H,0}^\varepsilon \text{ such that } a^{\varepsilon,\mathsf{diff}}\left(u_H^\varepsilon, \phi_j^{\mathbb{P}_1}\right) = F\left(\phi_j^{\mathbb{P}_1}\right) \quad \text{for all } 1 \le j \le N_0, \tag{4.22}$$

based on the trial space $V_{H,0}^\varepsilon$ and the test space $V_{H,0}$ for both the bilinear and the linear form. The following result was shown in Lemma 3.4.

Lemma 4.5. *The non-intrusive MsFEM variant (4.19) coincides with the Petrov-Galerkin MsFEM (4.22).*

The non-intrusive MsFEM approach is generalized in Chapter 6 after the development of a general framework to define a wide variety of MsFEMs in Section 5.1.3. Lemma 4.5 does not generalize to the full framework. We will see the conditions under which the non-intrusive approach leads to a Petrov-Galerkin MsFEM in Lemma 6.4.

4.7. Relation to homogenization theory

We highlight in this section the fact that many ingredients of our non-intrusive MsFEM approach are reminiscent of standard quantities of homogenization theory, or the theory of H-convergence, which studies the limit of a sequence of solutions u^ε to a PDE as ε tends to 0. This relation to H-convergence provides an interesting interpretation of the effective tensor $\overline{A}$ introduced in (4.12).

Let us suppose in this section (and in this section only for the purposes of Part I, except for Section 7.3) that $A^\varepsilon(x) = A^{\mathsf{per}}(x/\varepsilon)$ for some bounded, $\mathbb{Z}^d$-periodic matrix A^{per} satisfying the coercivity property in (4.2). In this case, the sequence of matrices A^ε has a homogenized limit that is explicitly known. (An explicit characterization of the limit is not available for H-convergence in general.) We summarize the main results below. See, for instance, [28, 134] or [7, Chapter 1] for details on periodic homogenization.

Due to H-convergence of A^ε, the functions u^ε, solution to (4.1), converge to a limit function $u^\star$ (weakly in $H^1(\Omega)$, strongly in $L^2(\Omega)$) as $\varepsilon \to 0$. The homogenized limit $u^\star$ is

the solution to the homogenized equation (4.25) below.

Let Q denote the unit cube of $\mathbb{R}^d$. We introduce the corrector functions $w_1, \dots, w_d \in H^1_{per}(Q)$ solution to

$$\begin{cases} -\mathrm{div}(A^{\mathsf{per}} \nabla w_\alpha) = \mathrm{div}(A^{\mathsf{per}} e_\alpha) & \text{in } \mathbb{R}^d, \\ w_\alpha \text{ is } Q\text{-periodic}, \end{cases} \tag{4.23}$$

which uniquely defines w_α up to an irrelevant additive constant. The entries of the (constant) homogenized diffusion tensor $A^\star \in \mathbb{R}^{d\times d}$ are given by

$$A^\star_{\beta,\alpha} = \int_Q (e_\beta + \nabla w_\beta) \cdot A^{\mathsf{per}} (e_\alpha + \nabla w_\alpha), \qquad 1 \le \alpha,\, \beta \le d. \tag{4.24}$$

The homogenized limit $u^\star$ of u^ε is the unique solution in $H^1_0(\Omega)$ to the boundary value problem

$$\begin{cases} -\mathrm{div}(A^\star \nabla u^\star) = f & \text{in } \Omega, \\ u^\star = 0 & \text{on } \partial\Omega. \end{cases} \tag{4.25}$$

The truncated reconstruction of $u^\star$ that is called the first-order two-scale expansion takes the form

$$u^{\varepsilon,1}(x) = u^\star(x) + \varepsilon \sum_{\alpha=1}^{d} \partial_\alpha u^\star(x)\, w_\alpha\left(\frac{x}{\varepsilon}\right). \tag{4.26}$$

Under suitable regularity assumptions, the difference $u^\varepsilon - u^{\varepsilon,1}$ converges to 0 strongly in $H^1(\Omega)$ as $\varepsilon \to 0$. This property will be used for the convergence results in Section 7.3.

In the periodic setting, the expansion (4.26) can be used to construct a numerical approximation of u^ε, without the need of any computations at the fine scale. This approximation is presumably valid only in the regime of very small parameters ε and deteriorates if ε grows. Moreover, in more general settings, the corrector functions are not local nor explicit, for their definition involves a PDE posed on the whole domain Ω and that depends on an effective tensor that is itself defined in terms of the corrector functions. Details can be found, e.g., in [7, 124, 134]. This prevents the H-convergence theory from being directly applicable for the numerical approximation of u^ε.

Numerical homogenization techniques, that draw their inspiration from the various elements above, offer an alternative for the approximation of u^ε that can be applied in much more general contexts. We can see the similarities between the corrector functions w_α in (4.23) and the numerical correctors $\chi_K^{\varepsilon,\alpha}$ in (4.11). Note that the $\chi_K^{\varepsilon,\alpha}$ solve problems similar to (4.23), but that they need to be solved at the microscale and on each mesh element K. Similarly, we note the resemblance between the reconstruction (4.26) and the definition of u_H^ε in (4.19), and between the homogenized coefficient $A^\star$ defined in (4.24) and the effective macroscopic coefficient $\overline{A}$ from (4.12). However, contrary to $A^\star$, the MsFEM quantity $\overline{A}$ has to be computed on an element-by-element basis, and it is not necessarily constant throughout Ω. Finally, the MsFEM analogue of the homogenized problem (4.25) is the resolution of the effective macroscale problem (4.14).

Example 4.6. A particular setting, although academic in nature and only useful for pedagogical purposes, actually leads to an MsFEM approximation that is exactly equivalent to a discretization of the periodic homogenization setting. Consider (4.1) in 2D posed on the unit square. Let us consider a mesh consisting of squares that are per-

fectly aligned with the periodicity of A^ε. We solve the corrector problems (4.11) on all square mesh elements with periodic boundary conditions and subsequently compute the effective diffusion tensor $\overline{A}$ according to (4.12).
In this case, the problems for the numerical correctors all reduce to (4.23) and $\overline{A}$ is constant and equal to the homogenized coefficient $A^\star$ as defined by (4.24). A $\mathbb{Q}_1$ discretization of the effective problem (4.14) thus constitutes a non-intrusive MsFEM that is equivalent to the $\mathbb{Q}_1$ approximation of the homogenized equation (4.25).

Chapter 5

A general framework for multiscale finite element methods

5.1. Why develop a general framework?

In this chapter we develop a general framework for a wide variety of MsFEMs in an abstract setting. We motivate first why this general framework for MsFEMs is useful.

5.1.1. Local boundary conditions. First, let us explain why various MsFEMs have been proposed in the literature. One reason is that different equations than (4.1) (e.g. advection-diffusion equations) give rise to different choices of the local problem (4.5), depending on which terms of the global PDE are included (see, for instance, [114] and Part II of this thesis.)

The other reason is that, even for the pure diffusion problem (4.1), the choice of the basis functions defined in (4.5) has an important drawback. The definition of the multiscale basis functions requires a choice of *arbitrary* boundary conditions on the mesh element boundary ∂K, since the exact boundary condition satisfied by u^ε is unknown. In (4.5), affine boundary conditions are imposed. In view of this choice, we shall refer to the MsFEM defined above as the 'MsFEM-lin'.

The MsFEM-lin cannot yield an accurate representation of u^ε near ∂K if A^ε is highly oscillatory and the mesh $\mathscr{T}_H$ is coarse. Variations on the definition of the functions ϕ_i^ε have been proposed to improve the MsFEM. Here we summarize the ideas of *oversampling* and of MsFEM *à la Crouzeix-Raviart*, which together inspire the formulation of a general MsFEM framework in this chapter.

The oversampling variant of the MsFEM was introduced along with the variant based on (4.5) at the time of its first appearance in [98]. For this method, an oversampling domain S_K is associated to each mesh element K (details are provided in Section 5.4.1). The problems (4.5) are solved on the larger domain S_K rather than K, so the inadequate boundary conditions are pushed away from the actual mesh elements. To construct the multiscale basis functions, the resulting functions on S_K are restricted to the actual mesh elements K and suitably combined around each vertex x_i. The new multiscale basis functions oscillate on ∂K if the oversampling patch is taken large enough. We note that, in general, this strategy leads to discontinuous basis functions. Hence, the finite element space obtained is no longer conforming.

The MsFEM with Crouzeix-Raviart type boundary conditions for the local problems (which we shall abbreviate as 'MsFEM-CR') was introduced in [112]. It uses basis functions associated to the edges of the mesh (in contrast to the MsFEM-lin presented above, and its oversampling variant, where basis functions are associated to the vertices of the mesh). A typical basis function satisfies the following on ∂K: the flux through each face of K is constant, and the constants are determined by the condition that the average of the basis function be 1 over one particular face and 0 over all other faces. Again, this is a way to avoid imposing any conditions on the trace of the basis function directly. The multiscale functions can thus be oscillatory on the faces of the mesh. As is the case for oversampling methods, the resulting finite element space is non-conforming.

All of these variations, applied to any MsFEM for linear second-order PDEs, are covered by the general MsFEM framework.

5.1.2. The non-intrusive approach. The intrusiveness of the specific MsFEM-lin variant introduced in Section 4.2 is exemplary for all MsFEMs described in Section 5.1.1. It turns out that the non-intrusive MsFEM approach introduced in Chapter 3 and recalled in Section 4.5 can also be generalized to all these MsFEM variants. We summarize the key ingredients that allow for the formulation of the non-intrusive MsFEM approach of Algorithm 4.2 (corresponding to the identities in the blue boxes in Section 4.4).

The non-intrusive MsFEM follows from the expansion (4.10), namely the expression of the multiscale basis function as a $\mathbb{P}_1$ basis function and a linear combination of numerical correctors that are fully localized. We note that

- the full localization of the numerical correctors defined in (4.11) allows the pre-processing of the microstructure independently of the global approximation indices related to the finite element method;
- the expansion (4.10) follows from the fact that $\nabla\phi_i^{\mathbb{P}_1}$ is piecewise constant combined with linearity of the local problems (4.5);
- the stiffness matrix can be formulated in terms of a piecewise constant effective diffusion tensor in (4.13) thanks to full localization of the corrector functions, the piecewise constant gradient of $\phi_i^{\mathbb{P}_1}$ in the expansion (4.10) and bilinearity of the global problem (4.3).

These observations provide the main structure of the general framework. First, we choose an underlying, low-dimensional space of *piecewise affine* functions to which the MsFEM is associated (Definition 5.4). This will be the standard conforming Lagrange space of order 1 (for the MsFEM-lin), or the Crouzeix-Raviart space of order 1 (for the MsFEM-CR). Second we need to formulate the local problems for the numerical correctors (Definitions 5.11 and 5.16). This involves the definition of oversampling patches (for MsFEMs with oversampling, Definition 5.7), and an extension of the notion of degrees of freedom to define the boundary conditions for the numerical correctors (Definition 5.5, 5.8 and 5.9) on oversampling patches. It is then possible to define the multiscale basis functions by a generalization of (4.10) (see Definition 5.21) and finally to define the MsFEM for our general framework in Definition 5.28.

Remark 5.1. We note that our development of non-intrusive MsFEM approaches relies to a great extent on the fact that (4.10), and its generalization (5.10) in the general framework developed below, provide a description of the multiscale basis functions in

terms of $\mathbb{P}_1$ basis functions, without the need of higher-order functions, in a linear manner. Higher-order MsFEMs can be found in [9, 94] (see also [117]). Possible analogues of (5.10) for such MsFEMs and the subsequent techniques to design a non-intrusive MsFEM variant are more involved. We give some developments in this direction in Section 8.2.

5.1.3. Other motivations for the general framework. Besides a unified formulation of our non-intrusive MsFEM approach, our general framework can also be beneficial to concrete code development for the MsFEM. Common features among various multiscale methods have previously been used to design flexible and efficient software for the implementation of such methods on the DUNE platform [24, 23] within the Exa-Dune project [26]. For example, the distribution of local problems over multiple processors and subsequent coupling in a global problem are handled by designated software components [25]. Our work may contribute to the efficient implementation of all MsFEMs covered by our general framework in such a project and similar endeavours yet to come.

When formulating the general framework, we also clarify a few practical matters that are often left pending in the various research articles we are aware of. In particular, we give a rigorous definition of the oversampling procedure near the boundary $\partial\Omega$ of the global domain.

As we explore the general framework, we will also propose an MsFEM variant that has not yet appeared in the literature: the MsFEM-CR combined with the oversampling technique (see Example 5.25). We hope that our framework may also further the development of new MsFEM variants in an attempt to improve on the shortcomings of the methods known today.

Finally, the present study may also uncover a deeper understanding of MsFEMs by paving the way to a unified convergence analysis of different variants. A first step in this direction is made in Part III of this thesis.

We develop here a general framework for multiscale finite element methods. The ultimate aim is to generalize the key identities of Section 4.4. This is done in Definitions 5.11 and 5.16 for the numerical correctors introduced in (4.11), and in Definition 5.21 for the expansion (4.10) of the multiscale basis functions. This allows the reformulation of the linear system of the MsFEM as the linear system of an effective problem in (6.8) (for a Petrov-Galerkin MsFEM) and (6.12) (for a Galerkin MsFEM) in Chapter 6. The other notions introduced in this chapter, although rather technical and abstract, are necessary tools to capture a wide variety of MsFEMs in our general framework.

5.2. The continuous problem

The abstract variational problem for our general MsFEM framework is as follows. Let a^ε be a continuous bilinear form on $H^1(\Omega) \times H^1(\Omega)$. We are interested in the solution to the problem

$$\text{Find } u^\varepsilon \in H^1_0(\Omega) \text{ such that } a^\varepsilon(u^\varepsilon, v) = F(v) \text{ for any } v \in H^1_0(\Omega), \tag{5.1}$$

where F is defined as in (4.4) for any $f \in L^2(\Omega)$. To ensure well-posedness of (5.1), we suppose that the bilinear form a^ε is coercive on $H^1_0(\Omega)$. The bilinear form a^ε may contain coefficients that oscillate on a microscopically small scale.

The oversampling and Crouzeix-Raviart variants of the MsFEM introduced in Section 5.1.1 show that we need to accommodate for approximation spaces with discontinuities at the interfaces. This requires some additional assumptions on the formulation of the abstract problem. We suppose that the bilinear form a^ε is in fact defined on the broken Sobolev space $H^1(\mathscr{T}_H) \times H^1(\mathscr{T}_H)$. More precisely, we assume that we can represent it as $a^\varepsilon = \sum_{K \in \mathscr{T}_H} a^\varepsilon_K$, where, for each $K \in \mathscr{T}_H$, a^ε_K is a continuous bilinear form defined on $H^1(K) \times H^1(K)$.

To ensure well-posedness of MsFEMs, which may use non-conforming approximation spaces, coercivity on $H^1_0(\Omega)$ may be insufficient. Therefore, we add the following coercivity hypothesis for the bilinear forms a^ε_K:

$$\begin{gathered}\text{for all } K \in \mathscr{T}_H, \text{ there exists } \alpha_K > 0 \text{ such that} \\ \forall\, u \in H^1(K), \quad a^\varepsilon_K(u,u) \geq \alpha_K \, \|\nabla u\|^2_{L^2(K)}.\end{gathered} \tag{5.2}$$

In order to perform a convergence analysis, one also has to assume that the α_K are bounded from below by some $\tilde{\alpha} > 0$ that does not depend on H. We provide convergence results in Chapter 7 for the pure diffusion problem (4.1), in which case we have $\alpha_K = m$ from (4.2).

As an example, the introductory problem (4.1) with the associated bilinear form $a^{\varepsilon,\mathsf{diff}}$ is covered by this framework as is made explicit in Example 5.2 below. Other second-order PDEs that fit in our abstract variational formulation are given in Example 5.3.

Example 5.2. The diffusion problem (4.1) is covered by the abstract variational formulation above. Indeed, we can set

$$a^\varepsilon = a^{\varepsilon,\mathsf{diff}},$$

where $a^{\varepsilon,\mathsf{diff}}$ is the bilinear form defined in (4.4). Further, we define

$$a^\varepsilon_K(u,v) = a^{\varepsilon,\mathsf{diff}}_K(u,v) := \int_K \nabla v \cdot A^\varepsilon \nabla u,$$

for all $u, v \in H^1(\mathscr{T}_H)$, so that we have indeed $a^{\varepsilon,\mathsf{diff}} = \sum_{K \in \mathscr{T}_H} a^{\varepsilon,\mathsf{diff}}_K$. Clearly, each $a^{\varepsilon,\mathsf{diff}}_K$ satisfies (5.2) with $\alpha_K = m$ the coercivity constant from (4.2).

Example 5.3. The reaction-advection-diffusion equation,

$$-\mathrm{div}(A^\varepsilon \nabla u^\varepsilon) + b \cdot \nabla u^\varepsilon + \sigma u^\varepsilon = f,$$

with a divergence-free advection field $b : \Omega \mapsto \mathbb{R}^d$ and a non-negative reaction coefficient $\sigma : \Omega \mapsto \mathbb{R}$, can be modelled (under some regularity hypotheses that we do not state here) with the bilinear forms

$$a^\varepsilon_K(u,v) = \int_K \nabla v \cdot A^\varepsilon \nabla u + v\, b \cdot \nabla u + \sigma u v.$$

However, these bilinear forms a^ε_K do not satisfy (5.2) even though the bilinear form a^ε is coercive on $H^1_0(\Omega)$. To this end, a skew-symmetrized formulation of the transport term

can be used. The skew-symmetrized formulation uses the bilinear form

$$a_K^\varepsilon(u,v) = \int_K \nabla v \cdot A^\varepsilon \nabla u + \frac{1}{2} v\, b \cdot \nabla u - \frac{1}{2} u\, b \cdot \nabla v + \sigma u v, \tag{5.3}$$

which does satisfy (5.2). Assumption (5.2) is used for proving well-posedness of the MsFEM in Lemma 5.29, but note that both choices for a_K^ε mentioned here can be studied in practice. We refer e.g. to [108, 115] and to Remark 11.3 in Part II for more details. Within the general MsFEM framework, b and σ are allowed to be highly oscillatory, and this may impact the specific MsFEM strategy to be preferred.

5.3. Piecewise affine structure

In Section 4.2, we have seen that the relation between multiscale basis functions and piecewise affine functions is essential for the development of our non-intrusive MsFEM. For the MsFEM definition in the general framework, we start by choosing such a structure in the following definition.

Definition 5.4. Let a mesh $\mathscr{T}_H$ be given. The **underlying $\mathbb{P}_1$ space** for the MsFEM, denoted V_H, is one of the following two spaces: the Lagrange approximation space

$$V_H^L = \{v \in \mathbb{P}_1(\mathscr{T}_H) \mid v \text{ is continuous on } \Omega\},$$

in which case we shall refer to the associated MsFEM as the MsFEM-lin, or the Crouzeix-Raviart approximation space

$$V_H^{CR} = \left\{ v \in \mathbb{P}_1(\mathscr{T}_H) \mid \forall\, K \in \mathscr{T}_H,\ \forall e \in \mathscr{F}(K) \text{ such that } e \subset \Omega : \int_e [\![v]\!] = 0 \right\},$$

in which case the associated MsFEM shall be called the MsFEM-CR. We use the notation $\mathscr{F}(K)$ for the set of faces of K and $[\![v]\!]$ denotes the jump of v over the face e. The space V_H^L is a subspace of $H^1(\Omega)$, but V_H^{CR} is not. Note that no restrictions apply on faces lying on $\partial\Omega$.

We note that the underlying $\mathbb{P}_1$ space has the following property: if $v \in V_H$ is piecewise constant on the mesh $\mathscr{T}_H$, then v is constant in Ω. Contrary to the space V_H^L, functions in the Crouzeix-Raviart space V_H^{CR} are discontinuous in general. They are continuous, however, at the centroids of all faces of the mesh.

For standard finite elements, the notion of degrees of freedom allows to characterize any finite element function. The idea of the MsFEM is to preserve this notion of degrees of freedom (in a suitable way made precise below) in the definition of a multiscale approximation space, while adapting the piecewise affine structure to the microstructure of the PDE. We formalize this notion for the two underlying $\mathbb{P}_1$ spaces that we introduced in Definition 5.4. The definition involves an arbitrary simplex K, which is typically an element of the mesh $\mathscr{T}_H$, or an associated oversampling patch (for the oversampling technique of the MsFEM) that we shall define in Definition 5.7. The latter is not always a simplex, and we extend Definition 5.5 to such oversampling patches in Definition 5.8 and 5.9.

Definition 5.5. A **degree of freedom operator** (*DOF* operator) Γ associates to any simplex $K \subset \mathbb{R}^d$ and $v \in \mathbb{P}_1(K)$ a vector $\Gamma(K, v) \in \mathbb{R}^{d+1}$, whose components are called the **degrees of freedom** of v on K, in such a way that the application $v \mapsto \Gamma(K, v)$ is a linear bijection from $\mathbb{P}_1(K)$ to $\mathbb{R}^{d+1}$. More precisely, $\Gamma(K, \cdot)$ will denote in the sequel one of the following two operators:

1. (*DOF* operator for the MsFEM-lin.) Let $x_0, \ldots, x_d$ denote the vertices of K. We set
$$\forall\, v \in \mathbb{P}_1(K), \qquad \Gamma^L(K, v) = (v(x_0), \ldots, v(x_d))\,.$$
For $K \in \mathscr{T}_H$, the degree of freedom $[\Gamma^L(K, \cdot)]_j$ is said to be **associated to the boundary** if, for all $v \in \mathbb{P}_1(K)$, $[\Gamma^L(K, v)]_j = v(x)$ for a vertex x of the mesh that lies on $\partial\Omega$.

2. (*DOF* operator for the MsFEM-CR.) Let $e_0, \ldots, e_d$ denote the faces of K. We set
$$\forall\, v \in \mathbb{P}_1(K), \qquad \Gamma^{CR}(K, v) = \left(\frac{1}{|e_0|}\int_{e_0} v, \ldots, \frac{1}{|e_d|}\int_{e_d} v\right).$$
For $K \in \mathscr{T}_H$, the degree of freedom $[\Gamma^{CR}(K, \cdot)]_j$ is said to be **associated to the boundary** if, for all $v \in \mathbb{P}_1(K)$, $[\Gamma^{CR}(K, v)]_j = \dfrac{1}{|e|}\displaystyle\int_e v$ for a face e of the mesh that lies on $\partial\Omega$.

The $\mathbb{P}_1$ **test space** is defined as
$$V_{H,0} = \left\{ v \in V_H \;\middle|\; \begin{array}{l} \forall\, K \in \mathscr{T}_H,\ \forall\, 1 \le j \le d+1, [\Gamma(K, v)]_j = 0 \text{ if the degree} \\ \text{of freedom } [\Gamma(K, \cdot)]_j \text{ is associated to the boundary} \end{array} \right\}.$$

The $\mathbb{P}_1$ test space is used in practice to approximate the subspace $H^1_0(\Omega)$ of $H^1(\Omega)$. The degrees of freedom are defined element per element and are thus local. Global properties of the underlying $\mathbb{P}_1$ space V_H are most easily made explicit through the identification of a basis for V_H.

Definition 5.6. Let V_H be an underlying $\mathbb{P}_1$ space as in Definition 5.4, and let Γ be the associated *DOF* operator. We shall denote by N the dimension of V_H. The $\mathbb{P}_1$ **basis functions** $\phi_1^{\mathbb{P}_1}, \ldots, \phi_N^{\mathbb{P}_1}$ are defined as follows:

- For the MsFEM-lin, let $x_1, \ldots, x_N$ be an enumeration of the (internal and boundary) vertices of $\mathscr{T}_H$. Then $\phi_i^{\mathbb{P}_1}$ is defined by $\phi_i^{\mathbb{P}_1}(x_j) = \delta_{i,j}$ for all $1 \le i, j \le N$.
- For the MsFEM-CR, let $e_1, \ldots, e_N$ be an enumeration of the (internal and boundary) faces of $\mathscr{T}_H$. Then $\phi_i^{\mathbb{P}_1}$ is defined by $\dfrac{1}{|e_j|}\displaystyle\int_{e_j} \phi_i^{\mathbb{P}_1} = \delta_{i,j}$ for all $1 \le i, j \le N$.

In both cases, these functions form a basis of the corresponding space V_H of Definition 5.4.

5.4. Local problems

5.4.1. Oversampling patches. To replace the (standard) underlying $\mathbb{P}_1$ space by a space of the same (low) dimension, adapted to the microstructure of a^ε, we associate to each mesh element $K \in \mathscr{T}_H$ an oversampling patch. It serves to avoid imposing artificial, non-oscillatory boundary conditions on K directly when computing numerical correctors to process the microstructure.

Definition 5.7. Let $K \in \mathscr{T}_H$ be any mesh element and let S'_K be a simplex obtained from K by homothety around the centroid of K with homothety ratio $\rho \geq 1$. The **oversampling patch** S_K is defined as $S_K = S'_K \cap \Omega$.

See Figure 5.1 for an illustration of the construction of oversampling patches in dimension 2. We allow for the trivial homothety ratio $\rho = 1$. In this case, the patch S_K coincides with K.

We will call an MsFEM **without oversampling** an MsFEM for which all oversampling patches satisfy $S_K = K$. Otherwise, the MsFEM is called an MsFEM **with oversampling**. We speak simply of an MsFEM when there are no assumptions on the oversampling patches.

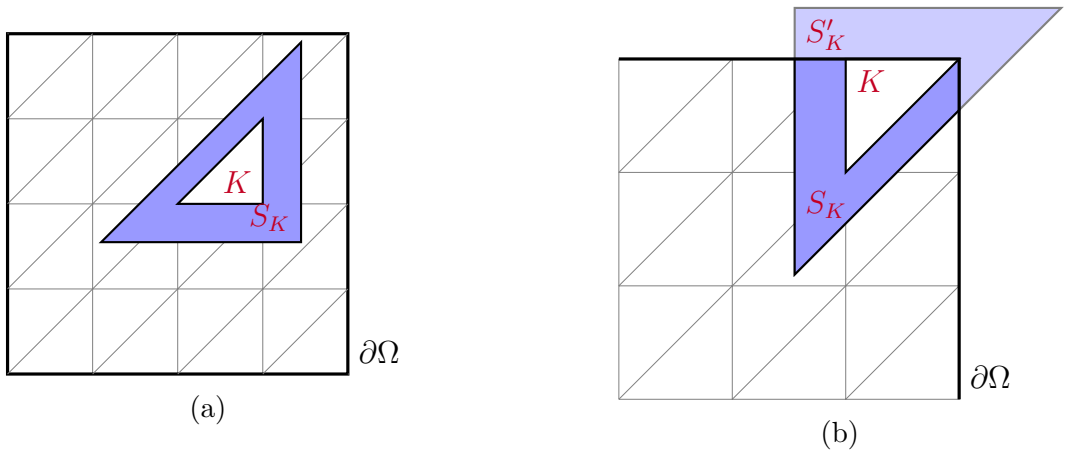

Figure 5.1: *Oversampling patches for the MsFEM in 2D. Left: the patch for the mesh element K is obtained from K by homothety. Right: The triangle S'_K partially lies outside the domain Ω and the oversampling patch S_K is not homothetic to K. It is not even a triangle.*

For most mesh elements K, the patch S_K in Definition 5.7 is a simplex. However, for mesh elements close to the boundary $\partial\Omega$, alternative constructions should be considered. We have not found any explicit description of such a construction in the literature. This complicates the reproducibility of the method as well as a rigorous convergence analysis. The precise definitions of this section provide a first step to address these issues. A fully rigorous convergence analysis of the MsFEM with oversampling as described here has not yet been accomplished and would be one of the interesting extensions of the analysis of Part III of this thesis.

5.4.2. Degrees of freedom on oversampling patches. Definition 5.5 provides the definition of *DOF* operators on any simplex. For the MsFEM, we wish to compute multiscale

functions on oversampling patches S_K, in which case Definition 5.5 may be insufficient. We illustrated this in Figure 5.1b. Indeed, the number of vertices/faces of the oversampling patch may be larger than $d+1$. In order to associate a multiscale basis function to every $\mathbb{P}_1$ basis function, we still need a notion of *DOF* operator such that $\Gamma(S_K, \cdot)$ is a linear bijection from $\mathbb{P}_1(S_K)$ to $\mathbb{R}^{d+1}$. Therefore, we extend the definition of the degrees of freedom operators Γ^L and Γ^{CR} in Definition 5.8 and 5.9.

Definition 5.8. Let $K \in \mathscr{T}_H$ and let S_K be its associated oversampling patch. Let $x_0, \ldots, x_d$ be a selection of $d+1$ distinct vertices of S_K. We define the *DOF* operator Γ^L by

$$\forall\, v \in \mathbb{P}_1(S_K), \qquad \Gamma^L(S_K, v) = (v(x_0), \ldots, v(x_d))\,.$$

We note that any choice of $d+1$ nodal values unequivocally characterizes an affine function on S_K. Hence, $\Gamma^L(S_K, \cdot)$ is indeed a bijection. Now the precise choice of the vertices in Definition 5.8 is unimportant, because $\Gamma^L(S_K, \cdot)$ will only be used in the sequel to describe the trace of $\mathbb{P}_1$ functions on ∂S_K in boundary value problems. For any $\mathbb{P}_1$ function, this trace is uniquely defined by its values in $d+1$ distinct vertices of S_K. Finally, when S_K is a simplex, it has only $d+1$ vertices and Definition 5.8 reduces to Definition 5.5.

To generalize the notion of degrees of freedom for the Crouzeix-Raviart space to non-simplicial patches, we need to introduce some additional notation. On the boundary of a non-simplicial oversampling patch, we can identify some faces that collapse to a single vertex if we shrink S_K to K. We call these faces the additional faces and denote the set containing them by $\mathscr{F}_a(S_K)$. The other faces of S_K are referred to as the dilated faces, collected in the set $\mathscr{F}_d(S_K)$. When the patch S_K does not touch $\partial\Omega$, we have $\mathscr{F}_d(S_K) = \mathscr{F}(S_K)$ and $\mathscr{F}_a(S_K) = \emptyset$. In Figure 5.2a, for example, the additional faces are exactly those faces that lie on $\partial\Omega$. This is not always the case, as is illustrated by Figure 5.2b.

For the definition of $\Gamma^{CR}(S_K, \cdot)$, we shall rely on the existence of $d+1$ dilated faces, because we need $\Gamma^{CR}(S_K, \cdot)$ to be a bijection between $\mathbb{P}_1(S_K)$ and $\mathbb{R}^{d+1}$. This imposes a constraint on the choice of the homothety ratio used to construct S_K. For example, in the case of Figure 5.2a, the lower right dilated face falls outside Ω if the homothety ratio is too large, and the oversampling patch S_K only has two dilated faces (edges here) and two additional faces. We do not consider this case hereafter.

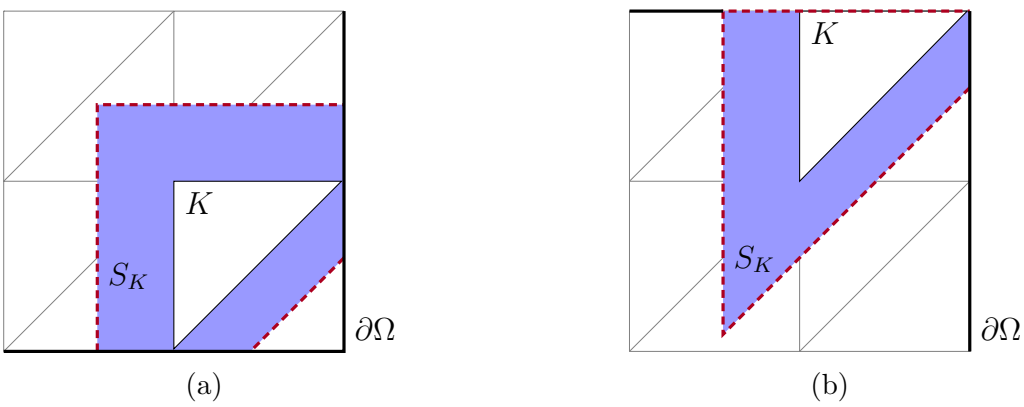

Figure 5.2: *Non-simplicial oversampling patches in 2D. The dilated edges of the patch S_K, those that 'correspond' to the edges of the original triangle K, are dashed and drawn in red.*

Definition 5.9. Let $K \in \mathscr{T}_H$ and let S_K be its associated oversampling patch. We assume that S_K has $d+1$ dilated faces, and we denote them by $e_0, \dots, e_d$. We define the *DOF* operator Γ^{CR} by

$$\forall\, v \in \mathbb{P}_1(S_K), \qquad \Gamma^{CR}(S_K, v) = \left(\frac{1}{|e_0|} \int_{e_0} v, \dots, \frac{1}{|e_d|} \int_{e_d} v \right).$$

When S_K is a simplex, we have $\mathscr{F}_d(S_K) = \mathscr{F}(S_K)$, and Definition 5.9 coincides with the respective elements of Definition 5.5.

5.4.3. Numerical correctors: first oversampling strategy. We now provide the precise assumptions under which we will consider local problems, i.e., the analogues of (4.5) defining the MsFEM-lin basis functions and the definition of the numerical correctors in (4.11). In fact, since the numerical correctors play an essential role in the construction of non-intrusive MsFEM approaches, we define the numerical correctors first and use them to define the multiscale basis functions in Definition 5.21.

We discuss two definitions of the numerical correctors, corresponding to two ways to define the oversampling technique for the MsFEM. The functional settings for these constructions are provided by Definition 5.10 and 5.15. These definitions involve a 'sampling space', whose name is inspired by the idea that only a limited number of local problems will be solved to encode the microstructure of the PDE in the numerical model. The choice of sampling space has to accommodate for the boundary conditions that one wishes to impose on the numerical correctors and basis functions (e.g. essential or natural; see Examples 5.12 and 5.13).

Definition 5.10. Let $K \in \mathscr{T}_H$, let S_K be its associated oversampling patch and let Γ be a *DOF* operator from Definition 5.5, 5.8 or 5.9. A subspace V_K of $H^1(S_K)$ and bilinear form $s_K^\varepsilon : V_K \times V_K \to \mathbb{R}$ are called **sampling space** and **sampling form**, respectively, if they satisfy the following:

1. the space V_K contains the space of affine functions $\mathbb{P}_1(S_K)$;
2. the operator $\Gamma(S_K, \cdot)$ is well-defined on V_K;
3. the ***DOF*-extended local problem**: find $v \in V_K$ such that

$$\begin{cases} s_K^\varepsilon(v, w) = \langle g, w \rangle \text{ for all } w \in V_{K,0}, \\ \Gamma(S_K, v) = \text{given}, \end{cases} \tag{5.4}$$

has a unique solution for any $g \in (H^1(S_K))'$. Here, $V_{K,0} = \{w \in V_K \mid \Gamma(S_K, w) = 0\}$ is the **sampling test space**.

Problem (5.4) is called '*DOF*-extended' because the degrees of freedom, controlling the boundary conditions associated to the local problem, are imposed on the oversampling patch S_K rather than the (generally smaller) mesh element K.

The sampling form s_K^ε shall be used to encode the oscillations of the bilinear form a^ε and thus the microstructure of the problem in the multiscale finite element functions. There is some flexibility in choosing the sampling form; one may choose to include all the same terms as those in the bilinear form a_K^ε of the original problem (5.1), or only some of them. When the MsFEM was first proposed in [98], it was suggested that s_K^ε should

include those terms that correspond to the highest-order terms of the PDE that is to be solved. In the context of the advection-diffusion equation, one may thus choose to include in our MsFEM framework only the diffusion terms, or both the diffusion and advection terms. Both options have been studied e.g. in [114, 115].

In the functional setting of Definition 5.10, the generalization of (4.11) to define the numerical correctors for the general MsFEM framework is as follows.

Definition 5.11. For all $K \in \mathscr{T}_H$, for any $0 \leq \alpha \leq d$, we introduce the function $\chi_{S_K}^{\varepsilon,\alpha,\mathsf{e}} \in V_{K,0}$ as the unique solution to the **corrector problem**

$$\boxed{\forall\, w \in V_{K,0}, \quad s_K^\varepsilon\left(\chi_{S_K}^{\varepsilon,\alpha,\mathsf{e}}, w\right) = \begin{cases} -s_K^\varepsilon\left(1, w\right) & \text{if } \alpha = 0, \\ -s_K^\varepsilon\left(x^\alpha - x_{c,K}^\alpha, w\right) & \text{if } 1 \leq \alpha \leq d. \end{cases}} \tag{5.5}$$

The ***DOF*-extended numerical corrector** $\chi_K^{\varepsilon,\alpha,\mathsf{e}}$ is defined as the restriction of $\chi_{S_K}^{\varepsilon,\alpha,\mathsf{e}}$ to K, extended to all of Ω by 0.

Note that the above definition introduces one more numerical corrector than introduced in (4.11) (namely the corrector for $\alpha = 0$). The precise definition of the numerical correctors is chosen such that the analogous expansion of (4.10) for the general framework (see (5.10)) leads to a PDE for the multiscale basis functions analogous to (4.5); we show this in Lemma 5.22 and (for a second oversampling strategy introduced below) in Lemma 5.23. In the following example, we see that Definition 5.11 is indeed a generalization of the numerical correctors defined by (4.11) in Section 4.4.

Example 5.12 (MsFEM-lin for diffusion problems)**.** We consider $V_H = V_H^L$ and $\Gamma = \Gamma^L$ from Definition 5.5. For the diffusion problem (4.1), we have $a^\varepsilon = a^{\varepsilon,\mathsf{diff}}$ and we set $s_K^\varepsilon = a_K^{\varepsilon,\mathsf{diff}}$ (see Example 5.2). The sampling space for the MsFEM-lin is defined as

$$V_K = V_K^L := \left\{ v \in H^1(S_K) \;\middle|\; \exists\, w \in \mathbb{P}_1(S_K) \text{ such that } v|_{\partial S_K} = w|_{\partial S_K} \right\}.$$

Then the sampling test space $V_{K,0}^L$ is the space $H_0^1(S_K)$. In this case, it holds $a_K^{\varepsilon,\mathsf{diff}}(1, w) = 0$ for all $w \in V_{K,0}^L$. Consequently, the *DOF*-extended numerical corrector $\chi_K^{\varepsilon,0,\mathsf{e}}$ is identically equal to 0; we obtain indeed exactly d numerical correctors as in Section 4.4. For the non-trivial numerical correctors, Definition 5.11 corresponds to the weak formulation of the following boundary value problem:

$$-\mathrm{div}(A^\varepsilon \nabla \chi_{S_K}^{\varepsilon,\alpha,\mathsf{e}}) = \mathrm{div}(A^\varepsilon e_\alpha) \;\text{ in } S_K, \quad \chi_{S_K}^{\varepsilon,\alpha,\mathsf{e}} = 0 \;\text{ on } \partial S_K, \tag{5.6}$$

which is clearly well-posed.

Example 5.13 (MsFEM-CR for diffusion problems)**.** Taking a^ε, a_K^ε and s_K^ε as in the previous example, we construct the MsFEM-CR with the sampling space $V_K^{CR} := H^1(S_K)$. With $V_H = V_H^{CR}$ and $\Gamma = \Gamma^{CR}$ from Definition 5.5, the corrector problem (5.5) for $\alpha = 0$ reduces to $\chi_K^{\varepsilon,0,\mathsf{e}} = 0$, as in Example 5.12. For $1 \leq \alpha \leq d$, the *DOF*-extended

numerical corrector $\chi_K^{\varepsilon,\alpha,\mathsf{e}}$ is obtained from the boundary value problem:

$$\begin{cases} -\mathrm{div}(A^\varepsilon \nabla \chi_{S_K}^{\varepsilon,\alpha,\mathsf{e}}) = \mathrm{div}(A^\varepsilon e_\alpha) & \text{in } S_K, \\ \vec{n} \cdot A^\varepsilon \nabla \chi_{S_K}^{\varepsilon,\alpha,\mathsf{e}} = -\vec{n} \cdot A^\varepsilon e_\alpha & \text{on each } h \in \mathscr{F}_a(S_K), \\ \vec{n} \cdot A^\varepsilon \nabla \chi_{S_K}^{\varepsilon,\alpha,\mathsf{e}} = c_h - \vec{n} \cdot A^\varepsilon e_\alpha & \text{on each } h \in \mathscr{F}_d(S_K), \\ \dfrac{1}{|h|} \displaystyle\int_h \chi_{S_K}^{\varepsilon,\alpha,\mathsf{e}} = 0 & \text{for each } h \in \mathscr{F}_d(S_K), \end{cases} \tag{5.7}$$

where $\vec{n}$ denotes the outward unit vector on ∂S_K and c_h is a constant whose value is uniquely determined by the above problem. We note that the condition for the flux on the additional faces of S_K is entirely determined by the right-hand side in (5.5), whereas the flux on the dilated faces of S_K involves an additional constant, due to the fact that the test functions in $V_{K,0}^{CR}$ cannot take arbitrary values on the dilated faces. Indeed, their mean vanishes on these faces according to Definition 5.10.
When $S_K = K$ and when the faces of K do not lie on $\partial\Omega$, this corresponds to the setting of the original MsFEM-CR defined in [112]. The latter work also provides an alternative characterization of the multiscale Crouzeix-Raviart space.
When a face e of K lies on $\partial\Omega$, the basis functions that we will define below in Section 5.5 do not satisfy $\phi_e^\varepsilon = 0$ on e, but only satisfy a weak boundary condition in the average sense on e (and so does the corresponding MsFEM approximation to (5.1) defined below). This does not correspond to the original definition of the MsFEM-CR in [112, 113]. The MsFEM-CR with local boundary conditions as defined here was studied in [57, 123, 105].

Remark 5.14. In both Examples 5.12 and 5.13, the numerical corrector $\chi_K^{\varepsilon,0,\mathsf{e}}$ vanishes, because $s_K^\varepsilon(1, w) = 0$ for all w in the sampling test space. This is no longer the case e.g. for an MsFEM for advection-diffusion problems in which the sampling problem uses the skew-symmetrized bilinear form defined in (5.3). In this case, the numerical corrector $\chi_K^{\varepsilon,0,\mathsf{e}}$ does not vanish. In the corresponding effective numerical scheme that we will derive in (6.11), this leads to a term of order 0 even if such a term is not present in the advection-diffusion equation itself.

When $S_K = K$ (i.e., in the absence of oversampling), the *DOF* operator allows us to prescribe certain continuity properties on the faces of the mesh elements K. More precisely, when the MsFEM-lin with *DOF* operator Γ^L is employed, the numerical correctors $\chi_K^{\varepsilon,\alpha,\mathsf{e}}$ vanish at the vertices of the mesh, and, with the correct choice of sampling space (see Example 5.12), they vanish on all faces of K and are thus continuous on Ω. When the MsFEM-CR with *DOF* operator Γ^{CR} is considered, we obtain weak continuity of the numerical correctors over all faces of the mesh. The definition of the multiscale basis functions that we give below (see Definition 5.21, in the vein of the expansion (4.10)) shows that the continuity properties of the $\mathbb{P}_1$ basis functions of the underlying $\mathbb{P}_1$ space are not perturbed when building the multiscale basis functions.

In the general case, when the oversampling patch S_K is larger than K, we cannot preserve any of these continuity properties if we use *DOF*-extended local problems for our local computations, since the values on ∂K are not controlled by the degrees of freedom $\Gamma(S_K, \cdot)$ on ∂S_K. Therefore, we introduce another variant of the local problems to define *DOF*-continuous numerical correctors in the next section.

5.4.4. Numerical correctors: second oversampling strategy.

Definition 5.15. Let $K \in \mathscr{T}_H$ and let V_K and s_K^ε be a sampling space and sampling form, respectively, according to Definition 5.10. Additionally, suppose that the operator $\Gamma(K,\cdot)$ is well-defined on V_K. Then a ***DOF*-continuous local problem** is to find $v \in V_K$ such that

$$\begin{cases} s_K^\varepsilon(v,w) = \langle g, w\rangle \text{ for all } w \in V_{K,0}, \\ \Gamma(K,v) = \text{given}, \end{cases} \tag{5.8}$$

for some $g \in (H^1(S_K))'$.

Definition 5.16. Suppose any *DOF*-continuous local problem in Definition 5.15 is well-posed. Then we introduce, for all $K \in \mathscr{T}_H$ and all $0 \le \alpha \le d$, the functions $\chi_{S_K}^{\varepsilon,\alpha,\mathsf{c}}$ as the unique functions in V_K with $\Gamma\left(K, \chi_{S_K}^{\varepsilon,\alpha,\mathsf{c}}\right) = 0$ satisfying the corrector problem (5.5). We define the ***DOF*-continuous numerical correctors** $\chi_K^{\varepsilon,\alpha,\mathsf{c}}$ as the restriction of $\chi_{S_K}^{\varepsilon,\alpha,\mathsf{c}}$ to K, extended to all of Ω by 0.

We emphasize that the local problems of Definition 5.11 and 5.16 use test functions w in *the same space* $V_{K,0}$. This means that the test functions satisfy $\Gamma(S_K, w) = 0$ rather than $\Gamma(K,w) = 0$. The difference between *DOF*-extended and *DOF*-continuous numerical correctors is that the former satisfy $\Gamma(S_K, \chi_K^{\varepsilon,\alpha,\mathsf{e}}) = 0$, whereas the latter satisfy $\Gamma(K, \chi_K^{\varepsilon,\alpha,\mathsf{c}}) = 0$.

Remark 5.17. Clearly, when $S_K = K$, there is no difference between the *DOF*-extended and *DOF*-continuous problems (5.4) and (5.8). We shall in this case simply refer (5.4) (or (5.8)) as local problems, and we write $\chi_K^{\varepsilon,\alpha,\bullet} = \chi_K^{\varepsilon,\alpha}$ for the numerical correctors of MsFEMs without oversampling.

Example 5.18 (MsFEM-lin for diffusion problems)**.** Continuing Example 5.12, consider now the *DOF*-continuous numerical corrector $\chi_K^{\varepsilon,\alpha,\mathsf{c}}$. Equation (5.8) solves the following problem for $1 \le \alpha \le d$: there exists $w \in \mathbb{P}_1(S_K)$ such that

$$\begin{aligned} &-\operatorname{div}(A^\varepsilon \nabla \chi_K^{\varepsilon,\alpha,\mathsf{c}}) = \operatorname{div}(A^\varepsilon e_\alpha) \text{ in } S_K, \quad \chi_K^{\varepsilon,\alpha,\mathsf{c}} = w \text{ on } \partial S_K, \\ &\text{and } \chi_K^{\varepsilon,\alpha,\mathsf{c}} = 0 \text{ at the vertices of } K. \end{aligned}$$

The boundary condition on ∂S_K is complemented by a condition at the vertices of K. Except when A^ε is constant (and a solution is $\chi_K^{\varepsilon,\alpha,\mathsf{c}} = 0$), it is not evident whether a solution to this problem exists. For $\alpha = 0$, the numerical corrector $\chi_K^{\varepsilon,0,\mathsf{c}}$ vanishes, as in the *DOF*-extended case.

Example 5.19 (MsFEM-CR for diffusion problems)**.** For the MsFEM-CR considered in Example 5.13, the *DOF*-continuous numerical correctors satisfy the same problem (5.7) (for $1 \le \alpha \le d$) as the *DOF*-extended numerical correctors, but with the average condition (the final equation in (5.7)) replaced by $\frac{1}{|h|}\int_h \chi_K^{\varepsilon,\alpha,\mathsf{c}} = 0$ for each $h \in \mathscr{F}(K)$. As we saw for the MsFEM-lin in Example 5.18, this is not a standard boundary value problem on S_K. For the case $\alpha = 0$, we have $\chi_K^{\varepsilon,0,\mathsf{c}} = 0$, which clearly satisfies the constraints $\frac{1}{|h|}\int_h \chi_K^{\varepsilon,0,\mathsf{c}} = 0$ for each $h \in \mathscr{F}(K)$.

Examples 5.12 and 5.13 show that a *DOF*-extended local problem is typically equivalent to a PDE with boundary conditions on S_K. Under reasonable assumptions, these problems have a unique solution as required by Definition 5.10. We have seen in Examples 5.18 and 5.19 that this is not the case for *DOF*-continuous problems, for which one finds some boundary conditions on ∂S_K (because the degrees of freedom of test functions in $V_{K,0}$ are prescribed on S_K) and another set of conditions on ∂K that are explicitly imposed through the degrees of freedom on K in (5.8). Well-posedness is not obvious in general, and cannot always be deduced from well-posedness of the *DOF*-extended counterpart (5.4). We address the well-posedness of *DOF*-continuous problems in more detail in Section 5.4.5. The advantage of *DOF*-continuous oversampling is that it imposes certain continuity properties on the multiscale basis functions, and we will see in Section 7.4 that it yields better numerical approximations than *DOF*-extended oversampling.

Remark 5.20. Other oversampling strategies for the MsFEM-CR than those defined above are proposed in Section 8.1. These were formulated after the publication of the contents of the present chapter in [31].

5.4.5. Well-posedness of *DOF*-continuous numerical correctors. We have seen in Examples 5.18 and 5.19 that *DOF*-continuous local problems lead to non-standard boundary conditions. This poses not only a theoretical issue, but also a computational challenge. To complete our study of the general MsFEM framework, we now present a computational strategy to obtain the *DOF*-continuous numerical correctors, and we use this strategy to discuss the well-posedness of the associated local problems.

In Definition 5.10 we assume the well-posedness of *DOF*-extended problems, and we have seen in Examples 5.12 and 5.13 that this is a natural assumption. It is also natural to assume that we can compute *DOF*-extended numerical correctors numerically. We compute the *DOF*-continuous numerical correctors from the *DOF*-extended numerical correctors, by subtracting a linear combination of suitable functions W^β from the *DOF*-extended numerical correctors. The W^β must all satisfy the homogeneous equation $s_K^\varepsilon\left(W^\beta, w\right) = 0$ for all $w \in V_{K,0}$, in order not to perturb the local problem (5.5) that is already satisfied by both types of numerical correctors. We shall use the functions $W^0 := 1 + \chi_{S_K}^{\varepsilon,0,\mathsf{e}}$ and $W^\beta := x^\beta - x_{c,K}^\beta + \chi_{S_K}^{\varepsilon,\beta,\mathsf{e}}$ for $1 \le \beta \le d$, where $\chi_{S_K}^{\varepsilon,\beta,\mathsf{e}}$ is defined in Definition 5.11. The precise strategy is as follows.

Fix $0 \le \alpha \le d$. We look for coefficients $c_0^\alpha, \dots, c_d^\alpha$ such that $\chi_{S_K}^{\varepsilon,\alpha,\mathsf{c}} = \chi_{S_K}^{\varepsilon,\alpha,\mathsf{e}} - \sum_{\beta=0}^{d} c_\beta^\alpha W^\beta$ on K, where we recall that $\chi_{S_K}^{\varepsilon,\alpha,\mathsf{c}}$ is defined by Definition 5.16. Note that both sides of the equation clearly satisfy (5.5). The desired equality thus holds if and only if $\Gamma\left(K, \chi_{S_K}^{\varepsilon,\alpha,\mathsf{e}} - \sum_{\beta=0}^{d} c_\beta^\alpha W^\beta\right) = 0$. Since the *DOF* operators are linear, this leads to the linear system

$$\underbrace{\begin{bmatrix} | & | & & | \\ \Gamma(K, W^0) & \Gamma(K, W^1) & \dots & \Gamma(K, W^d) \\ | & | & & | \end{bmatrix}}_{=:\,\mathbb{M}} \begin{bmatrix} c_0^\alpha \\ c_1^\alpha \\ \vdots \\ c_d^\alpha \end{bmatrix} = \Gamma\left(K, \chi_{S_K}^{\varepsilon,\alpha,\mathsf{e}}\right). \tag{5.9}$$

Invertibility of the matrix $\mathbb{M}$ is thus a sufficient condition for the existence of all *DOF*-continuous numerical correctors, and the resolution of the linear system (5.9) for each α (where all *DOF*-extended numerical correctors are replaced by their numerical approximation) allows to compute the *DOF*-continuous numerical correctors numerically.

Before studying the invertibility of the matrix $\mathbb{M}$ in a few special cases, let us consider the matrix composed of the degrees of freedom on S_K, i.e., the matrix

$$\widetilde{\mathbb{M}} := \begin{bmatrix} | & | & & | \\ \Gamma(S_K, W^0) & \Gamma(S_K, W^1) & \dots & \Gamma(S_K, W^d) \\ | & | & & | \end{bmatrix}.$$

By definition of the functions $\chi_{S_K}^{\varepsilon,\beta,\mathsf{c}}$, we have $\Gamma(S_K, W^\beta) = \Gamma(S_K, x^\beta - x_{c,K}^\beta)$ for $1 \le \beta \le d$, and $\Gamma(S_K, W^0) = \Gamma(S_K, 1)$. Note that the constant function together with the coordinate functions $x^\beta - x_{c,K}^\beta$ $(1 \le \beta \le d)$ span $\mathbb{P}_1(S_K)$. Since $\Gamma(S_K, \cdot)$ is a bijection, the vectors $\Gamma(S_K, W^0), \dots, \Gamma(S_K, W^d)$ are linearly independent. Hence the matrix $\widetilde{\mathbb{M}}$ is invertible. One may hope that the linear independence of the vectors $\Gamma(S_K, W^\beta)$ is preserved for the degrees of freedom on the interior boundary ∂K instead of ∂S_K, yielding invertibility of $\mathbb{M}$. We found this to hold for all numerical tests that we performed, involving both the MsFEM-lin and the MsFEM-CR.

We can prove invertibility of $\mathbb{M}$ in a few special cases. When s_K^ε is the sampling form that was used in Example 5.12 (corresponding to a diffusion problem; we will consider this case until the end of this section) and if A^ε is constant, all numerical correctors vanish on S_K and the foregoing argument for the matrix $\widetilde{\mathbb{M}}$ shows invertibility of $\mathbb{M}$.

In the periodic setting (see Section 4.7), even though A^ε itself is not constant, its homogenized limit $A^\star$ is. In this case, the $\chi_{S_K}^{\varepsilon,\beta,\mathsf{e}}$ converge to zero weakly in $H^1(S_K)$. (We show this in Lemma 7.7 in the absence of oversampling, but the argument can be generalized to *DOF*-extended oversampling.) Now consider the MsFEM-CR. The weak convergence of the $\chi_{S_K}^{\varepsilon,\beta,\mathsf{e}}$ in $H^1(S_K)$ ensures weak convergence on each face of K in the $H^{1/2}$-norm by continuity of the trace operator. Since the embedding of $H^{1/2}(\partial K)$ in $L^2(\partial K)$ is compact, the $\chi_{S_K}^{\varepsilon,\beta,\mathsf{e}}$ converge to 0 strongly in L^2 on each face of K. Consequently, the degrees of freedom $\Gamma(K, \chi_{S_K}^{\varepsilon,\beta,\mathsf{e}})$ (the averages on the faces of K) converge to zero as $\varepsilon \to 0$. Thus, $\Gamma(K, W^0) \to \Gamma(K, 1)$ and $\Gamma(K, W^\beta) \to \Gamma(K, x^\beta - x_{c,K}^\beta)$ as $\varepsilon \to 0$ for all $1 \le \beta \le d$ and, by the above argument for the matrix $\widetilde{\mathbb{M}}$, the matrix $\mathbb{M}$ is invertible in this limit. By continuity of the determinant function, the matrix $\mathbb{M}$ is invertible when ε is small enough, and the *DOF*-continuous basis functions exist in this regime.

The study of the *DOF*-continuous numerical correctors for the MsFEM-lin is more delicate, since pointwise operations are involved in evaluating the degrees of freedom, which are ill-defined on $H^1(S_K)$. One can invoke the De Giorgi-Nash result, which can be found e.g. in [81, Theorem 8.22], to see that the multiscale basis functions, obtained from the numerical correctors in Definition 5.21 below, are in fact continuous for any bounded diffusion tensor. (See Example 5.24 for a definition of the multiscale basis functions for the MsFEM-lin independent of the numerical correctors.) Pointwise evaluation is then justified. It would therefore be convenient to study the *DOF*-continuous basis functions directly, without the intermediate step of the numerical correctors. We do not further pursue this topic here.

5.5. The multiscale basis functions

We can now define the multiscale basis functions for the approximation of the abstract problem (5.1) in terms of the numerical correctors. We recall that in Section 4.2, the numerical correctors were derived from the definition of the basis functions. An equivalent definition of the multiscale basis functions, independent of the numerical correctors, is given in Lemmas 5.22 and 5.23. Recall that $\phi_1^{\mathbb{P}_1}, \dots, \phi_N^{\mathbb{P}_1}$ is a basis of the space V_H (see Definition 5.6). We can suppose that the first N_0 basis functions form a basis of $V_{H,0}$. The following definition is the generalization of (4.10) to the general MsFEM framework.

Definition 5.21. For each $i = 1, \dots, N$, the **multiscale basis function** ϕ_i^ε is defined by

$$\forall\, K \in \mathscr{T}_H, \qquad \boxed{\phi_i^\varepsilon|_K = \phi_i^{\mathbb{P}_1}\big|_K + \phi_i^{\mathbb{P}_1}(x_{c,K})\,\chi_K^{\varepsilon,0,\bullet} + \sum_{\alpha=1}^{d} \partial_\alpha\big(\phi_i^{\mathbb{P}_1}\big|_K\big)\chi_K^{\varepsilon,\alpha,\bullet},} \tag{5.10}$$

where $\bullet = \mathsf{e}$ corresponds to *DOF*-extended multiscale basis functions and $\bullet = \mathsf{c}$ corresponds to *DOF*-continuous multiscale basis functions.

The *DOF*-extended multiscale basis functions satisfy a variational problem on the oversampling patches S_K as shown by the following lemma.

Lemma 5.22. *Let K be any mesh element and let $1 \le i \le N$. Consider an MsFEM with DOF-extended basis functions. Define an extension of ϕ_i^ε from K to S_K by*

$$\widehat{\phi_i^\varepsilon} = \widehat{\phi_i^{\mathbb{P}_1}\big|_K} + \phi_i^{\mathbb{P}_1}(x_{c,K})\,\chi_{S_K}^{\varepsilon,0,\mathsf{e}} + \sum_{\alpha=1}^{d} \partial_\alpha\big(\phi_i^{\mathbb{P}_1}\big|_K\big)\chi_{S_K}^{\varepsilon,\alpha,\mathsf{e}} \quad \text{in } S_K, \tag{5.11}$$

where $\widehat{\phi_i^{\mathbb{P}_1}\big|_K}$ denotes the affine extension of $\phi_i^{\mathbb{P}_1}\big|_K$ to S_K, and $\chi_K^{\varepsilon,\alpha,\mathsf{e}}$ is as in Definition 5.11. Then $\widehat{\phi_i^\varepsilon}$ is the unique solution in V_K to

$$\begin{cases} s_K^\varepsilon\left(\widehat{\phi_i^\varepsilon}, w\right) = 0 \text{ for all } w \in V_{K,0}, \\ \Gamma\left(S_K, \widehat{\phi_i^\varepsilon}\right) = \Gamma\left(S_K, \widehat{\phi_i^{\mathbb{P}_1}\big|_K}\right). \end{cases} \tag{5.12}$$

In the case of the MsFEM-lin for the diffusion problem (4.1), problem (5.12) with $S_K = K$ coincides with the definition of the multiscale basis functions in (4.5); see Example 5.24.

Proof. Problem (5.12) has a unique solution in view of Definition 5.10. It thus suffices to show that $\widehat{\phi_i^\varepsilon}$ satisfies (5.12). Since the numerical correctors $\chi_K^{\varepsilon,\alpha,\mathsf{e}}$ belong to $V_{K,0}$ for all $0 \le \alpha \le d$, it is clear from (5.11) that $\Gamma\left(S_K, \widehat{\phi_i^\varepsilon}\right) = \Gamma\left(S_K, \widehat{\phi_i^{\mathbb{P}_1}\big|_K}\right)$.

Inserting (5.11) into (5.12) and applying (5.5) to all $\chi_K^{\varepsilon,\alpha,\mathsf{e}}$, we find, for any $w \in V_{K,0}$,

$$s_K^\varepsilon\left(\widehat{\phi_i^\varepsilon}, w\right) = s_K^\varepsilon\left(\widehat{\phi_i^{\mathbb{P}_1}\big|_K}, w\right) + \phi_i^{\mathbb{P}_1}(x_{c,K})\, s_K^\varepsilon\left(\chi_{S_K}^{\varepsilon,0,\mathsf{e}}, w\right) + \sum_{\alpha=1}^{d} \left(\partial_\alpha \phi_i^{\mathbb{P}_1}\right)\big|_K\, s_K^\varepsilon\left(\chi_{S_K}^{\varepsilon,\alpha,\mathsf{e}}, w\right)$$

$$= s_K^\varepsilon\left(\widehat{\phi_i^{\mathbb{P}_1}\big|_K}, w\right) - \phi_i^{\mathbb{P}_1}(x_{c,K})\, s_K^\varepsilon(1, w) - \sum_{\alpha=1}^{d}\left(\partial_\alpha \phi_i^{\mathbb{P}_1}\right)\big|_K\, s_K^\varepsilon\left(x^\alpha - x_{c,K}^\alpha, w\right)$$

$$= s_K^\varepsilon\left(\widehat{\phi_i^{\mathbb{P}_1}\big|_K}, w\right) - s_K^\varepsilon\left(\phi_i^{\mathbb{P}_1}(x_{c,K}) + \sum_{\alpha=1}^{d}\left(\partial_\alpha \phi_i^{\mathbb{P}_1}\right)\big|_K\left(x^\alpha - x_{c,K}^\alpha\right), w\right).$$

Here we use that s_K^ε is a bilinear form on V_K, that all piecewise affine functions are contained in V_K according to Definition 5.10 (this ensures that $\widehat{\phi_i^\varepsilon}$ indeed lies in the domain of s_K^ε), and the property that $\nabla\phi_i^{\mathbb{P}_1}$ is piecewise constant. Finally, we use (4.20) for $\varphi = \widehat{\phi_i^{\mathbb{P}_1}}$ to conclude that $s_K^\varepsilon\left(\widehat{\phi_i^\varepsilon}, w\right) = s_K^\varepsilon\left(\widehat{\phi_i^{\mathbb{P}_1}\big|_K}, w\right) - s_K^\varepsilon\left(\widehat{\phi_i^{\mathbb{P}_1}\big|_K}, w\right) = 0$, which establishes the desired variational formulation satisfied by $\widehat{\phi_i^\varepsilon}$. ■

If the *DOF*-continuous problems (5.8) are well-posed, we obtain by the same arguments the following result for *DOF*-continuous multiscale basis functions.

Lemma 5.23. *Let K be any mesh element and let $1 \le i \le N$. Assume that any DOF-continuous local problem (5.8) is well-posed. Consider an MsFEM with DOF-continuous basis functions. Define an extension of ϕ_i^ε from K to S_K by*

$$\widehat{\phi_i^\varepsilon} = \widehat{\phi_i^{\mathbb{P}_1}\big|_K} + \phi_i^{\mathbb{P}_1}(x_{c,K})\,\chi_{S_K}^{\varepsilon,0,\mathsf{c}} + \sum_{\alpha=1}^{d}\partial_\alpha\big(\phi_i^{\mathbb{P}_1}\big|_K\big)\chi_{S_K}^{\varepsilon,\alpha,\mathsf{c}} \quad \text{in } S_K,$$

where $\chi_K^{\varepsilon,\alpha,\mathsf{c}}$ is as in Definition 5.16, and $\widehat{\phi_i^{\mathbb{P}_1}\big|_K}$ is as defined in Lemma 5.22. Then $\widehat{\phi_i^\varepsilon}$ is the unique solution in V_K to

$$\begin{cases} s_K^\varepsilon\left(\widehat{\phi_i^\varepsilon}, w\right) = 0 \text{ for all } w \in V_{K,0}, \\ \Gamma\left(K, \widehat{\phi_i^\varepsilon}\right) = \Gamma\left(K, \phi_i^{\mathbb{P}_1}\right). \end{cases} \tag{5.13}$$

Example 5.24 (MsFEM-lin for diffusion problems)**.** In the setting of Example 5.12, any *DOF*-extended multiscale basis function ϕ_i^ε for the MsFEM-lin constructed in (5.12) is obtained, in each mesh element K, as the restriction of a function $\widehat{\phi_i^\varepsilon}$, which is the unique solution in $H^1(S_K)$ to $-\mathrm{div}(A^\varepsilon\nabla\widehat{\phi_i^\varepsilon}) = 0$ in S_K with $\widehat{\phi_i^\varepsilon} = \widehat{\phi_i^{\mathbb{P}_1}}$ on ∂S_K. For a *DOF*-continuous basis function, $\widehat{\phi_i^\varepsilon}$ solves the same PDE in S_K, is affine on ∂S_K, and satisfies $\widehat{\phi_i^\varepsilon}(x_j) = \phi_i^{\mathbb{P}_1}(x_j)$ at all vertices x_j of K.

Example 5.25 (MsFEM-CR for diffusion problems)**.** In the continuation of Example 5.13, the *DOF*-extended multiscale basis function ϕ_i^ε for the MsFEM-CR is the restriction to K of $\widehat{\phi_i^\varepsilon}$, the unique solution in $H^1(S_K)$ to

$$\begin{cases} -\mathrm{div}(A^\varepsilon\nabla\widehat{\phi_i^\varepsilon}) = 0 & \text{in } S_K, \\ \vec{n}\cdot A^\varepsilon\nabla\widehat{\phi_i^\varepsilon} = 0 & \text{on each } h \in \mathscr{F}_a(S_K), \\ \vec{n}\cdot A^\varepsilon\nabla\widehat{\phi_i^\varepsilon} = c_h & \text{on each } h \in \mathscr{F}_d(S_K), \\ \dfrac{1}{|h|}\displaystyle\int_h \widehat{\phi_i^\varepsilon} = \dfrac{1}{|h|}\displaystyle\int_h \widehat{\phi_i^{\mathbb{P}_1}} & \text{for each } h \in \mathscr{F}_d(S_K), \end{cases}$$

where the constants c_h are uniquely determined by the problem. We recall that the sets of faces $\mathscr{F}_a(S_K)$ and $\mathscr{F}_d(S_K)$ are defined in Section 5.4.2. For *DOF*-continuous basis functions, the last condition is applied to the faces $h \in \mathscr{F}(K)$ (and all other conditions remain unchanged).

Our general framework allows two characterizations of the multiscale basis functions, namely (5.10) and (5.12) or (5.13), as was the case for the MsFEM studied in Section 4.2 (where ϕ_i^ε is given by (4.5) or (4.10)). The essential advantage of (5.10) is that the microscale is fully encoded in the numerical correctors $\chi_K^{\varepsilon,\alpha,\bullet}$, that can be computed element per element without any global information. In particular, the *global* index i of the multiscale basis function ϕ_i^ε is irrelevant for the computation of the numerical correctors. The expression in (5.10) is therefore the crucial relationship that we will employ to develop non-intrusive MsFEMs within the general framework in Chapter 6, just as was (4.10) in Sections 4.4 and 4.5.

The second formulation of the multiscale basis functions, as solutions to the local problems (5.12) or (5.13), provides a more direct interpretation of the multiscale basis functions in terms of the sampling form chosen. It also gives a relation between the degrees of freedom of the $\mathbb{P}_1$ basis functions and the associated multiscale basis function. This is useful in particular for the well-posedness of the MsFEM, that we study in Lemma 5.29.

Remark 5.26. Our definition of the multiscale basis functions in (5.10) is reminiscent of the Variational Multiscale Method, a framework developed in [101, 102] to adapt Galerkin approximations on low-dimensional spaces to the presence of multiscale features. In this context, our formulation of the MsFEM also exhibits a link with residual-free bubbles, see e.g. [41, 38, 102].

Remark 5.27. The first introduction of the MsFEM in [98] corresponds to the idea of oversampling with *DOF*-continuous basis functions. Although their existence cannot be established in general, they are computed numerically by taking linear combinations of *DOF*-extended basis functions (following an analogous strategy to the one we discussed in Section 5.4.5). The MsFEM with *DOF*-extended basis functions is studied in the works [70, 100] dealing with the convergence analysis of the MsFEM-lin with oversampling.
Let us also note that the combination of Crouzeix-Raviart MsFEM and oversampling has, to the best of our knowledge, not yet been proposed in the literature. This method, for which the basis functions are given explicitly in Example 5.25, is a natural by-product of the identification of the abstract MsFEM framework.

5.6. The global problem

We can now define the multiscale trial and test spaces, respectively V_H^ε and $V_{H,0}^\varepsilon$, as follows:

$$V_H^\varepsilon = \{\phi_i^\varepsilon \mid 1 \le i \le N\}, \qquad V_{H,0}^\varepsilon = \{\phi_i^\varepsilon \mid 1 \le i \le N_0\}.$$

We recall that we have assumed the first N_0 basis functions of V_H to form a basis of $V_{H,0}$ in Section 5.5. Note that we only use $V_{H,0}^\varepsilon$ in the present section, because (5.1) is posed with homogeneous Dirichlet boundary conditions, but that the larger space V_H^ε is useful for more general boundary conditions (see Section 6.3). Applying (5.10), we have the

equivalent characterization in terms of the $\mathbb{P}_1$ space V_H,

$$V_H^\varepsilon = \left\{ v_H^\varepsilon = v_H + \sum_{K\in\mathscr{T}_H} \left(v_H(x_{c,K})\, \chi_K^{\varepsilon,0,\bullet} + \sum_{\alpha=1}^{d} \partial_\alpha(v_H|_K)\chi_K^{\varepsilon,\alpha,\bullet} \right) \middle| \; v_H \in V_H \right\}. \tag{5.14}$$

Definition 5.28. Let V_H be an underlying $\mathbb{P}_1$ space defined in Definition 5.4 with the associated *DOF* operator Γ from Definition 5.5 and Definition 5.8-5.9. Define for each mesh element $K \in \mathscr{T}_H$ an oversampling patch (Definition 5.7), a sampling space and sampling form in accordance with Definition 5.10. Let the multiscale basis functions ϕ_i^ε be given as in Definition 5.21. Then a **Multiscale Finite Element Method** (MsFEM) for problem (5.1) is: find $u_H^\varepsilon \in V_{H,0}^\varepsilon$ such that

$$\forall\, v_H^\varepsilon \in V_{H,0}^\varepsilon, \qquad \sum_{K\in\mathscr{T}_H} a_K^\varepsilon\left(u_H^\varepsilon, v_H^\varepsilon\right) = F\left(v_H^\varepsilon\right). \tag{5.15}$$

In the following lemma, we investigate the well-posedness of the MsFEM.

Lemma 5.29. *Consider an MsFEM without oversampling, or an MsFEM with oversampling using DOF-continuous basis functions (assuming the associated basis functions are well-defined). When a^ε satisfies (5.2), the MsFEM (5.15) has a unique solution.*

Proof. Note that, with *DOF*-continuous oversampling, but also without oversampling, the multiscale basis functions satisfy (5.13). In particular, all degrees of freedom of u_H^ε related to the boundary vanish. Also note that, the dimension of $V_{H,0}^\varepsilon$ being finite, it suffices to show that $u_H^\varepsilon = 0$ is the unique solution to problem (5.15) with $F = 0$.

If $0 = F(u_H^\varepsilon) = a^\varepsilon(u_H^\varepsilon, u_H^\varepsilon)$, it follows from (5.2) that u_H^ε is piecewise constant. Let us write $u_H^\varepsilon = \sum_{i=1}^{N_0} \alpha_i\, \phi_i^\varepsilon$ for some coefficients $\alpha_i \in \mathbb{R}$ and introduce the function $u_H = \sum_{i=1}^{N_0} \alpha_i\, \phi_i^{\mathbb{P}_1} \in V_H$. Because of (5.13), we have $\Gamma(K, u_H^\varepsilon) = \Gamma(K, u_H)$ for all mesh elements K. Since u_H^ε is piecewise constant and $\Gamma(K,\cdot)$ is a bijection from $\mathbb{P}_1(K)$ to $\mathbb{R}^{d+1}$ (recall Definition 5.5), it follows that $u_H^\varepsilon = u_H$. In particular, the multiscale function u_H^ε in fact belongs to the underlying $\mathbb{P}_1$ space V_H.

We remarked immediately below Definition 5.4 that, for either of the two spaces $V_H = V_H^L$ or V_H^{CR}, the above implies that u_H^ε is constant throughout Ω. Since the degrees of freedom of u_H^ε associated to the boundary vanish, we readily deduce that $u_H^\varepsilon = 0$. ■

We do not know of the existence of a result on the well-posedness of MsFEMs with oversampling using *DOF*-extended multiscale basis functions. In [100], the authors establish an inf-sup result for a variant of the MsFEM-lin with oversampling that uses $\mathbb{P}_1$ test functions (see also Definition 6.1). This result is obtained for a periodic diffusion coefficient in the limit of sufficiently small ε.

Chapter 6

Non-intrusive MsFEM for the general framework

We show in this chapter how to develop a non-intrusive implementation for the general MsFEM framework of Chapter 5. We have seen in Lemma 4.5 that, for a particular MsFEM variant, the non-intrusive Galerkin MsFEM approach coincides with a Petrov-Galerkin MsFEM. This does not hold true for all MsFEMs in the general framework. We first develop a non-intrusive MsFEM approach for a Petrov-Galerkin MsFEM in the general framework. We show that the non-intrusive approach for the Petrov-Galerkin MsFEM is actually equivalent to the Petrov-Galerkin MsFEM itself. In a second step, we introduce a non-intrusive approximation of the Galerkin MsFEM. Before doing so, let us summarize the main steps of Sections 4.4 and 4.5 to obtain a non-intrusive MsFEM approach:

(1) the expansion (4.10) allows to recast the matrix $\mathbb{A}^\varepsilon$ of the linear system for the MsFEM as the matrix $\mathbb{A}^{\mathbb{P}_1}$ associated to the $\mathbb{P}_1$ discretization of an effective problem;

(2) we approximate the right-hand side $\mathbb{F}^\varepsilon$ of the MsFEM problem by the right-hand side $\mathbb{F}^{\mathbb{P}_1}$ of this $\mathbb{P}_1$ discretization;

(3) the post-processing step (4.21) applied to the $\mathbb{P}_1$ approximation of the effective problem yields the MsFEM approximation.

6.1. The Petrov-Galerkin MsFEM

We recall that the abstract continuous problem for which we developed the MsFEM in Section 5.1.3 is given by (5.1) and that it can be rewritten in terms of the bilinear forms a_K^ε satisfying (5.2). Petrov-Galerkin variants of the multiscale finite element method with $\mathbb{P}_1$ test functions were previously studied in [100, 94]. In our general MsFEM framework, the adaptation of Definition 5.28 to a Petrov-Galerkin MsFEM is the following.

Definition 6.1. Let V_H be an underlying $\mathbb{P}_1$ space defined in Definition 5.4 with the associated *DOF* operator Γ from Definition 5.5 and Definition 5.8-5.9. Define for each mesh element $K \in \mathscr{T}_H$ an oversampling patch (Definition 5.7), a sampling space and sampling form in accordance with Definition 5.10. Let the multiscale basis functions ϕ_i^ε

be given as in Definition 5.21. Then a **Petrov-Galerkin Multiscale Finite Element Method** (PG-MsFEM) for problem (5.1) is: find $u_H^\varepsilon \in V_{H,0}^\varepsilon$ such that

$$\forall\, v_H \in V_{H,0}, \qquad \sum_{K\in\mathscr{T}_H} a_K^\varepsilon(u_H^\varepsilon, v_H) = F(v_H). \tag{6.1}$$

When confusion may arise, we shall refer to the MsFEM defined in Definition 5.28 as the Galerkin MsFEM (G-MsFEM). To study well-posedness of the PG-MsFEM, it is most convenient to relate this method to the G-MsFEM. Therefore, we postpone well-posedness of (6.1) to Lemma 6.4.

We now execute step (1) of the summary of the non-intrusive MsFEM approach at the beginning of this chapter. The matrix $\mathbb{A}^\varepsilon$ of the linear system associated to (6.1) is defined by

$$\mathbb{A}_{j,i}^\varepsilon = \sum_{K\in\mathscr{T}_H} a_K^\varepsilon\big(\phi_i^\varepsilon,\, \phi_j^{\mathbb{P}_1}\big), \quad 1 \le i,j \le N_0. \tag{6.2}$$

To find an effective $\mathbb{P}_1$ formulation with the same linear system, we will use the definition (5.10) of the multiscale basis functions in the general framework, but first we combine it with (4.20) applied to $\varphi = \phi_i^{\mathbb{P}_1}$ to rewrite (5.10) as

$$\begin{aligned}\phi_i^\varepsilon\big|_K &= \phi_i^{\mathbb{P}_1}(x_{c,K}) + \phi_i^{\mathbb{P}_1}(x_{c,K})\,\chi_K^{\varepsilon,0,\bullet} + \sum_{\alpha=1}^d \partial_\alpha\phi_i^{\mathbb{P}_1}\big|_K\,\big(x^\alpha - x_{c,K}^\alpha + \chi_K^{\varepsilon,\alpha,\bullet}\big)\\ &= \phi_i^{\mathbb{P}_1}(x_{c,K})\,\Lambda_K^{\varepsilon,0} + \sum_{\alpha=1}^d \partial_\alpha\phi_i^{\mathbb{P}_1}\big|_K\,\Lambda_K^{\varepsilon,\alpha},\end{aligned} \tag{6.3}$$

where

$$\Lambda_K^{\varepsilon,0} := 1 + \chi_K^{\varepsilon,0,\bullet}, \quad \Lambda_K^{\varepsilon,\alpha} := x^\alpha - x_{c,K}^\alpha + \chi_K^{\varepsilon,\alpha,\bullet}, \tag{6.4}$$

for all $1 \le \alpha \le d$ and each $K \in \mathscr{T}_H$. We recall that $\bullet \in \{\mathsf{e},\mathsf{c}\}$ indicates the choice of *DOF*-extended or *DOF*-continuous basis functions. Inserting (6.3) into (6.2) for ϕ_i^ε and (4.20) for $\varphi = \phi_j^{\mathbb{P}_1}$ yields

$$\begin{aligned}\mathbb{A}_{j,i}^\varepsilon = \sum_{K\in\mathscr{T}_H}\Bigg(&\phi_i^{\mathbb{P}_1}(x_{c,K})\; a_K^\varepsilon\big(\Lambda_K^{\varepsilon,0}, 1\big)\;\phi_j^{\mathbb{P}_1}(x_{c,K}) + \sum_{\alpha=1}^d \big(\partial_\alpha\phi_i^{\mathbb{P}_1}\big)\big|_K\; a_K^\varepsilon(\Lambda_K^{\varepsilon,\alpha}, 1)\,\phi_j^{\mathbb{P}_1}(x_{c,K})\\ &+ \sum_{\beta=1}^d \phi_i^{\mathbb{P}_1}(x_{c,K})\; a_K^\varepsilon\Big(\Lambda_K^{\varepsilon,0}, x^\beta - x_{c,K}^\beta\Big)\;\big(\partial_\beta\phi_j^{\mathbb{P}_1}\big)\big|_K\\ &+ \sum_{\alpha,\beta=1}^d \big(\partial_\alpha\phi_i^{\mathbb{P}_1}\big)\big|_K\; a_K^\varepsilon\Big(\Lambda_K^{\varepsilon,\alpha}, x^\beta - x_{c,K}^\beta\Big)\;\big(\partial_\beta\phi_j^{\mathbb{P}_1}\big)\big|_K\Bigg),\end{aligned}$$

and therefore,

$$\boxed{\begin{aligned}\mathbb{A}_{j,i}^\varepsilon = &\sum_{K\in\mathscr{T}_H} |K|\;\big(\overline{M}\phi_i^{\mathbb{P}_1}\,\phi_j^{\mathbb{P}_1}\big)(x_{c,K})\\ &\qquad + \int_K \phi_j^{\mathbb{P}_1}\,\overline{B}^1\cdot\nabla\phi_i^{\mathbb{P}_1} + \phi_i^{\mathbb{P}_1}\,\overline{B}^2\cdot\nabla\phi_j^{\mathbb{P}_1} + \nabla\phi_j^{\mathbb{P}_1}\cdot\overline{A}\,\nabla\phi_i^{\mathbb{P}_1},\end{aligned}} \tag{6.5}$$

where we have defined the effective mass $\overline{M}$, (adjoint) advection vector $\overline{B}^1$ and $\overline{B}^2$, and the effective diffusion tensor $\overline{A}$, for all $1 \leq \alpha, \beta \leq d$ and for each $K \in \mathscr{T}_H$, as

$$\begin{aligned} \overline{M}\big|_K &= \frac{1}{|K|}\, a_K^\varepsilon\big(\Lambda_K^{\varepsilon,0}, 1\big), & \overline{B}^1_\alpha\Big|_K &= \frac{1}{|K|}\, a_K^\varepsilon(\Lambda_K^{\varepsilon,\alpha}, 1), \\ \overline{B}^2_\beta\Big|_K &= \frac{1}{|K|}\, a_K^\varepsilon\Big(\Lambda_K^{\varepsilon,0}, x^\beta - x^\beta_{c,K}\Big), & \overline{A}_{\beta,\alpha}\big|_K &= \frac{1}{|K|}\, a_K^\varepsilon\Big(\Lambda_K^{\varepsilon,\alpha}, x^\beta - x^\beta_{c,K}\Big). \end{aligned} \tag{6.6}$$

Note that $\overline{M}$, $\overline{B}^1$, $\overline{B}^2$ and $\overline{A}$ are all piecewise constant quantities. All integrals in (6.5) can be computed exactly by evaluating the integrand at the centroid. With this quadrature rule, we observe that the term $|K|\left(\overline{M}\phi_i^{\mathbb{P}_1}\,\phi_j^{\mathbb{P}_1}\right)(x_{c,K})$ also equals the numerical approximation of the integral $\displaystyle\int_K \overline{M}\phi_i^{\mathbb{P}_1}\phi_j^{\mathbb{P}_1}$.

The new expression (6.5) for the matrix of the linear system motivates us to introduce the effective bilinear forms $\overline{a}_K$ defined on $H^1(K) \times H^1(K)$ by

$$\begin{aligned} \overline{a}_K(u,v) = \int_K \nabla v \cdot \overline{A}\,\nabla u + v\left(\overline{B}^1 \cdot \nabla u\right) \\ + u\left(\overline{B}^2 \cdot \nabla v\right) + \overline{M}\,u\,v, \quad \text{for all } u,\, v \in H^1(K), \end{aligned} \tag{6.7}$$

and the associated $\mathbb{P}_1$ Galerkin approximation on the space $V_{H,0}$:

$$\text{Find } u_H \in V_{H,0} \text{ such that } \sum_{K\in\mathscr{T}_H} \overline{a}_K(u_H, v_H) = F(v_H) \quad \text{for all } v_H \in V_{H,0}. \tag{6.8}$$

This discrete problem leads to a linear system with the matrix

$$\mathbb{A}^{\mathbb{P}_1}_{j,i} = \overline{a}\left(\phi_i^{\mathbb{P}_1},\, \phi_j^{\mathbb{P}_1}\right) = \sum_{K\in\mathscr{T}_H} \overline{a}_K(\phi_i^{\mathbb{P}_1},\, \phi_j^{\mathbb{P}_1}), \quad 1 \leq i,j \leq N_0.$$

The identity (6.5) thus implies the following result, which generalizes Lemma 4.2 to the PG-MsFEM in the general framework.

Theorem 6.2. *The matrices $\mathbb{A}^\varepsilon$ and $\mathbb{A}^{\mathbb{P}_1}$ are identical if the integrals in (6.7) are evaluated at the centroid of each mesh element K for the computation of $\mathbb{A}^{\mathbb{P}_1}$. Then the PG-MsFEM (6.1) coincides with the resolution of the effective problem (6.8) combined with the post-processing step*

$$u_H^\varepsilon\big|_K = u_H(x_{c,K})\,\Lambda_K^{\varepsilon,0} + \sum_{\alpha=1}^d \partial_\alpha u_H\big|_K\,\Lambda_K^{\varepsilon,\alpha}. \tag{6.9}$$

Note that step (2) of the summary at the beginning of this chapter is irrelevant for the PG-MsFEM. The computation of the right-hand side in (6.1) is clearly part of any standard FEM software. We refer to Remark 4.3 and 4.4 for some additional comments on the post-processing step.

The computational approach described by Theorem 6.2 naturally fits within the non-intrusive workflow of Algorithm 4.2. The numerical correctors on line 4 are, of course, replaced by those of Definition 5.11 or Definition 5.16. Line 6 is replaced by the computation of all effective quantities in (6.6), where $\Lambda_K^{\varepsilon,\alpha}$ is related to the numerical correctors

by (6.4). The online phase in line 8 amounts to solving the $\mathbb{P}_1$ problem (6.8), where all integrations to construct the matrix of the linear system are to be performed by evaluation at the centroid. (This is not the case for the construction of the right-hand side, however.) Finally, in the post-processing phase, we construct u_H^ε from u_H by virtue of (6.9).

Next we generalize the above expansions to design a non-intrusive approximation of the G-MsFEM.

6.2. The non-intrusive Galerkin MsFEM

For the G-MsFEM (introduced in Definition 5.28), we need to replace the $\mathbb{P}_1$ test space $V_{H,0}$ of the PG-MsFEM by the multiscale test space $V_{H,0}^\varepsilon$. The matrix of the linear system associated to (5.15) is given by

$$\mathbb{A}_{j,i}^{\varepsilon,\mathsf{G}} = \sum_{K\in\mathscr{T}_H} a_K^\varepsilon\big(\phi_i^\varepsilon, \phi_j^\varepsilon\big), \quad 1 \le i,j \le N_0.$$

Upon inserting (5.10) for the test function ϕ_j^ε, we find, for all $1 \le i,j \le N_0$,

$$\mathbb{A}_{j,i}^{\varepsilon,\mathsf{G}} = \mathbb{A}_{j,i}^{\varepsilon} + \sum_{K\in\mathscr{T}_H} \left(\phi_j^{\mathbb{P}_1}(x_{c,K})\, a_K^\varepsilon\big(\phi_i^\varepsilon, \chi_K^{\varepsilon,0,\bullet}\big) + \sum_{\beta=1}^{d} \big(\partial_\beta \phi_j^{\mathbb{P}_1}\big)\big|_K\, a_K^\varepsilon\Big(\phi_i^\varepsilon, \chi_K^{\varepsilon,\beta,\bullet}\Big)\right),$$

where $\mathbb{A}^\varepsilon$ is the matrix of the Petrov-Galerkin MsFEM, see (6.2) and (6.5).

An effective formulation can again be derived by inserting (6.3) for the ϕ_i^ε. We obtain

$$\boxed{\begin{aligned}\mathbb{A}_{j,i}^{\varepsilon,\mathsf{G}} = \sum_{K\in\mathscr{T}_H} |K| \left(\overline{M}^{\mathsf{G}} \phi_i^{\mathbb{P}_1}\, \phi_j^{\mathbb{P}_1}\right)(x_{c,K}) \\ + \int_K \phi_j^{\mathbb{P}_1}\, \overline{B}^{1,\mathsf{G}} \cdot \nabla\phi_i^{\mathbb{P}_1} + \phi_i^{\mathbb{P}_1}\, \overline{B}^{2,\mathsf{G}} \cdot \nabla\phi_j^{\mathbb{P}_1} + \nabla\phi_j^{\mathbb{P}_1} \cdot \overline{A}^{\mathsf{G}}\, \nabla\phi_i^{\mathbb{P}_1},\end{aligned}}$$

where the effective mass, (adjoint) advection vectors and diffusion tensor are given by (using those defined in (6.6))

$$\begin{aligned}
\overline{M}^{\mathsf{G}}\Big|_K &= \overline{M}\big|_K + \frac{1}{|K|}\, a_K^\varepsilon\big(\Lambda_K^{\varepsilon,0}, \chi_K^{\varepsilon,0,\bullet}\big), \\
\overline{B}_\alpha^{1,\mathsf{G}}\Big|_K &= \overline{B}_\alpha^{1}\Big|_K + \frac{1}{|K|}\, a_K^\varepsilon\big(\Lambda_K^{\varepsilon,\alpha}, \chi_K^{\varepsilon,0,\bullet}\big), \\
\overline{B}_\beta^{2,\mathsf{G}}\Big|_K &= \overline{B}_\beta^{2}\Big|_K + \frac{1}{|K|}\, a_K^\varepsilon\Big(\Lambda_K^{\varepsilon,0}, \chi_K^{\varepsilon,\beta,\bullet}\Big), \\
\overline{A}_{\beta,\alpha}^{\mathsf{G}}\Big|_K &= \overline{A}_{\beta,\alpha}\big|_K + \frac{1}{|K|}\, a_K^\varepsilon\Big(\Lambda_K^{\varepsilon,\alpha}, \chi_K^{\varepsilon,\beta,\bullet}\Big).
\end{aligned} \tag{6.10}$$

Again, these quantities are all piecewise constant. We can now introduce $\overline{a}^{\mathsf{G}} = \sum_{K\in\mathscr{T}_H} \overline{a}_K^{\mathsf{G}}$, the effective bilinear forms $\overline{a}_K^{\mathsf{G}}$, for all $K \in \mathscr{T}_H$, being defined by

$$\overline{a}_K^{\mathsf{G}}(u,v) = \int_K \nabla v \cdot \overline{A}^{\mathsf{G}}\, \nabla u + v\left(\overline{B}^{1,\mathsf{G}} \cdot \nabla u\right) + u\left(\overline{B}^{2,\mathsf{G}} \cdot \nabla v\right) + \overline{M}^{\mathsf{G}}\, u\, v. \tag{6.11}$$

This leads to the formulation of the following effective variational problem:

$$\text{Find } u_H \in V_{H,0} \text{ such that } \sum_{K\in\mathscr{T}_H} \overline{a}_K^{\mathsf{G}}(u_H, v_H) = F(v_H) \quad \text{for all } v_H \in V_{H,0}. \tag{6.12}$$

The associated linear system has coefficients $\mathbb{A}_{j,i}^{\mathbb{P}_1,\mathsf{G}} = \overline{a}^{\mathsf{G}}\left(\phi_i^{\mathbb{P}_1}, \phi_j^{\mathbb{P}_1}\right)$. We have the following analogue of Theorem 6.2, which generalizes Lemma 4.2 to the G-MsFEM in the general framework.

Theorem 6.3. *The matrices $\mathbb{A}^{\varepsilon,\mathsf{G}}$ and $\mathbb{A}^{\mathbb{P}_1,\mathsf{G}}$ are identical if the integrals in (6.11) are evaluated at the centroid of each mesh element K in the computation of $\mathbb{A}^{\mathbb{P}_1,\mathsf{G}}$.*

Contrary to the matrices, the right-hand sides of the effective problem (6.12) and the Galerkin MsFEM (5.15) are not equal in general. We apply step (2) formulated at the beginning of this chapter: the right-hand side of the G-MsFEM is approximated by the right-hand side of the effective problem to obtain an approximate, but non-intrusive, MsFEM. The non-intrusive G-MsFEM becomes:

$$\text{Find } u_H^\varepsilon \in V_{H,0}^\varepsilon \text{ such that } \sum_{K\in\mathscr{T}_H} a_K^\varepsilon\left(u_H^\varepsilon, \phi_j^\varepsilon\right) = F\left(\phi_j^{\mathbb{P}_1}\right) \quad \text{for all } 1 \le j \le N_0. \tag{6.13}$$

This problem is no longer a Galerkin approximation of (4.1), because different test spaces are used for the bilinear and for the linear form. In view of Theorem 6.3, the non-intrusive MsFEM can equivalently be formulated as

$$\text{compute } u_H \in V_{H,0} \text{ solution to (6.12) and compute } u_H^\varepsilon \text{ from } u_H \text{ by (6.9)},$$

provided all integrals in (6.11) are evaluated at the centroid for the construction of the matrix of the linear system in (6.12).

The latter formulation of the non-intrusive MsFEM immediately suggests how to effectively implement the non-intrusive MsFEM in a non-intrusive way similar to Algorithm 4.2. For completeness, we provide the algorithm for the non-intrusive G-MsFEM in Algorithm 6.1.

Algorithm 6.1 Non-intrusive G-MsFEM for the general framework

```
Let 𝒯_H be the mesh used by the legacy code, let • ∈ {e, c} be the chosen oversampling variant
for all K ∈ 𝒯_H do
    for 0 ≤ α ≤ d do
        Solve for the applicable χ_K^{ε,α,•} from Definition 5.11 or 5.16
    end for
    Compute the effective tensors defined in (6.10)
end for
Use the legacy code to construct the matrix 𝔸^{ℙ1} by evaluating (6.11) at the centroid of each mesh element and to solve for u_H defined by (6.12)
Save {u_H(x_{c,K})}_{K∈𝒯_H} and {(∂_α u_H)|_K}_{K∈𝒯_H, 1≤α≤d}
Obtain the MsFEM approximation u_H^ε from (6.9)
```

The discussion surrounding Algorithm 4.2 regarding the advantages for the implementation of this non-intrusive MsFEM approach also applies here.

Let us now comment on the well-posedness of the MsFEMs for the general framework introduced above. We recall that the hypotheses of the general framework without oversampling, or with *DOF*-continuous oversampling, provide well-posedness of the G-MsFEM (5.15) by Lemma 5.29. In this case, the non-intrusive approximation (6.13) is also well-posed, because the matrices associated to both MsFEM variants are the same. Regarding the PG-MsFEM (6.1), we can only establish well-posedness if the associated matrix coincides with the matrix of the corresponding Galerkin MsFEM. This is stated in the following lemma, which generalizes Lemma 4.5 to the general framework.

Lemma 6.4. *Consider a G-MsFEM as defined by Definition 5.28 without oversampling and suppose that the sampling form s_K^ε equals the local bilinear form a_K^ε. Then the matrix associated to this G-MsFEM coincides with the matrix associated to the corresponding PG-MsFEM of Definition 6.1. Consequently, the non-intrusive Galerkin MsFEM (6.13) coincides with the Petrov-Galerkin MsFEM (6.1) and in particular, the Petrov-Galerkin MsFEM is well-posed.*

Proof. To prove the lemma, we show that the matrices corresponding to the linear problems defined in (6.13) and (6.1) are equal. Using that $s_K^\varepsilon = a_K^\varepsilon$, we have for all $1 \leq i,\, j \leq N_0$,

$$\mathbb{A}_{j,i}^{\varepsilon,\mathsf{G}} - \mathbb{A}_{j,i}^{\varepsilon} = \sum_{K\in\mathscr{T}_H} a_K^\varepsilon\left(\phi_i^\varepsilon, \phi_j^\varepsilon - \phi_j^{\mathbb{P}_1}\right) = \sum_{K\in\mathscr{T}_H} s_K^\varepsilon\left(\phi_i^\varepsilon, \phi_j^\varepsilon - \phi_j^{\mathbb{P}_1}\right) = 0. \tag{6.14}$$

The last equality stems from the fact that the multiscale basis functions satisfy $\Gamma(K, \phi_i^\varepsilon) = \Gamma(K, \phi_i^{\mathbb{P}_1})$ for all K, so that $\phi_j^\varepsilon - \phi_j^{\mathbb{P}_1} \in V_{K,0}$ (see (5.12) with $S_K = K$ and recall Definition 5.10 for the sampling test space $V_{K,0}^\varepsilon$), and the variational problem in (5.12) (with $S_K = K$) shows that the above quantity vanishes. ■

6.3. Further extensions of the non-intrusive MsFEM

We sketch some other FEM settings to which we have applied the above strategy to develop non-intrusive MsFEM approaches.

Stabilized finite element formulations. In the context of advection-diffusion problems, stabilized finite element formulations add mesh-dependent terms to a discrete variational formulation (such as (5.15)) to remove numerical instabilities, for example caused by sharp boundary layers of the exact solution. See [114] for such a variant of the MsFEM and see [43, 103, 129] for the stabilization of single-scale problems. The expansion (6.3) can also be inserted in these additional terms to find a non-intrusive implementation of the associated MsFEM.

Petrov-Galerkin formulations. Other test spaces than the $\mathbb{P}_1$ space $V_{H,0}$ can be considered in Petrov-Galerkin formulations. An example would be to use multiscale test functions that locally solve the adjoint problem rather than the direct problem, introducing yet another bilinear form than s_K^ε in (5.12) or (5.13). See e.g. [77]. An expansion of the kind (6.3) can still be found for such test functions, with a suitably adapted definition of the numerical correctors. This way, a non-intrusive formulation can be found using the techniques of Part I of this thesis.

Non-homogeneous Dirichlet conditions. Suppose that a legacy FEM code can provide a solution to an effective problem such as (6.8) posed on the space $V_{H,0}$ and complemented with non-homogeneous Dirichlet conditions for u_H on $\partial\Omega$. This solution can directly be used to construct a multiscale approximation $u_H^\varepsilon \in V_H^\varepsilon$ from (6.9). The translation of the Dirichlet condition to the MsFEM approximation is as follows: if *DOF*-continuous oversampling is applied, the function u_H^ε satisfies $[\Gamma(K, u_H^\varepsilon)]_j = [\Gamma(K, u_H)]_j$ for all degrees of freedom associated to the boundary. Here, $[\Gamma(K, u_H)]_j$ is determined by the legacy code. When *DOF*-extended oversampling is used, the degrees of freedom associated to the boundary are equal to the sum of $[\Gamma(K, u_H)]_j$ and a perturbation due to the fact that the degrees of freedom of the numerical correctors do not vanish.

Neumann conditions. To apply Neumann conditions on $\partial\Omega$, one solves a Galerkin approximation of the variational formulation in the space V_H^ε. The suitable adaptation of (5.15) can be approximated by a non-intrusive Galerkin MsFEM following the same methodology as above. The effective $\mathbb{P}_1$ approximation that is obtained corresponds to the resolution of an effective PDE with Neumann conditions, for which a legacy code can be used. In the case of the diffusion problem (4.1), the Neumann boundary condition in the effective problem is imposed on the effective flux $\vec{n} \cdot \overline{A}\nabla u_H$, where $\overline{A}$ is defined in (4.12).

Parabolic equations. When a parabolic equation is discretized in time, problems of the form (5.1) are typically obtained for each time step, but with a right-hand side that depends on the solution of the previous time step. This term belongs to the space V_H^ε, so it varies on the microscale and cannot be integrated numerically by the legacy code that operates on the coarse mesh. The non-intrusive strategy of the foregoing sections cannot be applied directly to find a non-intrusive MsFEM. In the vein of our non-intrusive approach, one could introduce an additional approximation by replacing the multiscale solution of the previous time step by its underlying $\mathbb{P}_1$ representation in the $\mathbb{P}_1$ space V_H. Studying the effect of this approximation is beyond the scope of the present work.

6.4. Intrusiveness of other multiscale methods

Some work on the formulation of effective $\mathbb{P}_1$ problems in multiscale methods, and the related question of non-intrusive approaches, can be found in the literature. We discuss here the case of the Heterogeneous Multiscale Method (HMM) and the localized orthogonal decomposition (LOD) in the context of numerical homogenization, and provide some additional references to other fields at the end of this section.

6.4.1. The heterogeneous multiscale method. Let us briefly describe the finite element HMM such as introduced e.g. in [5]. It is *assumed* that (4.1) can be solved by applying a finite element to an effective equation like (4.14) for an effective diffusion tensor $\overline{A}$ that is to be approximated based on the microstructure. The effective model will be resolved with existing finite element software. The HMM is thus non-intrusive by construction. Let us focus on a legacy code using a $\mathbb{P}_1$ finite element method and denote by x_K the centroid of the mesh element K for each $K \in \mathscr{T}_H$. Then the bilinear form in the variational formulation of the effective equation (see (4.16)) can be written

$$\overline{a}^{\mathsf{diff}}(u_H, v_H) = \sum_{K \in \mathscr{T}_H} |K|\, \bar{A}(x_K)\nabla u_H(x_K) \cdot \nabla v_H(x_K). \tag{6.15}$$

The effective coefficient $\bar{A}$ is thus to be computed (or approximated) only at the centroid of each coarse mesh element K. To this end, small sampling domains K_δ are introduced around each x_K. On each sampling domain, numerical correctors $\chi_{K_\delta}^{\varepsilon,\alpha}$ are computed that solve the equation

$$-\operatorname{div}\left(A^\varepsilon \nabla(\chi_{K_\delta}^{\varepsilon,\alpha} + x^\alpha)\right) = 0 \quad \text{in } K_\delta,$$

equipped with some choice of boundary conditions. These are used to compute $\bar{A}$ according to the formula

$$\overline{A}_{\beta,\alpha}(x_K) := \frac{1}{|K_\delta|}\int_{K_\delta} e_\beta \cdot A^\varepsilon(e_\alpha + \nabla\chi_{K_\delta}^{\varepsilon,\alpha}) \quad \text{for each } K \in \mathscr{T}_H.$$

When one chooses $K_\delta = K$ and uses homogeneous Dirichlet boundary conditions on ∂K, it can be shown that this effective tensor corresponds exactly to (4.12). In this sense, the HMM is a generalization of the MsFEM. When we consider more general problems than the diffusion problem, there is an important difference between the two methods. For the MsFEM, the form of the effective equation and the definition of the effective coefficients follow directly from the choice of basis functions, and thus from the choice of local problems. For the HMM, the local problems and the effective equation are formulated independently, and the link between the two is only justified heuristically, drawing inspiration from homogenization theory.

In terms of intrusiveness, the (non-intrusive) Petrov-Galerkin MsFEM (Definition 6.1), the non-intrusive Galerkin MsFEM (6.13) and the HMM are much alike. Similar problems have to be solved to compute the effective macroscopic coefficient in the offline stage. With both methods, a legacy code can be used for the effective problem as soon as the effective coefficient has been computed externally and can be read by the legacy code.

In practice, the sampling domains K_δ used for the HMM are much smaller than an entire coarse mesh element K that is used for the local problems of the MsFEM. One must ensure that K_δ captures the microstructure sufficiently well. Another difference between the two methods is that the solution of the effective problem of the HMM does not impose an immediate reconstruction of the microscopic scale that approximates u^ε in the H^1-norm, since the microscopic structure is only sampled in the subdomains K_δ and not throughout the entire domain. In contrast, the MsFEM yields an approximation of the solution u^ε in the L^2- and H^1-norms. However, periodic extensions of the microscopic information in each K_δ may be considered to restore the microscale with the HMM. We refer e.g. to [2].

6.4.2. The localized orthogonal decomposition. Here we compare the implementation of the MsFEM to the LOD. See [120] for the original introduction of the method for symmetric elliptic problems, and [12] for a more general framework.

Like the MsFEM, the method relies on the computation of numerical correctors. These correctors are, in contrast, not supported by a single mesh element, but by an element patch around a central mesh element K. We denote these numerical correctors by $q_{K,l}^\alpha$, where l is an integer indicating the size of the patch that supports the corrector, and α indicates the space direction to which the corrector is associated ($1 \le \alpha \le d$), as before. We do not further detail the definition of the numerical correctors, since it is carried out in an offline stage independently of the legacy code. Let us simply mention that the computation of $q_{K,l}^\alpha$ becomes more expensive as l increases.

To compare the implementation of the LOD to our non-intrusive MsFEM variants, it

is most illustrative to consider the Petrov-Galerkin variant discussed in [79]. The discrete problem on the coarse mesh is defined on the conforming $\mathbb{P}_1$ space that we denote by $V_{H,0}$. It reads: find $u_{H,l} \in V_{H,0}$ such that

$$a^{\varepsilon,\mathsf{diff}}\left(u_{H,l},\, v_H + \mathscr{C}^{(l)} v_H\right) = F(v_H) \quad \forall\, v_H \in V_{H,0}, \tag{6.16}$$

where, for any $v_H \in V_H$, the corrector $\mathscr{C}^{(l)} v_H$ is defined as

$$\mathscr{C}^{(l)} v_H = \sum_{K \in \mathscr{T}_H} \sum_{\alpha=1}^{d} (\partial_\alpha v_H)|_K \, q^\alpha_{K,l}. \tag{6.17}$$

A post-processing step as in our Algorithm 4.2 can be applied to compute

$$u^\varepsilon_{H,l} = (1 + \mathscr{C}^{(l)}) u_{H,l}.$$

Remark 6.5. In the (non-localized) limit $l \to \infty$, the discrete problem (6.16) is equivalent to finding $u_{H,\infty} \in V_{H,0}$ such that

$$\forall\, v_H \in V_{H,0}, \qquad a^{\varepsilon,\mathsf{diff}}\left(u_{H,\infty} + \mathscr{C}^{(\infty)} u_{H,\infty},\, v_H\right) = F(v_H).$$

This shows that the LOD presented in [79], before localization, is indeed a Petrov-Galerkin approximation of (4.3) on the trial space $(1 + \mathscr{C}^{(\infty)}) V_{H,0}$. We refer e.g. to [71] for more details on Galerkin and Petrov-Galerkin LOD methods, in particular for a discussion of the advantages regarding the implementation of Petrov-Galerkin variants with respect to Galerkin variants.

Although the corrector definition (6.17) resembles the expansion (4.10) for the MsFEM, the fact that the correctors $q^\alpha_{K,l}$ are not supported by a single mesh element has severe implications for the effective problem, as we shall see now. The matrix $\mathbb{A}^\varepsilon$ for the linear system associated to (6.16) is given by

$$\begin{aligned}
\mathbb{A}^\varepsilon_{j,i} &= \sum_{T \in \mathscr{T}_H} \sum_{\alpha,\beta=1}^{d} \left(\partial_\beta \phi^{\mathbb{P}_1}_j\right)\big|_T \left(\int_T e_\beta \cdot A^\varepsilon e_\alpha\right) \left(\partial_\alpha \phi^{\mathbb{P}_1}_i\right)\big|_T + \\
&\qquad \sum_{K \in \mathscr{T}_H} \sum_{\beta=1}^{d} \left(\partial_\beta \phi^{\mathbb{P}_1}_j\right)\big|_K \int_\Omega \nabla q^\beta_{K,l} \cdot A^\varepsilon \nabla \phi^{\mathbb{P}_1}_i \\
&= \sum_{T,K \in \mathscr{T}_H} \sum_{\alpha,\beta=1}^{d} \left(\partial_\beta \phi^{\mathbb{P}_1}_j\right)\big|_K \left(\int_T \left\{\delta_{T,K} e_\beta + \nabla q^\beta_{K,l}\right\} \cdot A^\varepsilon e_\alpha\right) \left(\partial_\alpha \phi^{\mathbb{P}_1}_i\right)\big|_T \\
&= \int_\Omega \int_\Omega \nabla \phi^{\mathbb{P}_1}_j(y) \cdot \mathscr{A}^{(l)}(x,y) \nabla \phi^{\mathbb{P}_1}_i(x) \,\mathrm{d}y \,\mathrm{d}x,
\end{aligned} \tag{6.18}$$

where the piecewise constant tensor $\mathscr{A}^{(l)} : \Omega \times \Omega \to \mathbb{R}^{d \times d}$ is defined for any $T, K \in \mathscr{T}_H$ as

$$\mathscr{A}^{(l)}_{\beta,\alpha}\Big|_{T \times K} = \frac{1}{|T|\,|K|} \int_T \left\{\delta_{T,K} e_\beta + \nabla q^\beta_{K,l}\right\} \cdot A^\varepsilon e_\alpha, \quad 1 \le \alpha, \beta \le d.$$

We observe that the effective macroscopic problem (6.18) for the LOD involves a bilinear form with a *double* integral. It is not natural to expect an existing code for

diffusion problems to be equipped for the discretization of such terms. The original version of the LOD is thus much more intrusive than the MsFEM, unless $l = 1$, in which case the numerical correctors are defined on a single mesh element.

In order to obtain an effective discrete problem that resembles the discretization of a diffusion problem, the following is suggested in [79]. Note that for any mesh element $K \in \mathscr{T}_H$, the effective tensor $\mathscr{A}^{(l)}(\bullet, K)$ contains the contributions to the effective scheme of the numerical correctors associated to K. In particular, if $l = 1$, we have $\mathscr{A}^{(1)}(T, K) = 0$ when $T \neq K$. The idea is to concentrate all contributions in all of Ω associated to the correctors $q^1_{K,l}, \dots q^d_{K,l}$ in an effective diffusion coefficient whose support is K. This is done by summing the contributions over the entire domain. We introduce the piecewise constant tensor $\overline{A}^{(l)} : \Omega \to \mathbb{R}^{d\times d}$ as

$$\begin{aligned}\overline{A}^{(l)}_{\beta,\alpha}\Big|_K &= \int_\Omega \mathscr{A}^{(l)}_{\beta,\alpha}(x, K)\,\mathrm{d}x \\ &= \frac{1}{|K|}\left(\int_K e_\beta \cdot A^\varepsilon e_\alpha + \int_\Omega \nabla q^\beta_{K,l} \cdot A^\varepsilon e_\alpha\right), \quad 1 \le \alpha, \beta \le d,\ K \in \mathscr{T}_H.\end{aligned}$$

The LOD (6.16) is subsequently replaced by: find $u_H \in V_{H,0}$ such that

$$\forall\, v_H \in V_{H,0}, \qquad \int_\Omega \nabla \phi^{\mathbb{P}_1}_j \cdot \overline{A}^{(l)}_{\beta,\alpha} \nabla \phi^{\mathbb{P}_1}_i = F(v_H). \tag{6.19}$$

Despite a more expensive offline stage, the macroscopic problem (6.19) has exactly the same structure as the Petrov-Galerkin MsFEM (7.4) and yields a non-intrusive LOD variant. It has to be noted, however, that well-posedness of the approximate problem (6.19) cannot be guaranteed a priori and can only be checked after the construction of the matrix $\overline{A}^{(l)}$.

6.4.3. Non-intrusive methods in other fields of computing. The question of non-intrusive implementations of multiscale algorithms is an interesting and relevant question in many more fields of scientific computing than we can discuss here. Beyond the field of finite element methods, we mention the multiscale finite volume method [106, 88], in which a non-intrusive coupling between the local and global computations is natural, since the local computations lead to transmissibilities that can be used in a separate, global finite volume simulator. Other than numerical homogenization methods, there are mixed finite element methods for multiscale modelling [50, 14, 16] and domain decomposition techniques (such as the generalized FEM, patches of finite elements, numerical zoom; see [39, 82, 13]), for which non-intrusive approaches can e.g. be found in [66, 87]. Finally, we would like to mention the reduced basis method for the efficient resolution of parameterized PDEs. Non-intrusive adaptations of this method (both for finite element and finite volume schemes) have been proposed and analysed e.g. in [48, 49, 86].

Chapter 7

Comparison of the classical and non-intrusive MsFEM for diffusion problems

We study in this chapter a particular setting within the general MsFEM framework, namely that of MsFEMs for diffusion problems. To this end, we adopt in this chapter the choice $a_K^\varepsilon = a_K^{\varepsilon,\mathsf{diff}}$ defined in Example 5.2, and for the sampling form we set $s_K^\varepsilon = a_K^{\varepsilon,\mathsf{diff}}$.

7.1. The general framework for diffusion problems

For the convenience of the reader, we first give an explicit description of the simplifications of the general framework in the diffusion setting. In Definition 5.11 and 5.16 for the numerical correctors, Equation (5.5) reduces to

$$a_K^{\varepsilon,\mathsf{diff}}\left(\chi_{S_K}^{\varepsilon,\alpha,\bullet}, w\right) = -a_K^{\varepsilon,\mathsf{diff}}\left(x^\alpha, w\right), \tag{7.1}$$

for all $w \in V_{K,0}$ (where $V_{K,0}$ is the sampling test space for either the MsFEM-lin or the MsFEM-CR; see Examples 5.12 and 5.13) when $1 \leq \alpha \leq d$, whereas $\chi_{S_K}^{\varepsilon,0,\bullet} = 0$. (The notation $\chi_K^{\varepsilon,\alpha}$ will be used in the absence of oversampling, see Remark 5.17.) This means that $\Lambda_K^{\varepsilon,0} = 1$ in (6.3). Consequently, regarding the formulation of the effective $\mathbb{P}_1$ problem, only the effective diffusion coefficient does not vanish in (6.6) and (6.10). Its definition in (6.10) is identical to the formula in (4.12) for the applicable choice of the numerical correctors.

The definition of the multiscale basis functions by (5.10) reduces to (4.10) (again upon replacing the numerical correctors $\chi_K^{\varepsilon,\alpha}$ by the relevant ones for the MsFEM under consideration). Hence, we can associate a multiscale counterpart in V_H^ε to any $v_H \in V_H$, given by

$$v_H^\varepsilon = v_H + \sum_{K\in\mathscr{T}_H} \sum_{\alpha=1}^{d} (\partial_\alpha v_H)|_K \, \chi_K^{\varepsilon,\alpha,\bullet}. \tag{7.2}$$

The non-intrusive MsFEM (6.13) becomes

$$\text{Find } u_H^\varepsilon \in V_{H,0}^\varepsilon \text{ such that } \sum_{K\in\mathscr{T}_H} a_K^{\varepsilon,\mathsf{diff}}\left(u_H^\varepsilon, \phi_j^\varepsilon\right) = F\left(\phi_j^{\mathbb{P}_1}\right) \quad \text{for all } 1 \le j \le N_0. \tag{7.3}$$

Lemma 6.4 now amounts to the following.

Lemma 7.1. *Let 'MsFEM' refer to the MsFEM-lin or the MsFEM-CR, both without oversampling. The non-intrusive Galerkin MsFEM (7.3) coincides with the following Petrov-Galerkin MsFEM:*

$$\textit{Find } u_H^\varepsilon \in V_{H,0}^\varepsilon \textit{ such that } \sum_{K\in\mathscr{T}_H} a_K^{\varepsilon,\mathsf{diff}}\left(u_H^\varepsilon, \phi_j^{\mathbb{P}_1}\right) = F\left(\phi_j^{\mathbb{P}_1}\right) \quad \textit{for all } 1 \le j \le N_0, \tag{7.4}$$

We will specify for all results in this section to which specific MsFEMs they apply among the MsFEM-lin and the MsFEM-CR, with or without oversampling. Lemmas 7.2 and 7.4 and Theorem 7.10 are generalizations of results in Chapter 3, where the MsFEM-lin without oversampling is considered.

7.2. Convergence results

We estimate here the difference between the solutions to the (intrusive) Galerkin approximation (5.15) and the non-intrusive MsFEM (7.3), which coincides with the Petrov-Galerkin MsFEM (7.4). We first show coercivity of the effective diffusion tensor $\overline{A}$.

Lemma 7.2. *Consider the MsFEM-lin or the MsFEM-CR, without oversampling, or the MsFEM-CR with DOF-continuous oversampling. The effective tensor $\overline{A}$ defined by (4.12) with the appropriate numerical correctors satisfies*

$$\forall \xi \in \mathbb{R}^d, \quad m|\xi|^2 \le \xi \cdot \overline{A}\,\xi.$$

Here, m is the same coercivity constant as in (4.2).

Proof. Let $\xi = (\xi_1, \dots, \xi_d) \in \mathbb{R}^d$, and let K be any simplex of the mesh $\mathscr{T}_H$. We have

$$\begin{aligned} |K|\,\xi \cdot \overline{A}\big|_K \xi &= \sum_{\alpha,\beta=1}^{d} a_K^{\varepsilon,\mathsf{diff}}\left(\xi_\alpha\left(x^\alpha + \chi_K^{\varepsilon,\alpha}\right), \xi_\beta\left(x^\beta + \chi_K^{\varepsilon,\beta}\right)\right) \\ &= \int_K (\xi + \nabla\chi^\xi) \cdot A^\varepsilon(\xi + \nabla\chi^\xi), \end{aligned}$$

denoting by χ^ξ the function $\chi^\xi = \sum_{\alpha=1}^{d} \xi_\alpha \chi_K^{\varepsilon,\alpha}$. Using (4.2), we obtain

$$|K|\,\xi \cdot \overline{A}\big|_K \xi \ge m \int_K \left|\xi + \nabla\chi^\xi\right|^2 \ge m\,|K|\,|\xi|^2 + 2m \int_K \xi \cdot \nabla\chi^\xi.$$

Using an integration by parts, we see that $\int_K \xi \cdot \nabla\chi^\xi = \int_{\partial K} \chi^\xi\, n \cdot \xi$, where n is the unit outward normal vector on ∂K. In the case of the MsFEM-lin, the function χ^ξ vanishes on ∂K. In the case of the MsFEM-CR with *DOF*-continuous oversampling, or without

oversampling, the function χ^ξ has average zero on each face of K. Since the factor $n \cdot \xi$ is constant on each face, the integral again vanishes. In conclusion, we have $\int_K \xi \cdot \nabla \chi^\xi = 0$.

We thus obtain the inequality $\xi \cdot \overline{A}\big|_K \xi \geq m|\xi|^2$. Since $K \in \mathscr{T}_H$ is arbitrary here, this shows coercivity of $\overline{A}$ and completes the proof. ■

Coercivity of $\overline{A}$ implies coercivity of the bilinear form $\overline{a}^{\mathsf{diff}}$ on $H^1_0(\Omega)$. By an application of the Lax-Milgram Theorem, we conclude that the (continuous) effective problem (4.14) is well-posed for the MsFEM-lin and the MsFEM-CR without oversampling, and for the MsFEM-CR with *DOF*-continuous oversampling.

Remark 7.3. The proof of the above lemma does not extend to the MsFEM-lin with oversampling, because there is no global information about $\chi^{\varepsilon,\alpha}_K$ on the faces of K.

The following lemma provides a variational characterization of the bijection (7.2) on the space $V^\varepsilon_{H,0}$.

Lemma 7.4. *Consider the MsFEM-lin or the MsFEM-CR, both without oversampling. Let $v^\varepsilon_H \in V^\varepsilon_{H,0}$. The unique $v_H \in V_{H,0}$ for which (7.2) holds, is the unique solution in $V_{H,0}$ to the problem*

$$\forall\, w_H \in V_{H,0}, \quad \overline{a}^{\mathsf{diff}}(v_H, w_H) = a^{\varepsilon,\mathsf{diff}}(v^\varepsilon_H, w_H). \tag{7.5}$$

In addition, we have, with the constants m and M from (4.2), the estimate

$$\|\nabla v_H\|_{L^2(\mathscr{T}_H)} \leq \frac{M}{m} \|\nabla v^\varepsilon_H\|_{L^2(\mathscr{T}_H)}.$$

Proof. Let $v_H \in V_{H,0}$ be the unique element of $V_{H,0}$ such that v^ε_H and v_H satisfy (7.2). Take any $w_H \in V_{H,0}$. Using that ∇v_H and ∇w_H are piecewise constant, we compute

$$a^{\varepsilon,\mathsf{diff}}(v^\varepsilon_H, w_H) = \sum_{K \in \mathscr{T}_H} \sum_{\alpha,\beta=1}^{d} (\partial_\beta w_H)|_K \, a^{\varepsilon,\mathsf{diff}}_K\big(x^\alpha + \chi^{\varepsilon,\alpha}_K, x^\beta\big)(\partial_\alpha v_H)|_K.$$

For the MsFEM without oversampling, the numerical correctors belong to the sampling test space $V_{K,0}$. We can thus use (7.1) to obtain

$$\forall\, 1 \leq \alpha,\, \beta \leq d, \quad a^{\varepsilon,\mathsf{diff}}_K\big(x^\alpha + \chi^{\varepsilon,\alpha}_K, x^\beta\big) = a^{\varepsilon,\mathsf{diff}}_K\Big(x^\alpha + \chi^{\varepsilon,\alpha}_K, x^\beta + \chi^{\varepsilon,\beta}_K\Big).$$

Using the definitions of $\overline{A}$ in (4.12) and of $\overline{a}^{\mathsf{diff}}$ in (4.16) (we recall that these expressions hold true here upon replacing the numerical correctors by those under consideration), we conclude that

$$a^{\varepsilon,\mathsf{diff}}(v^\varepsilon_H, w_H) = \sum_{K \in \mathscr{T}_H} \sum_{\alpha,\beta=1}^{d} \int_K \partial_\beta w_H \, \overline{A}_{\beta,\alpha} \, \partial_\alpha v_H = \overline{a}^{\mathsf{diff}}(v_H, w_H).$$

It follows that v_H satisfies (7.5). In addition, in view of the coercivity of $\overline{A}$ established in Lemma 7.2 and by the Lax-Milgram Theorem, problem (7.5) uniquely characterizes v_H.

The estimate on v_H follows by testing the characterization (7.5) against $w_H = v_H$.

This yields

$$m \left\|\nabla v_H\right\|^2_{L^2(\mathscr{T}_H)} \leq \overline{a}^{\mathsf{diff}}(v_H, v_H) = a^{\varepsilon,\mathsf{diff}}(v_H^\varepsilon, v_H) = \sum_{K\in\mathscr{T}_H} \int_K \nabla v_H \cdot A^\varepsilon \nabla v_H^\varepsilon$$
$$\leq M \sum_{K\in\mathscr{T}_H} \left\|\nabla v_H\right\|_{L^2(K)} \left\|\nabla v_H^\varepsilon\right\|_{L^2(K)}.$$

The first inequality follows from coercivity of $\overline{A}$ and the second inequality from the upper bound on A^ε in (4.2) and the Cauchy-Schwarz inequality. With a discrete Cauchy-Schwarz inequality, we obtain

$$m \left\|\nabla v_H\right\|^2_{L^2(\mathscr{T}_H)} \leq M \sum_{K\in\mathscr{T}_H} \left\|\nabla v_H\right\|_{L^2(K)} \left\|\nabla v_H^\varepsilon\right\|_{L^2(K)} \leq M \left\|\nabla v_H\right\|_{L^2(\mathscr{T}_H)} \left\|\nabla v_H^\varepsilon\right\|_{L^2(\mathscr{T}_H)}.$$

The proof is completed upon simplifying by $\left\|\nabla v_H\right\|_{L^2(\mathscr{T}_H)}$. ■

For the remainder of this chapter, we consider MsFEMs without oversampling. Let $u_H^{\varepsilon,\mathsf{G}}$ denote the solution to the MsFEM approximation (5.15) (we use the superscript G to stress that this is a *Galerkin* approximation) and let $u_H^{\varepsilon,\mathsf{PG}}$ denote the solution to the non-intrusive MsFEM (7.3) (which is equivalent to the *Petrov-Galerkin* MsFEM (7.4), since we do not apply the oversampling technique).

We first study the error $u_H^{\varepsilon,\mathsf{G}} - u_H^{\varepsilon,\mathsf{PG}}$ when $\varepsilon \to 0$. In this case, we do not need a rate of convergence in H and we shall relax the condition $f \in L^2(\Omega)$ to the condition $f \in H^{-1}(\Omega)$. Then the definition of the linear form F in (4.4) has to be adapted. Given $f \in H^{-1}(\Omega)$, there exist $f_0, f_1, \ldots, f_d \in L^2(\Omega)$ such that $F(v) = \sum_{K\in\mathscr{T}_H} \left(\int_K f_0\, v + \sum_{\beta=1}^d \int_K f_\beta\, \partial_\beta v \right)$, which is in fact well-defined for any $v \in H^1(\mathscr{T}_H)$ and thus in particular on V_H, the underlying affine space for the MsFEM, and the multiscale space V_H^ε.

We consider in Theorem 7.5 a sequence of diffusion tensors A^ε that H-converges to a constant diffusion tensor. This means that u^ε converges weakly in $H^1(\Omega)$ as $\varepsilon \to 0$ towards a function $u^\star \in H_0^1(\Omega)$, solution to the homogenized problem (4.25), and $A^\varepsilon \nabla u^\varepsilon \rightharpoonup A^\star \nabla u^\star$ weakly in $L^2(\Omega)$.

Theorem 7.5. *Consider the MsFEM-lin or the MsFEM-CR, both without oversampling. Suppose that $(A^\varepsilon)_{\varepsilon>0}$ is a sequence of matrices satisfying (4.2) that H-converges to a constant matrix. Let $f \in H^{-1}(\Omega)$. Then $\left\|u_H^{\varepsilon,\mathsf{G}} - u_H^{\varepsilon,\mathsf{PG}}\right\|_{H^1(\mathscr{T}_H)} \to 0$ as $\varepsilon \to 0$.*

Remark 7.6. A rate of convergence can be obtained under some additional structural assumptions on A^ε; see Theorem 7.12.

We need a few auxiliary results to establish Theorem 7.5. The first result below concerns the convergence of the numerical correctors as $\varepsilon \to 0$.

Lemma 7.7. *Suppose that A^ε H-converges to a constant homogenized matrix $A^\star$. Consider the MsFEM-lin or the MsFEM-CR, both without oversampling. Then, for all $K \in \mathscr{T}_H$ and all $1 \leq \alpha \leq d$, we have $\chi_K^{\varepsilon,\alpha} \rightharpoonup 0$ weakly in $H^1(K)$ as $\varepsilon \to 0$.*

Proof. We introduce for each $\alpha = 1, \ldots, d$ the function $\tau^{\varepsilon,\alpha} = x^\alpha + \chi_K^{\varepsilon,\alpha}$. Then (7.1) implies

the equation $-\mathrm{div}(A^\varepsilon \nabla \tau^{\varepsilon,\alpha}) = 0$ in K. For the MsFEM-lin, the boundary conditions of the local problems for $\chi_K^{\varepsilon,\alpha}$ (see (5.6) with $S_K = K$) lead to $\tau^{\varepsilon,\alpha} = x^\alpha$ on ∂K. The boundary conditions associated to the MsFEM-CR follow from (5.7) and are as follows: the flux $\vec{n}\cdot A^\varepsilon \nabla \tau^{\varepsilon,\alpha}$ is constant on each face of K (but may depend on ε) and $\displaystyle\int_h \tau^{\varepsilon,\alpha} = \int_h x^\alpha$ for all faces h of K.

It follows that the homogenized limit $\tau^{\star,\alpha}$ of $\tau^{\varepsilon,\alpha}$ satisfies the equation

$$-\mathrm{div}(A^\star \nabla \tau^{\star,\alpha}) = 0 \quad \text{in } K.$$

For the MsFEM-lin, the boundary condition for the homogenized problem is $\tau^{\star,\alpha} = x^\alpha$ on ∂K. The boundary conditions associated to the MsFEM-CR are a constant flux $\vec{n} \cdot A^\star \nabla \tau^{\alpha,\star}$ on each face of K and $\displaystyle\int_h \tau^{\star,\alpha} = \int_h x^\alpha$ for all faces h of K.

Both for the MsFEM-lin and the MsFEM-CR, the homogenized equation has a unique solution, which is easily seen to be $\tau^{\star,\alpha} = x^\alpha$, because $A^\star$ is constant. Therefore, $\tau^{\star,\alpha} \rightharpoonup x^\alpha$ weakly in $H^1(K)$. Subtracting the function x^α, we deduce the desired convergence. ■

We will also use the following result, which is a straightforward generalization of the extended Poincaré inequality in [73, Lemma 3.31].

Lemma 7.8. *Let W be the subspace of $H^1(\mathscr{T}_H)$ defined by*

$$W = \left\{ v \in H^1(\mathscr{T}_H) \;\middle|\; \int_h [\![v]\!] = 0 \text{ for each face } h \text{ of } \mathscr{T}_h,\ \int_h v = 0 \text{ for each face } h \subset \partial\Omega \right\}.$$

There exists a constant $C > 0$ depending only on Ω but not on H such that

$$\forall\, v \in W, \qquad \|v\|_{L^2(\Omega)} \le C\, \|\nabla v\|_{L^2(\mathscr{T}_H)}.$$

Note that the multiscale space $V_{H,0}^\varepsilon$ is contained in W for both the MsFEM-lin and the MsFEM-CR, without oversampling. Finally, we provide a number of useful bounds for the difference between $u_H^{\varepsilon,\mathsf{G}}$ and $u_H^{\varepsilon,\mathsf{PG}}$.

Lemma 7.9. *Let $f \in H^{-1}(\Omega)$ and consider the MsFEM-lin or the MsFEM-CR, both without oversampling. Let $e_H^\varepsilon = u_H^{\varepsilon,\mathsf{G}} - u_H^{\varepsilon,\mathsf{PG}}$. There exists a unique $e_H^{\mathbb{P}_1} \in V_{H,0}$ and a linear combination of the numerical correctors, that we denote by e_H^{osc}, such that $e_H^\varepsilon = e_H^{\mathbb{P}_1} + e_H^{\mathsf{osc}}$, and it holds, with the constants m, M from (4.2) and the constant C from Lemma 7.8,*

$$a^{\varepsilon,\mathsf{diff}}(e_H^\varepsilon,\, e_H^\varepsilon) = F(e_H^{\mathsf{osc}}), \tag{7.6}$$

$$\|\nabla e_H^{\mathsf{osc}}\|_{L^2(K)} \le \frac{M}{m} \left\|\nabla e_H^{\mathbb{P}_1}\right\|_{L^2(K)} \quad \text{for all } K \in \mathscr{T}_H, \tag{7.7}$$

$$\left\|\nabla e_H^{\mathbb{P}_1}\right\|_{L^2(\mathscr{T}_H)} \le \frac{M}{m} \left\|\nabla e_H^\varepsilon\right\|_{L^2(\mathscr{T}_H)}, \tag{7.8}$$

$$\|\nabla e_H^\varepsilon\|_{L^2(\mathscr{T}_H)} \le \sqrt{1 + C^2}\, \frac{M^2}{m^3} \|F\|_{\mathscr{L}(H^1(\mathscr{T}_H))}, \tag{7.9}$$

where $\|\cdot\|_{\mathscr{L}(H^1(\mathscr{T}_H))}$ is the operator norm on $\mathscr{L}(H^1(\mathscr{T}_H))$.

Proof. Since the numerical approximations $u_H^{\varepsilon,\mathsf{G}}$ and $u_H^{\varepsilon,\mathsf{PG}}$ both belong to the multiscale approximation space $V_{H,0}^\varepsilon$, it follows that $e_H^\varepsilon \in V_{H,0}^\varepsilon$, and we are in a position to use (7.2) on $V_{H,0}^\varepsilon$: there exists a unique $e_H^{\mathbb{P}_1} \in V_{H,0}$ such that

$$e_H^\varepsilon = e_H^{\mathbb{P}_1} + e_H^{\mathsf{osc}}, \quad e_H^{\mathsf{osc}} = \sum_{K\in\mathscr{T}_H} \sum_{\alpha=1}^{d} \left(\partial_\alpha e_H^{\mathbb{P}_1}\right)\big|_K \, \chi_K^{\varepsilon,\alpha}. \tag{7.10}$$

Applying Lemma 7.4 to $v_H^\varepsilon = e_H^\varepsilon$,we immediately obtain (7.8).

Now recall that the numerical correctors are defined by (7.1). Using the fact that $\nabla e_H^{\mathbb{P}_1}$ is piecewise constant, this implies that e_H^{osc} satisfies the following variational problem in each $K \in \mathscr{T}_H$:

$$\forall\, w \in V_{K,0}, \quad a_K^{\varepsilon,\mathsf{diff}}\left(e_H^{\mathsf{osc}},\, w\right) = -a_K^{\varepsilon,\mathsf{diff}}\left(e_H^{\mathbb{P}_1},\, w\right).$$

Without oversampling, it holds $\chi_K^{\varepsilon,\alpha} \in V_{K,0}$ for each $1 \le \alpha \le d$, so e_H^{osc} can be used as a test function here. With the bounds in (4.2), implying continuity and coercivity of $a_K^{\varepsilon,\mathsf{diff}}$, we obtain (7.7).

Next using (7.10), we can write

$$a^{\varepsilon,\mathsf{diff}}(e_H^\varepsilon,\, e_H^\varepsilon) = a^{\varepsilon,\mathsf{diff}}\left(u_H^{\varepsilon,\mathsf{G}},\, e_H^\varepsilon\right) - a^{\varepsilon,\mathsf{diff}}\left(u_H^{\varepsilon,\mathsf{PG}},\, e_H^{\mathbb{P}_1}\right) - a^{\varepsilon,\mathsf{diff}}\left(u_H^{\varepsilon,\mathsf{PG}},\, e_H^{\mathsf{osc}}\right).$$

We deduce from (6.14) that $a^{\varepsilon,\mathsf{diff}}\left(u_H^{\varepsilon,\mathsf{PG}},\, e_H^{\mathsf{osc}}\right) = 0$. Since e_H^ε can be used as a test function in the discrete problem (5.15) and $e_H^{\mathbb{P}_1}$ in (7.4), we have $a^{\varepsilon,\mathsf{diff}}\left(u_H^{\varepsilon,\mathsf{G}},\, e_H^\varepsilon\right) - a^{\varepsilon,\mathsf{diff}}\left(u_H^{\varepsilon,\mathsf{PG}},\, e_H^{\mathbb{P}_1}\right) = F\left(e_H^{\mathsf{osc}}\right)$, which shows (7.6). It follows that

$$a^{\varepsilon,\mathsf{diff}}(e_H^\varepsilon,\, e_H^\varepsilon) \le \|F\|_{\mathscr{L}(H^1(\mathscr{T}_H))}\, \|e_H^{\mathsf{osc}}\|_{H^1(\mathscr{T}_H)} \le \|F\|_{\mathscr{L}(H^1(\mathscr{T}_H))} \sqrt{1+C^2}\, \|\nabla e_H^{\mathsf{osc}}\|_{L^2(\mathscr{T}_H)},$$

where C is the Poincaré constant from Lemma 7.8. Now applying (7.7) and (7.8) on the right, and using coercivity of $a^{\varepsilon,\mathsf{diff}}$ on the left, we find

$$m\, \|\nabla e_H^\varepsilon\|_{L^2(\mathscr{T}_H)}^2 \le \sqrt{1+C^2} \left(\frac{M}{m}\right)^2 \|F\|_{\mathscr{L}(H^1(\mathscr{T}_H))}\, \|\nabla e_H^\varepsilon\|_{L^2(\mathscr{T}_H)},$$

from which we deduce (7.9). ■

Proof of Theorem 7.5. Let $e_H^\varepsilon = u_H^{\varepsilon,\mathsf{G}} - u_H^{\varepsilon,\mathsf{PG}}$. We will use (7.10). By Lemma 7.9, we have (7.6). Combined with (4.2) and Lemma 7.8, this implies

$$C \left\| u_H^{\varepsilon,\mathsf{G}} - u_H^{\varepsilon,\mathsf{PG}} \right\|_{H^1(\mathscr{T}_H)}^2 \le a^{\varepsilon,\mathsf{diff}}(e_H^\varepsilon,\, e_H^\varepsilon) = F\left(e_H^{\mathsf{osc}}\right) = \sum_{K\in\mathscr{T}_H} \sum_{\alpha=1}^{d} \left(\partial_\alpha e_H^{\mathbb{P}_1}\right)\big|_K \, F\left(\chi_K^{\varepsilon,\alpha}\right).$$

By Lemma 7.7, we know that $\chi_K^{\varepsilon,\alpha} \rightharpoonup 0$ as $\varepsilon \to 0$ weakly in $H^1(K)$ for each K and for each α. Therefore, $F\left(\chi_K^{\varepsilon,\alpha}\right) \to 0$ as $\varepsilon \to 0$. In view of (7.8) and (7.9), every derivative $\left(\partial_\alpha e_H^{\mathbb{P}_1}\right)\big|_K$ is bounded independently of ε. It follows that $F\left(e_H^{\mathsf{osc}}\right) \to 0$ as $\varepsilon \to 0$. The conclusion now follows from the above inequality. ■

We next study the convergence of $u_H^{\varepsilon,\mathsf{G}} - u_H^{\varepsilon,\mathsf{PG}}$ as $H \to 0$. To this end, we return to the original hypotheses of Chapter 4, i.e., $f \in L^2(\Omega)$. Note that for the next result, the additional H-convergence hypothesis of Theorem 7.5 for A^ε is not needed.

Theorem 7.10. *Consider the MsFEM-lin or the MsFEM-CR, both without oversampling. Assume that $f \in L^2(\Omega)$. Then there exists a constant C independent of ε, H and f such that*

$$\left\| u_H^{\varepsilon,\mathsf{G}} - u_H^{\varepsilon,\mathsf{PG}} \right\|_{H^1(\mathscr{T}_H)} \leq CH\|f\|_{L^2(\Omega)}.$$

To prove this lemma, we will use some Poincaré-Friedrichs inequalities, for which we refer e.g. to [112, Lemma 4.3], [73, Lemma B.66].

Proof. Let $e_H^\varepsilon = u_H^{\varepsilon,\mathsf{G}} - u_H^{\varepsilon,\mathsf{PG}}$ and recall the results of Lemma 7.9. We have $e_H^\varepsilon = e_H^{\mathbb{P}_1} + e_H^{\mathsf{osc}}$ (see (7.10)), and (7.6) provides, for $f \in L^2(\Omega)$, the equality $a^{\varepsilon,\mathsf{diff}}(e_H^\varepsilon, e_H^\varepsilon) = (f, e_H^{\mathsf{osc}})_{L^2(\Omega)}$. Hence, by the Cauchy-Schwarz inequality,

$$a^{\varepsilon,\mathsf{diff}}(e_H^\varepsilon, e_H^\varepsilon) \leq \|f\|_{L^2(\Omega)} \|e_H^{\mathsf{osc}}\|_{L^2(\Omega)}. \tag{7.11}$$

For the MsFEM-lin (without oversampling), it holds that $\chi_K^{\varepsilon,\alpha} = 0$ on ∂K for all mesh elements K and all $1 \leq \alpha \leq d$, and it follows that $e_H^{\mathsf{osc}} = 0$ on the boundaries of all mesh elements. In the case of the MsFEM-CR (without oversampling), it holds that $\int_h \chi_K^{\varepsilon,\alpha} = 0$ for all faces h of the mesh and all $1 \leq \alpha \leq d$. (Note that the average of $\chi_K^{\varepsilon,\alpha}$ over any face h is well-defined even if $\chi_K^{\varepsilon,\alpha}$ is in general discontinuous along faces.) Since $\partial_\alpha e_H^{\mathbb{P}_1}$ is constant on each mesh element K, we also have $\int_h e_H^{\mathsf{osc}} = 0$. Hence, both for the MsFEM-lin and for the MsFEM-CR, an appropriate variant of the Poincaré-Friedrichs inequality yields a constant C independent of K but dependent on the regularity of the mesh, such that

$$\|e_H^{\mathsf{osc}}\|_{L^2(K)} \leq CH \|\nabla e_H^{\mathsf{osc}}\|_{L^2(K)}. \tag{7.12}$$

Upon inserting the inequalities (7.12), (7.7) and (7.8) into (7.11), it follows that

$$a^{\varepsilon,\mathsf{diff}}(e_H^\varepsilon, e_H^\varepsilon) \leq CH \left(\frac{M}{m}\right)^2 \|\nabla e_H^\varepsilon\|_{L^2(\mathscr{T}_H)} \|f\|_{L^2(\Omega)}.$$

One more time using the lower bound in (4.2), we find

$$\|\nabla e_H^\varepsilon\|_{L^2(\mathscr{T}_H)} \leq CH\frac{M^2}{m^3}\|f\|_{L^2(\Omega)}.$$

The proof is concluded by application of Lemma 7.8 to e_H^ε. ■

7.3. Convergence results in the periodic setting

We now study the MsFEM-lin applied to the periodic setting introduced in Section 4.7 in some more detail. To the best of our knowledge, all convergence results known for the MsFEM are obtained in this periodic setting (see e.g. [70, 100, 69, 9, 94, 112, 113, 116, 115]). The analysis in these works relies on the explicit description of the microstructure that we summarized in Section 4.7. In particular, recall the existence of a homogenized diffusion coefficient given by (4.24) and the first-order two-scale expansion (4.26). We emphasize, however, that the *application* of the MsFEM does not require the periodic setting, nor does it even suppose the PDE under consideration to be embedded in a

sequence of PDEs for a family of parameters ε that tend 0. We refer to Section 7.4 for examples of such numerical experiments.

Applying the MsFEM to a sequence of matrices $A^\varepsilon = A^{\mathsf{per}}(\cdot/\varepsilon)$, we obtain a sequence of effective tensors $\overline{A}(\varepsilon)$. Each $\overline{A}(\varepsilon)$ is defined by (4.12) for a fixed value of ε. We have the following convergence result.

Lemma 7.11. *Let $\overline{A}(\varepsilon)$ be the sequence of effective tensors obtained in (4.12) by applying the MsFEM-lin without oversampling to $A^\varepsilon = A^{\mathsf{per}}(\cdot/\varepsilon)$. We have $\overline{A}(\varepsilon) \to A^\star$ as $\varepsilon \to 0$.*

Proof. We fix a mesh element $K \in \mathscr{T}_H$. First observe that $\overline{A}(\varepsilon)$ and $A^\star$ satisfy

$$\overline{A}_{\beta,\alpha}(\varepsilon)\big|_K = \frac{1}{|K|} a_K^{\varepsilon,\mathsf{diff}}\big(x^\alpha + \chi_K^{\varepsilon,\alpha},\, x^\beta\big), \qquad A^\star_{\beta,\alpha} = \int_Q e_\beta \cdot A^{\mathsf{per}}(e_\alpha + \nabla w_\alpha), \tag{7.13}$$

for each $1 \le \alpha, \beta \le d$, in view of the variational formulations satisfied by $\chi_K^{\varepsilon,\alpha}$ (solution to the PDE (4.11)) and w_α (solution to the PDE (4.23)). We recall that Q is the unit cube of $\mathbb{R}^d$.

Now let $\tau^{\varepsilon,\alpha} = x^\alpha + \chi_K^{\varepsilon,\alpha}$. In view of Lemma 7.7, $\tau^{\varepsilon,\alpha} \rightharpoonup \tau^{\star,\alpha}$ as $\varepsilon \to 0$ weakly in $H^1(K)$, with $\tau^{\star,\alpha}(x) = x^\alpha$. Writing the two-scale expansion (4.26) of $\tau^{\varepsilon,\alpha}$, we thus have, when ε is small,

$$\tau^{\varepsilon,\alpha}(x) \approx \tau^{\star,\alpha}(x) + \varepsilon \sum_{\gamma=1}^{d} w_\gamma\left(\frac{x}{\varepsilon}\right) \partial_\gamma \tau^{\star,\alpha}(x) = x^\alpha + \varepsilon\, w_\alpha\left(\frac{x}{\varepsilon}\right),$$

and the difference tends to zero in $H^1(K)$ as $\varepsilon \to 0$. Inserting this convergence in (7.13), we deduce that

$$\lim_{\varepsilon\to 0} \overline{A}_{\beta,\alpha}(\varepsilon)\big|_K = \lim_{\varepsilon\to 0} \frac{1}{|K|} \int_K e_\beta \cdot A^{\mathsf{per}}\left(\frac{x}{\varepsilon}\right)\left(e_\alpha + \nabla w_\alpha\left(\frac{x}{\varepsilon}\right)\right) \mathrm{d}x = A^\star_{\beta,\alpha}.$$

The convergence to the mean on the unit cube in the last equality follows from the Q-periodicity of the function $e_\beta \cdot A^{\mathsf{per}}\,(e_\alpha + \nabla w_\alpha)$. ■

The following theorem studies the convergence of $u_H^{\varepsilon,\mathsf{G}} - u_H^{\varepsilon,\mathsf{PG}}$ towards 0 as $\varepsilon \to 0$ for the MsFEM-lin without oversampling. As was stated in Remark 7.6, thanks to the periodic setting, we now obtain a rate for the convergence stated in Theorem 7.5.

Theorem 7.12. *Let $f \in L^2(\Omega)$. Consider the MsFEM-lin without oversampling. For $A^\varepsilon = A^{\mathsf{per}}(\cdot/\varepsilon)$ sufficiently regular, we have*

$$\left\| u_H^{\varepsilon,\mathsf{G}} - u_H^{\varepsilon,\mathsf{PG}} \right\|_{H^1(\Omega)} \le C\varepsilon \, \|f\|_{L^2(\Omega)},$$

where the constant C depends on the dimension d and the constants m, M in (4.2), but not on ε, H or f.

Proof. Let $e_H^\varepsilon = u_H^{\varepsilon,\mathsf{G}} - u_H^{\varepsilon,\mathsf{PG}}$. Lemma 7.9 applies, so we can use (7.6) and a Cauchy-Schwarz inequality to find

$$a^{\varepsilon,\mathsf{diff}}(e_H^\varepsilon,\, e_H^\varepsilon) \leq \|f\|_{L^2(\Omega)}\, \|e_H^{\mathsf{osc}}\|_{L^2(\Omega)} = \|f\|_{L^2(\Omega)} \left\| \sum_{K\in\mathscr{T}_H} \sum_{\alpha=1}^{d} \left(\partial_\alpha e_H^{\mathbb{P}_1}\right)\big|_K\, \chi_K^{\varepsilon,\alpha} \right\|_{L^2(\Omega)} . \quad (7.14)$$

Next we seek a bound on $\chi_K^{\varepsilon,\alpha}$ in $L^2(K)$. Using (4.11) and (4.23), we have

$$\operatorname{div}\left(A^{\mathsf{per}}\left(\frac{\cdot}{\varepsilon}\right)\nabla\left[\chi_K^{\varepsilon,\alpha} - \varepsilon\, w_\alpha\left(\frac{\cdot}{\varepsilon}\right)\right]\right) = 0 \quad \text{in } K.$$

Since $\chi_K^{\varepsilon,\alpha}$ vanishes on ∂K (recall that we consider the MsFEM-lin without oversampling), the maximum principle [81, Theorem 8.1] yields

$$\left\|\chi_K^{\varepsilon,\alpha} - \varepsilon\, w_\alpha\left(\frac{\cdot}{\varepsilon}\right)\right\|_{L^2(K)} \leq \sup_{\partial K}\left|\chi_K^{\varepsilon,\alpha} - \varepsilon\, w_\alpha\left(\frac{\cdot}{\varepsilon}\right)\right| \sqrt{\int_K 1} = \varepsilon\, |K|^{1/2} \sup_{\partial K}\left|w_\alpha\left(\frac{\cdot}{\varepsilon}\right)\right|.$$

When A^{per} is sufficiently regular, the corrector functions w_α are uniformly bounded. Then for each $K \in \mathscr{T}_H$ and each $1 \leq \alpha \leq d$, we have

$$\|\chi_K^{\varepsilon,\alpha}\|_{L^2(K)} \leq \left\|\chi_K^{\varepsilon,\alpha} - \varepsilon\, w_\alpha\left(\frac{\cdot}{\varepsilon}\right)\right\|_{L^2(K)} + \varepsilon\, \left\|w_\alpha\left(\frac{\cdot}{\varepsilon}\right)\right\|_{L^2(K)} \leq C\varepsilon |K|^{1/2}.$$

Since all $\chi_K^{\varepsilon,\alpha}$ have disjoint supports, we can use the latter estimate to bound

$$\begin{aligned}
\left\| \sum_{K\in\mathscr{T}_H} \sum_{\alpha=1}^{d} \left(\partial_\alpha e_H^{\mathbb{P}_1}\right)\big|_K\, \chi_K^{\varepsilon,\alpha} \right\|_{L^2(\Omega)}^2 &= \sum_{K\in\mathscr{T}_H} \left\| \sum_{\alpha=1}^{d} \left(\partial_\alpha e_H^{\mathbb{P}_1}\right)\big|_K\, \chi_K^{\varepsilon,\alpha} \right\|_{L^2(K)}^2 \\
&\leq C\varepsilon^2 \sum_{K\in\mathscr{T}_H} \sum_{\alpha=1}^{d} |K| \left(\left(\partial_\alpha e_H^{\mathbb{P}_1}\right)\big|_K\right)^2 \\
&= C\varepsilon^2 \sum_{K\in\mathscr{T}_H} \sum_{\alpha=1}^{d} \left\|\partial_\alpha e_H^{\mathbb{P}_1}\right\|_{L^2(K)}^2 \\
&= C\varepsilon^2 \left\|\nabla e_H^{\mathbb{P}_1}\right\|_{L^2(\Omega)}^2 . \qquad (7.15)
\end{aligned}$$

We insert (7.15) combined with (7.8) into (7.14) to find

$$a^{\varepsilon,\mathsf{diff}}(e_H^\varepsilon,\, e_H^\varepsilon) \leq C\varepsilon\, \|f\|_{L^2(\Omega)}\, \|\nabla e_H^\varepsilon\|_{L^2(\Omega)} .$$

Applying the coercivity property in (4.2) on the left-hand side and a Poincaré inequality on Ω, we obtain the desired result. ■

The classical error estimate for the Galerkin MsFEM approach (4.6) is obtained in the periodic setting and under some regularity assumption on A^{per} and on the homogenized limit $u^\star$. The bound obtained in [69, Theorem 6.5] reads

$$\left\|u^\varepsilon - u_H^{\varepsilon,\mathsf{G}}\right\|_{H^1(\Omega)} \leq C\left(H + \varepsilon + \sqrt{\varepsilon/H}\right), \qquad (7.16)$$

for some C independent of ε and H. Theorem 7.12 shows that the same estimate holds true for $u_H^{\varepsilon,\mathsf{PG}}$, the Petrov-Galerkin MsFEM approximation, under the correct regularity assumptions. We note that the bound for $u_H^{\varepsilon,\mathsf{PG}}$ can also be inferred from Theorem 7.10. However, since the MsFEM is applied in the regime where $\varepsilon < H$, the result of Theo-

rem 7.12 is more precise, thanks to the extra structural assumptions made on the diffusion tensor A^ε.

7.4. Numerical study of non-intrusive MsFEMs

In this section, we compare the Galerkin MsFEM (5.15), its non-intrusive approximation (6.13) and the Petrov-Galerkin MsFEM (6.1) on a concrete numerical example in 2D ($d = 2$). The numerical approximations obtained for these various MsFEMs shall be denoted $u_H^{\varepsilon,\mathsf{G}}$, $u_H^{\varepsilon,\mathsf{G\text{-}ni}}$ and $u_H^{\varepsilon,\mathsf{PG}}$, respectively.

7.4.1. Description of the numerical experiments. We consider the pure diffusion equation (4.1) on the domain $\Omega = (0,1) \times (0,1)$. Thus, the local bilinear forms are $a_K^\varepsilon = a_K^{\varepsilon,\mathsf{diff}}$ defined in Example 5.2, where we consider the three diffusion tensors

$$A^{\varepsilon,\mathsf{per}}(x) = \nu^\varepsilon(x)\,\mathrm{Id}, \quad \nu^\varepsilon(x) = 1 + 100\,\cos^2(\pi\,x_1/\varepsilon)\sin^2(\pi\,x_2/\varepsilon), \tag{7.17a}$$

$$A^{\varepsilon,\mathsf{lp}}(x) = \left(1 + \cos^2(2\pi x_1)\right)\,A^{\varepsilon,\mathsf{per}}(x), \tag{7.17b}$$

$$A^{\varepsilon,\mathsf{np}}(x) = \nu^{\varepsilon,\mathsf{np}}(x)\,\mathrm{Id}, \tag{7.17c}$$

$$\nu^{\varepsilon,\mathsf{np}}(x) = 1 + \left(1 + 100\,\cos^2(\pi\,x_1/\varepsilon)\sin^2(\pi\,x_2/\varepsilon)\right)\cos^2\left(\frac{x_1^2 + x_2^2}{\varepsilon}\right).$$

We fix $f(x) = \sin(x_1)\sin(x_2)$.

The coefficient $A^{\varepsilon,\mathsf{per}}$ is ε-periodic with period $\varepsilon = \pi/150 \approx 0.02$. The coefficient $A^{\varepsilon,\mathsf{lp}}$ is locally periodic and, although a homogenized coefficient exists (see [28]), it is not constant. Consequently, a certain number of lemmas established in Chapter 7 are not known to hold true. Finally, we include the coefficient $A^{\varepsilon,\mathsf{np}}$ as an example of a multiscale problem for which we are not aware of any explicit homogenization results. We will see nevertheless that the non-intrusive MsFEMs that we introduced above provide good approximations compared to their intrusive G-MsFEM counterparts for all test cases.

A reference solution u_h^ε is computed on a uniform 1024×1024 mesh $\mathscr{T}_h$ by means of a standard $\mathbb{P}_1$ finite element method using FreeFEM++ [91]. The mesh $\mathscr{T}_h$ (as well as the coarse mesh introduced below) consists of squares cut in two along a diagonal that is in the same direction for all squares, i.e., such as the meshes in Figure 5.1. The FreeFEM++ scripts to perform all different MsFEMs can be found at [29].

We compare the reference solution u_h^ε to MsFEM solutions obtained on a coarse mesh $\mathscr{T}_H$ for varying H. The mesh $\mathscr{T}_H$ is a uniform $1/H \times 1/H$ triangulation of Ω. We test the MsFEM-lin and the MsFEM-CR using the sampling operator $s_K^\varepsilon = a_K^{\varepsilon,\mathsf{diff}}$. All oversampling methods in this chapter use a homothety ratio of 3 for the construction of the oversampling patches in Definition 5.7. A precise definition of the associated basis functions can be found in Examples 5.24 and 5.25. The mesh $\mathscr{T}_h$ is a refinement of $\mathscr{T}_H$ for all values of H. Therefore, for each $K \in \mathscr{T}_H$, we use the corresponding submesh of $\mathscr{T}_h$ (consisting of all triangles included in K) for the numerical approximation of the numerical correctors in (5.5) by $\mathbb{P}_1$ Lagrange finite elements.

Remark 7.13. We provide a few remarks on the computation of the error, which takes place in the post-processing step of the MsFEM. Evidently, these computations have to be carried out by integration on the fine scale and one may try to perform these computations on the global mesh $\mathscr{T}_h$. However, the legacy code does not, in general,

operate on the global fine mesh. Moreover, we stress that the approximation u_H^ε is in general discontinuous across element edges (for the MsFEM-CR, and for all MsFEMs with oversampling), and can therefore not be represented globally by e.g. a piecewise $\mathbb{P}_1$ function on the fine mesh $\mathscr{T}_h$ (even if one supposes that $\mathscr{T}_h$ is conformal). Thus, one has to compute the error element by element, using the code for the microscale, according to the sum

$$\|u^\varepsilon - u_H^\varepsilon\|^2_{H^1(\mathscr{T}_H)} = \sum_{K\in\mathscr{T}_H} \|u^\varepsilon - u_H^\varepsilon\|^2_{H^1(K)}\,.$$

To do so, Equation (6.9) can be used on each element K to find the correct values of u_H^ε, and the global fine mesh $\mathscr{T}_h$ is never used.

7.4.2. Results. We first compare the approximations $u_H^{\varepsilon,\mathsf{G}}$ and $u_H^{\varepsilon,\mathsf{G\text{-}ni}}$ for varying H in Figure 7.1 for MsFEMs without oversampling and MsFEMs with *DOF*-continuous oversampling. Without oversampling (OS), the approximation $u_H^{\varepsilon,\mathsf{G\text{-}ni}}$ equals $u_H^{\varepsilon,\mathsf{PG}}$ due to Lemma 6.4. We also report the error committed by the G-MsFEM. We observe that, without oversampling, the difference $u_H^{\varepsilon,\mathsf{G}} - u_H^{\varepsilon,\mathsf{G\text{-}ni}}$ is much smaller than this error. As a result, the errors obtained with the G-MsFEM and its non-intrusive approximation are of the same size. Indeed, the error of the non-intrusive G-MsFEM-lin deviates from the error of the G-MsFEM-lin by at most 0.05% for all tests that we report here. For the MsFEM-CR, this is at most 1.2%. In both cases, the two MsFEM variants thus have practically the same accuracy. This is in agreement with the theoretical result of Theorem 7.10.

The estimates obtained in Chapter 7 do not apply to MsFEMs with oversampling. From Figure 7.1, we can see that the difference $u_H^{\varepsilon,\mathsf{G}} - u_H^{\varepsilon,\mathsf{G\text{-}ni}}$ is still small with respect to the error committed by the G-MsFEM when *DOF*-continuous oversampling is applied. The approximation errors for the non-intrusive G-MsFEMs with *DOF*-continuous oversampling differ by at most 1.3% from the error of the G-MsFEM. Similar conclusions hold for the MsFEM-lin with *DOF*-extended oversampling. The difference between the G-MsFEM and the non-intrusive G-MsFEM is larger for the MsFEM-CR with *DOF*-extended oversampling. We do not include these results in the comparison of Figure 7.1 because both methods perform particularly badly when compared to the G-MsFEM without oversampling.

Let us also point out the qualitative and quantitative similarities between the performance of the MsFEM for the periodic and the non-periodic diffusion coefficients. Although the study of the homogenized limit of u^ε becomes increasingly difficult for the various coefficients (7.17a) to (7.17c), the non-intrusive approximation does not deteriorate the accuracy of the MsFEM in these numerical tests.

Before moving on to a comparison with the Petrov-Galerkin MsFEMs with oversampling, let us discuss a phenomenon in Figure 7.1 and 7.2 known as the 'resonance effect' in the literature, preventing convergence of the MsFEM if the coarse scale H is close to ε. Upon further decreasing H, convergence is found only when H is sufficiently small with respect to the microscale ε, in which case we are in the regime of classical FEMs. From a theoretical point of view, this is explained by the term $\sqrt{\varepsilon/H}$ in the error estimate (7.16) (or ε/H for the MsFEM-lin with oversampling; see [70]). We note that the same error estimate was obtained in [112] for the MsFEM-CR (without oversampling). Figure 7.2 shows that the resonance effect is more pronounced for the MsFEM-lin with oversampling than for the MsFEM-CR with oversampling.

We consider next in Figure 7.2 MsFEMs with the two different oversampling strategies of Section 5.1.3: *DOF*-continuous and *DOF*-extended oversampling. The PG-MsFEM

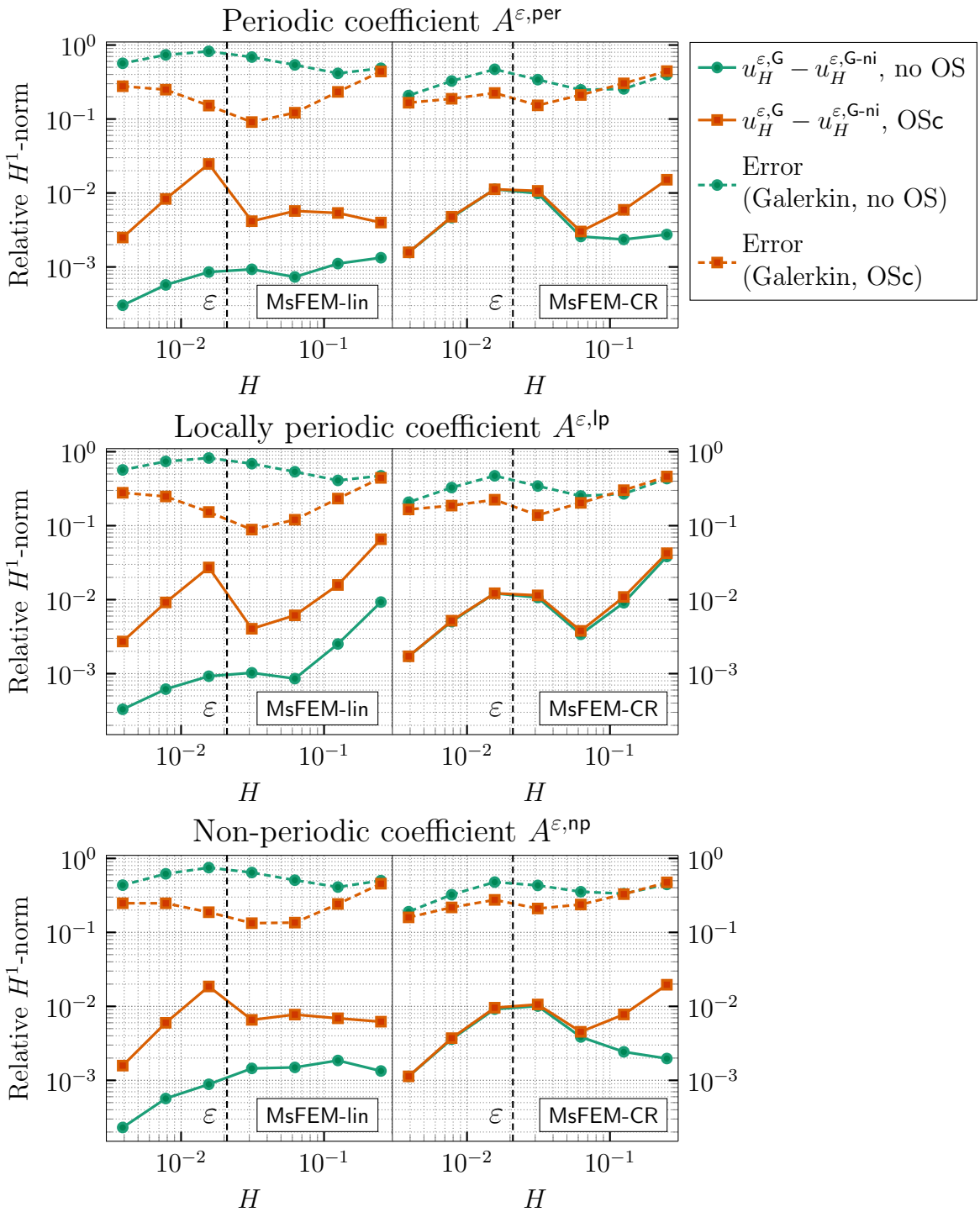

Figure 7.1: *Solid lines: difference between the Galerkin MsFEM approximation ($u_H^{\varepsilon,\mathsf{G}}$ defined by (5.15)) and the non-intrusive Galerkin MsFEM approximation ($u_H^{\varepsilon,\mathsf{G\text{-}ni}}$ defined by (6.13)), without oversampling (no OS) and with DOF-continuous oversampling (OSc), for the diffusion coefficients in (7.17) as the mesh size H varies. Dashed lines: error of the Galerkin MsFEM with respect to the reference solution. All values are normalized with respect to the H^1 norm of the reference solution.*

variant, with or without oversampling, is completely equivalent to its non-intrusive implementation by virtue of Theorem 6.2. With oversampling, however, it does not coincide with the (intrusive or non-intrusive) G-MsFEM.

With oversampling, the matrices of the linear systems for the G-MsFEM and PG-MsFEM are different; Lemma 6.4 does not apply. The result is that the differences $u_H^{\varepsilon,\mathsf{G}} - u_H^{\varepsilon,\mathsf{PG}}$ are larger than the differences $u_H^{\varepsilon,\mathsf{G}} - u_H^{\varepsilon,\mathsf{G\text{-}ni}}$. This is reflected in the numerical errors of the methods. We show the errors of the PG-MsFEM and the G-MsFEM with respect to the reference solution u_h^ε in Figure 7.2. (The non-intrusive G-MsFEM is too close to the G-MsFEM to be distinguishable on the scale of Figure 7.2 for all MsFEMs except the MsFEM with *DOF*-extended oversampling.) The G-MsFEM without oversampling is also shown to highlight the effect of oversampling.

Let us first consider the two different oversampling strategies. For all Galerkin MsFEMs, it is clear that the *DOF*-continuous variant performs (much) better than the *DOF*-extended variant. For the Petrov-Galerkin MsFEMs, the difference between the two oversampling strategies is smaller, but the *DOF*-continuous version of oversampling continues to perform better over all.

Although clear differences in the performance of the Galerkin and Petrov-Galerkin MsFEMs with *DOF*-continuous oversampling can be observed, these differences are small and both MsFEM approaches have a comparable accuracy. There is no systematic disadvantage in choosing the non-intrusive PG-MsFEM over the (intrusive or non-intrusive) G-MsFEM. Moreover, the non-periodic test cases again show the robustness of all MsFEM variants when going beyond the setting of periodic homogenization. In particular, this demonstrates the robustness of the non-intrusive approaches for the MsFEM developed in this thesis.

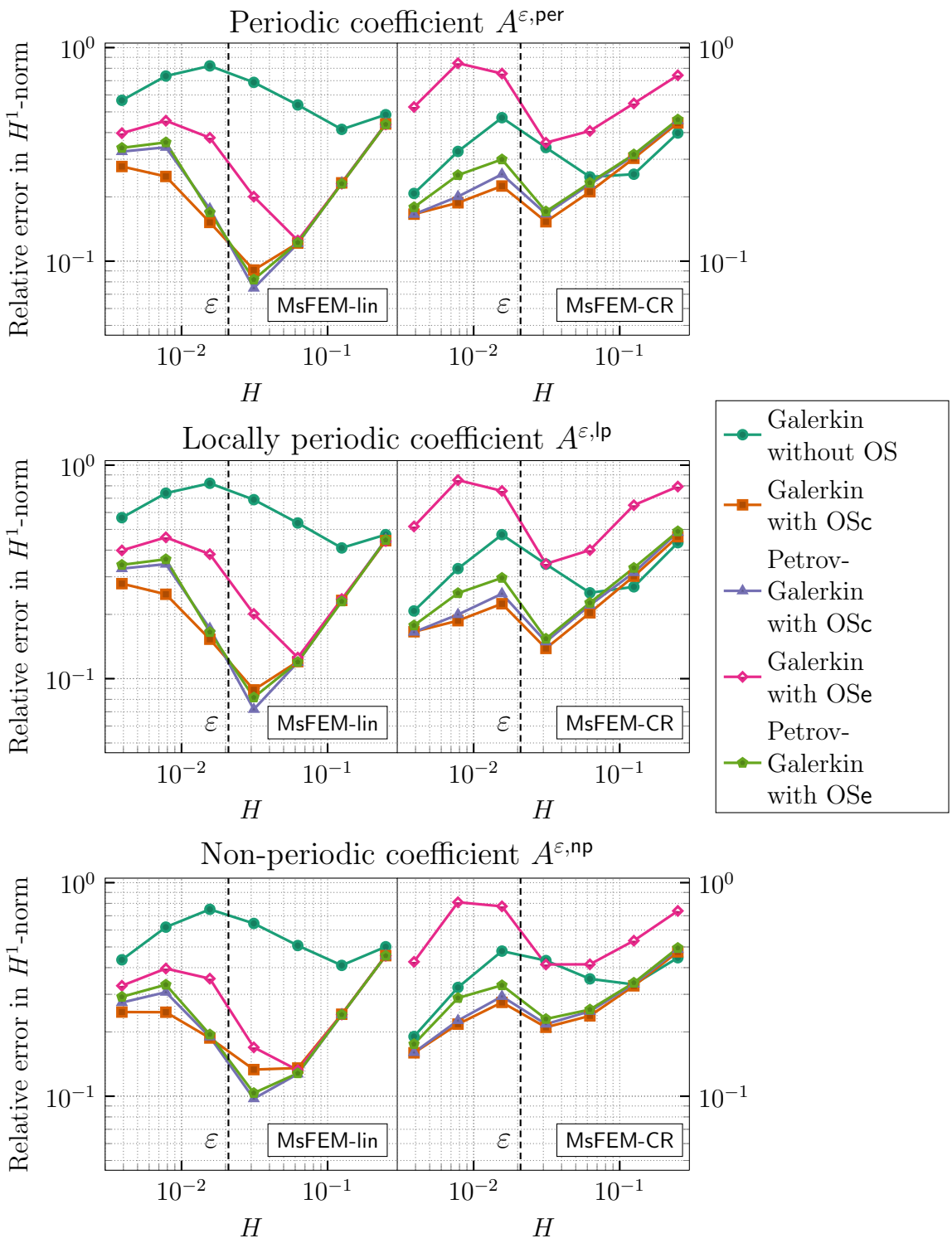

Figure 7.2: *Comparison of the errors of the (intrusive) Galerkin MsFEM* (5.15) *and the (non-intrusive) Petrov-Galerkin MsFEM* (6.1) *for the diffusion coefficients in* (7.17) *as the mesh size H varies. Different oversampling strategies are applied: DOF-continuous (OSc, Definition 5.16) and DOF-extended (OSe, Definition 5.11). The Galerkin MsFEM without OS is included to illustrate the effect of the OS strategies.*

Chapter 8

Some further considerations

In this chapter we collect two topics related to the developments of Chapters 4 to 7. We first discuss in Section 8.1 alternative oversampling techniques for the MsFEM-CR that were not introduced in the published work [31], and then consider some aspects of a non-intrusive implementation of higher-order MsFEMs in Section 8.2.

8.1. Different oversampling techniques for the MsFEM-CR

In this section we propose two variations on the oversampling technique for the MsFEM-CR that was first defined in the general framework of Chapter 5. The difference resides in the definition of the numerical correctors for those mesh elements that touch the boundary $\partial\Omega$. The oversampling variants presented below have not been included in the presentation of the general MsFEM framework of this thesis (even though the framework could be modified accordingly), because we followed the presentation of the published work [31].

We focus on the pure diffusion problem of Example 5.2 as in Chapter 7. Any multiscale function is then defined in terms of a $\mathbb{P}_1$ Crouzeix-Raviart function v_H as in (7.2), i.e.,

$$v_H^\varepsilon = v_H + \sum_{K\in\mathscr{T}_H} \sum_{\alpha=1}^{d} (\partial_\alpha v_H)|_K \, \chi_K^{\varepsilon,\alpha,\bullet}, \tag{8.1}$$

We recall that $\bullet \in \{\mathsf{e}, \mathsf{c}\}$ denotes the choice of *DOF*-extended or *DOF*-continuous oversampling according to Definitions 5.11 and 5.16. Definitions of the numerical correctors for diffusion problems used in Chapter 5 were given in Examples 5.13 and 5.19. Different numerical correctors are proposed in this section.

Motivation for a different oversampling strategy. In (8.1), the coarse part v_H of the multiscale function is used for the resolution of the effective problem resulting from the MsFEM (6.12). A difference between the MsFEM-lin and the MsFEM-CR is that the Dirichlet boundary conditions of the exact solution are respected exactly by the $\mathbb{P}_1$ Lagrange space (corresponding to the MsFEM-lin), but only in a weak sense (on average on each face of the mesh lying on $\partial\Omega$) by the $\mathbb{P}_1$ Crouzeix-Raviart space. The convergence analysis for both the $\mathbb{P}_1$ Lagrange and Crouzeix-Raviart FEMs is well-established (see, e.g., [73, Theorems 3.16 and 3.38]) and, in spite of this difference in the treatment of the

boundary conditions, both methods commit an error of order H in the approximation of the effective PDE. The oscillatory behaviour of the solution u^ε is encoded in the numerical correctors.

The purpose of oversampling is to better reflect the oscillations of u^ε near the mesh element boundaries in the numerical correctors. The oversampling strategy for the MsFEM-CR of Chapter 5 does not exploit the fact that the exact boundary conditions of u^ε are known along $\partial\Omega$ (contrary to the MsFEM-lin, where the numerical correctors are always defined with homogeneous Dirichlet conditions for all mesh elements). Therefore, the oversampling strategy does not seem optimal. We thus propose below two different ways to incorporate (strong) Dirichlet conditions on $\partial\Omega$ in the numerical correctors, rather than the weak boundary conditions that are used in the definitions of Chapter 5, to which we shall refer as "weak boundary condition" (WBC) oversampling. Our numerical results at the end of this section show that other oversampling strategies can indeed perform better than the WBC oversampling variant.

The "vanishing boundary condition" variant. Let $K \in \mathscr{T}_H$ be a mesh element and S_K its associated oversampling patch. The first option we consider is to impose the same Dirichlet conditions as those for the correctors of the MsFEM-lin on those faces of S_K that lie on $\partial\Omega$. We call this option the "vanishing boundary condition" variant because the numerical correctors vanish on $\partial\Omega$. We recall the distinction between the set of dilated faces $\mathscr{F}_d(S_K)$ of S_K and the set of additional faces $\mathscr{F}_a(S_K)$ that was made in Section 5.4.2. Note that the set of additional faces $\mathscr{F}_a(S_K)$ only contains faces lying on $\partial\Omega$, since they are obtained from intersecting a homothetic trasformation of K with $\partial\Omega$. On the other hand, some dilated faces of S_K may also lie on $\partial\Omega$. The definition of the numerical correctors in Examples 5.13 and 5.19 should thus be modified as follows to impose strong Dirichlet conditions on $\partial\Omega$.

Definition 8.1. For all $1 \leq \alpha \leq d$, the vanishing boundary condition (VBC) *DOF*-extended numerical corrector $\chi_K^{\varepsilon,\alpha,\mathsf{e}}$ is defined as the restriction to K of the unique function $\chi_{S_K}^{\varepsilon,\alpha,\mathsf{e}}$ in $H^1(S_K)$ such that

$$\begin{cases} -\mathrm{div}(A^\varepsilon \nabla \chi_{S_K}^{\varepsilon,\alpha,\mathsf{e}}) = \mathrm{div}(A^\varepsilon e_\alpha) & \text{in } S_K, \\ \chi_{S_K}^{\varepsilon,\alpha,\mathsf{e}} = 0 & \text{on } \partial S_K \cap \partial\Omega, \\ \vec{n} \cdot A^\varepsilon \nabla \chi_{S_K}^{\varepsilon,\alpha,\mathsf{e}} = c_h - \vec{n} \cdot A^\varepsilon e_\alpha & \text{on each } h \in \mathscr{F}_d(S_K) \text{ that does not lie on } \partial\Omega, \\ \dfrac{1}{|h|}\displaystyle\int_h \chi_{S_K}^{\varepsilon,\alpha,\mathsf{e}} = 0 & \text{for each } h \in \mathscr{F}_d(S_K) \text{ that does not lie on } \partial\Omega, \end{cases}$$

where the constants c_h are uniquely determined by the above problem. We define the VBC *DOF*-continuous numerical corrector $\chi_K^{\varepsilon,\alpha,\mathsf{c}}$ as the restrction to K of the solution to the same problem where the average condition in the last line is replaced by $\dfrac{1}{|h|}\displaystyle\int_h \chi_K^{\varepsilon,\alpha,\mathsf{c}} = 0$ for each face $h \in \mathscr{F}(K)$ that does not lie on $\partial\Omega$.

As announced above, when $\partial S_K \cap \partial\Omega = \varnothing$, this definition coincides with the definition of the numerical correctors in Chapter 5.

The multiscale functions v_H^ε in (8.1) constructed with the VBC numerical correctors satisfy $v_H^\varepsilon = v_H$ on $\partial\Omega$, where v_H is a $\mathbb{P}_1$ Crouzeix-Raviart function and is thus discontinuous along $\partial\Omega$ in general. Consequently, the multiscale functions are discontinuous along $\partial\Omega$ in general, and may not reproduce the exact boundary condition of u^ε on $\partial\Omega$

even if $u^\varepsilon = 0$ on $\partial\Omega$. The fact that the boundary conditions is not interpolated exactly need not be a problem to obtain an accurate FEM. Indeed, the same holds true for the standard $\mathbb{P}_1$ Crouzeix-Raviart FEM, for which the same type of convergence estimates have been established as for the $\mathbb{P}_1$ Lagrange FEM. The numerical results of Figure 8.1 confirm that a numerical approximation is obtained with VBC oversampling whose accuracy is comparable to that of the MsFEM-lin with oversampling.

The "affine boundary condition" variant. We now present another variant such that constant boundary conditions on $\partial\Omega$ are reproduced exactly by the multiscale space. The MsFEM-CR (with or without oversampling) implements a boundary condition by fixing the average of the approximation over each face lying on $\partial\Omega$. Let $K \in \mathscr{T}_H$ be such that (at least) one of its faces h lies on $\partial\Omega$. If we use *DOF*-continuous numerical correctors, we have, for any multiscale function v_H^ε defined in (8.1),

$$\frac{1}{|h|}\int_h v_H^\varepsilon = \frac{1}{|h|}\int_h v_H + \sum_{\alpha=1}^d (\partial_\alpha v_H)|_K \frac{1}{|h|}\int_h \chi_K^{\varepsilon,\alpha,\mathsf{c}} = \frac{1}{|h|}\int_e v_H = v_H(x_{c,h}),$$

where $x_{c,h}$ is the centroid of the face h. The MsFEM-CR thus sets the value of v_H at $x_{c,h}$ equal to the average of the boundary condition of the global problem over h. If we want to encode a constant Dirichlet boundary condition *exactly* in the multiscale approximation, we should construct multiscale functions such that $v_H^\varepsilon = v_H(x_{c,h})$ on h.

We shall do so now for both *DOF*-extended and *DOF*-continuous oversampling. To find the correct boundary conditions to be used for the numerical correctors, we use the identity (4.20) (noting that we can indeed replace the centroid of K by the centroid of h here). This yields

$$v_H^\varepsilon = v_H(x_{c,h}) + \sum_{\alpha=1}^d (\partial_\alpha v_H)|_K \left(x^\alpha - x_{c,h}^\alpha + \chi_K^{\varepsilon,\alpha,\bullet}\right) \quad \text{on } h.$$

Hence, $v_H^\varepsilon = v_H(x_{c,h})$ on h if and only if the sum over α vanishes. Since this is to hold for all $v_H \in V_H$, we obtain the necessary and sufficient condition, for all $1 \le \alpha \le d$,

$$x^\alpha - x_{c,h}^\alpha + \chi_K^{\varepsilon,\alpha,\bullet} = 0 \text{ on } h \text{ if } h \text{ lies on } \partial\Omega. \tag{8.2}$$

We conclude that, to exactly reproduce a constant Dirichlet condition along $\partial\Omega$, the numerical correctors have to satisfy the affine Dirichlet condition (8.2). Hence, we use the name "affine boundary condition" variant for the numerical correctors in the next definition.

Definition 8.2. For all $1 \le \alpha \le d$, the affine boundary condition (ABC) *DOF*-extended numerical corrector $\chi_K^{\varepsilon,\alpha,\mathsf{e}}$ is defined as the restriction to K of the unique function $\chi_{S_K}^{\varepsilon,\alpha,\mathsf{e}}$ in $H^1(S_K)$ such that

$$\begin{cases} -\mathrm{div}(A^\varepsilon \nabla \chi_{S_K}^{\varepsilon,\alpha,\mathsf{e}}) = \mathrm{div}(A^\varepsilon e_\alpha) & \text{in } S_K, \\ \chi_{S_K}^{\varepsilon,\alpha,\mathsf{e}} = x_{c,h}^\alpha - x^\alpha & \text{on each } h \in \mathscr{F}(S_K) \text{ that lies on } \partial\Omega, \\ \vec{n}\cdot A^\varepsilon \nabla \chi_{S_K}^{\varepsilon,\alpha,\mathsf{e}} = c_h - \vec{n}\cdot A^\varepsilon e_\alpha & \text{on each } h \in \mathscr{F}_d(S_K) \text{ that does not lie on } \partial\Omega, \\ \dfrac{1}{|h|}\displaystyle\int_h \chi_{S_K}^{\varepsilon,\alpha,\mathsf{e}} = 0 & \text{for each } h \in \mathscr{F}_d(S_K) \text{ that does not lie on } \partial\Omega, \end{cases}$$

where the constants c_h are uniquely determined by the above problem. We define the ABC *DOF*-continuous numerical corrector $\chi_K^{\varepsilon,\alpha,\mathsf{c}}$ as the restriction to K of the solution to the same problem where the average condition in the last line is replaced by $\frac{1}{|h|}\int_h \chi_K^{\varepsilon,\alpha,\mathsf{c}} = 0$ for each face $h \in \mathscr{F}(K)$ that does not lie on $\partial\Omega$.

For non-constant boundary conditions on $\partial\Omega$, the choice of ABC numerical correctors yields an MsFEM approximation that is piecewise constant on the boundary.

Remark 8.3. An ABC adaptation of the numerical correctors for the MsFEM-CR without oversampling can be defined similarly in order to reproduce constant Dirichlet conditions on $\partial\Omega$ exactly. This corresponds to the original definition of the MsFEM-CR in [112]. In this case, however, the Dirichlet condition is not encoded in all mesh elements touching $\partial\Omega$. Consider for example Figure 5.2a. The triangle K in this figure touches $\partial\Omega$ in two of its vertices while all its faces lie inside Ω. Changing the boundary conditions on Ω therefore has no influence on the local problems for this mesh element. We observed that the ABC variant of the MsFEM-CR without oversampling does not lead to a significant improvement of its accuracy, in contrast to the oversampling variants that are reported in Figure 8.1.

Numerical results. We compare the performance of the different oversampling strategies defined above in Figure 8.1. The corresponding MsFEMs are tested in both the Galerkin formulation of Definition 5.28 and the Petrov-Galerkin formulation of Definition 6.1. (As was observed in Section 7.4, the non-intrusive Galerkin MsFEM (6.13) still yields the same accuracy as the Galerkin MsFEM, also for the new oversampling variants.) The test case corresponds exactly to the one of Section 7.4 with the periodic diffusion coefficient (7.17a). We show the relative H^1 error with respect to the reference solution for varying coarse mesh sizes H. The homothety ratio used for the definition of the oversampling patches equals 3, and we only consider *DOF*-continuous oversampling. It was observed in the numerical experiments that *DOF*-continuous oversampling yields better results than *DOF*-extended oversampling (and even much better for the Galerkin MsFEM), like in Section 7.4. Finally, we reproduce the results of Section 7.4 for the Galerkin MsFEM-lin with *DOF*-continuous oversampling for comparison.

We observe in Figure 8.1 that both of the new oversampling variants (VBC and ABC) significantly improve on the MsFEM-CR with oversampling as it was defined in Chapter 5. Moreover, both variations improve on the MsFEM-lin with oversampling in the regime $H > \varepsilon$ (which is the regime of interest for the MsFEM). It can also be seen that the Galerkin and Petrov-Galerkin formulations of the MsFEM-CR are still close for all oversampling strategies. The particular choice of the Galerkin MsFEM with ABC *DOF*-continuous numerical correctors is the most accurate method in these tests.

8.2. Non-intrusive implementation of a $\mathbb{P}_2$ MsFEM

The developments of Chapters 4 to 7 rely to a great extent on the fact that the multiscale basis functions are expressed (or defined) in terms of piecewise affine functions in (5.10). This was already observed in Remark 5.1. We have used at multiple occasions the fact that the gradients of the $\mathbb{P}_1$ basis functions are constant. In this section, we consider a possible extension of the non-intrusive approach to the higher-order MsFEM of [9]. (To

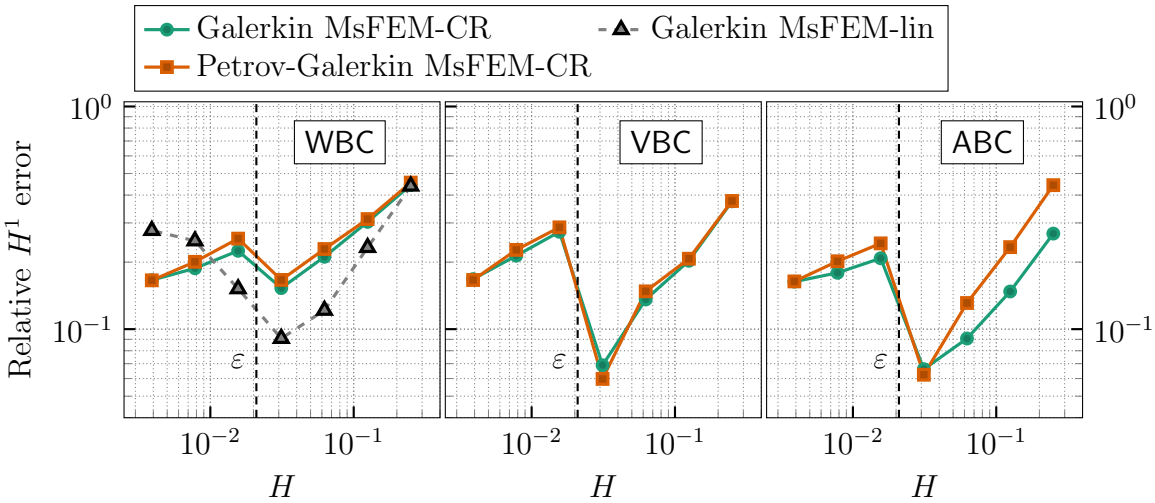

Figure 8.1: *Comparison of different oversampling strategies for the MsFEM-CR applied to the diffusion coefficient in (7.17a) as the mesh size H varies. The Crouzeix-Raviart MsFEM is considered for DOF-continuous numerical correctors with weak, vanishing and affine boundary conditions. All methods shown use oversampling and a homothety ratio of 3. The results of the MFEM-lin correspond to those of Section 7.4, without a modified oversampling strategy.*

be precise, we will actually consider a Petrov-Galerkin variant of the method.) Another high-order MsFEM was proposed in [94]. We only treat the example of the pure diffusion equation, which is sufficient to reveal a number of complications in the generalization of the non-intrusive approach.

8.2.1. Definition of a high-order MsFEM. For the pure diffusion problem (4.1), we recall that the numerical correctors $\chi_K^{\varepsilon,\alpha}$ (without oversampling) are defined, for $1 \leq \alpha \leq d$, by (4.10). The multiscale basis functions for the MsFEMs of the previous chapters are then defined as

$$\phi_i^\varepsilon|_K = \phi_i^{\mathbb{P}_1}|_K + \sum_{\alpha=1}^{d} (\partial_\alpha \phi_i^{\mathbb{P}_1})|_K \chi_K^{\varepsilon,\alpha} \quad \text{for all } K \in \mathscr{T}_H.$$

The high-order MsFEM of [9] is based on the observation that this is equivalent to the change of coordinates on K given by

$$\phi_i^\varepsilon|_K(x) = \phi_i^{\mathbb{P}_1}\big|_K(x + \mathbb{X}_K^\varepsilon(x)) \quad \text{on } K, \tag{8.3}$$

where we introduce the vector $\mathbb{X}_K^\varepsilon = [\chi_K^{\varepsilon,\alpha}]_{\alpha=1}^d$.

Let us now introduce for any integer $k > 0$ the $\mathbb{P}_k$ Lagrange finite element space

$$V_H^k = \{v_H \in \mathscr{C}(\Omega) \,|\, \forall\, K \in \mathscr{T}_H : v_H|_K \in \mathbb{P}_k(K), \text{ and } v_H|_{\partial\Omega} = 0\}.$$

For any $v_H \in V_H^k$, the change of coordinates (8.3) can be used to define a multiscale function, on each $K \in \mathscr{T}_H$, by

$$v_H|_K(x) = v_H|_K(x + \mathbb{X}_K^\varepsilon(x)) \quad \text{on } K. \tag{8.4}$$

We define the multiscale approximation space

$$V_H^{k,\varepsilon} = \left\{ v_H^\varepsilon \,|\, v_H \in V_H^k \right\},$$

that is used for the definition of a high-order MsFEM.

The MsFEM of [9] is a Galerkin approximation on V_H^ε. We have already seen in Chapter 5 that the computations to obtain an effective finite element scheme are simplified if we consider a Petrov-Galerkin formulation with standard test functions. The Galerkin case can be studied similarly. Hence, we consider in this chapter the following MsFEM: find $u_H^\varepsilon \in V_H^{k,\varepsilon}$ such that

$$\int_\Omega \nabla v_H \cdot A^\varepsilon \nabla u_H^\varepsilon = \int_\Omega f\, v_H \quad \text{for all } v_H \in V_H^k. \tag{8.5}$$

Moreover, we restrict ourselves to the $\mathbb{P}_2$ variant of the above MsFEM in this chapter.

To obtain a non-intrusive MsFEM workflow for the above method in the spirit of Algorithm 6.1, the first step, i.e., the computation of the numerical correctors, remains unchanged. The question that we aim to answer in the following sections is if we can express the stiffness matrix of the MsFEM in terms of the standard $\mathbb{P}_2$ basis functions and appropriately defined effective quantities. Such a formulation of the stiffness matrix can be used in a non-intrusive formulation of the $\mathbb{P}_2$ MsFEM if the expression for the stiffness matrix can be computed by a standard $\mathbb{P}_2$ finite element code.

Let $(\phi_i^{\mathbb{P}_k})_{1\le i\le \mathscr{N}}$ be a basis for V_H^k, and for each $1 \le i \le N$, associate a multiscale basis function ϕ_i^ε to $\phi_i^{\mathbb{P}_2}$ according to (8.4). The stiffness matrix $\mathbb{A}^\varepsilon$ of the MsFEM (8.5) is then given by

$$\mathbb{A}_{j,i}^\varepsilon = \int_\Omega \nabla \phi_j^{\mathbb{P}_2} \cdot A^\varepsilon \nabla \phi_i^\varepsilon, \quad 1 \le i, j \le \mathscr{N}. \tag{8.6}$$

For a non-intrusive implementation of the $\mathbb{P}_2$ MsFEM, we must find an expression for these integrals in terms of integrals of piecewise $\mathbb{P}_2$ functions only. We start with a study of integrals like the one in (8.6) for an arbitrary matrix A in Section 8.2.2. This leads to a reformulation of the integral that is used to obtain an effective formulation of the $\mathbb{P}_2$ MsFEM in Section 8.2.3.

8.2.2. Exact quadrature for quadratic functions. Fix a mesh element $K \in \mathscr{T}_H$. Let $A \in L^\infty(K)^{d\times d}$ be any $d \times d$ matrix, and let g, h be two arbitrary functions belonging to $\mathbb{P}_2(K)$. We look for an equivalent expression of the integral

$$\int_K \nabla h \cdot A \nabla g \tag{8.7}$$

in terms of integrals of $\mathbb{P}_2(K)$ functions only. The main ingredient for our reformulation of the integral is the expansion of g and h around the vertices of a quadrature formula for K. Let $\left(x_l^K, \omega_l^K\right)_{l=1}^{d+1}$ be a set of quadrature points and weights such that we have the equality $\displaystyle\int_K \varphi = \sum_{l=1}^{d+1} \omega_l^K \varphi\left(x_l^K\right)$ for any $\varphi \in \mathbb{P}_2(K)$. In particular, it holds

$$\sum_{l=1}^{d+1} \omega_l = |K|. \tag{8.8}$$

To simplify the notation, we will write (x_l, ω_l) instead of (x_l^K, ω_l^K) since we consider a fixed mesh element.

Since g is a polynomial of degree 2, it holds, for all $1 \le l \le d+1$,

$$\nabla g(x) = \nabla g(x_l) + \sum_{\alpha=1}^{d} (x^\alpha - x_l^\alpha)\partial_\alpha \nabla g = \nabla g(x_l) + D^2(g)\,[x - x_l], \quad x \in K, \tag{8.9}$$

where $D^2 g\,[x - x_i]$ is to be read as a matrix-vector product. Note that the second derivatives of g are constant on K. Clearly, the same expansion holds for h.

Using (8.8) and inserting the expansion (8.9) in (8.7) for g and h, we obtain

$$\begin{aligned}
\int_K \nabla h \cdot A \nabla g &= \sum_{l=1}^{d+1} \frac{\omega_l}{|K|} \int_K \nabla h \cdot A \nabla g \\
&= \sum_{l=1}^{d+1} \frac{\omega_l}{|K|} \int_K \left(\nabla h(x_l) + D^2(h)\,[x - x_l]\right) \cdot A \left(\nabla g(x_l) + D^2(g)\,[x - x_l]\right) \\
&= \sum_{l=1}^{d+1} \frac{\omega_l}{|K|} \Bigg\{ \nabla h(x_l) \cdot \left(\int_K A\right) \nabla g(x_l) + \\
&\qquad \sum_{\alpha=1}^{d} \partial_\alpha \nabla h \left(\int_K (x^\alpha - x_l^\alpha)\, A\right) \nabla g(x_l) + \\
&\qquad \sum_{\alpha=1}^{d} \nabla h(x_l) \cdot \left(\int_K (x^\alpha - x_l^\alpha)\, A\right) \partial_\alpha \nabla g + \\
&\qquad \sum_{\alpha,\beta=1}^{d} \partial_\beta \nabla h \cdot \left(\int_K \left(x^\beta - x_l^\beta\right)(x^\alpha - x_l^\alpha)\, A\right) \partial_\alpha \nabla g \Bigg\}.
\end{aligned}$$

We collect the above moments of A in the three tensors $\overline{\mathscr{A}}_0(A) \in \mathbb{P}_0(K, \mathbb{R}^{d\times d})$, $\overline{\mathscr{A}}_1(A) \in \mathbb{P}_1(K, \mathbb{R}^{d\times d\times d})$ and $\overline{\mathscr{A}}_2(A) \in \mathbb{P}_2(K, \mathbb{R}^{d\times d\times d\times d})$ defined by

$$\begin{cases}
\overline{\mathscr{A}}_0(A)^{\alpha,\beta} = \dfrac{1}{|K|} \displaystyle\int_K A^{\beta,\alpha}, & \\
\overline{\mathscr{A}}_1(A)^{\alpha,\beta,\gamma}(y) = \dfrac{1}{|K|} \displaystyle\int_K (x^\gamma - y^\gamma)\, A^{\beta,\alpha}, & \text{for } l = 1, \dots, d+1, \\
\overline{\mathscr{A}}_2(A)^{\alpha,\beta,\gamma,\delta}(y) = \dfrac{1}{|K|} \displaystyle\int_K (x^\gamma - y^\gamma)\left(x^\delta - y^\delta\right) A^{\beta,\alpha}, & \text{for } l = 1, \dots, d+1.
\end{cases} \tag{8.10}$$

With these definitions, the above computations can be summarized as

$$\begin{aligned}
\int_K \nabla h \cdot A \nabla g = \sum_{l=1}^{d+1} \omega_l \Big\{ &\partial_\beta h\, \overline{\mathscr{A}}_0(A)^{\alpha,\beta}\, \partial_\alpha g + \partial_\gamma \partial_\beta h\, \overline{\mathscr{A}}_1(A)^{\alpha,\beta,\gamma}\, \partial_\alpha g + \\
&\partial_\beta h\, \overline{\mathscr{A}}_1(A)^{\alpha,\beta,\gamma}\, \partial_\gamma \partial_\alpha g + \partial_\delta \partial_\beta h\, \overline{\mathscr{A}}_2(A)^{\alpha,\beta,\gamma,\delta}\, \partial_\gamma \partial_\alpha g \Big\}(x_l).
\end{aligned} \tag{8.11}$$

Here and in the sequel, we apply the Einstein summation convention to repeated Greek indices. The right-hand side in (8.11) can be interpreted as the application of the quadrature rule $\left(x_l^K, \omega_l^K\right)_{l=1}^{d+1}$ to the function in curly brackets.

Note that all terms in the curly brackets are polynomials of degree at most 2. For instance, $\partial_\beta h$ and $\partial_\alpha g$ are polynomials of degree at most 1, and $\overline{\mathscr{A}}_0(A)^{\alpha,\beta}$ is constant, for all $1 \leq \alpha, \beta \leq d$. Also recall that the quadrature rule $\left(x_l^K, \omega_l^K\right)_{l=1}^{d+1}$ is exact on $\mathbb{P}_2(K)$. Hence, the numerical quadrature on the right-hand side of (8.11) is equal to the integral over K, i.e.,

$$\begin{aligned}\int_K \nabla h \cdot A \nabla g = \int_K \partial_\beta h\, \overline{\mathscr{A}}_0(A)^{\alpha,\beta}\, \partial_\alpha g + \partial_\gamma \partial_\beta h\, \overline{\mathscr{A}}_1(A)^{\alpha,\beta,\gamma}\, \partial_\alpha g + \\ \partial_\beta h\, \overline{\mathscr{A}}_1(A)^{\alpha,\beta,\gamma}\, \partial_\gamma \partial_\alpha g + \partial_\delta \partial_\beta h\, \overline{\mathscr{A}}_2(A)^{\alpha,\beta,\gamma,\delta}\, \partial_\gamma \partial_\alpha g.\end{aligned} \tag{8.12}$$

In Section 8.2.3, the identity (8.12) will be our main tool in the reformulation of $\mathbb{P}_2$ MsFEM as an effective scheme involving only piecewise $\mathbb{P}_2$ functions.

Remark 8.4. Even though we derived Equation (8.12) with the help of one given quadrature formula, none of the quantities on the right-hand side depend on this choice. In particular, the effective tensors $\overline{\mathscr{A}}_0(A)$, $\overline{\mathscr{A}}_1(A)$ and $\overline{\mathscr{A}}_2(A)$ only depend on the matrix A and the mesh element K.

8.2.3. Effective formulation of the $\mathbb{P}_2$ MsFEM. In this section, we address the computation of the stiffness matrix $\mathbb{A}^\varepsilon_{j,i}$ from (8.6). Let us fix i and j between 1 and $\mathscr{N}$. First we compute $\nabla \phi_i^\varepsilon$. The chain rule shows that, for any mesh element K and all $x \in K$,

$$\nabla \phi_i^\varepsilon|_K(x) = (\mathrm{Id} + \nabla \mathbb{X}_K^\varepsilon(x))\, \nabla \phi_i^{\mathbb{P}_2}(x + \mathbb{X}_K^\varepsilon(x)),$$

where $\nabla \mathbb{X}_K^\varepsilon$ denotes the matrix

$$\nabla \mathbb{X}_K^\varepsilon = \begin{pmatrix} \partial_1 \chi_K^{\varepsilon,1} & \cdots & \partial_1 \chi_K^{\varepsilon,d} \\ \vdots & \ddots & \vdots \\ \partial_d \chi_K^{\varepsilon,1} & \cdots & \partial_d \chi_K^{\varepsilon,d} \end{pmatrix}.$$

Since $\nabla \phi_i^{\mathbb{P}_2}$ is piecewise $\mathbb{P}_1$, it follows, for all $x \in K$,

$$\nabla \phi_i^\varepsilon|_K(x) = (\mathrm{Id} + \nabla \mathbb{X}_K^\varepsilon(x)) \left(\nabla \phi_i^{\mathbb{P}_2}(x) + D^2\left(\phi_i^{\mathbb{P}_2}\right)\big|_K \mathbb{X}_K^\varepsilon(x)\right). \tag{8.13}$$

We can thus expand the matrix element $\mathbb{A}^\varepsilon_{j,i}$ as

$$\begin{aligned}\mathbb{A}^\varepsilon_{j,i} &= \sum_{K \in \mathscr{T}_H} \int_K \nabla \phi_j^{\mathbb{P}_2} \cdot A^\varepsilon\, (\mathrm{Id} + \nabla \mathbb{X}_K^\varepsilon) \left(\nabla \phi_i^{\mathbb{P}_2} + D^2\left(\phi_i^{\mathbb{P}_2}\right) \mathbb{X}_K^\varepsilon\right) \\ &= \sum_{K \in \mathscr{T}_H} \underbrace{\int_K \nabla \phi_j^{\mathbb{P}_2} \cdot A^\varepsilon\, (\mathrm{Id} + \nabla \mathbb{X}_K^\varepsilon)\, \nabla \phi_i^{\mathbb{P}_2}}_{=:\, I_K} + \\ &\qquad \sum_{\zeta=1}^d \underbrace{\int_K \nabla \phi_j^{\mathbb{P}_2} \cdot A^\varepsilon\, (\mathrm{Id} + \nabla \mathbb{X}_K^\varepsilon)\, \chi_K^{\varepsilon,\zeta}\, \nabla\left(\partial_\zeta \phi_i^{\mathbb{P}_2}\right)}_{=:\, II_K(\zeta)}.\end{aligned}$$

We can compute the terms I_K by applying (8.12) to the matrix $A = (\mathrm{Id} + \nabla \mathbb{X}_K^\varepsilon)$ for

each mesh element K. Let us define the tensors $\overline{A}_0$, $\overline{A}_1$ and $\overline{A}_2$ by

$$\begin{aligned} \overline{A}_0\big|_K &= \overline{\mathscr{A}_0}(\mathrm{Id} + \nabla \mathbb{X}_K^\varepsilon), \\ \overline{A}_1\big|_K &= \overline{\mathscr{A}_1}(\mathrm{Id} + \nabla \mathbb{X}_K^\varepsilon), \qquad \text{for all } K \in \mathscr{T}_H. \\ \overline{A}_2\big|_K &= \overline{\mathscr{A}_2}(\mathrm{Id} + \nabla \mathbb{X}_K^\varepsilon), \end{aligned} \tag{8.14}$$

referring to (8.10) for detailed definitions. Then it holds, for all $K \in \mathscr{T}_H$,

$$\begin{aligned} I_K = \int_K \partial_\beta \phi_j^{\mathbb{P}_2} \, \overline{A_0}^{\alpha,\beta} \, \partial_\alpha \phi_i^{\mathbb{P}_2} + \partial_\gamma \partial_\beta \phi_j^{\mathbb{P}_2} \, \overline{A_1}^{\alpha,\beta,\gamma} \, \partial_\alpha \phi_i^{\mathbb{P}_2} + \\ \partial_\beta \phi_j^{\mathbb{P}_2} \, \overline{A_1}^{\alpha,\beta,\gamma} \, \partial_\gamma \partial_\alpha \phi_i^{\mathbb{P}_2} + \partial_\delta \partial_\beta \phi_j^{\mathbb{P}_2} \, \overline{A_2}^{\alpha,\beta,\gamma,\delta} \, \partial_\gamma \partial_\alpha \phi_i^{\mathbb{P}_2}. \end{aligned}$$

For all $K \in \mathscr{T}_H$ and $1 \le \zeta \le d$, we can compute $II_K(\zeta)$ by applying (8.12) to $h = \phi_j^{\mathbb{P}_2}$, $g = \partial_\zeta \phi_i^{\mathbb{P}_2}$, and $A = (\mathrm{Id} + \nabla \mathbb{X}_K^\varepsilon)\, \chi_K^{\varepsilon,\zeta}$. Note that g is affine on K in this case, so all its second derivatives vanish. Hence, we define the tensors $\overline{D}_0$ and $\overline{D}_1$ by

$$\begin{aligned} \overline{D}_0^{\alpha,\beta,\zeta}\Big|_K &= \overline{\mathscr{A}_0}\Big((\mathrm{Id} + \nabla \mathbb{X}_K^\varepsilon)\, \chi_K^{\varepsilon,\zeta} \Big)^{\alpha,\beta}, \\ \overline{D}_1^{\alpha,\beta,\zeta,\gamma}\Big|_K &= \overline{\mathscr{A}_1}\Big((\mathrm{Id} + \nabla \mathbb{X}_K^\varepsilon)\, \chi_K^{\varepsilon,\zeta} \Big)^{\alpha,\beta,\gamma}, \end{aligned} \qquad \text{for all } K \in \mathscr{T}_H. \tag{8.15}$$

Then we can express $II_K(\zeta)$ as

$$II_K(\zeta) = \int_K \partial_\beta \phi_j^{\mathbb{P}_2} \, \overline{D_0}^{\alpha,\beta,\zeta} \, \partial_\zeta \partial_\alpha \phi_i^{\mathbb{P}_2} + \partial_\gamma \partial_\beta \phi_j^{\mathbb{P}_2} \, \overline{D_1}^{\alpha,\beta,\zeta,\gamma} \, \partial_\zeta \partial_\alpha \phi_i^{\mathbb{P}_2}.$$

Remark 8.5. Note that the tensor $\overline{A}_2$ is symmetric with respect to its third and fourth index, but that $\overline{D}_1$ is not.

Now summing all the above contributions, we find

$$\begin{aligned} \mathbb{A}_{j,i}^\varepsilon = \sum_{K \in \mathscr{T}_H} \int_K \partial_\beta \phi_j^{\mathbb{P}_2} \, \overline{A}_0^{\alpha,\beta} \, \partial_\alpha \phi_i^{\mathbb{P}_2} + \partial_\gamma \partial_\beta \phi_j^{\mathbb{P}_2} \, \overline{A}_1^{\alpha,\beta,\gamma} \, \partial_\alpha \phi_i^{\mathbb{P}_2} + \\ \partial_\beta \phi_j^{\mathbb{P}_2} \left[\overline{A}_1^{\alpha,\beta,\gamma} + \overline{D}_0^{\alpha,\beta,\gamma} \right] \partial_\gamma \partial_\alpha \phi_i^{\mathbb{P}_2} + \partial_\delta \partial_\beta \phi_j^{\mathbb{P}_2} \left[\overline{A}_2^{\alpha,\beta,\gamma,\delta} + \overline{D}_1^{\alpha,\beta,\gamma,\delta} \right] \partial_\gamma \partial_\alpha \phi_i^{\mathbb{P}_2}. \end{aligned} \tag{8.16}$$

Upon introducing, for all $K \in \mathscr{T}_H$, the effective bilinear form

$$\begin{aligned} \overline{a}_K^{\mathbb{P}_2}(u,v) = \int_K \partial_\beta v \, \overline{A}_0^{\alpha,\beta} \, \partial_\alpha u + \partial_\gamma \partial_\beta v \, \overline{A}_1^{\alpha,\beta,\gamma} \, \partial_\alpha u + \partial_\beta v \left[\overline{A}_1^{\alpha,\beta,\gamma} + \overline{D}_0^{\alpha,\beta,\gamma} \right] \partial_\gamma \partial_\alpha u + \\ \partial_\delta \partial_\beta v \left[\overline{A}_2^{\alpha,\beta,\gamma,\delta} + \overline{D}_1^{\alpha,\beta,\gamma,\delta} \right] \partial_\gamma \partial_\alpha u \qquad \text{for all } u, v \in H^2(\mathscr{T}_H), \end{aligned}$$

we can rewrite the above as the identity

$$\mathbb{A}_{j,i}^\varepsilon = \sum_{K \in \mathscr{T}_H} \overline{a}_K^{\mathbb{P}_2}\big(\phi_i^{\mathbb{P}_2}, \phi_j^{\mathbb{P}_2}\big).$$

This corresponds to the $\mathbb{P}_2$ discretization of a fourth order PDE. Recall that the original MsFEM problem (8.5) is a discretization of a second order PDE. The structure of the effective problem is thus considerably more invovled than that of the MsFEM.

If a standard $\mathbb{P}_2$ finite element code is available that can solve general fourth-order PDEs, one can use it to solve the linear system

$$\mathbb{A}^\varepsilon U^\varepsilon = \mathbb{F}^{\mathbb{P}_2},$$

where $\mathbb{F}_j^{\mathbb{P}_2} = \int_\Omega f\, \phi_j^{\mathbb{P}_2}$, once the numerical correctors and the effective tensors from (8.14) and (8.15) have been computed in the offline stage. Note that, in contrast to the MsFEM studied in Chapter 6, the effective tensors are no longer all constant, but are piecewise $\mathbb{P}_2$ functions. One should thus compute all their coefficients as input to the legacy FEM software. Once the linear system has been solved in the online stage of the MsFEM, the solution to (8.5) is given by

$$u_H^\varepsilon = \sum_{i=1}^{\mathscr{N}} U_i^\varepsilon\, \phi_i^\varepsilon.$$

In conclusion, we see that an effective PDE can be formulated such that its $\mathbb{P}_2$ discretization is equivalent to the MsFEM problem (8.5), with the property that all effective tensors are $\mathbb{P}_2$ functions. In comparison to the $\mathbb{P}_1$ case studied in detail before, the effective PDE is no longer of second order and its formulation requires the computation of many more coefficients. The order of the effective PDE and the number of coefficients to be computed will further increase when higher-order MsFEMs are considered. The implementation of the effective PDE in a given legacy code may become a problem in itself. Therefore, we do not pursue the development of non-intrusive $\mathbb{P}_k$ MsFEMs in as much generality as was done for the $\mathbb{P}_1$ MsFEM.

Part II

Multiscale Finite Element Methods for Advection-Dominated Problems

Chapter 9

Introduction and classical stabilization methods

We have seen in the Introduction that a standard FEM shows instabilities for the approximation of advection-diffusion problems with dominant advection terms, and that the same holds for an MsFEM that encodes only the diffusive terms in the basis functions. The development of stable numerical methods for the approximation of PDEs in heterogeneous media and in the advection-dominated regime is the topic of Part II of this thesis. The contents of this part of the thesis are being prepared for publication in [30].

We illustrate the instability of the $\mathbb{P}_1$ FEM in this chapter in some more detail, and we briefly review classical stabilization methods. In particular, we recall the connection between the SUPG method and the use of residual-free bubbles. These results are well-known and the reader familiar with stabilization methods may wish to skip some parts of this chapter and only look at Sections 9.2, 9.4.1 and 9.4.2 for the introduction of some notation that is used in the sequel.

In Chapter 10 we recall the basic principles of the MsFEM in order to keep Part II self-contained, and then derive an MsFEM from the residual-free bubble framework, with basis functions adapted to both the advective and diffusive parts of the differential operator. This identification with the residual-free bubble framework is used to show stability of the method in 1D as well as to give an explanation for the instability of the method in higher dimension, which was previously observed numerically in [114]. Even in the one-dimensional setting, we observe that this MsFEM cannot achieve high accuracy in spite of its stability, and we solve this problem through the addition of suitable bubble functions to the approximation space in Section 10.3. The performance of this method is illustrated numerically in 1D in Section 10.4 and later, in Chapter 12, in 2D.

For higher-dimensional problems, we introduce the concept of weak bubbles in Chapter 11, and we will see that these bubbles can be used to define an MsFEM with Crouzeix-Raviart type boundary conditions (denoted adv-MsFEM-CR here), an idea originally introduced in [112]. The enrichment of the approximation space by bubble functions (this time by weak bubbles) is also proposed, following the developments of the one-dimensional setting. In Section 11.4, we summarize the non-intrusive implementation approach for MsFEMs developed in Part I and extend it to MsFEMs with additional bubble functions.

Finally, the numerical results of Chapter 12 show that the adv-MsFEM-CR enriched with weak bubbles is stable. The results also show that the non-intrusive implementation

of the additional bubble functions yields the largest accuracy among all numerical methods investigated here. The adv-MsFEM-CR with bubbles is the first stable MsFEM that maintains a competitive accuracy in both the advection- and diffusion-dominated regimes and does not depend on an additional stabilization parameter that has to be properly adjusted.

9.1. Advection-dominated problems

We recall the instability of the finite element method on a coarse mesh in the advection-dominated regime for a PDE with constant coefficients in 1D. To this end, we consider the following boundary value problem for u:

$$\begin{cases} -m\,u'' + b\,u' = 1 & \text{in } (0,1), \\ u(0) = 0, & u(1) = 0, \end{cases} \tag{9.1}$$

where b is a positive constant for now. Then u is given by

$$u(x) = \frac{x}{b} - \frac{1}{b}\,\frac{\mathrm{e}^{\frac{b}{m}x} - 1}{\mathrm{e}^{\frac{b}{m}} - 1}.$$

When $b/m \gg 1$, the solution u displays a sharp boundary layer near $x = 1$, where the derivative of u is much larger than outside the boundary layer. In this sense (9.1) leads to multiscale phenomena even with constant coefficients.

It is insightful to note that u can be decomposed into a slowly varying part v^s and a multiscale part v^ε such that $u = v^s + v^\varepsilon$, where $v^s(x) = \dfrac{x}{b}$ is the solution to

$$\begin{cases} -m\,(v^s)'' + b\,(v^s)' = 1 & \text{in } \Omega, \\ v^s(0) = 0, & v^s(1) = \dfrac{1}{b}, \end{cases} \tag{9.2a}$$

and v^ε is thus the solution to the following boundary value problem without source term:

$$\begin{cases} -m\,(v^\varepsilon)'' + b\,(v^\varepsilon)' = 0 & \text{in } \Omega, \\ v^\varepsilon(0) = 0, & v^\varepsilon(1) = -\dfrac{1}{b}. \end{cases} \tag{9.2b}$$

From this decomposition, it is clear that the multiscale behaviour of u is due to the Dirichlet conditions that do not match the source term of the PDE in (9.1), contrary to the conditions imposed in (9.2a). Problem (9.2b) shows that a boundary layer can emerge in the advection-dominated regime even in the absence of a source term.

Now consider the $\mathbb{P}_1$ finite element approximation of u on the grid $0 = x_0, x_1, \ldots, x_N = 1$ with $x_i - x_{i-1} = H$ $(1 \le i \le N)$. We split the approximation of u into two problems according to (9.2). In this simple case, the approximations of both v^s and v^ε can be computed explicitly. It is easy to see that the finite element approximation of (9.2a) is exact, whereas the approximation v_H^ε of v^ε in (9.2b) is of the form

$$v_H^\varepsilon(x_i) = -\frac{1}{b}\frac{1-\gamma^i}{1-\gamma^N}, \quad \gamma = \frac{1+\mathsf{Pe}_H}{1-\mathsf{Pe}_H}, \quad x_i = i\,H, \quad i = 0, \ldots, N.$$

Here, $\mathsf{Pe}_H = \dfrac{bH}{2m}$ is the *local* or *numerical Péclet number*. We see that the numerical approximation of v^ε oscillates in the domain $(0,1)$ when $\mathsf{Pe}_H > 1$, whereas v^ε itself is monotone. In other words, when the mesh size H is too large, the finite element approximation of u^ε displays *spurious oscillations* that are unphysical. This phenomenon generalizes to higher-dimensional settings, and the spurious oscillations become more pronounced as the strength of the advection field b further increases. The standard finite element approximation of (9.3) is therefore said to be *unstable*.

Stabilization methods aim to provide an accurate numerical approximation of u outside the boundary layer even when a coarse mesh is used (with a large local Péclet number), thus capturing the correct behaviour of v^s. In dimension 1, adapted finite element strategies are known that yield a nodally exact approximation for u when the coefficients of the PDE and the source term are piecewise constant, thus removing the spurious oscillations of a standard FEM. For higher-dimensional problems, a method yielding nodal exactness is not known, and the performance of stabilization methods is judged by stronger stability properties, convergence estimates with an improved dependence on the advection field, and the extent to which spurious oscillations are suppressed in practice. We recall some stabilization methods in Sections 9.3 and 9.4.

9.2. The multiscale setting

The next chapters of Part II focus on the numerical approximation of $u^\varepsilon \in H^1(\Omega)$ defined as the solution to the PDE

$$\begin{cases} \mathscr{L}^\varepsilon u^\varepsilon = -\operatorname{div}(A^\varepsilon \nabla u^\varepsilon) + b \cdot \nabla u^\varepsilon = f & \text{in } \Omega, \\ u^\varepsilon = g & \text{on } \partial\Omega, \end{cases} \tag{9.3}$$

with a Dirichlet boundary condition $g \in H^{1/2}(\partial\Omega)$ and a source term $f \in L^2(\Omega)$. The problem is posed on $\Omega \subset \mathbb{R}^d$, an open, bounded polytope in d-dimensional space (a polygon in dimension 2, a polyhedron in dimension 3). Since Ω has a Lipschitz boundary, the boundary condition g is the trace of a function $g \in H^1(\Omega)$ (denoted here by the same symbol g; see [85, Theorem 1.5.1.3]).

The diffusion tensor $A^\varepsilon \in L^\infty\big(\Omega, \mathbb{R}^{d\times d}\big)$ is bounded and coercive, that is,

$$\text{for almost all } x \in \Omega, \quad \begin{cases} \forall\, \xi \in \mathbb{R}^d, & m|\xi|^2 \le \xi \cdot A^\varepsilon(x)\xi, \\ \forall\, \xi_1, \xi_2 \in \mathbb{R}^d, & |\xi_2 \cdot A^\varepsilon(x)\xi_1| \le M|\xi_2|\,|\xi_1|, \end{cases} \tag{9.4}$$

for constants $0 < m \le M$ (that are independent of ε). We write the diffusion tensor with a superscript ε, because we focus on highly heterogeneous diffusion coefficients that may oscillate on a length scale ε much smaller than the diameter of Ω. Note that we shall use no further assumptions (such as periodicity) on A^ε for the design of the numerical approaches in Chapters 10 and 11. Finally, we assume that the advection field $b \in L^\infty\big(\Omega, \mathbb{R}^d\big)$ satisfies

$$\operatorname{div}(b) = 0 \tag{9.5}$$

in the sense of distributions. Then the problem (9.3) has a unique solution. Other conditions can also be considered that ensure well-posedness of (9.3). For instance, the weaker conditions $\operatorname{div}(b) \in L^{d/2}(\Omega)$ and $\operatorname{div}(b) \le 0$ almost everywhere on Ω are in fact

sufficient for our purposes, but we assume (9.5) to simplify the exposition of strongly consistent stabilization methods in Section 9.3. The general case can be found in [129, Chapter 13].

The variational (or weak) formulation of (9.3) that we will use is: find $u^\varepsilon \in H^1(\Omega)$ such that $u^\varepsilon - g$ belongs to $H^1_0(\Omega)$ and satisfies

$$a^\varepsilon(u^\varepsilon, v) = F(v) \quad \text{for all } v \in H^1_0(\Omega), \tag{9.6}$$

where, for all $u, v \in H^1(\Omega)$,

$$a^\varepsilon(u, v) = \int_\Omega \nabla v \cdot A^\varepsilon \nabla u + v\, b \cdot \nabla u, \quad F(v) = \int_\Omega f\, v.$$

Under the above assumptions (9.4) and (9.5), it is classical to show that a^ε is coercive on $H^1_0(\Omega)$, such that a unique solution to (9.6) exists by the Lax-Milgram Theorem (see, e.g., [129, Chapter 13]).

We recall that an FEM for the approximation of (9.3) is obtained upon restricting the variational formulation (9.6) to finite-dimensional trial and test spaces of functions with localized supports. To this end, we introduce a conformal mesh $\mathscr{T}_H$ of Ω and define the trial space

$$V_H = \{v \in \mathscr{C}(\Omega) \,|\, \forall\, K \in \mathscr{T}_H,\, v|_K \in \mathbb{P}_1(K)\},$$

that is, the space of all continuous functions that are piecewise affine. Note that $V_H \subset H^1(\Omega)$. We also define the test space

$$V_{H,0} = V_H \cap H^1_0(\Omega).$$

Finally, let $\mathscr{I}_H : H^1(\Omega) \mapsto V_H$ be a suitable interpolation operator for the boundary condition. The (standard, conforming) Lagrange $\mathbb{P}_1$ finite element method then is to find $u_H \in V_H$ such that

$$\begin{cases} a^\varepsilon(u_H, v_H) = F(v_H) & \text{for all } v_H \in V_{H,0}, \\ u_H - \mathscr{I}_H(g) \in V_{H,0}. \end{cases} \tag{9.7}$$

We have seen in Section 9.1 that the exact solution u^ε may have a strong boundary layer near the outflow boundary if the advection is dominant over the diffusive effects in (9.3). We also recalled that the $\mathbb{P}_1$ FEM (9.7) produces a numerical approximation with unphysical oscillations propagating through the entire domain, if the underlying mesh is not sufficiently fine to resolve the boundary layer well, and this remains true in higher dimension. In Chapters 10 and 11, we focus on stabilizing properties of multiscale finite element methods aimed at removing such oscillations from the numerical approximation, while also incorporating the strongly heterogeneous character of A^ε properly. The aim is to identify numerical methods that are robust when we pass from the advection-dominated to the diffusion-dominated regime. References to related contributions in the field were given in Section 2.3.2.

Remark 9.1. It is common practice in the literature to only consider (9.3) with homogeneous boundary conditions ($g = 0$), because the resolution of the problem with non-homogeneous boundary conditions by the FEM only requires some standard adaptations. One can use a lifting of the boundary conditions or use a penalization technique.

We refer to [73, Section 8.4] for details. However, for the case of advection-dominated problems, we emphasized in Section 9.1 that the instability of standard FEMs is caused by the Dirichlet boundary conditions, even when $f = 0$. In this case, the problem (9.3) becomes trivial when homogeneous boundary conditions are imposed. It is therefore more insightful for the understanding of stabilizing properties of the methods introduced in Chapters 10 and 11 to treat the general case of possibly non-homogeneous boundary conditions. See for instance Theorem 10.4 and Corollary 11.5 in this regard.

9.3. Strongly consistent stabilization methods

We recall here the concept of strongly consistent stabilization methods for problems without a multiscale diffusion coefficient. Therefore, we consider the single-scale operator

$$\mathscr{L}u = -m\Delta u + b \cdot \nabla u, \tag{9.8}$$

where $m > 0$ and $b \in \mathbb{R}^d$ are constant. We denote (using (9.5)) by $\mathscr{L}_s v = -m\Delta v$ and $\mathscr{L}_{ss} v = b \cdot \nabla v$ the symmetric and skew-symmetric part of $\mathscr{L}$, respectively. In this case, u can equivalently be defined by the variational formulation

$$a(u, v) = \int_\Omega m\nabla u \cdot \nabla v + v\, b \cdot \nabla u = F(v) \quad \text{for all } v \in H_0^1(\Omega),$$

where F is as in (9.6). The finite element approximation (9.7) becomes: find $u_H \in V_H$ such that

$$\begin{cases} a(u_H, v_H) = F(v_H) & \text{for all } v_H \in V_{H,0}, \\ u_H - \mathscr{I}_H(g) \in V_{H,0}. \end{cases} \tag{9.9}$$

Strongly consistent stabilization methods consist of adding the residue of the PDE in each mesh element $K \in \mathscr{T}_H$ to the discrete variational problem (9.9), with a weight (τ below) that depends on the advection field. The additional terms are chosen such that stronger stability properties hold for the numerical scheme, in particular in the streamline direction. More precisely, a strongly consistent stabilization method consists in finding $u_H \in V_H$ such that

$$\begin{cases} a(u_H, v_H) + a_H(u_H, v_H) = F(v_H) + F_H(v_H) & \text{for all } v_H \in V_{H,0}, \\ u_H - \mathscr{I}_H(g) \in V_{H,0}, \end{cases} \tag{9.10}$$

where, for all $u, v \in V_H$, we introduce the stabilization terms

$$\begin{aligned} a_H(u_H, v_H) &= \sum_{K \in \mathscr{T}_H} \int_K \tau\, (\mathscr{L}u_H)\, ((\mathscr{L}_{ss} + \rho\mathscr{L}_s)v_H)\,, \\ F_H(v_H) &= \sum_{K \in \mathscr{T}_H} \int_K \tau\, f\, ((\mathscr{L}_{ss} + \rho\mathscr{L}_s)v_H)\,. \end{aligned} \tag{9.11}$$

Note that $\mathscr{L}_s$ vanishes on $\mathbb{P}_1(K)$ for all $K \in \mathscr{T}_H$, and the parameter ρ thus disappears from the above definitions. When higher-order polynomial approximation spaces are used for the finite element method, different schemes emerge for different choices of ρ. The choice $\rho = -1$ yields the Douglas-Wang method [65, 75], the choice $\rho = 1$ leads to the Galerkin Least Squares method [103], and the Streamline Upwind/Petrov-Galerkin

(SUPG) method [43] corresponds to $\rho = 0$. We restrict ourselves to the SUPG method in this work.

Remark 9.2. In our numerical tests for the $\mathbb{P}_1$ SUPG method, even when the diffusion coefficient is not constant, we still replace $\mathscr{L}u_H$ by $\mathscr{L}_{ss}u_H$ in (9.11).

These methods are called strongly consistent because any solution $u \in H^1(\Omega)$ of (9.8) satisfies $a_H(u, v_H) = F_H(v_H)$ for all $v_H \in V_{H,0}$ and thus satisfies the stabilized discrete formulation. In 1D, the stabilization term a_H corresponds to elementary techniques such as upwinding and adding artificial diffusion. The stabilization term F_H and subsequent consistency of the stabilization methods secure high-order convergence when high-order polynomial spaces are used [109, 131].

The stabilization parameter τ that appears in the definition of the stabilization terms must be carefully adjusted to the coefficients of the PDE. This is the topic of many research articles and we refer e.g. to [107] for a review of some choices and their motivations. Roughly speaking, in the advection dominated regime $\mathsf{Pe}_H > 1$, a suitable choice for τ is of the order of $\dfrac{\operatorname{diam}(K)}{2\,|b_K|}$ in each mesh element K, where b_K is a characteristic value of b in K. This scaling of τ results in the advection-dominated regime in a coercivity constant of $a + a_H$ of the order of $m + \tau|b|^2 \approx m + |b|H \approx |b|H$ on V_H, while the continuity constant is of the order of $m + |b|H + \tau|b|^2 \approx m + \frac{3}{2}|b|H \approx \frac{3}{2}|b|H$. The two constants are thus of the same order for all values of m. When no stabilization is applied, the coercivity constant is just m and coercivity is lost in the limit $m \to 0$. For higher-order finite elements, it is suggested that τ should be taken smaller (see [78]).

9.4. Variational stabilization methods

9.4.1. The variational multiscale framework. We now return to the approximation of u^ε, solution to the multiscale PDE (9.3). The variational multiscale framework (VMF) [101, 102] is a now classical approach for the adaptation of standard finite element methods to multiscale phenomena. It relies on the concept of *resolved* and *unresolved* scales. The space of resolved scales is the space in which the finite element approximation is sought. The unresolved scales are then all components of u^ε outside this space. In [102], the resolved scales in the context of the FEM equal the $\mathbb{P}_1$ space V_H. In order to localize the unresolved scales to each mesh element $K \in \mathscr{T}_H$ separately, the bubble space

$$\mathscr{B}_H = \bigoplus_{K \in \mathscr{T}_H} H_0^1(K) \tag{9.12}$$

is used for the unresolved scales. One hopes that the space $V_H \oplus \mathscr{B}_H$ captures sufficiently many multiscale features of u^ε in order to design an accurate finite element method. This is true in 1D, since $V_H \oplus \mathscr{B}_H = H_0^1(\Omega)$, but in higher dimension, this space discards all possible oscillations of u^ε on the interfaces of the mesh. In the context of stabilization methods, the result is that full stabilization is not achieved by the residual-free bubble method that we recall below. In the context of the multiscale finite element method, this problem has lead to the introduction of the so-called oversampling technique, which seeks for a better approximation of u^ε on the mesh interfaces (see Section 10.1.)

A concrete instance of the VMF requires the choice of a discrete subspace of $\mathscr{B}_H$, which will be used in the numerical scheme. One aims to capture the effect of the bubble func-

tions on the space of resolved scales V_H. (We provide a concrete example of this approach in Section 9.4.2.) It was observed in [54, 41, 101] that a generic, problem-independent choice of bubble functions is not effective. On the other hand, it was established in [22] that, given certain stabilized finite element formulations, a set of bubbles exist from which the stabilization terms can be derived. This justifies the attempt to search for a suitable choice of bubble functions within the VMF. The residual-free bubble (RFB) method is of particular interest in combination with the MsFEM as we will see in Chapter 10.

9.4.2. The residual-free bubble method. We now recall the RFB method [76, 38] in the context of the highly oscillatory PDE (9.3), and recall how it is related to stabilization. Let us mention the more general framework studied in [40], where the coarse space includes functions whose traces on the interfaces of the mesh are higher-order polynomials.

Consider a Galerkin approximation of (9.6) on the (infinite-dimensional) space $V_H \oplus \mathscr{B}_H$. The residual-free bubble approximation to (9.6) is the unique function $u_H + u_B \in V_H \oplus \mathscr{B}_H$ such that

$$\begin{cases} a^\varepsilon(u_H + u_B, v) = F(v) & \text{for all } v \in V_{H,0} \oplus \mathscr{B}_H, \\ u_H - \mathscr{I}_H(g) \in V_{H,0}. \end{cases} \tag{9.13}$$

Restricting the test function v to the bubble space $\mathscr{B}_H$, it follows that u_B is the unique solution in $\mathscr{B}_H$ to

$$\forall\, v \in \mathscr{B}_H, \quad a^\varepsilon(u_B, v) = F(v) - a^\varepsilon(u_H, v). \tag{9.14}$$

Equivalently, the bubble part u_B solves, on each $K \in \mathscr{T}_H$, the PDE

$$\mathscr{L}_K^\varepsilon u_B = -\mathscr{L}_K^\varepsilon u_H + f, \tag{9.15}$$

with homogeneous Dirichlet boundary conditions on ∂K. Here, $\mathscr{L}_K^\varepsilon$ denotes the restriction of the differential operator $\mathscr{L}^\varepsilon$ to K. The bubble function u_B is called 'residual-free' because (9.15) ensures that the RFB approximation satisfies $\mathscr{L}_K^\varepsilon(u_H + u_B) = f = \mathscr{L}_K^\varepsilon u^\varepsilon$ for each K, i.e., the local residue of the solution vanishes.

Although the bubble part u_B of the solution is defined in an infinite-dimensional space and depends on the coarse part u_H, the PDE (9.15) shows that u_B can actually be found in the finite-dimensional space

$$B_H^\varepsilon(f) = \bigoplus_{K \in \mathscr{T}_H} (\mathscr{L}_K^\varepsilon)^{-1} \left(\{ \mathscr{L}_K^\varepsilon v_H|_K \mid v_H \in V_H \} \right) \oplus \operatorname{span} \left\{ (\mathscr{L}_K^\varepsilon)^{-1}(f|_K) \right\} \tag{9.16}$$

where $(\mathscr{L}_K^\varepsilon)^{-1}$ is the inverse operator of $\mathscr{L}_K^\varepsilon$ on $H_0^1(K)$. For later reference, let us define, for all $K \in \mathscr{T}_H$, the spaces

$$B_K^\varepsilon(f) = \operatorname{span} \left\{ (\mathscr{L}_K^\varepsilon)^{-1}(f|_K) \right\}. \tag{9.17}$$

Since $u_H + u_B$ belongs to the RFB space $V_H \oplus B_H^\varepsilon(f)$, a Galerkin approximation of (9.13) on the RFB space has exactly the same solution as (9.13). In other words, the RFB method is equivalent to the following finite-dimensional problem: find $u_H + u_B \in V_H \oplus B_H^\varepsilon(f)$ such that

$$\begin{cases} a^\varepsilon(u_H + u_B, v_{H,B}) = F(v_{H,B}) & \text{for all } v_{H,B} \in V_{H,0} \oplus B_H^\varepsilon(f), \\ u_H - \mathscr{I}_H(g) \in V_{H,0}. \end{cases} \tag{9.18}$$

The RFB method is an interesting tool to inspire the design of a stable FEM in dimension 1 due to the following result.

Lemma 9.3. *In dimension 1, the residual-free bubble method, that is, the Galerkin approximation of (9.6) on the space $V_H \oplus B_H^\varepsilon(f)$, is exact. Consequently, since the bubble part of the solution vanishes at the nodes, the coarse part u_H is a nodally exact approximation of u^ε.*

This result is a consequence of the fact that the decomposition $H^1(\Omega) = V_H \oplus \mathscr{B}_H$ holds in dimension 1. Indeed, this is essential to ensure that the solution u^ε to (9.3) lies in the RFB space $V_H \oplus B_H^\varepsilon(f)$. In particular, the residual-free bubble method provides a stable finite-dimensional reformulation of (9.3) for any choice of boundary conditions and for any right-hand side in dimension 1. We discuss the stabilizing effect obtained by following the RFB methodology in Section 9.4.3.

Let us note that the exact computation of the bubble space $B_H^\varepsilon(f)$ is impossible except for simplified one-dimensional cases. Moreover, it depends on the right-hand side of the PDE, and can thus not be used directly as a numerical method for the approximation of (9.3). It was therefore suggested in [76, 38] to use an analytic approximation of the space $B_H^\varepsilon(f)$ to enrich the space V_H in practice, as is done e.g. in [41]. We will see in Chapter 10, however, that it is common to compute a numerical approximation of the RFB space during the so-called offline stage of modern methods for numerical homogenization (see Remark 10.6).

9.4.3. Deriving the SUPG method from the RFB method. We restrict the RFB method here to the single-scale PDE (9.8) with a constant advection field and a piecewise constant right-hand side f. Let us summarize the classical analysis of [38, 41]. The bubble space $B_H^\varepsilon(f)$ is now spanned by a single bubble per mesh element K, that we denote by b_K, and that is the unique solution in $H_0^1(K)$ to

$$-m\Delta b_K + b \cdot \nabla b_K = 1.$$

Then it is clear from (9.15) that the bubble part u_B equals, in terms of the coarse part of the solution $u_H \in V_H$,

$$u_B = \sum_{K \in \mathscr{T}_H} (f - b \cdot \nabla u_H)|_K \, b_K. \tag{9.19}$$

Here we use that u_H satisfies $\Delta u_H = 0$ in each mesh element K since it is a piecewise affine function, and that b and f are (piecewise) constant.

Inserting this expression for u_B in (9.18) and testing against $v_H \in V_H$, one finds a discrete problem for u_H on the space V_H. (This procedure is known as *static condensation* in the finite element literature.) Since b and f are (piecewise) constant, the scheme for u_H can be rewritten as

$$\begin{cases} a(u_H, v_H) + \displaystyle\sum_{K \in \mathscr{T}_H} \int_K \tau^B \, (b \cdot \nabla u_H)(b \cdot \nabla v_H) = F(v_H) + \\ \qquad\qquad \displaystyle\sum_{K \in \mathscr{T}_H} \int_K \tau^B \, f \, b \cdot \nabla v_H \quad \text{for all } v_H \in V_{H,0}, \\ \qquad u_H - \mathscr{I}_H(g) \in V_{H,0}. \end{cases} \tag{9.20}$$

where the stabilization parameter τ^B appears, which is given in each mesh element $K \in \mathscr{T}_H$ by

$$\tau^B\big|_K = \frac{1}{|K|}\int_K b_K. \tag{9.21}$$

We note that this is precisely the SUPG scheme, see (9.11) with $\rho = 0$, and we can expect stabilizing properties. The stabilizing effect of the RFB is directly linked to the bubble function b_K through the value of the stabilization parameter obtained from (9.21).

In the one-dimensional case, the parameter τ^B can easily be computed analytically and equals the unique value for which the SUPG method is known to provide a solution that is exact at the vertices of the mesh. It then corresponds to the Il'in-Allen-Southwell scheme [11]. The scheme was also derived in [51]. Note that nodal exactness can directly be inferred from Lemma 9.3 with the interpretation of the RFB method.

In dimension larger than 1, $V_H \oplus \mathscr{B}_H$ is no longer an exact decomposition of $H^1(\Omega)$, and no exactness results are known for either the SUPG or the RFB method. The parameter τ^B given by (9.21) is in fact too small to achieve full stabilization [41]. The stabilization parameter that is actually used with the SUPG method is a generalization to higher dimension of the formula of the ideal parameter for the one-dimensional setting (see [107]).

In Section 10.3, we propose an MsFEM enriched with bubbles. We will exploit a link with the RFB method to show exactness properties of the MsFEM approximation, and thus stability, in dimension 1. See Theorems 10.4 and 10.7. We will explain why such results cannot be expected to hold true for higher-dimensional problems. Then we consider in Chapter 11 an MsFEM based on unresolved scales that only vanish weakly (in the sense of the average) on the interfaces of the mesh. Equivalently, we will speak of 'weak bubbles'. The stabilizing effect of this framework is established in the numerical results of Chapter 12.

Chapter 10

Multiscale finite element methods for advection-diffusion problems

In this chapter and the following, we focus on the PDE (9.3) with a strongly heterogeneous diffusion coefficient as introduced in Section 9.2. We have seen in the Introduction that the $\mathbb{P}_1$ FEM is incapable of providing an approximation of u^ε on a coarse mesh, and in Chapter 9 that, moreover, spurious oscillations appear in the advection-dominated regime. We consider in this chapter and the next MsFEM type approaches (see Section 10.1) for problems with a multiscale diffusion coefficient and a possibly dominant advection field. For the convenience of the reader, we first recall the principle of the MsFEM that was also introduced in the Introduction.

10.1. The multiscale finite element method

The multiscale finite element method (MsFEM) seeks a Galerkin approximation of (9.3) on an approximation space that is adapted to the differential operator $\mathscr{L}^\varepsilon$. This idea was first introduced in [20]. One hopes (and this is indeed the case) that by 'correctly' encoding the multiscale features in the approximation space, an accurate finite element method is obtained even with a coarse mesh.

The original MsFEM proposed in [98] uses multiscale basis functions that locally, inside each mesh element $K \in \mathscr{T}_H$, resolve the oscillations of the leading order elliptic part of the differential operator and satisfy affine boundary conditions on ∂K. We shall refer to it here as the MsFEM-lin. More precisely, let $\phi_1^{\mathbb{P}_1}, \dots, \phi_N^{\mathbb{P}_1}$ denote the standard basis of V_H defined by $\phi_i^{\mathbb{P}_1}(x_j) = \delta_{i,j}$ for all vertices x_j of the mesh $\mathscr{T}_H$. Then define, for $1 \le i \le N$, the multiscale basis function $\phi_i^\varepsilon \in H^1(\Omega)$ by the boundary value problems

$$\forall\, K \in \mathscr{T}_H, \quad \begin{cases} -\mathrm{div}(A^\varepsilon \nabla \phi_i^\varepsilon) = 0 & \text{in } K, \\ \phi_i^\varepsilon = \phi_i^{\mathbb{P}_1} & \text{on } \partial K. \end{cases} \tag{10.1}$$

Note that ϕ_i^ε indeed belongs to $H^1(\Omega)$ because continuity is imposed on the interfaces of the mesh. Also note that ϕ_i^ε has the same support as the corresponding $\mathbb{P}_1$ basis function $\phi_i^{\mathbb{P}_1}$.

Now define the multiscale trial space $V_H^\varepsilon = \mathrm{span}\{\, \phi_i^\varepsilon \mid 1 \le i \le N\}$ and the multiscale

test space $V_{H,0}^\varepsilon = V_H^\varepsilon \cap H_0^1(\Omega)$, and introduce an interpolation operator $\mathscr{I}_H^\varepsilon : H^1(\Omega) \mapsto V_H^\varepsilon$ for the boundary condition in (9.3) as follows: we replace each basis function $\phi_i^{\mathbb{P}_1}$ in the definition of $\mathscr{I}_H$ (the interpolation operator to the space V_H) by ϕ_i^ε. Then the MsFEM-lin is defined as finding $u_H^\varepsilon \in V_H^\varepsilon$ such that

$$\begin{cases} a^\varepsilon(u_H^\varepsilon, v_H^\varepsilon) = F(v_H^\varepsilon) & \text{for all } v_H^\varepsilon \in V_{H,0}^\varepsilon, \\ u_H^\varepsilon - \mathscr{I}_H^\varepsilon(g) \in V_{H,0}^\varepsilon. \end{cases} \tag{10.2}$$

In order to put the MsFEM into practice, the multiscale basis functions ϕ_i^ε have to be computed numerically. This requires another discretization, for instance by a $\mathbb{P}_1$ Lagrange FEM on a fine mesh of K that resolves the microstructure. Note, however, that these problems are localized and might therefore be solved by modest computational resources even when a direct discretization of (9.3) cannot be solved numerically. Moreover, the problems (10.1) on all K and for all different i are independent and can thus be solved in parallel. These computations form the *offline stage*. The global problem (10.2) on the low-dimensional space $V_{H,0}^\varepsilon$ is solved in the *online stage*. The number of unknowns in the online stage is thus small. The online stage is repeated each time the right-hand side or the boundary conditions on $\partial\Omega$ change. Note that the matrix related to the linear system resulting from (10.2) can be computed once and for all after the computation of the multiscale basis functions in the offline stage.

One of the main drawbacks of the MsFEM-lin is the fact that *affine* boundary conditions are imposed in the local problems (10.1). The 'best' boundary conditions, namely those of u^ε, are of course unknown, and some choice of boundary conditions is required to localize the multiscale basis functions. The affine conditions in (10.1) suppress all oscillations near the boundary of the mesh elements.

The design of MsFEMs after its first introduction can be characterized as a search for improved boundary conditions for the multiscale basis functions. We mention here the Crouzeix-Raviart type boundary conditions (see [112]), to which we will come back in Chapter 11, and the oversampling technique, which places the (affine) boundary conditions of (10.1) on an extended domain larger than K. In the context of diffusion problems, it was proposed along with the MsFEM-lin in [98]. For the Crouzeix-Raviart type boundary conditions it is introduced in Chapter 5 of this thesis. Hierarchical enrichment of the multiscale space has been considered in [68, 97, 46, 117].

Remark 10.1. All oversampling strategies described in Chapter 5 and Section 8.1 have been investigated for the approximation of (9.3), but large numerical instabilities were observed in the advection-dominated regime. They are not further reported in this thesis.

In spite of the development of improved boundary conditions for the MsFEM, it is easy to understand that all these MsFEM variants cannot provide an accurate approximation of u^ε in the advection-dominated regime. Indeed, the MsFEM reduces to an (unstable) $\mathbb{P}_1$ finite element method in the particular case when A^ε is constant. The MsFEM-lin was stabilized by application of the SUPG method in [114]. Introducing a stabilization parameter τ, the stabilized formulation of (10.2), which we call the MsFEM-lin SUPG,

reads

$$\begin{cases} a^\varepsilon\left(u_H^{\varepsilon,\mathsf{SUPG}}, v_H^\varepsilon\right) + \sum_{K\in\mathscr{T}_H} \int_K \tau\left(b\cdot\nabla u_H^{\varepsilon,\mathsf{SUPG}}\right)(b\cdot\nabla v_H^\varepsilon) \\ \qquad\qquad = F(v_H^\varepsilon) + \sum_{K\in\mathscr{T}_H}\int_K f\,\tau\,(b\cdot\nabla v_H^\varepsilon) \quad \text{for all } v_H^\varepsilon \in V_{H,0}^\varepsilon, \\ u_H^{\varepsilon,\mathsf{SUPG}} - \mathscr{I}_H^\varepsilon(g) \in V_{H,0}^\varepsilon. \end{cases} \tag{10.3}$$

10.2. A residual-free bubble point of view

Another idea to build a stable MsFEM was also proposed in [114], replacing the definition of the multiscale basis functions in (10.1) by multiscale functions that also encode the advective effects. We are going to recover the same method here from a link with the RFB framework.

Remark 10.2. Let us remark that the adv-MsFEM-lin that we define in (10.6) below was actually found not to provide stability in dimension larger than 1 in [114]. We choose to recall the method here because our new stabilization method in Chapter 11 can be seen as a variation on this earlier idea. We also provide new insights into the adv-MsFEM-lin, explaining why stability is achieved in dimension 1 but not beyond.

Given a space of coarse scales V_H, the RFB method introduces a space of bubbles defined on each mesh element by $B_H^\varepsilon(f)$ in (9.16). In the spirit of the MsFEM, we can replace the space of coarse scales V_H by a space encoding some properties of the differential operator $\mathscr{L}^\varepsilon$. We propose here to choose a coarse space that reduces the size of the space $B_H^\varepsilon(f)$, hoping that in doing so, we transfer some stabilization properties of the RFB method (recall Lemma 9.3) to the coarse space. We explained in Section 9.1 that instabilities for advection-dominated problems are caused by boundary conditions that are incompatible with the flow problem, even when $f = 0$. Let us thus consider, at least as a first step, the space $B_H^\varepsilon(f = 0)$, for which we recall that

$$B_H^\varepsilon(f=0) = \bigoplus_{K\in\mathscr{T}_H} (\mathscr{L}_K^\varepsilon)^{-1}\left(\{\,\mathscr{L}_K^\varepsilon v_H|_K \mid v_H \in V_H\}\right).$$

This space *vanishes* if we choose the space of coarse scales such that $v_H \in V_H$ satisfies $\mathscr{L}_K^\varepsilon v_H = 0$ for all $K \in \mathscr{T}_H$. Therefore, we define the space

$$V_H^{\varepsilon,\mathsf{adv}} = \left\{ v_H^{\varepsilon,\mathsf{adv}} \in V_H \oplus \mathscr{B}_H \;\middle|\; a^\varepsilon\left(v_H^{\varepsilon,\mathsf{adv}}, v\right) = 0 \text{ for all } v \in \mathscr{B}_H \right\}. \tag{10.4}$$

We recall the definition of $\mathscr{B}_H$ in (9.12). Applying the RFB-method to the space $V_H^{\varepsilon,\mathsf{adv}}$, the space for the bubble part $B_H^\varepsilon(f = 0)$ is empty. We recall that, according to Lemma 9.3, the RFB method gives an exact characterizaton of u^ε in dimension 1. Now the coarse space $V_H^{\varepsilon,\mathsf{adv}}$ includes all properties needed to obtain the same result without an additional bubble space when $f = 0$. This is the content of Theorem 10.4 below.

We add both the superscripts ε and adv to the name of the space to emphasize that this multiscale space is adapted to both the heterogeneities of A^ε and to the advection field. The results of the following lemma are easy to show.

Lemma 10.3. *The space $V_H^{\varepsilon,\mathsf{adv}}$ has finite dimension $N = \dim(V_H)$, and a basis is given by the functions $\phi_i^{\varepsilon,\mathsf{adv}}$ solving, for $i = 1, \dots, N$,*

$$\forall\ K \in \mathscr{T}_H, \quad \begin{cases} -\mathrm{div}(A^\varepsilon \nabla \phi_i^{\varepsilon,\mathsf{adv}}) + b \cdot \nabla \phi_i^{\varepsilon,\mathsf{adv}} = 0, & \text{in } K, \\ \phi_i^{\varepsilon,\mathsf{adv}} = \phi_i^{\mathbb{P}_1}, & \text{on } \partial K. \end{cases} \tag{10.5}$$

As in (10.1), each basis function $\phi_i^{\varepsilon,\mathsf{adv}}$ is associated to the vertex x_i of the mesh. In view of the similarities between (10.5) and (10.1), we call the restriction of (9.6) to the finite-dimensional space $V_H^{\varepsilon,\mathsf{adv}}$ the adv-MsFEM-lin: find $u_H^{\varepsilon,\mathsf{adv}} \in V_H^{\varepsilon,\mathsf{adv}}$ such that

$$\begin{cases} a^\varepsilon\left(u_H^{\varepsilon,\mathsf{adv}}, v_H^{\varepsilon,\mathsf{adv}}\right) = F\left(v_H^{\varepsilon,\mathsf{adv}}\right), \quad \text{for all } v_H^{\varepsilon,\mathsf{adv}} \in V_{H,0}^{\varepsilon,\mathsf{adv}} \\ u_H^{\varepsilon,\mathsf{adv}} - \mathscr{I}_H^{\varepsilon,\mathsf{adv}}(g) \in V_{H,0}^{\varepsilon,\mathsf{adv}}. \end{cases} \tag{10.6}$$

The interpolation operator $\mathscr{I}_H^{\varepsilon,\mathsf{adv}} : H^1(\Omega) \to V_H^{\varepsilon,\mathsf{adv}}$ is defined by replacing each basis function $\phi_i^{\mathbb{P}_1}$ in the definition of $\mathscr{I}_H$ by $\phi_i^{\varepsilon,\mathsf{adv}}$.

We can show that the solution of the RFB method (9.18) coincides with the adv-MsFEM-lin approximation (10.6) when $f = 0$. This link between the adv-MsFEM and the RFB method yields exactness of the adv-MsFEM in 1D, as is stated in the following theorem. The interpretation of the MsFEM as an RFB method is essentially contained in (10.7) below, which is precisely the representation of the multiscale finite element space $V_H^{\varepsilon,\mathsf{adv}}$ used in the general framework of Chapter 5; see also (5.14).

Theorem 10.4. *When $f = 0$, the adv-MsFEM-lin approximation $u_H^{\varepsilon,\mathsf{adv}}$ equals the RFB solution defined in (9.18). In particular, in dimension 1 and when $f = 0$, the adv-MsFEM-lin is exact for any choice of boundary conditions.*

The above theorem implies that the adv-MsFEM-lin provides a stable approximation of (9.3) in dimension 1 when $f = 0$. Since the instability of a finite element method is in fact related to the boundary conditions rather than the right-hand side (as explained in Section 9.1), we expect this stability to be preserved for generic right-hand sides f. This is indeed the case, as we will see from numerical evidence in Section 10.3.

Proof of Theorem 10.4. The second assertion of the theorem follows from the first one due to Lemma 9.3. Let us show that $u_H^{\varepsilon,\mathsf{adv}}$ belongs to the space $V_H \oplus B_H^\varepsilon(f)$ and solves (9.18) for $f = 0$.

We start by showing that $V_H^{\varepsilon,\mathsf{adv}} \subset V_H \oplus B_H^\varepsilon(f = 0)$. Let us note that

$$V_H^{\varepsilon,\mathsf{adv}} = \left\{ v_H + \sum_{K \in \mathscr{T}_H} \sum_{\alpha=1}^{d} \partial_\alpha(v_H|_K) \chi_K^{\varepsilon,\mathsf{adv},\alpha} \,\middle|\, v_H \in V_H \right\}, \tag{10.7}$$

where, for each $K \in \mathscr{T}_H$ and $1 \le \alpha \le d$, the function $\chi_K^{\varepsilon,\mathsf{adv},\alpha} \in H_0^1(K)$ is defined by $\mathscr{L}_K^\varepsilon\left(\chi_K^{\varepsilon,\mathsf{adv},\alpha}\right) = -\mathscr{L}_K^\varepsilon(x^\alpha)$ and extended by 0 outside K, and x^α denotes the α-th coordinate function. This is the characterization (5.14) of the multiscale space given in the general MsFEM framework of Part I in the setting of the adv-MsFEM-lin.

For any $v_H \in V_H$, set $v_H^{\mathsf{osc}} = \sum_{K \in \mathscr{T}_H} \sum_{\alpha=1}^{d} \partial_\alpha(v_H|_K) \chi_K^{\varepsilon,\mathsf{adv},\alpha}$. Then, for each $K \in \mathscr{T}_H$, since

$\partial_\alpha v_H$ is constant on K, it holds

$$\begin{aligned}\mathscr{L}_K^\varepsilon(v_H^{\mathsf{osc}}) &= \sum_{\alpha=1}^d \partial_\alpha(v_H|_K)\mathscr{L}_K^\varepsilon\left(\chi_K^{\varepsilon,\mathsf{adv},\alpha}\right)\\ &= -\sum_{\alpha=1}^d \partial_\alpha(v_H|_K)\mathscr{L}_K^\varepsilon(x^\alpha)\\ &= -\mathscr{L}_K^\varepsilon\left(\sum_{\alpha=1}^d \partial_\alpha(v_H|_K)x^\alpha\right) = \mathscr{L}_K^\varepsilon(-v_H),\end{aligned}$$

where we use in the final equality that $\mathscr{L}_K^\varepsilon$ only acts on the gradient of its argument. According to (9.16), v_H^{osc} thus belongs to $B_H^\varepsilon(f=0)$, from which we conclude that $V_H^{\varepsilon,\mathsf{adv}} \subset V_H \oplus B_H^\varepsilon(f=0)$. Hence, $u_H^{\varepsilon,\mathsf{adv}}$ indeed belongs to the residual-free bubble space $V_H \oplus B_H^\varepsilon(f=0)$.

We next need to establish that $u_H^{\varepsilon,\mathsf{adv}}$ is a solution to (9.18). According to (10.7), there exists $u_H \in V_H$ (which is in fact unique) such that $u_H^{\varepsilon,\mathsf{adv}} = u_H + u_H^{\mathsf{osc}}$. By the construction of the interpolation operator $\mathscr{I}_H^{\varepsilon,\mathsf{adv}}$, and since $u_H^{\mathsf{osc}} \in B_H^\varepsilon(f=0)$ vanishes on all interfaces of the mesh, we deduce from (10.6) that u_H equals $\mathscr{I}_H(g)$ on $\partial\Omega$. Thus, $u_H - \mathscr{I}_H(g) \in V_{H,0}$.

Finally, let us compute $a^\varepsilon\left(u_H^{\varepsilon,\mathsf{adv}}, v_{H,B}\right)$ for an arbitrary test function $v_{H,B} = v_H + v_B$ belonging to the space $V_{H,0} \oplus B_H^\varepsilon(f=0)$. We may write $v_{H,B} = v_H + v_H^{\mathsf{osc}} + (v_B - v_H^{\mathsf{osc}})$. The function $v_H + v_H^{\mathsf{osc}}$ belongs to $V_H^{\varepsilon,\mathsf{adv}}$ by (10.7), so (10.6) yields

$$a^\varepsilon\left(u_H^{\varepsilon,\mathsf{adv}}, v_H + v_H^{\mathsf{osc}}\right) = F(v_H + v_H^{\mathsf{osc}}) = 0,$$

since $f=0$. We also note that v_B and v_H^{osc} both vanish on all interfaces of the mesh, i.e., $v_B - v_H^{\mathsf{osc}} \in \mathscr{B}_H$. Thus, we see from (10.4) that

$$a^\varepsilon\left(u_H^{\varepsilon,\mathsf{adv}}, v_B - v_H^{\mathsf{osc}}\right) = 0.$$

Combining the two preceding equalities gives

$$a^\varepsilon\left(u_H^{\varepsilon,\mathsf{adv}}, v_H + v_B\right) = 0.$$

This shows that $u_H^{\varepsilon,\mathsf{adv}}$ solves (9.18).

Since the solution to (9.18) is unique in the space $V_H \oplus B_H^\varepsilon(f=0)$, we have shown that $u_H^{\varepsilon,\mathsf{adv}}$ equals the RFB solution. ■

Remark 10.5. In practice, when the multiscale basis functions $\phi_i^{\varepsilon,\mathsf{adv}}$ are obtained from a numerical approximation of (10.5), the numerical approximation provided by the adv-MsFEM-lin cannot be equal to u^ε. Under the hypotheses of Theorem 10.4, if the $\phi_i^{\varepsilon,\mathsf{adv}}$ are computed by a $\mathbb{P}_1$ FEM on a fine mesh of each $K \in \mathscr{T}_H$, it can be shown that $u_H^{\varepsilon,\mathsf{adv}}$ is equal to the $\mathbb{P}_1$ approximation of (9.3) on the global fine mesh obtained from combining all fine meshes of the coarse mesh elements.

Remark 10.6. The above theorem provides us with the interpretation of the adv-MsFEM-lin as a particularly efficient implementation of the RFB space when $f = 0$. Rather than *enlarging* the $\mathbb{P}_1$ approximation space V_H by $B_H^\varepsilon(f = 0)$, the space V_H is *replaced* by the multiscale space $V_H^{\varepsilon,\mathsf{adv}}$ of the same dimension, and which produces the same solution as the RFB method. In particular, the (relevant) bubble functions of the space $B_H^\varepsilon(f = 0)$ are captured by the (numerical) computation of the basis functions $\phi_i^{\varepsilon,\mathsf{adv}}$ and do not need to be approximated analytically to capture their effect at the coarse scale.

In spite of the stability provided by Theorem 10.4 in dimension 1 when $f = 0$, there are two important drawbacks of the adv-MsFEM-lin as such. The first is related to the very shape of the multiscale basis functions themselves. This problem is addressed in Section 10.3. The second issue concerns the generalization to higher dimension that we discuss in Section 10.5, and for which we shall propose a different method in Chapter 11.

10.3. Enrichment by additional residual-free bubble functions

We provide a one-dimensional illustration of some MsFEMs in Figure 10.1 for the following choice of the coefficients in (9.3):

$$a^\varepsilon(x) = \alpha\left(2 + \cos\left(\frac{2\pi x}{\varepsilon}\right)\right), \tag{10.8}$$

where $\alpha = 2^{-7}$, $\varepsilon = 2^{-5}$, and we further set $b = 1$ and $f(x) = \sin^2(3\pi x)$. We used $H = 2^{-3}$ and all basis functions were computed by a $\mathbb{P}_1$ FEM on a fine mesh of size $h = 2^{-9}$.

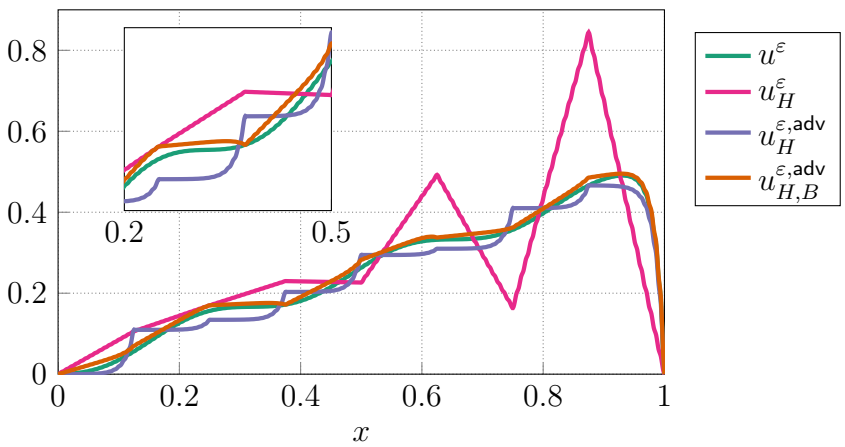

Figure 10.1: *Comparison of the exact solution u^ε of (9.3) and its approximation by the MsFEM-lin (u_H^ε defined by (10.2)), the adv-MsFEM-lin ($u_H^{\varepsilon,\mathsf{adv}}$ defined by (10.6)) and the adv-MsFEM-lin-B ($u_{H,B}^{\varepsilon,\mathsf{adv}}$ defined by (10.10)). The zoom clearly shows that the adv-MsFEM-lin basis functions are close to step functions.*

It is clear that the MsFEM-lin approximation u_H^ε is unstable. On the contrary, we can observe the stability of the adv-MsFEM-lin. Although the nodal exactness property of Theorem 10.4 is not observed here for the adv-MsFEM-lin (this is not a contradiction

with Theorem 10.4, because the right-hand side of the PDE does not vanish), the spurious oscillations of the unstable MsFEM-lin have vanished. We thus see numerically that the result of Theorem 10.4 is sufficient to ensure a stable approximation of (9.3) for generic right-hand sides.

One clear disadvantage of the adv-MsFEM-lin is also visible in Figure 10.1: the basis functions $\phi_i^{\varepsilon,\mathsf{adv}}$ are heavily deformed by the advection field. In combination with the boundary conditions imposed in the local problems (10.5), this results in basis functions having sharp boundary layers inside each coarse mesh element and being close to step functions. On the contrary, the exact solution varies smoothly and only shows a boundary layer near the outflow at $x = 1$. This prevents an accurate approximation of the exact solution u^ε of (9.3) by the adv-MsFEM-lin in spite of the stability of the method.

To design an improved MsFEM (at least for 1D problems), we return our attention to the RFB method, which gives an exact description of u^ε according to Lemma 9.3. Inserting the space V_H^ε in (9.16) for V_H, we see that the components of the RFB method that are missing in the adv-MsFEM-lin are contained in the space $\bigoplus_{K\in\mathscr{T}_H} B_K^\varepsilon(f)$, where we recall the definition of the spaces $B_K^\varepsilon(f)$ in (9.17). We propose to enrich the approximation space $V_H^{\varepsilon,\mathsf{adv}}$ by an approximate version of the spaces $B_K^\varepsilon(f)$, which cannot be used themselves in an FEM, because they depend on the right-hand side f.

We enrich the adv-MsFEM-lin space by the span of a single bubble function per mesh element that corresponds to $B_K^\varepsilon(f)$ if f is piecewise constant. For any $K \in \mathscr{T}_H$, we define the bubble function $B_K^{\varepsilon,\mathsf{adv}} \in H_0^1(K)$ as the unique solution to $\mathscr{L}_K^\varepsilon B_K^{\varepsilon,\mathsf{adv}} = 1$ in K, and extend it by 0 outside K. Equivalently, $B_K^{\varepsilon,\mathsf{adv}}$ is the unique solution in $\mathscr{B}_H$ to

$$a^\varepsilon\left(B_K^{\varepsilon,\mathsf{adv}}, v\right) = \int_K v \quad \text{for all } v \in \mathscr{B}_H. \tag{10.9}$$

We next define the spaces

$$V_{H,B}^{\varepsilon,\mathsf{adv}} = V_H^{\varepsilon,\mathsf{adv}} \bigoplus_{K\in\mathscr{T}_H} \operatorname{span}\left\{B_K^{\varepsilon,\mathsf{adv}}\right\}, \qquad V_{H,B,0}^{\varepsilon,\mathsf{adv}} = V_{H,0}^{\varepsilon,\mathsf{adv}} \bigoplus_{K\in\mathscr{T}_H} \operatorname{span}\left\{B_K^{\varepsilon,\mathsf{adv}}\right\},$$

and the adv-MsFEM-lin with bubbles, abbreviated adv-MsFEM-lin-B: find $u_{H,B}^{\varepsilon,\mathsf{adv}} \in V_{H,B}^{\varepsilon,\mathsf{adv}}$ such that

$$\begin{cases} a^\varepsilon\left(u_{H,B}^{\varepsilon,\mathsf{adv}}, v_{H,B}^{\varepsilon,\mathsf{adv}}\right) = F\left(v_{H,B}^{\varepsilon,\mathsf{adv}}\right) & \text{for all } v_{H,B}^{\varepsilon,\mathsf{adv}} \in V_{H,B,0}^{\varepsilon,\mathsf{adv}}, \\ u_{H,B}^{\varepsilon,\mathsf{adv}} - \mathscr{I}_H^{\varepsilon,\mathsf{adv}}(g) \in V_{H,B,0}^{\varepsilon,\mathsf{adv}}. \end{cases} \tag{10.10}$$

Here, the interpolation operator $\mathscr{I}_H^{\varepsilon,\mathsf{adv}}$ is the same as used in the adv-MsFEM-lin (10.6). The computation of the multiscale space $V_{H,B}^{\varepsilon,\mathsf{adv}}$ requires one additional computation per mesh element in the offline stage of the MsFEM with respect to the adv-MsFEM in order to compute the additional bubble functions $B_K^{\varepsilon,\mathsf{adv}}$.

We have the following property. The proof follows the same steps as the proof of Theorem 10.4 and is omitted here.

Theorem 10.7. *When f is piecewise constant, the adv-MsFEM-lin-B approximation $u_{H,B}^{\varepsilon,\mathsf{adv}}$ equals the RFB solution defined in (9.18). In particular, in dimension 1 and when f is piecewise constant, the adv-MsFEM-lin-B is exact for any choice of boundary conditions.*

This theorem shows an improved accuracy of the adv-MsFEM-lin-B with respect to the adv-MsFEM-lin for any piecewise constant f. The improved accuracy is observed numerically also when f is not piecewise constant. See Figures 10.1 and 10.2.

10.4. Numerical experiment in 1D

In this section we compare the numerical methods introduced above on a one-dimensional example. It is in this setting that Theorem 10.7 guarantees an exact approximation for piecewise constant f. The numerical results here go beyond that assumption. Although a one-dimensional setting may be an overly simplified situation, we will draw some conclusions that are important for the assessment of the more challenging two-dimensional situation of Chapter 12.

The test case in this section is based on the diffusion coefficient (10.8) with $b = 1$ and $\varepsilon = 2^{-8}$, and on the right-hand side $f(x) = \sin^2(3\pi x)$ on the domain $\Omega = (0, 1)$. We used $H = 2^{-6}$ as the mesh size for the MsFEM. For the fine mesh, on which the reference solution (denoted u_h^ε) and the multiscale basis functions are computed, we used $h = 2^{-5} \min\{\varepsilon, \alpha\}$, such that the fine mesh resolves the microstructure and the local Péclet number of the fine mesh satisfies $\mathsf{Pe}_h < 2^{-6}$ for all tests. For the MsFEM-lin SUPG, we used the stabilization parameter

$$\tau = \frac{H}{2|b|}\left(\coth \mathsf{Pe}_H - \frac{1}{\mathsf{Pe}_H}\right) \quad \text{with } \mathsf{Pe}_H = \frac{|b|H}{2\alpha},$$

which is the ideal value (9.21) for the $\mathbb{P}_1$ SUPG method in 1D for a constant diffusion coefficient equal to α.

In Figure 10.2, we aim to distinguish between unstable methods, which develop spurious oscillations propagating from the boundary layer at $x = 1$ for small values of α, and stable methods. Therefore, we measure the error outside the mesh element where the boundary layer lies, i.e., on $\Omega_{\mathsf{OBLE}} = (0, 1 - H)$ (OBLE for 'outside the boundary layer element'). The errors are normalized with respect to the norm of the reference solution u_h^ε on the same domain Ω_{OBLE}. We comment on this choice of error measure in Remark 12.1.

The results of Figure 10.2 confirm that the $\mathbb{P}_1$ method and the MsFEM-lin are not stable, since they suffer from spurious oscillations due to which the error explodes even when measured on Ω_{OBLE}. The $\mathbb{P}_1$ and $\mathbb{P}_1$ SUPG methods, as well as the MsFEM-lin and MsFEM-lin SUPG, yield identical results in the diffusion-dominated regime. This is natural because no stabilization is required in that regime, and in fact the stabilization parameter τ is negligible here. The point where stabilized and unstabilized methods start to differ can also be used as an indication of when the advection starts to dominate. We discuss this further in Section 12.1.3.

Among the stable methods, we find the $\mathbb{P}_1$ SUPG method, the MsFEM-lin SUPG, the adv-MsFEM-lin and the adv-MsFEM-lin-B. We note first that the adv-MsFEM-lin is not accurate in the advection-dominated regime, even though it does not suffer from spurious oscillations in Ω_{OBLE}. This was anticipated above as a result of the inappropriate shape of the basis functions $\phi_i^{\varepsilon,\mathsf{adv}}$ under the influence of a strong advection field (recall Figure 10.1). The error of the $\mathbb{P}_1$ (SUPG) FEM is larger than that of the multiscale methods by one order of magnitude in the diffusion-dominated regime, as can be expected from the fact that a^ε is highly oscillatory with 4 periods per coarse mesh element ($H = 4\varepsilon$).

On the other hand, we observe in the advection-dominated regime that the accuracy of

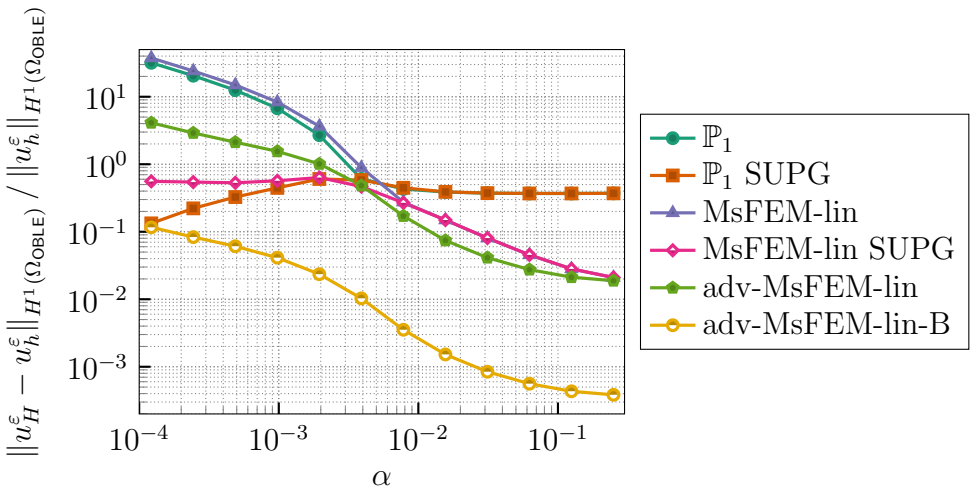

Figure 10.2: *Relative errors outside the boundary layer element between the reference solution u_h^ε and various numerical approximations u_H^ε, for the one-dimensional test case (10.8), for varying α, with $b = 1$, $\varepsilon = 2^{-8}$ and $H = 2^{-6}$. The $\mathbb{P}_1$ and $\mathbb{P}_1$ SUPG methods, as well as the MsFEM-lin and MsFEM-lin SUPG, yield identical results in the diffusion-dominated regime.*

the $\mathbb{P}_1$ SUPG method is comparable to the adv-MsFEM-lin-B, and that it even performs better than the MsFEM-lin SUPG. This confirms the earlier findings of [114], stating that the multiscale character of the diffusion is overshadowed by the advective effects when those dominate the diffusive effects. A more intuitive understanding of this phenomenon is provided by Figure 10.3, which shows the derivative of the reference solution u_h^ε and several numerical approximations on a coarse mesh. The two cases shown correspond to the values $\alpha = 2^{-9}$ and $\alpha = 2^{-13}$ in Figure 10.2.

It is clear from Figure 10.3 that the amplitude of the oscillations of $(u_h^\varepsilon)'$ decreases with decreasing α. However, the basis functions of the MsFEM SUPG are independent of the multiplicative factor α, which cancels in (10.1). Consequently, the oscillations of the basis functions of the MsFEM SUPG are too large when the advective term strongly dominates the diffusion. On the other hand, the $\mathbb{P}_1$ SUPG method encodes no fine-scale oscillations, which becomes a better approximation of the actual behaviour of u_h^ε in the H^1-norm when α decreases. The only method that captures the oscillations correctly throughout the entire regime of diffusion strengths is the adv-MsFEM-lin-B.

As a final observation for the 1D test case, we point out that the accuracy of the adv-MsFEM-lin-B decreases over almost three orders of magnitude when α decreases in the range studied here. Nevertheless, the method would be exact for all α if f were piecewise constant. The results of Figure 10.2 show that a perturbation of the piecewise constant situation has a relatively small impact on the accuracy of the adv-MsFEM-lin-B in the diffusion-dominated regime, but a much larger impact in the advection-dominated regime. The large increase in the error if we deviate from the piecewise constant situation when the advection is dominant shows that we cannot expect high accuracy in more challenging situations such as the advection-dominated regime in two-dimensional problems.

In Section 10.5, we explain why the above findings do not all generalize to higher dimension. We consider numerical experiments in 2D with a more suitable MsFEM variant in Chapter 12.

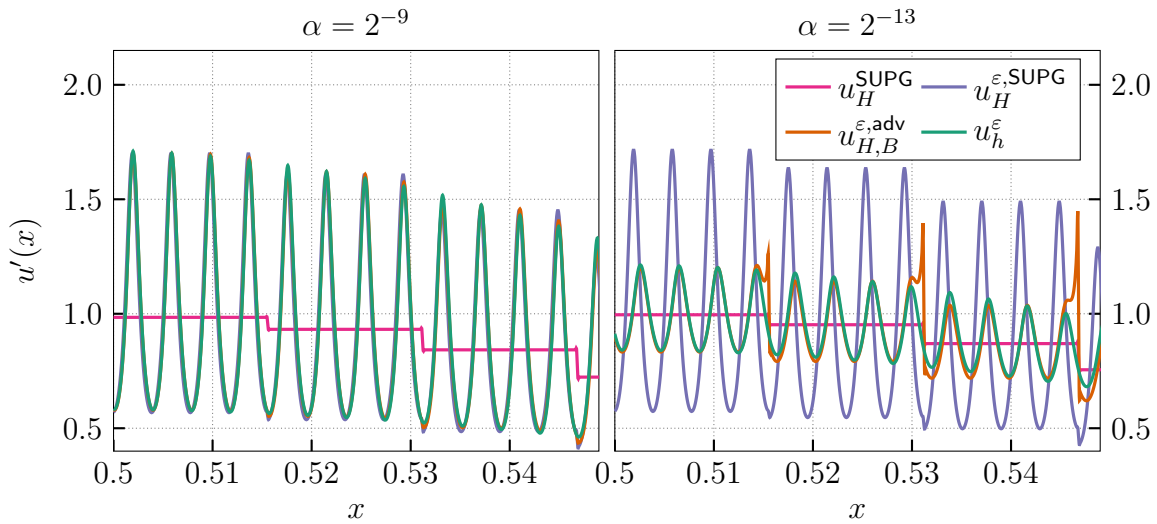

Figure 10.3: *Fine-scale oscillations of the derivative of the reference solution u_h^ε and three stable (Ms)FEM approximations, for two different values of the diffusion strength α. The $\mathbb{P}_1$ SUPG approximation is denoted by u_H^{SUPG}. For $\alpha = 2^{-9}$, the MsFEM SUPG approximation $u_H^{\varepsilon,\mathsf{SUPG}}$ and adv-MsFEM-lin-B approximation $u_{H,B}^{\varepsilon,\mathsf{adv}}$ visually coincide with u_h^ε on the scale of this plot. For $\alpha = 2^{-13}$, only $u_{H,B}^{\varepsilon,\mathsf{adv}}$ captures the oscillations of u_h^ε correctly (except close the boundary of mesh elements).*

Remark 10.8. The adv-MsFEM-lin-B can be enriched with more bubbles in order to extend the exactness results of Theorem 10.7 to more general right-hand sides f. For example, if f is any (piecewise) polynomial of degree p, the exact solution u^ε lies in an adv-MsFEM space enriched with $p+1$ suitable bubble functions per mesh element.

10.5. On the generalization to higher dimension

It was observed in numerical experiments in [114] that the adv-MsFEM-lin is not stable in dimension 2, unlike the one-dimensional setting in which we have Theorem 10.4 and for which our numerical results also confirm stability. Here we provide a previously unknown explanation for those observations.

The exactness results of Sections 10.2 and 10.3 cannot hold in dimension larger than 1, because they rely on the exactness of the RFB method, a property that is only true when $V_H \oplus \mathscr{B}_H$ (or $V_H^{\varepsilon,\mathsf{adv}} \oplus \mathscr{B}_H$) is an exact decomposition of $H_0^1(\Omega)$. Besides the fact that these theoretical results no longer hold, the loss of stability in higher dimension observed in practice can be understood as follows.

We first consider the adv-MsFEM-lin-B and draw some conclusions for the method without bubbles below. Let us rewrite the multiscale approximation $u_{H,B}^{\varepsilon,\mathsf{adv}}$ as a sum of coarse scale and multiscale parts. Following the characterization (10.7) of $V_H^{\varepsilon,\mathsf{adv}}$, we have

$$u_{H,B}^{\varepsilon,\mathsf{adv}} = u_H + \sum_{K\in\mathscr{T}_H} \sum_{\alpha=1}^{d} \partial_\alpha(u_H|_K)\chi_K^{\varepsilon,\mathsf{adv},\alpha} + \sum_{K\in\mathscr{T}_H} \beta_K\, B_K^{\varepsilon,\mathsf{adv}},$$

for some $u_H \in V_H$ and $\beta_K \in \mathbb{R}$. We recall that $B_K^{\varepsilon,\mathsf{adv}}$ is defined in (10.9). The coefficients β_K can be expressed in terms of u_H upon testing (10.10) against $B_K^{\varepsilon,\mathsf{adv}}$. Inserting

the expression in (10.10), and testing against $v_H^{\varepsilon,\mathsf{adv}} \in V_H^{\varepsilon,\mathsf{adv}}$ (that we also expand as in (10.7)), we obtain a numerical scheme for u_H. This scheme can be rewritten as a generalized form of (9.20) with $d+1$ different stabilization parameters per mesh element K: one for each function $\chi_K^{\varepsilon,\mathsf{adv},\alpha}$ and one related to $B_K^{\varepsilon,\mathsf{adv}}$.

The most insightful case is that of constant coefficients. It then holds that $\chi_K^{\varepsilon,\mathsf{adv},\alpha} = -b_\alpha B_K^{\varepsilon,\mathsf{adv}}$, where $b_\alpha = b \cdot e_\alpha$, and the effective scheme can be formulated in terms of a single stabilization parameter given by (9.21). (Note that $B_K^{\varepsilon,\mathsf{adv}}$ coincides with the bubble function b_K used in (9.21) in the case of constant coefficients.) We refer to [41] for the details of the derivation of the effective scheme. In fact, we know from Theorem 10.7 that the adv-MsFEM-B coincides with the RFB method for a piecewise constant right-hand side. Hence, the discussion of Section 9.4.3 applies, and the scheme for u_H takes exactly the form (9.20) with a single stabilization parameter taking the value (9.21). As we recalled in Section 9.4.3, this is the ideal parameter yielding nodal exactness of u_H in 1D, but in higher dimension this value is too small to achieve full stabilization and some spurious oscillations remain in u_H. The full multiscale solution $u_{H,B}^{\varepsilon,\mathsf{adv}}$ suffers from the same spurious oscillations as u_H, because all $\chi_K^{\varepsilon,\mathsf{adv},\alpha}$ and $B_K^{\varepsilon,\mathsf{adv}}$ vanish on the mesh element boundaries.

Let us now explain what the above observations imply for the adv-MsFEM-lin (without bubbles) that was previously found to be unstable in dimension 2, see [114]. An effective scheme for u_H can be obtained following again the steps of [41]. We obtain

$$\begin{cases} a(u_H, v_H) + \displaystyle\sum_{K\in\mathscr{T}_H} \int_K \tau^B\,(b\cdot\nabla u_H)(b\cdot\nabla v_H) = F(v_H) + \\ \qquad\qquad - \displaystyle\sum_{K\in\mathscr{T}_H} \int_K \tau^B\, f\, b\cdot\nabla v_H \quad \text{for all } v_H \in V_{H,0}, \\ \qquad\qquad u_H - \mathscr{I}_H(g) \in V_{H,0}, \end{cases}$$

which differs from the SUPG scheme (9.20) only by the minus sign in front of the sum on the second line. However, we have emphasized throughout that the stability or instability of the FEM is not related to the right-hand side (in particular because it persists in the case when $f = 0$), and thus the left-hand side of the above scheme is decisive for the stability of the FEM. Hence, the same conclusions as above with regard to the effectiveness of the stabilization parameter τ^B apply to the adv-MsFEM-lin: it encodes the perfect stabilization parameter in the one-dimensional situation, but does not achieve full stability beyond that setting. This can also be observed in Figure 12.2d when we consider numerical experiments in 2D.

Remark 10.9. An expansion of the type (10.7) also holds for the basis functions of the MsFEM-lin (see (10.1)) for a suitable counterpart of the functions $\chi_K^{\varepsilon,\mathsf{adv},\alpha}$. We refer to Part I for details, where these representations were used to design non-intrusive implementations of MsFEMs. (See also Section 11.4.) However, unlike the space $V_H^{\varepsilon,\mathsf{adv}}$, the multiscale space V_H^ε of the MsFEM-lin is not a subspace of the RFB space defined in (9.16) (except in the pure diffusion case). Therefore, no connection with classical stabilization methods can be made for the MsFEM-lin.

In a general way, we can summarize the above conclusions regarding the higher-dimensional setting as follows: the bubble space (9.12), with bubble functions that *vanish* on all interfaces of the mesh, is too small a choice for the unresolved scales to stabilize

a finite element method. In the next chapter we relax the condition on the interfaces of the mesh. We will consider an MsFEM based on unresolved scales that only vanish in a weak sense (on average on each face) on the coarse mesh element boundaries.

Chapter 11

An MsFEM with weak bubbles

In Chapter 10, we have given a new interpretation of the adv-MsFEM-lin with bubbles that allows to explain why the method is stable in dimension 1, but not in higher dimension. In the present chapter, we consider a variant of the MsFEM with Crouzeix-Raviart type boundary conditions, which we abbreviate as MsFEM-CR. This method was first introduced in [112] for pure diffusion problems. The multiscale basis functions introduced in that work reduce to the classical $\mathbb{P}_1$ Crouzeix-Raviart element when applied to constant diffusion, hence the name of the method. The MsFEM-CR was found to be particularly advantageous when enriched with bubble functions for the resolution of PDEs in perforated domains in [113]. The method has been adapted in the spirit of the adv-MsFEM-lin for the numerical approximation of advection-diffusion problems in [114], but without the bubble enrichment that we will propose below to obtain a sufficiently accurate MsFEM. The enrichment by bubble functions was used in [115, 57], again in the context of perforated domains. To the best of our knowledge, the insights into the stabilizing properties of the approximation space that we present in this thesis are new.

The MsFEM-CR relies on unresolved scales that only vanish weakly, i.e., on average, on the mesh element interfaces, in contrast to the space $\mathscr{B}_H$. More precisely, we define, for each $K \in \mathscr{T}_H$, the space

$$H_0^{1,w}(K) = \left\{ v \in H^1(K) \;\middle|\; \int_e v = 0 \;\text{ for all } e \in \mathscr{E}_H(K) \right\},$$

where $\mathscr{E}_H(K)$ denotes the set of faces of the mesh element K. We define the space of weak bubbles as

$$\mathscr{B}_H^w = \bigoplus_{K \in \mathscr{T}_H} H_0^{1,w}(K).$$

The weak bubbles are continuous across mesh elements in a weak sense, namely, in the sense that the average jump of the bubble functions over each interface vanishes. In particular, $\mathscr{B}_H^w$ is not a subspace of $H^1(\Omega)$. We thus extend our functional setting to the broken H^1 space with weak continuity conditions, that is,

$$H^{1,w}(\mathscr{T}_H) = \left\{ v \in L^2(\Omega) \;\middle|\; v|_K \in H^1(K) \text{ for all } K \in \mathscr{T}_H \text{ and } \int_e [\![v]\!] = 0 \text{ for all } e \in \mathscr{E}_H^{in} \right\},$$

where $\mathscr{E}_H^{in}$ is the set of all internal interfaces of the mesh $\mathscr{T}_H$ and $[\![v]\!]$ denotes the jump

of v over such an interface e. We also define $\mathscr{E}_H^\partial$ as those interfaces of the mesh that lie on $\partial\Omega$ and $\mathscr{E}_H = \mathscr{E}_H^{in} \cup \mathscr{E}_H^\partial$ as the set of all interfaces of $\mathscr{T}_H$. Equipped with the broken H^1 norm,

$$\|v\|_{H^1(\mathscr{T}_H)} = \left(\sum_{K \in \mathscr{T}_H} \|v\|^2_{H^1(K)} \right)^{1/2},$$

we endow $H^{1,w}(\mathscr{T}_H)$ with the structure of a Hilbert space. We also define the subspace of functions that vanish on average on the boundary faces of the mesh as

$$H_0^{1,w}(\mathscr{T}_H) = \left\{ v \in H^{1,w}(\mathscr{T}_H) \,\middle|\, \int_e v = 0 \text{ for all } e \in \mathscr{E}_H^\partial \right\}.$$

Note that the broken H^1 space can be written as the direct sum $H^{1,w}(\mathscr{T}_H) = V_H^w \oplus \mathscr{B}_H^w$, where V_H^w is the $\mathbb{P}_1$ Crouzeix-Raviart space defined as

$$V_H^w = \left\{ v \in \mathbb{P}_1(\mathscr{T}_H) \,\middle|\, \int_e [\![v]\!] = 0 \text{ for all } e \in \mathscr{E}_H^{in} \right\}.$$

Also note that the exact solution u^ε to (9.3) belongs to $H^{1,w}(\mathscr{T}_H)$ (because $H^1(\Omega) \subset H^{1,w}(\mathscr{T}_H)$). This is in sharp contrast to the bubble space used in Chapter 10, for which it holds in general that $u^\varepsilon \notin V_H \oplus \mathscr{B}_H$ when the ambient dimension is larger than 1.

11.1. The coarse scales

Generalizing (10.4) to the space of weak bubbles, we propose the multiscale approximation space

$$W_H^{\varepsilon,\mathsf{adv}} = \left\{ w_H^{\varepsilon,\mathsf{adv}} \in H^{1,w}(\mathscr{T}_H) \,\middle|\, a^\varepsilon\left(w_H^{\varepsilon,\mathsf{adv}}, w\right) = 0 \text{ for all } w \in \mathscr{B}_H^w \right\}.$$

We introduce one multiscale basis function for $W_H^{\varepsilon,\mathsf{adv}}$ associated to each interface $e \in \mathscr{E}_H$. The basis function $\phi_e^{\varepsilon,\mathsf{adv}}$ is defined by the variational problem

$$\forall\, K \in \mathscr{T}_H, \quad \begin{cases} a_K^\varepsilon\left(\phi_e^{\varepsilon,\mathsf{adv}}, v\right) = 0 & \text{for all } v \in H_0^{1,w}(K), \\ \dfrac{1}{|h|} \displaystyle\int_h \phi_e^{\varepsilon,\mathsf{adv}} = \delta_{e,h} & \text{for each } h \in \mathscr{E}_H(K). \end{cases} \tag{11.1}$$

Here, $\delta_{e,h}$ is the Kronecker delta and a_K^ε is the restriction of the bilinear form a^ε to $H^1(K) \times H^1(K)$. We do not know how to establish well-posedness of these problems because the bilinear form a_K^ε is not coercive on $H_0^{1,w}(K)$ in general. However, if the $\phi_e^{\varepsilon,\mathsf{adv}}$ are well-defined, it is easy to verify that they form a basis of $W_H^{\varepsilon,\mathsf{adv}}$ and one can show by standard analysis arguments that they satisfy the equivalent PDE

$$\begin{cases} -\operatorname{div}(A^\varepsilon \nabla \phi_e^{\varepsilon,\mathsf{adv}}) + b \cdot \nabla \phi_e^{\varepsilon,\mathsf{adv}} = 0 & \text{in } K, \\ \vec{n} \cdot A^\varepsilon \nabla \phi_e^{\varepsilon,\mathsf{adv}} = \lambda_h & \text{on each } h \in \mathscr{F}(K), \\ \dfrac{1}{h} \displaystyle\int_h \phi_e^{\varepsilon,\mathsf{adv}} = \delta_{e,h} & \text{for each } h \in \mathscr{F}(K), \end{cases} \tag{11.2}$$

where $\vec{n}$ is the outward unit normal vector on ∂K and λ_h is a constant that depends on h and that is uniquely determined by this problem. To circumvent the problem of

well-posedness, one can choose to work with a different bilinear form based on a skew-symmetric formulation of the advective term in (9.3). We provide some more details on this possibility in Remark 11.3. In practice, a discrete approximation of (11.2) can be solved. See Chapter 12 for details on our computational approach.

The adv-MsFEM-CR is now defined as follows: find $w_H^{\varepsilon,\mathsf{adv}} \in W_H^{\varepsilon,\mathsf{adv}}$ such that

$$\begin{cases} \displaystyle\sum_{K\in\mathscr{T}_H} a_K^\varepsilon\left(w_H^{\varepsilon,\mathsf{adv}}, v_H^{\varepsilon,\mathsf{adv}}\right) = F\left(v_H^{\varepsilon,\mathsf{adv}}\right) & \text{for all } v_H^{\varepsilon,\mathsf{adv}} \in W_{H,0}^{\varepsilon,\mathsf{adv}}, \\ \displaystyle\int_e w_H^{\varepsilon,\mathsf{adv}} = \int_e g & \text{for all } e \in \mathscr{E}_H^\partial, \end{cases} \tag{11.3}$$

where the multiscale test space $W_{H,0}^{\varepsilon,\mathsf{adv}}$ is defined as $W_{H,0}^{\varepsilon,\mathsf{adv}} = W_H^{\varepsilon,\mathsf{adv}} \cap H_0^{1,w}(\mathscr{T}_H)$.

Remark 11.1. The original MsFEM-CR is obtained upon setting $b = 0$ in the definition of the space $W_H^{\varepsilon,\mathsf{adv}}$.

Let us stress that the approximation space $W_H^{\varepsilon,\mathsf{adv}}$ is not a subspace of $H^1(\Omega)$ and thus that the adv-MsFEM-CR (11.3) is a non-conforming approximation of (9.6). Moreover, an interpolation operator in the spirit of $\mathscr{I}_H$ (see (9.7)) based on nodal values cannot be defined on $W_H^{\varepsilon,\mathsf{adv}}$ due to discontinuities on $\partial\Omega$. Therefore, the boundary condition in (11.3) is imposed in a weak sense, like the continuity condition of the space $H^{1,w}(\mathscr{T}_H)$. Here we deviate from the definition of the MsFEM-CR in [112, 113]. Our choice of boundary conditions was also employed in [57, 123, 105].

In dimension 1, the adv-MsFEM-lin and the adv-MsFEM-CR basis functions coincide. It thus follows from our study in dimension 1 (see Section 10.3 and Figure 10.1) that the basis functions are substantially deformed under the influence of the advection field when it is dominant. This carries over to the two-dimensional case (both for the adv-MsFEM-lin and the adv-MsFEM-CR) as is illustrated for the adv-MsFEM-CR in Figure 11.1. The multiscale space $W_H^{\varepsilon,\mathsf{adv}}$ is thus unable to provide a sufficiently accurate solution. Hence, we follow the development of Section 10.3, and enrich the multiscale space $W_H^{\varepsilon,\mathsf{adv}}$ with additional bubble functions from the space of unresolved scales $\mathscr{B}_H^w$.

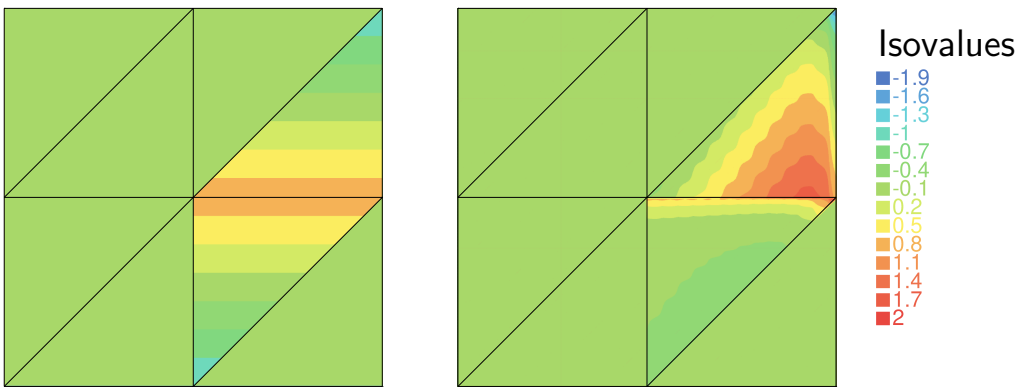

Figure 11.1: *Comparison of a $\mathbb{P}_1$ CR basis function (left) and an adv-MsFEM-CR basis function (right) in the presence of a strong advection field.*

11.2. Additional bubbles for the adv-MsFEM-CR

The adaptation of the bubble functions $B_K^{\varepsilon,\mathsf{adv}} \in \mathscr{B}_H$ (see (10.9)) to the space of weak bubbles $\mathscr{B}_H^w$ takes the following form. We define for each $K \in \mathscr{T}_H$ the weak bubble function $B_K^{\varepsilon,\mathsf{adv},w}$ as the unique solution in $\mathscr{B}_H^w$ to

$$a_K^\varepsilon\Big(B_K^{\varepsilon,\mathsf{adv},w}, v\Big) = \int_K v \quad \text{for all } v \in H_0^{1,w}(K). \tag{11.4}$$

Note that $B_K^{\varepsilon,\mathsf{adv},w}$ vanishes outside K, and that $B_K^{\varepsilon,\mathsf{adv},w}$ solves $\mathscr{L}_K^\varepsilon B_K^{\varepsilon,\mathsf{adv},w} = 1$ in K.

Then we define the augmented multiscale spaces

$$W_{H,B}^{\varepsilon,\mathsf{adv}} = W_H^{\varepsilon,\mathsf{adv}} \bigoplus_{K\in\mathscr{T}_H} \operatorname{span}\Big\{B_K^{\varepsilon,\mathsf{adv},w}\Big\}, \quad W_{H,B,0}^{\varepsilon,\mathsf{adv}} = W_{H,0}^{\varepsilon,\mathsf{adv}} \bigoplus_{K\in\mathscr{T}_H} \operatorname{span}\Big\{B_K^{\varepsilon,\mathsf{adv},w}\Big\},$$

and the adv-MsFEM-CR with (weak) bubbles, abbreviated as adv-MsFEM-CR-B, as: find $w_{H,B}^{\varepsilon,\mathsf{adv}} \in W_{H,B}^{\varepsilon,\mathsf{adv}}$ such that

$$\begin{cases} \displaystyle\sum_{K\in\mathscr{T}_H} a_K^\varepsilon\Big(w_{H,B}^{\varepsilon,\mathsf{adv}}, v_{H,B}^{\varepsilon,\mathsf{adv}}\Big) = F\Big(v_{H,B}^{\varepsilon,\mathsf{adv}}\Big) & \text{for all } v_{H,B}^{\varepsilon,\mathsf{adv}} \in W_{H,B,0}^{\varepsilon,\mathsf{adv}}, \\ \displaystyle\int_e w_{H,B}^{\varepsilon,\mathsf{adv}} = \int_e g & \text{for all } e \in \mathscr{E}_H^\partial. \end{cases} \tag{11.5}$$

This MsFEM with weak bubbles satisfies a result analogous to Theorem 10.7 for a generalization of the continuous problem (9.3) on the space with weak continuity. Let us introduce these notions now. On the space $H^{1,w}(\mathscr{T}_H)$ we consider the following problem for ν_H^ε:

$$\begin{cases} \displaystyle\sum_{K\in\mathscr{T}_H} a_K^\varepsilon(\nu_H^\varepsilon, v) = F(v) & \text{for all } v \in H_0^{1,w}(\mathscr{T}_H), \\ \displaystyle\int_e \nu_H^\varepsilon = \int_e g & \text{for all } e \in \mathscr{E}_H^\partial. \end{cases} \tag{11.6}$$

With respect to (9.6), the interelement continuity is relaxed. Jumps are allowed as long as the weak continuity condition of the space $H^{1,w}(\mathscr{T}_H)$ is satisfied. Again, we cannot show well-posedness of (11.6) unless we change the bilinear form. Supposing that a unique solution exists, we have the following result. Contrary to Theorems 10.4 and 10.7 concerning the adv-MsFEM-lin, it holds true in any dimension.

Theorem 11.2. *Suppose that f is piecewise constant and that the problems (11.1), (11.4), (11.5) and (11.6) all have a unique solution. Then the adv-MsFEM-CR-B provides the exact solution to (11.6), that is, $w_{H,B}^{\varepsilon,\mathsf{adv}} = \nu_H^\varepsilon$.*

Proof. We show that ν_H^ε belongs to the finite-dimensional space $W_{H,B}^{\varepsilon,\mathsf{adv}}$. The function $\varphi = \nu_H^\varepsilon - \sum_{K\in\mathscr{T}_H} f|_K\, B_K^{\varepsilon,\mathsf{adv},w}$ satisfies

$$\forall\, K \in \mathscr{T}_H,\ \forall\, w \in \mathscr{B}_K^w, \qquad a_K^\varepsilon(\varphi, w) = a_K^\varepsilon(\nu_H^\varepsilon, w) - f|_K\, a_K^\varepsilon\Big(B_K^{\varepsilon,\mathsf{adv},w}, w\Big)$$

$$= \int_K f\, w - f|_K \int_K w$$
$$= 0,$$

using (11.6) and (11.4) in the second equality and the fact that f is piecewise constant in the third equality. Thus, $\varphi \in W_H^{\varepsilon,\mathsf{adv}}$ and this concludes the proof by the classical Céa Lemma. ■

In order to assess the quality of $w_{H,B}^{\varepsilon,\mathsf{adv}}$ as an approximation of u^ε, solution to (9.3), the question is of course to what extent ν_H^ε and u^ε are close. To the best of our knowledge this is an open question, and this could be an interesting research direction to further understand the stabilizing properties of the adv-MsFEM-CR. Our numerical results in Chapter 12 show that $w_{H,B}^{\varepsilon,\mathsf{adv}}$ is indeed a stable approximation of u^ε in the advection-dominated regime.

Remark 11.3 (Alternative variational formulation)**.** We noted above that the bilinear form a_K^ε is not coercive on the space $H_0^{1,w}(K)$, so the standard Lax-Milgram theory cannot be applied to show well-posedness of the definition (11.1) of the adv-MsFEM-CR basis functions. A skew-symmetrized version of the advective term is frequently used in the literature, see e.g. [108]. It is defined, for any $u, v \in H^1(K)$, as

$$a_K^{\varepsilon,\mathsf{SS}}(u,v) = \int_K \nabla v \cdot A^\varepsilon \nabla u + \frac{1}{2} v\, b \cdot \nabla u - \frac{1}{2} u\, b \cdot \nabla v - \frac{1}{2} u\, v \operatorname{div}(b),$$

where the last term vanishes under the assumption (9.5). One can show that $a_K^{\varepsilon,\mathsf{SS}}$ is coercive on $H_0^1(K)$ as long as $\operatorname{div}(b) \leq 0$.
It is easily seen that for any $u, v \in H_0^1(\Omega)$, we have $\sum_{K \in \mathscr{T}_H} a_K^{\varepsilon,\mathsf{SS}}(u,v) = a^\varepsilon(u,v)$, by integration by parts. We could thus replace a^ε by $a^{\varepsilon,\mathsf{SS}}$ throughout without modifying the original solution of the problem (9.3). The adv-MsFEM-lin and adv-MsFEM-CR spaces do change. We did not adopt the bilinear form $a_K^{\varepsilon,\mathsf{SS}}$ in this thesis, because our numerical experiments show that the versions of the adv-MsFEM with this bilinear form are less accurate than those with the form a_K^ε. It is not clear why. We would like to point out, however, that Theorem 11.2 (and Corollary 11.5 below) remain true when a_K^ε is replaced by $a_K^{\varepsilon,\mathsf{SS}}$, and well-posedness of (11.1), (11.4), (11.5) and (11.6) is guaranteed in this case.

Remark 11.4. Whether (11.5) can be used to stabilize (9.6) may also be studied in the constant coefficient case. Then (11.5) corresponds to a $\mathbb{P}_1$ Crouzeix-Raviart method with bubble functions. For the adv-MsFEM-lin, studies of the RFB method for constant coefficient problems have led to multiple insights even for the multiscale case in Chapter 10. We are not aware of similar studies for the $\mathbb{P}_1$ Crouzeix-Raviart FEM. For alternative stabilization approaches designed specifically for the $\mathbb{P}_1$ Crouzeix-Raviart FEM we refer to [108, 110, 64] and the references therein.

11.3. A closer look at the bubbles

We now investigate the role of the bubble functions in the linear system resulting from the two adv-MsFEM variants with bubbles (10.10) and (11.5). The notation of the adv-

MsFEM-CR-B is employed, but the analysis directly carries over to the adv-MsFEM-lin-B.

We use the basis $\left\{\phi_e^{\varepsilon,\mathsf{adv}}\right\}_{e\in\mathscr{E}_H^{in}}$ for $W_{H,0}^{\varepsilon,\mathsf{adv}}$ and $\left\{B_K^{\varepsilon,\mathsf{adv},w}\right\}_{K\in\mathscr{T}_H}$ for the bubble space. The matrix of the linear system corresponding to (11.5) then is

$$\mathbb{A}^{\varepsilon,\mathsf{adv}} = \left(\begin{array}{c|c} \mathbb{A}^{W,W} & \mathbb{A}^{W,B} \\ \hline \mathbb{A}^{B,W} & \mathbb{A}^{B,B} \end{array}\right), \tag{11.7}$$

where

$$\begin{aligned} \mathbb{A}_{h,e}^{W,W} &= \sum_{T\in\mathscr{T}_H} a_T^\varepsilon\left(\phi_e^{\varepsilon,\mathsf{adv}}, \phi_h^{\varepsilon,\mathsf{adv}}\right) && \text{for all } e,h\in\mathscr{E}_H^{in}, \\ \mathbb{A}_{K',K}^{B,B} &= \sum_{T\in\mathscr{T}_H} a_T^\varepsilon\left(B_K^{\varepsilon,\mathsf{adv},w}, B_{K'}^{\varepsilon,\mathsf{adv},w}\right) && \text{for all } K,K'\in\mathscr{T}_H, \\ \mathbb{A}_{h,K}^{W,B} &= \sum_{T\in\mathscr{T}_H} a_T^\varepsilon\left(B_K^{\varepsilon,\mathsf{adv},w}, \phi_h^{\varepsilon,\mathsf{adv}}\right) && \text{for all } K\in\mathscr{T}_H,\ h\in\mathscr{E}_H^{in}, \\ \mathbb{A}_{K',e}^{B,W} &= \sum_{T\in\mathscr{T}_H} a_T^\varepsilon\left(\phi_e^{\varepsilon,\mathsf{adv}}, B_{K'}^{\varepsilon,\mathsf{adv},w}\right) = 0 && \text{for all } e\in\mathscr{E}_H^{in},\ K'\in\mathscr{T}_H. \end{aligned} \tag{11.8}$$

The lower left block vanishes because $\phi_e^{\varepsilon,\mathsf{adv}}$ solves (11.1) and $B_{K'}^{\varepsilon,\mathsf{adv},w}\in H_0^{1,w}(K')$. Moreover, the right lower block $\mathbb{A}^{B,B}$ is diagonal because all bubble functions have disjoint supports. Its diagonal entries are

$$\mathbb{A}_{K,K}^{B,B} = a_K^\varepsilon\left(B_K^{\varepsilon,\mathsf{adv},w}, B_K^{\varepsilon,\mathsf{adv},w}\right) = \int_K B_K^{\varepsilon,\mathsf{adv},w},$$

where we used (11.4). (Note that we could show positivity of this quantity if a_K^ε were coercive on $H_0^{1,w}(K)$.) The bubble part $w_B^{\varepsilon,\mathsf{adv}}\in B_H^{\varepsilon,\mathsf{adv},w}$ of the adv-MsFEM-CR-B approximation $w_{H,B}^{\varepsilon,\mathsf{adv}}$ can thus be explicitly computed and equals

$$w_B^{\varepsilon,\mathsf{adv}} = \sum_{K\in\mathscr{T}_H} \frac{\displaystyle\int_K f B_K^{\varepsilon,\mathsf{adv},w}}{\displaystyle\int_K B_K^{\varepsilon,\mathsf{adv},w}} B_K^{\varepsilon,\mathsf{adv},w}, \tag{11.9}$$

which reduces to

$$w_B^{\varepsilon,\mathsf{adv}} = \sum_{K\in\mathscr{T}_H} f|_K B_K^{\varepsilon,\mathsf{adv},w} \tag{11.10}$$

if f is piecewise constant.

With an explicit expression for $w_B^{\varepsilon,\mathsf{adv}}$ at hand, we obtain a scheme for the coarse scale part $w_W^{\varepsilon,\mathsf{adv}} = w_{H,B}^{\varepsilon,\mathsf{adv}} - w_B^{\varepsilon,\mathsf{adv}}$ of $w_{H,B}^{\varepsilon,\mathsf{adv}}$ (as pointed out above, this is generally known as static condensation in the FEM literature). The addition of bubble functions therefore does not increase the size of the linear system that has to be solved in order to compute $w_{H,B}^{\varepsilon,\mathsf{adv}}$ from (11.5) (with respect to the size of the linear system associated to (11.3)).

In the particular case that f is piecewise constant, upon inserting (11.10), the scheme

for $w_W^{\varepsilon,\mathsf{adv}}$ writes

$$\begin{cases} \displaystyle\sum_{K\in\mathscr{T}_H} a_K^\varepsilon\left(w_W^{\varepsilon,\mathsf{adv}}, v_H^{\varepsilon,\mathsf{adv}}\right) = F\left(v_H^{\varepsilon,\mathsf{adv}}\right) - \\ \qquad\qquad \displaystyle\sum_{K\in\mathscr{T}_H}\left(\frac{1}{|K|}\int_K f\right) a_K^\varepsilon\left(B_K^{\varepsilon,\mathsf{adv},w}, v_H^{\varepsilon,\mathsf{adv}}\right) & \text{for all } v_H^{\varepsilon,\mathsf{adv}} \in W_{H,0}^{\varepsilon,\mathsf{adv}}, \\ \qquad\qquad \displaystyle\int_e w_W^{\varepsilon,\mathsf{adv}} = \int_e g & \text{for all } e \in \mathscr{E}_H^\partial. \end{cases} \tag{11.11a}$$

In fact, one can also compute $w_W^{\varepsilon,\mathsf{adv}}$ from (11.11a) when f is not piecewise constant. This results in a new numerical method that no longer coincides with the adv-MsFEM-CR-B in general.

More precisely, we formulate the adv-MsFEM-CR-β as follows:

$$\text{Set } w_{H,\beta}^{\varepsilon,\mathsf{adv}} = w_W^{\varepsilon,\mathsf{adv}} + \sum_{K\in\mathscr{T}_H}\left(\frac{1}{|K|}\int_K f\right) B_K^{\varepsilon,\mathsf{adv},w}, \quad \text{where } w_W^{\varepsilon,\mathsf{adv}} \text{ solves (11.11a).} \tag{11.11b}$$

Directly computing the coefficients of the bubble functions according to either (11.9) or (11.10) is advantageous because it reduces the number of unknowns in $w_{H,B}^{\varepsilon,\mathsf{adv}}$ and thus results in a smaller linear system to be solved. An additional advantage of the adv-MsFEM-CR-β is that the computation of these coefficients does not require any integrations at the microscale. The implications for the implementation of the adv-MsFEM-CR-β are further considered in Section 11.4. The accuracy of the adv-MsFEM-B and the adv-MsFEM-CR-β is compared in Chapter 12.

In the special case $f = 0$, it is clear from (11.10) that $w_B^{\varepsilon,\mathsf{adv}} = 0$. Consequently, the adv-MsFEM-CR and the adv-MsFEM-CR-B coincide. We thus obtain the following property as a corollary to Theorem 11.2.

Corollary 11.5. *Suppose that $f = 0$ and that (11.5) and (11.6) both have a unique solution. Then the adv-MsFEM-CR (11.3) provides the exact solution to (11.6), that is, $w_H^{\varepsilon,\mathsf{adv}} = \nu_H^\varepsilon$.*

Besides the fact that (11.10) allows one to compute the coefficients of the bubble function, it also explains why it is important to add bubble functions to the multiscale approximation space when advective effects are dominant. Consider Equation (9.3) for a decreasing magnitude of the diffusion tensor A^ε. The solution u^ε then stays of the same order of magnitude. Since the coefficients in front of the bubble functions in (11.10) are independent of A^ε, the relative importance of the bubble functions in the numerical approximation is directly determined by the size of the bubble functions. In dimension 1, and for piecewise constant coefficients, the bubble functions are easily computed explicitly. (The problem defining the bubble functions is a rescaled version of (9.1).) They become larger when the diffusion parameter m decreases. This is illustrated in Figure 11.2. At the same time, the boundary layers of the multiscale functions (in both the spaces $V_H^{\varepsilon,\mathsf{adv}}$ and $W_H^{\varepsilon,\mathsf{adv}}$) inside each coarse mesh element become more pronounced, and the bubble functions compensate these boundary layers. In higher dimension, an explicit computation is not obvious, but numerical computations of the bubble functions confirm that the bubble functions become larger when the diffusion coefficient decreases. See Figure 11.3.

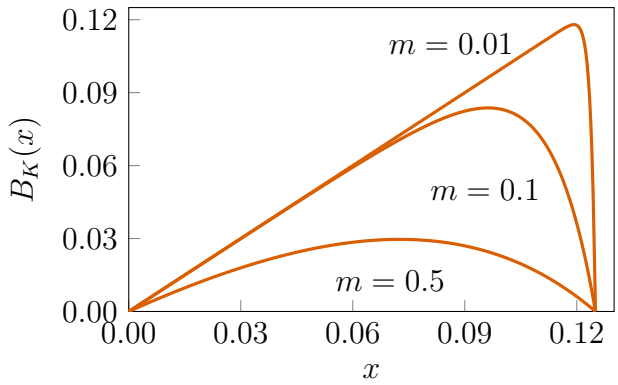

Figure 11.2: *Bubble functions B_K on the one-dimensional domain $(0, 0.125)$ solving $-mB_K'' + B_K' = 1$ as m varies.*

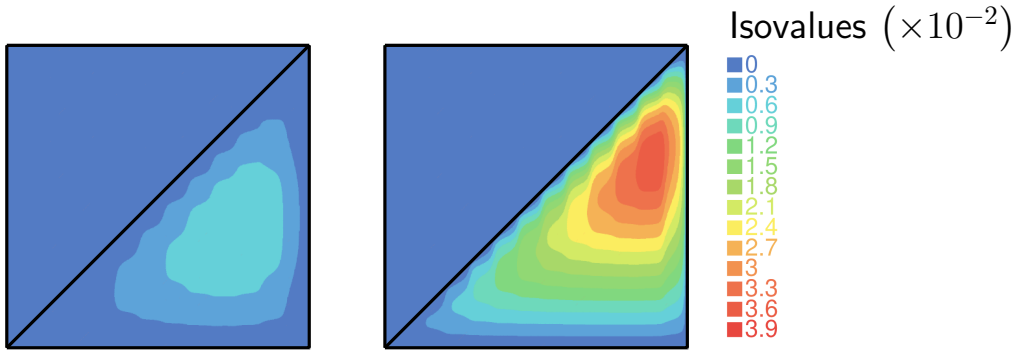

Figure 11.3: *Bubble functions for the adv-MsFEM-lin-B with $|b| = 1$ and $H = 2^{-4}$. Left: A^ε oscillates around the value 2^{-6}. Right: A^ε oscillates around the value 2^{-9}.*

11.4. Non-intrusive implementation

We focus in this section on the implementation of adv-MsFEM variants with bubbles. The central part of the implementation of the MsFEM is the construction and resolution of the linear system associated to (11.5). We write

$$w_{H,B}^{\varepsilon,\mathsf{adv}} - \sum_{e\in\mathscr{E}_H^\partial} \left(\frac{1}{|e|}\int_e g\right)\phi_e^{\varepsilon,\mathsf{adv}} = \sum_{e\in\mathscr{E}_H^{in}} \mathscr{W}_e^{\varepsilon,\mathsf{adv}}\phi_e^{\varepsilon,\mathsf{adv}} + \sum_{K\in\mathscr{T}_H} \mathscr{W}_K^{\varepsilon,\mathsf{adv}} B_K^{\varepsilon,\mathsf{adv},w} \in H_0^{1,w}(\mathscr{T}_H),$$

for some coefficients $\left(\mathscr{W}_e^{\varepsilon,\mathsf{adv}}\right)_{e\in\mathscr{E}_H^{in}}$ and $\left(\mathscr{W}_K^{\varepsilon,\mathsf{adv}}\right)_{K\in\mathscr{T}_H}$. Then the MsFEM approximation $w_{H,B}^{\varepsilon,\mathsf{adv}}$ is found upon computing $\mathscr{W}^{\varepsilon,\mathsf{adv}} = (\mathscr{W}_e^{\varepsilon,\mathsf{adv}}, \mathscr{W}_K^{\varepsilon,\mathsf{adv}})$, solution to the linear system

$$\mathbb{A}^{\varepsilon,\mathsf{adv}}\,\mathscr{W}^{\varepsilon,\mathsf{adv}} = \mathbb{F}^{\varepsilon,\mathsf{adv}},$$

where $\mathbb{A}^{\varepsilon,\mathsf{adv}}$ is defined in (11.7) and the vector $\mathbb{F}^{\varepsilon,\mathsf{adv}}$, indexed by the internal edges of $\mathscr{T}_H$ and the mesh elements as in Section 11.3, is defined as

$$\begin{aligned}
\mathbb{F}_h^{\varepsilon,\mathsf{adv}} &= F\left(\phi_h^{\varepsilon,\mathsf{adv}}\right) \qquad \text{for all } h \in \mathscr{E}_H^{in},\\
\mathbb{F}_K^{\varepsilon,\mathsf{adv}} &= F\left(B_K^{\varepsilon,\mathsf{adv},w}\right) \qquad \text{for all } K \in \mathscr{T}_H.
\end{aligned}$$

Note that, for the sake of clarity, we discuss adv-MsFEM-CR variants explicitly in this section, but that all applies to the corresponding adv-MsFEM-lin variants as well.

An efficient construction of this linear system requires a laborious development process, as was discussed in Section 4.3. There it was also explained that it is not straightforward to adapt an existing finite element code, processing generic *polynomial* basis functions, to perform the numerical integrations involved in computing $\mathbb{A}^{\varepsilon,\mathsf{adv}}$ and $\mathbb{F}^{\varepsilon,\mathsf{adv}}$, which are defined in terms of the *multiscale* basis functions. An alternative MsFEM and implementation strategy were proposed to render the MsFEM less intrusive. It leads to the formulation of a standard FEM approximation of an effective PDE.

We next apply the methodology for a non-intrusive implementation of MsFEMs presented in Part I to the adv-MsFEM. We extend the methods of Part I with a non-intrusive approach for the multiscale bubble functions in the discrete formulation. Let us note that our non-intrusive formulation for MsFEMs with bubbles uses a right-hand side in $H^{-1}(\mathscr{T}_H)$, even if the right-hand side f of (9.3) belongs to $L^2(\Omega)$. The standard finite element code must be able to handle such terms. This is an additional requirement for the software used that was not present in the non-intrusive MsFEMs of Chapter 6.

11.4.1. The adv-MsFEM without bubbles. One non-intrusive MsFEM approach proposed in Chapter 6 (see Remark 11.9 for another possibility) is the following Petrov-Galerkin (PG) MsFEM: find $w_H^{\varepsilon,\mathsf{adv},\mathsf{PG}} \in W_H^{\varepsilon,\mathsf{adv}}$ such that

$$\begin{cases} \displaystyle\sum_{K\in\mathscr{T}_H} a_K^\varepsilon\Big(w_H^{\varepsilon,\mathsf{adv},\mathsf{PG}}, \phi_e^{\mathbb{P}_1}\Big) = \int_\Omega f\,\phi_e^{\mathbb{P}_1} & \text{for all } e\in\mathscr{E}_H^{in}, \\ \displaystyle\int_e w_H^{\varepsilon,\mathsf{adv},\mathsf{PG}} = \int_e g & \text{for all } e\in\mathscr{E}_H^{\partial}, \end{cases} \tag{11.12}$$

where *piecewise affine* test functions are used in the discrete problem. The test functions $\phi_e^{\mathbb{P}_1} \in V_H^w$ (we recall that this is the $\mathbb{P}_1$ Crouzeix-Raviart space) are piecewise affine functions defined by the property $\displaystyle\frac{1}{h}\int_h \phi_e^{\varepsilon,\mathsf{adv}} = \delta_{e,h}$ for each $h\in\mathscr{F}(K)$.

Due to the following result, the adv-MsFEM-CR (11.3) and the PG adv-MsFEM-CR coincide when $f=0$. In particular, Corollary 11.5 (concerning the adv-MsFEM without bubbles) also holds true for the Petrov-Galerkin formulation.

Theorem 11.6. *For any $h\in\mathscr{E}_H$, let $\phi_h\in H^{1,w}(\mathscr{T}_H)$ be any function such that $\displaystyle\int_e \phi_h = \int_e \phi_h^{\varepsilon,\mathsf{adv}}$ for all $e\in\mathscr{E}_H^{in}$. Consider the case $f=0$. Then the adv-MsFEM-CR (11.3) coincides with the adv-MsFEM-CR with test functions $(\phi_h)_{h\in\mathscr{E}_H^{in}}$.*

Proof. Since $f=0$, the proof amounts to showing that the matrix $\mathbb{A}^{W,W}$ defined in (11.8) coincides with the matrix $\mathbb{A}^{W,\phi}$ obtained upon replacing each test function $\phi_h^{\varepsilon,\mathsf{adv}}$ by ϕ_h, i.e., $\mathbb{A}_{h,e}^{W,\phi} = \displaystyle\sum_{K\in\mathscr{T}_H} a_K^\varepsilon\big(\phi_e^{\varepsilon,\mathsf{adv}},\phi_h\big)$. From (11.1), it readily follows that, for all $e,h\in\mathscr{E}_H^{in}$,

$$\mathbb{A}_{h,e}^{W,W} - \mathbb{A}_{h,e}^{W,\phi} = \sum_{K\in\mathscr{T}_H} a_K^\varepsilon\Big(\phi_e^{\varepsilon,\mathsf{adv}}, \phi_h^{\varepsilon,\mathsf{adv}} - \phi_h\Big) = 0.$$

Note that the function $\phi_h^{\varepsilon,\mathsf{adv}} - \phi_h$ can indeed be used as a test function in (11.1), because $\int_e \phi_h = \int_e \phi_h^{\varepsilon,\mathsf{adv}}$ for all $e \in \mathscr{E}_H^{in}$. ■

Remark 11.7. If, with the notation of Theorem 11.6, we choose the test functions ϕ_h as local solutions to the adjoint problem to (11.1), i.e.,

$$\forall\, K \in \mathscr{T}_H, \quad \begin{cases} a_K^\varepsilon(v, \phi_h) = 0, & \text{for all } v \in H_0^{1,w}(K), \\ \dfrac{1}{|e|}\displaystyle\int_e \phi_h = \delta_{h,e} & \text{for each } e \in \mathscr{E}_H(K), \end{cases}$$

it can be shown that the resulting finite element method is the same as the scheme for the coarse part of the adv-MsFEM-CR-B when f is piecewise constant (see (11.11a)). The idea that a Petrov-Galerkin method can provide stability is classical in the one-dimensional case. We refer e.g. to [131, pp. 82-84] and the references therein.
Even when f is not piecewise constant, one can show that the adv-MsFEM-CR with test functions solving the adjoint equation provides an approximation $w_H^{\varepsilon,\mathsf{adv}\star}$ satisfying $\int_e w_H^{\varepsilon,\mathsf{adv}\star} = \int_e \nu_H^\varepsilon$ (ν_H^ε was defined in (11.6)) for all $e \in \mathscr{E}_H$.

Let us now recall the non-intrusive MsFEM approach for solving (11.12). It is based on the expansion of the multiscale basis functions in terms of $\mathbb{P}_1$ Crouzeix-Raviart basis functions $\phi_e^{\mathbb{P}_1} \in V_H^w$ as

$$\phi_e^{\varepsilon,\mathsf{adv}} = \phi_e^{\mathbb{P}_1} + \sum_{K\in\mathscr{T}_H} \sum_{\alpha=1}^{d} \partial_\alpha\big(\phi_e^{\mathbb{P}_1}\big|_K\big)\chi_K^{\varepsilon,\mathsf{adv},\alpha}. \tag{11.13}$$

The so-called *numerical correctors* $\chi_K^{\varepsilon,\mathsf{adv},\alpha} \in H_0^{1,w}(K)$ ($\alpha = 1,\dots,d$) are defined by the problem $a^\varepsilon\Big(\chi_K^{\varepsilon,\mathsf{adv},\alpha} + x^\alpha, v\Big) = 0$ for all $v \in H_0^{1,w}(K)$. The terminology of numerical correctors stems from the close resemblance of (11.13) to the first-order expansion of u^ε in homogenization theory, for which corrector functions resolving the microstructure are introduced. A similar expansion was given for the adv-MsFEM-lin basis functions $\phi_i^{\varepsilon,\mathsf{adv}}$ in (10.7) (with suitably defined numerical correctors). Note that each numerical corrector depends only on the mesh element K to which it is associated and the local values of the coefficients of the PDE inside this mesh element.

The numerical correctors are used to define a piecewise constant diffusion matrix $\overline{A}$ and advection field $\overline{b}$ as follows:

$$\forall\, K \in \mathscr{T}_H, \quad \begin{aligned} \overline{A}_{\beta,\alpha} &= \frac{1}{|K|} a^\varepsilon\Big(x^\alpha + \chi_K^{\varepsilon,\mathsf{adv},\alpha}, x^\beta\Big), \quad 1 \le \alpha,\beta \le d, \\ \overline{b}_\alpha &= \frac{1}{|K|} a^\varepsilon\Big(x^\alpha + \chi_K^{\varepsilon,\mathsf{adv},\alpha}, 1\Big), \qquad 1 \le \alpha \le d. \end{aligned} \tag{11.14}$$

With these effective coefficients, we define the effective bilinear form

$$\overline{a}_K(u,v) = \int_K \nabla v \cdot \overline{A}\nabla u + v\,\overline{b}\cdot\nabla u \quad \text{for all } u,v \in H^1(K). \tag{11.15}$$

Denoting $\mathbb{A}^{W,\mathbb{P}_1}$ the matrix of the linear system associated to the PG method (11.12), we

have the identities, for all interfaces $e, h \in \mathscr{E}_H^{in}$,

$$\mathbb{A}_{h,e}^{W,\mathbb{P}_1} = \sum_{K\in\mathscr{T}_H} a_K^\varepsilon\big(\phi_e^{\varepsilon,\mathsf{adv}}, \phi_h^{\mathbb{P}_1}\big) = \sum_{K\in\mathscr{T}_H} \overline{a}_K\big(\phi_e^{\mathbb{P}_1}, \phi_h^{\mathbb{P}_1}\big). \tag{11.16}$$

These identities are purely algebraic and rely on the fact that $\nabla\phi_e^{\mathbb{P}_1}$ is constant on each mesh element and for each e. On the right, we recognize the expression for the linear system associated to a standard $\mathbb{P}_1$ Crouzeix-Raviart FEM that solves the following problem: find $\overline{w}_H^{\varepsilon,\mathsf{adv}} \in V_H^w$ such that

$$\begin{cases} \displaystyle\sum_{K\in\mathscr{T}_H} \overline{a}_K\Big(\overline{w}_H^{\varepsilon,\mathsf{adv}}, v_H\Big) = F(v_H) & \text{for all } v_H \in V_{H,0}^w, \\ \displaystyle\int_e \overline{w}_H^{\varepsilon,\mathsf{adv}} = \int_e g & \text{for all } e \in \mathscr{E}_H^\partial. \end{cases} \tag{11.17}$$

Once the effective coefficients in (11.14) have been computed, the problem (11.17) can be solved by a standard Crouzeix-Raviart finite element solver.

Since the right-hand sides of the discrete problems (11.12) and (11.17) are identical, and because of (11.16), the linear systems related to both problems are the same. We can thus compute the solution to (11.12) by solving (11.17) and expanding the solution of the linear system along the basis $\phi_e^{\varepsilon,\mathsf{adv}}$ rather than $\phi_e^{\mathbb{P}_1}$. This is equivalent to setting

$$w_H^{\varepsilon,\mathsf{adv,ni}} = \overline{w}_H^{\varepsilon,\mathsf{adv}} + \sum_{K\in\mathscr{T}_H}\sum_{\alpha=1}^d \partial_\alpha\Big(\overline{w}_H^{\varepsilon,\mathsf{adv}}\Big|_K\Big)\chi_K^{\varepsilon,\mathsf{adv},\alpha}, \text{ where } \overline{w}_H^{\varepsilon,\mathsf{adv}} \text{solves (11.17).} \tag{11.18}$$

This is called a non-intrusive implementation because only finite element problems based on standard $\mathbb{P}_1$ elements have to be solved.

Remark 11.8. The (Galerkin) adv-MsFEM-CR (11.3) and the PG variant (11.12) only differ in the right-hand side of the discrete formulation (as is shown by Theorem 11.6). The error analysis of Chapter 7 shows that, for pure diffusion problems, the difference between the two methods converges to 0 at the same rate as the mesh size H. Numerical examples showed that both MsFEM variants have the same accuracy (in both the case of the adv-MsFEM-CR and the adv-MsFEM-lin). Our numerical experiments (see Figure 12.7) investigate this question for advection-diffusion problems.

Remark 11.9. Another non-intrusive MsFEM approach was proposed in Part I, which corresponds to taking multiscale test functions on the left-hand side and $\mathbb{P}_1$ test functions on the right-hand side in (11.12). Although it was shown in Lemma 6.4 that this variant coincides with (11.12), this is no longer the case when we add bubble functions to the approximation space. (See also Remark 11.10.) Since our numerical tests indicate that this 'intermediate' approach in between (11.3) and (11.12) is, when enriched with bubble functions, less accurate than the Galerkin and Petrov-Galerkin variants defined above, we do not further detail it here.

11.4.2. Extension to MsFEMs with bubbles. We now turn our attention to a non-intrusive implementation of the adv-MsFEM-CR with bubbles. We can consider either the adv-MsFEM-CR-B (11.5) or the adv-MsFEM-CR-β (11.11b). For both methods, the coefficients for the bubble part can be computed element per element independently of

the degrees of freedom in the space $W_H^{\varepsilon,\mathsf{adv}}$, either according to (11.9) or as the average of the right-hand side f in (11.11b). For a non-intrusive implementation of the MsFEM, one must avoid integrals over the products of f and highly oscillatory functions, since the numerical quadrature in a standard finite element simulator on the coarse mesh $\mathscr{T}_H$ is not adapted to the approximation of such integrals. Such integrals appear in (11.9) but not in (11.11b).

For these reasons, we explicitly study the implementation of a PG variant of the adv-MsFEM-CR-β here. More precisely, we set

$$w_{H,\beta}^{\varepsilon,\mathsf{adv},\mathsf{PG}} = w_W^{\varepsilon,\mathsf{adv},\mathsf{PG}} + \sum_{K\in\mathscr{T}_H} \left(\frac{1}{|K|}\int_K f\right) B_K^{\varepsilon,\mathsf{adv},w}, \tag{11.19a}$$

where $w_W^{\varepsilon,\mathsf{adv},\mathsf{PG}} \in W_H^{\varepsilon,\mathsf{adv}}$ solves

$$\begin{cases} \displaystyle\sum_{K\in\mathscr{T}_H} a_K^\varepsilon\Big(w_W^{\varepsilon,\mathsf{adv},\mathsf{PG}}, v_H\Big) = F(v_H) \\ \qquad\qquad \displaystyle - \sum_{K\in\mathscr{T}_H} \left(\frac{1}{|K|}\int_K f\right) a_K^\varepsilon\Big(B_K^{\varepsilon,\mathsf{adv},w}, v_H\Big) & \text{for all } v_H \in V_{H,0}^w, \\ \displaystyle\int_e w_W^{\varepsilon,\mathsf{adv},\mathsf{PG}} = \int_e g & \text{for all } e \in \mathscr{E}_H^\partial. \end{cases} \tag{11.19b}$$

The discrete problem (11.19b) is obtained from (11.11a) upon replacing all test functions by their piecewise affine counterpart.

The matrix of the system (11.19b) is exactly the matrix $\mathbb{A}^{W,\mathbb{P}_1}$ from (11.16). It can thus be constructed in a non-intrusive fashion following (11.14) to (11.17). It remains to find a formulation of the right-hand side in terms of a $\mathbb{P}_1$ scheme on the coarse mesh that does not require any integrations on the microscale.

Fix any $\mathbb{P}_1$ Crouzeix-Raviart function $v_H \in V_H^w$. Note that any such function satisfies, in all $K \in \mathscr{T}_H$,

$$v_H|_K(x) = v_H(x_{c,K}) + \sum_{\alpha=1}^d \partial_\alpha(v_H|_K)\,\left(x^\alpha - x_{c,K}^\alpha\right) \quad \text{in } K,$$

because it is piecewise affine. Here $x_{c,K} = (x_{c,K}^1, \dots, x_{c,K}^d)$ denotes the centroid of K. Upon inserting this expression in the multiscale terms on the right-hand side of (11.19b), we obtain, for all $K \in \mathscr{T}_H$,

$$a_K^\varepsilon\Big(B_K^{\varepsilon,\mathsf{adv},w}, v_H\Big) = v_H(x_{c,K})\, a_K^\varepsilon\Big(B_K^{\varepsilon,\mathsf{adv},w}, 1\Big) + \sum_{\alpha=1}^d \partial_\alpha(v_H|_K)\, a_K^\varepsilon\Big(B_K^{\varepsilon,\mathsf{adv},w}, x^\alpha - x_{c,K}^\alpha\Big).$$

We propose to compute in the offline stage of the MsFEM the quantities $\mathscr{R}_0, \mathscr{R}_1, \dots, \mathscr{R}_d$ defined as

$$\begin{aligned} \mathscr{R}_0|_K &= \frac{1}{|K|}\, a_K^\varepsilon\Big(B_K^{\varepsilon,\mathsf{adv},w}, 1\Big), \\ \mathscr{R}_\alpha|_K &= \frac{1}{|K|}\, a_K^\varepsilon\Big(B_K^{\varepsilon,\mathsf{adv},w}, x^\alpha - x_{c,K}^\alpha\Big), \quad \alpha = 1, \dots, d. \end{aligned}$$

Then it holds

$$\sum_{K\in\mathscr{T}_H} \beta_K\, a_K^\varepsilon\Big(B_K^{\varepsilon,\mathsf{adv},w}, v_H\Big) = \sum_{K\in\mathscr{T}_H} \beta_K |K| \left(\mathscr{R}_0\, v_H(x_{c,K}) + \sum_{\alpha=1}^d \mathscr{R}_\alpha\, \partial_\alpha(v_H|_K)\right),$$

where $\beta_K = \left(\frac{1}{|K|}\int_K f\right)$. This can finally be rewritten as

$$\sum_{K\in\mathscr{T}_H} \beta_K\, a_K^\varepsilon\Big(B_K^{\varepsilon,\mathsf{adv},w}, v_H\Big) = \sum_{K\in\mathscr{T}_H} \beta_K \int_K \mathscr{R}_0\, v_H + \mathscr{R}\cdot\nabla v_H, \tag{11.20}$$

where we introduce the notation $\mathscr{R} = (\mathscr{R}_1,\dots,\mathscr{R}_d)$. Assuming a standard finite element solver has a routine to compute the averages of the function f, these terms can be computed once the quantities $\mathscr{R}_0,\dots,\mathscr{R}_d$ have been precomputed in the offline stage.

A non-intrusive formulation of the PG adv-MsFEM-CR-β can now be formulated as follows:

$$\begin{aligned}\text{Set } w_{H,\beta}^{\varepsilon,\mathsf{adv},\mathsf{PG}} = \overline{w}_H^{\varepsilon,\mathsf{adv},\mathsf{PG}} + \sum_{K\in\mathscr{T}_H}\sum_{\alpha=1}^d \partial_\alpha\Big(\overline{w}_H^{\varepsilon,\mathsf{adv},\mathsf{PG}}\Big|_K\Big)\chi_K^{\varepsilon,\mathsf{adv},\alpha} + \\ \sum_{K\in\mathscr{T}_H}\left(\frac{1}{|K|}\int_K f\right) B_K^{\varepsilon,\mathsf{adv},w},\end{aligned} \tag{11.21a}$$

where $\overline{w}_H^{\varepsilon,\mathsf{adv},\mathsf{PG}} \in V_H^w$ solves

$$\begin{cases} \displaystyle\sum_{K\in\mathscr{T}_H} \overline{a}_K\Big(\overline{w}_H^{\varepsilon,\mathsf{adv},\mathsf{PG}}, v_H\Big) = \int_\Omega f v_H + \\ \qquad\qquad \displaystyle\sum_{K\in\mathscr{T}_H} \beta_K \int_K \mathscr{R}_0\, v_H + \mathscr{R}\cdot\nabla v_H \quad \text{for all } v_H \in V_{H,0}^w, \\ \displaystyle\int_e \overline{w}_H^{\varepsilon,\mathsf{adv}} = \int_e g \qquad\qquad \text{for all } e \in \mathscr{E}_H^\partial. \end{cases} \tag{11.21b}$$

The latter problem no longer contains oscillatory coefficients and can be solved by a standard $\mathbb{P}_1$ Crouzeix-Raviart finite element solver.

Remark 11.10. For the Galerkin formulation (11.11) of the adv-MsFEM-CR-β, we obtain a similar non-intrusive formulation of the type (11.20) when the $\mathbb{P}_1$ function v_H is replaced by a multiscale function v_H^ε, upon replacing $\mathscr{R}_1,\dots,\mathscr{R}_d$ by

$$\mathscr{R}_\alpha^{\mathsf{G}}\big|_K = \mathscr{R}_\alpha|_K + \frac{1}{|K|}\, a_K^\varepsilon\Big(B_K^{\varepsilon,\mathsf{adv},w}, \chi_K^{\varepsilon,\mathsf{adv},\alpha}\Big), \quad \alpha = 1,\dots,d.$$

A non-intrusive implementation of (11.11a) requires replacing $F(v_H^\varepsilon)$ by $F(v_H)$. The resulting method is not equivalent to (11.11b) and was found in our experiments to produce less accurate results than both the Galerkin and the Petrov-Galerkin variant of the adv-MsFEM-CR-β. It is therefore not further reported here.

Chapter 12

Numerical results

We present in this chapter a comparison of various MsFEM and stabilization approaches presented in Chapters 10 and 11 on two representative test cases for (9.3) in dimension $d = 2$, on the domain $\Omega = (0,1)^2$.

12.1. First test case

Our first test case is

$$A^\varepsilon(x,y) = \mu^\varepsilon(x,y)\,\mathrm{Id}, \quad \mu^\varepsilon(x,y) = \alpha\left(1 + \frac{3}{4}\cos(2\pi x/\varepsilon)\sin(2\pi y/\varepsilon)\right), \tag{12.1a}$$

$$b(x,y) = \begin{pmatrix} 1+y \\ 2-x \end{pmatrix} / \sqrt{5 + 2y - 4x + y^2 + x^2}, \tag{12.1b}$$

$$f(x,y) = 2 + \sin(2\pi x) + x\cos(2\pi y), \tag{12.1c}$$

and $g = 0$, for varying values of α determining the relative importance of the advective and diffusive effects. The results are qualitatively the same for a similar test case with a constant advection field and constant right-hand side. Note that the advection field defined by (12.1b) is normalized and divergence-free and thus satisfies the assumptions set in Chapter 9. It is drawn in Figure 12.1, along with the reference solution for $\varepsilon = \alpha = 2^{-7}$, computed by a $\mathbb{P}_1$ Lagrange FEM on a mesh of size $h = 2^{-11}$. The boundary layer at the outflow can clearly be observed along the top and right sides of Ω.

For the MSFEM-lin SUPG (10.3), we need to define the stabilization parameter τ, that we take constant on each mesh element $K \in \mathscr{T}_H$. Following [107], we set

$$\tau = \frac{\mathrm{diam}(K;b)}{2|b|}\left(\coth \mathsf{Pe}_K - \frac{1}{\mathsf{Pe}_K}\right) \quad \text{in } K, \tag{12.2}$$

where $\mathrm{diam}(K;b)$ is the diameter of K in the direction of b and the element Péclet number Pe_K is defined as $\mathsf{Pe}_K = \dfrac{|b|\,\mathrm{diam}(K;b)}{2\alpha}$. In all these definitions, b is evaluated at the centroid of K. In the one-dimensional case with piecewise constant coefficients, this choice of τ corresponds to the optimal value yielding a nodally exact solution, which was also characterized as (9.21) in the context of the RFB method. Note that it is not obvious to propose the correct value of the diffusion field in the definition of Pe_K in the highly

oscillatory case, because one has to choose which value of the diffusion coefficient is used in the definition of Pe_K. Our choice here corresponds to the average of the maximum and minimum values of μ^ε in (12.1a) and is found to yield satisfactory results.

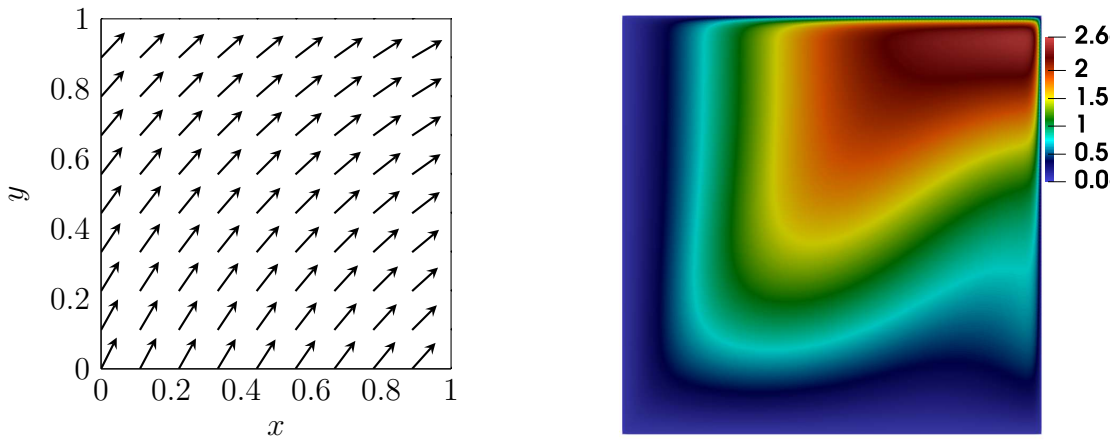

(a) (b)

Figure 12.1: *Test case* (12.1). *Left: the advection field* (12.1b). *Right: reference solution for* $\varepsilon = \alpha = 2^{-7}$.

12.1.1. Stability. We first assess the stability of some MsFEM approaches in Figure 12.2. The figure shows the $\mathbb{P}_1$ part of the MsFEM approximation for some parameter values in the advection-dominated regime. It is defined as follows: the numerical approximation is written as a sum of a piecewise affine function and numerical correctors (or bubble functions) as in (11.13), and the $\mathbb{P}_1$ part of the MsFEM approximation is the first mentioned piecewise affine function. This part of the solution is sufficient to investigate stability, since the numerical correctors vanish in all the vertices for the MsFEM-lin variants, and vanish on average on all edges for the MsFEM-CR variants. Therefore, they do not change the global behaviour of the numerical approximation.

Spurious oscillations that propagate far from the boundary layer are clearly visible for the (unstabilized) MsFEM-lin and MsFEM-CR. These spurious oscillations are removed from the MsFEM-lin when we add the SUPG stabilization that was proposed in [114]. On the other hand, the adv-MsFEM-lin approach reduces the spurious oscillations but is not able to suppress them completely. The effective stabilization captured by the adv-MsFEM-lin basis functions is too small, as was explained in Section 10.5. For the adv-MsFEM-CR, we see that no instabilities propagate outside the boundary layer. Stabilizing effects are better extracted from the numerical correctors in the space of weak bubbles $H_0^{1,w}(K)$ than in the traditional bubble space $H_0^1(K)$.

Let us also note that none of the MsFEM approximations in Figure 12.2 use the enrichment of the MsFEM space by additional bubble functions. Indeed, the bubble functions are introduced to maintain a good accuracy in the advection-dominated regime, when the multiscale basis functions are heavily deformed, but the stability properties are already encoded in the bubble functions that are identified with the numerical correctors in (11.13).

12.1.2. Error measurement outside the boundary layer. For a qualitative comparison of the different methods, we compute the error in the H^1-norm. The main objective

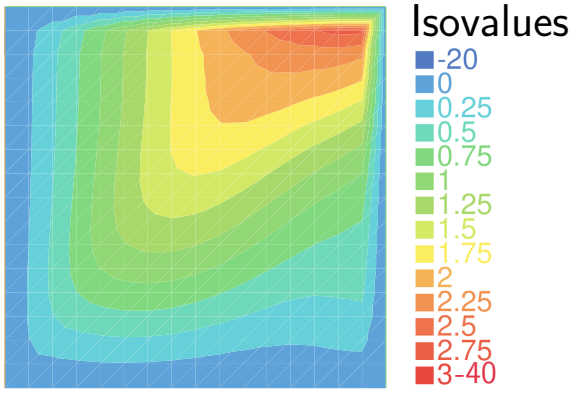

(a) *MsFEM-lin SUPG* (10.3)

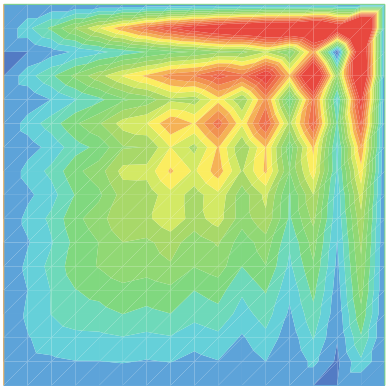

(b) *MsFEM-lin* (10.2)

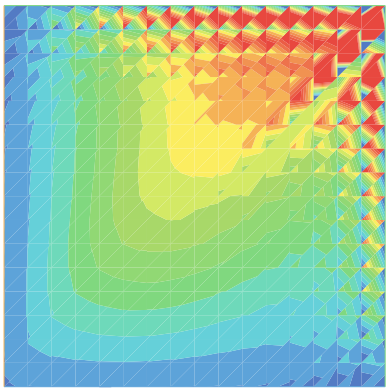

(c) *MsFEM-CR (see Remark 11.1)*

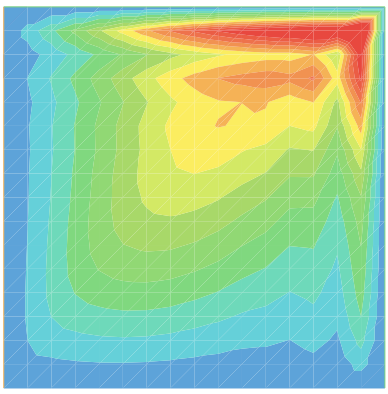

(d) *adv-MsFEM-lin* (10.6)

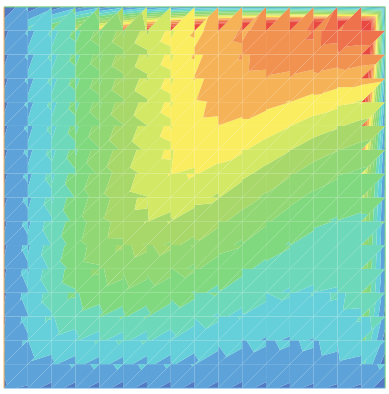

(e) *adv-MsFEM-CR* (11.3)

Figure 12.2: *The* $\mathbb{P}_1$ *part of various MsFEM approximations applied to the test case* (12.1) *when* $\varepsilon = 2^{-7}$, $\alpha = 2^{-8}$, *and* $H = 2^{-4}$. *Note that the colour code is not linear in the overshoot regions.*

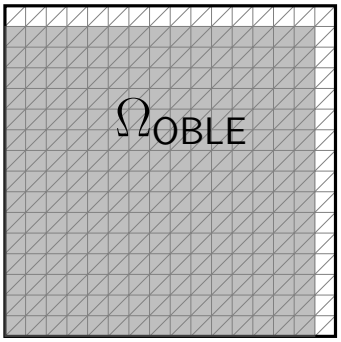

Figure 12.3: *We measure the error outside the boundary layer elements, that is, in Ω_{OBLE}, the domain highlighted in gray.*

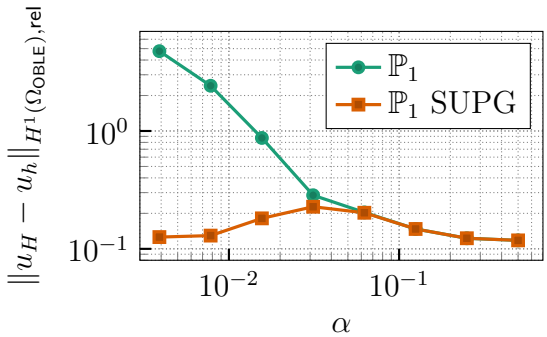

Figure 12.4: *Errors outside the boundary layer for $\mathbb{P}_1$ FEMs for the PDE $-\alpha\Delta u + b \cdot \nabla u = f$ on a coarse mesh $\mathscr{T}_H$ with $H = 2^{-4}$.*

of FEMs on a coarse mesh for advection-dominated problems is to capture the solution outside the boundary layer. The boundary layer itself cannot be resolved by standard finite elements due to the complex behaviour of the boundary layer within a single mesh element. The adv-MsFEM variants that we consider have problem-adapted basis functions that may in principle recover the boundary layer. We focus on this possibility in Figure 12.6.

Here we measure the error of the numerical approximation outside all mesh elements K that contain a part of the boundary layer of u^ε that is visualized in Figure 12.1b. We call this the region 'outside the boundary layer mesh elements' (OBLE), and denote it $\Omega_{\mathsf{OBLE}} = (0, 1 - H)^2$, where H is the length of the legs of the mesh elements. See Figure 12.3. To be precise, we compute the errors in the following relative norm:

$$\|u_H - u_h^\varepsilon\|_{H^1(\mathscr{T}_H;\Omega_{\mathsf{OBLE}}),\mathsf{rel}} = \frac{\sqrt{\sum_{K\in\mathscr{T}_H,\, K\subset\Omega_{\mathsf{OBLE}}} \|u_H - u_h^\varepsilon\|^2_{H^1(K)}}}{\|u_h^\varepsilon\|_{H^1(\Omega_{\mathsf{OBLE}})}},$$

for any u_H that is piecewise H^1. Here, $u_h^\varepsilon \in H^1(\Omega)$ is the $\mathbb{P}_1$ Lagrange approximation of (9.3) on a fine mesh of a mesh size h that is specified below.

Remark 12.1. Our definition of the relative error differs from the one in the earlier publication [114] in the normalization factor. We use $\|u_h^\varepsilon\|_{H^1(\Omega_{\mathsf{OBLE}})}$, whereas the earlier work used $\|u_h^\varepsilon\|_{H^1(\Omega)}$. Note that the latter norm (on the entire domain Ω) is unbounded as $\alpha \to 0$, because of the ever sharper boundary layer in $\Omega \setminus \Omega_{\mathsf{OBLE}}$ that is unbounded in $H^1(\Omega)$. This different choice does not, of course, change the classification of the performance of the numerical methods at a fixed value of α. However, the division by $\|u_h^\varepsilon\|_{H^1(\Omega)}$ may give the erroneous impression that certain methods perform exceptionally well in the advection-dominated regime (for small α) because of a large normalization factor. Our choice for normalizing by the norm of the reference solution on Ω_{OBLE} should give a better understanding of the actual accuracy of the numerical methods.

In Figure 12.4 we show the errors in this norm for a test case with constant coefficients and for the $\mathbb{P}_1$ FEM and its stabilization by the SUPG method. We observe that the error

of the $\mathbb{P}_1$ FEM grows by several orders of magnitude due to its instability. On the contrary, the error committed by the $\mathbb{P}_1$ SUPG method outside the boundary layer is stable for all values of the diffusion coefficient.

In Figure 12.5, we compare various numerical methods for the approximation of (9.3) with coefficients defined in (12.1) on a coarse mesh with legs of size $H = 2^{-4}$, and for α varying from 2^{-1} to $2^{-10} \approx 0.001$. We further set $\varepsilon = 2^{-7}$. The fine mesh, used for the computation of the reference solution and the multiscale basis functions, has legs of length $h = 2^{-11} = \varepsilon/16$ when $\alpha \geq 2^{-9}$ and $h = 2^{-12}$ when $\alpha = 2^{-10}$. The fine mesh is sufficiently fine to avoid instabilities of the Lagrange $\mathbb{P}_1$ FEM. For the smallest value of α, the fine mesh is refined because the choice $h = 2^{-11}$ did not allow to compute the adv-MsFEM-CR basis functions (see (11.2)) correctly in our computations. All computations are executed with FreeFEM [91]. The code used is available at [29].

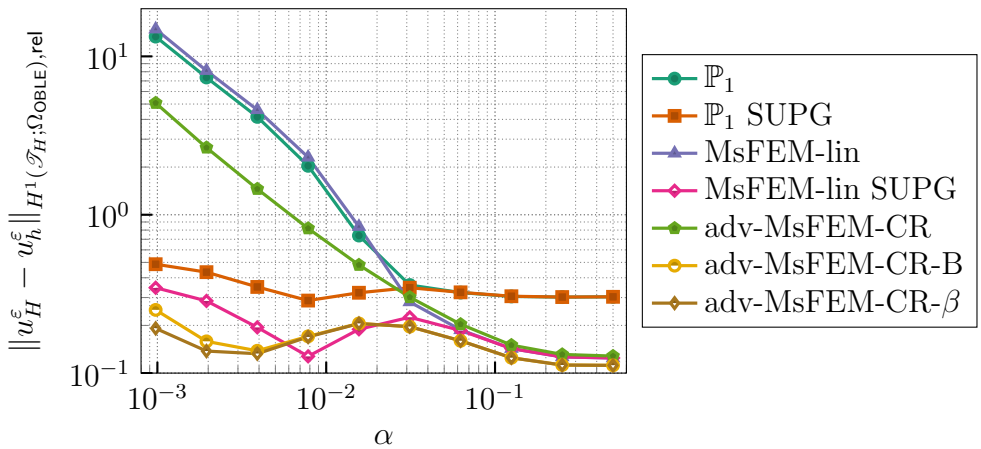

Figure 12.5: *Errors outside the boundary layer elements between the reference solution u_h^ε and various numerical approximations u_H^ε, for the test case (12.1) with $\varepsilon = 2^{-7}$, $H = 2^{-4}$ and varying α.*

The instability of the $\mathbb{P}_1$ FEM and the MsFEM is confirmed for small values of α by large relative errors even outside the boundary layer. In spite of the stability of the adv-MsFEM-CR that is observed in Figure 12.2, the accuracy of the adv-MsFEM-CR is also low. This is expected due to strongly deformed multiscale functions in the space $W_H^{\varepsilon,\mathsf{adv}}$. This phenomenon was also observed in the one-dimensional situation studied in Section 10.4. We further see that the accuracy of the MsFEM-lin SUPG and the adv-MsFEM-CR variants with bubble functions is robust with respect to α, showing the same fluctuations as the $\mathbb{P}_1$ SUPG method in the single-scale case of Figure 12.4. We point out that the adv-MsFEM-CR-B and adv-MsFEM-CR-β are the only methods considered here whose accuracy does not depend on an additional (stabilization) parameter that has to be chosen properly depending on the coefficients of the PDE.

For the one-dimensional test case of Figure 10.2, it was observed in the advection-dominated regime that the $\mathbb{P}_1$ SUPG method and the adv-MsFEM-lin-B have comparable accuracy and outperform the MsFEM-lin SUPG. This was explained by a decreasing amplitude of the oscillations of the derivative of the reference solution, which is not encoded in the MsFEM-lin basis functions. The same differences in the accuracy of the three methods cannot be observed for the two-dimensional tests in Figure 12.5.

12.1.3. Delineating the advection-dominated regime. In simulations with slowly varying coefficients, the values of α where the $\mathbb{P}_1$ FEM and the $\mathbb{P}_1$ SUPG method yield different results can be used as an indication of the advection-dominated regime, and it corresponds qualitatively to the regime where $\mathsf{Pe}_K > 1$. This same distinction is harder to make in the multiscale case, because it is not evident which value of A^ε should be used for the definition of an 'effective numerical Péclet number'. Although a precise definition of the advection-dominated regime may be hard to forumulate, the numerical comparison between the $\mathbb{P}_1$ FEM and the $\mathbb{P}_1$ SUPG method on the one hand, and between the MsFEM-lin and the MsFEM-lin SUPG on the other hand, indicates when the unstabilized methods start to suffer from instabilities.

One may notice in Figure 12.5 that the accuracy of the MsFEM-lin starts to degrade for larger values of α than the $\mathbb{P}_1$ FEM (and this difference is even more noticeable in Figure 12.8). This can be explained as follows. We recall that, for a pure diffusion problem, the $\mathbb{P}_1$ FEM is equivalent to the $\mathbb{P}_1$ approximation of a PDE with piecewise constant diffusion A^{av} given by $A^{\mathsf{av}}|_K = \dfrac{1}{|K|}\displaystyle\int_K A^\varepsilon$ for all $K \in \mathscr{T}_H$. This value is, for the diffusion coefficient in (12.1a), larger than the actual effective diffusion felt by u^ε. The MsFEM yields a better approximation of the effective diffusion, with a smaller value. The difference between the effective diffusion coefficients of the $\mathbb{P}_1$ FEM and the MsFEM increases as the contrast of the diffusion coefficient increases.

We now turn our attention to the case of non-zero advection. Effective, piecewise constant diffusion and advection coefficients $\overline{A}$ and $\overline{b}$, respectively, can be defined for the MsFEM-lin (SUPG) such that the resolution of each of these MsFEMs is equivalent to solving a $\mathbb{P}_1$ discretization of (11.15) with the corresponding effective coefficients (and possibly with additional stabilization terms) on the coarse mesh $\mathscr{T}_H$. For the $\mathbb{P}_1$ FEM, the effective coefficients are given, for all $K \in \mathscr{T}_H$, by

$$\overline{A}_{\beta,\alpha}\big|_K = \frac{1}{|K|}a^\varepsilon\big(x^\alpha, x^\beta\big), \quad \overline{b}_\alpha\big|_K = \frac{1}{|K|}a^\varepsilon(x^\alpha, 1), \quad 1 \le \alpha, \beta \le d,$$

and for the MsFEM-lin by

$$\begin{aligned} \overline{A}_{\beta,\alpha}\big|_K &= \frac{1}{|K|}a^\varepsilon\Big(x^\alpha + \chi_K^{\varepsilon,\alpha}, x^\beta + \chi_K^{\varepsilon,\beta}\Big), \\ \overline{b}_\alpha\big|_K &= \frac{1}{|K|}a^\varepsilon(x^\alpha + \chi_K^{\varepsilon,\alpha}, 1), \qquad\qquad 1 \le \alpha, \beta \le d, \end{aligned} \tag{12.3}$$

where $\chi_K^{\varepsilon,\alpha} \in H_0^1(K)$ solves $-\mathrm{div}\left(A^\varepsilon \nabla\left(\chi_K^{\varepsilon,\alpha} + x^\alpha\right)\right) = 0$. The start of the advection-dominated regime, in the sense that spurious oscillations appear in the numerical solution, depends on the Péclet number associated to the effective scheme and is thus method specific. It can be verified, for instance, that at a given value of α in (12.1), the eigenvalues of the effective diffusion tensor for the MsFEM-lin are smaller than those of the $\mathbb{P}_1$ FEM. Since the effective diffusion felt with the MsFEM-lin is smaller than for the $\mathbb{P}_1$ FEM, spurious oscillations already appear for larger values of α when one applies the MsFEM-lin.

12.1.4. Errors including the boundary layer. We consider in Figure 12.6 the relative errors on the entire domain Ω of those numerical methods that were previously identified

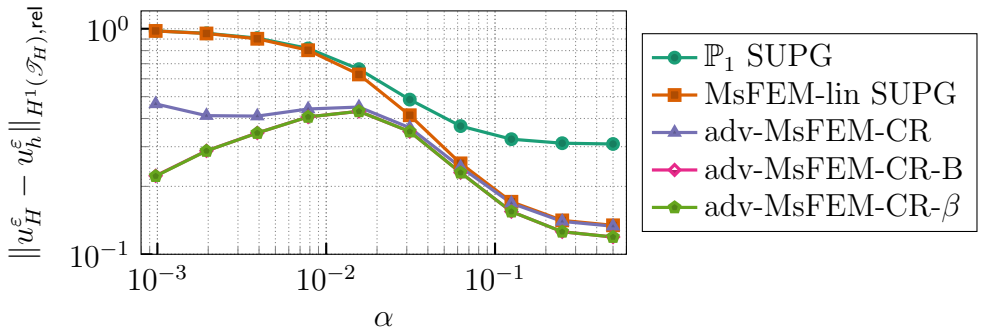

Figure 12.6: *Errors on the entire domain between the reference solution u_h^ε and various numerical approximations u_H^ε, for the test case (12.1) with $\varepsilon = 2^{-7}$, $H = 2^{-4}$, and for varying α. The results for the adv-MsFEM-CR-B and for the adv-MsFEM-CR-β coincide in the figure.*

as stable. We measure these errors in the relative H^1-norm defined as

$$\|u_H - u_h^\varepsilon\|_{H^1(\mathscr{T}_H),\mathsf{rel}} = \frac{\sqrt{\sum_{K\in\mathscr{T}_H} \|u_H - u_h^\varepsilon\|^2_{H^1(K)}}}{\|u_h^\varepsilon\|_{H^1(\Omega)}}.$$

Note that the normalization factor here is much larger than for the errors in Figure 12.5, because we include the H^1-norm of the reference solution in the boundary layer, which is characterized by a large gradient. The errors are by far dominated by the error in the boundary layer elements, i.e., in $\Omega \setminus \Omega_{\mathsf{OBLE}}$. The results are clear: the trial functions of the $\mathbb{P}_1$ SUPG method and the MsFEM-lin SUPG are not adapted to the exponential decay of u_h^ε and commit a large error in the advection-dominated regime. The only methods that are capable of resolving the boundary layer are the adv-MsFEM-CR variants with or without bubbles. Note that this is achieved while no a priori information about the location of the boundary layer of the exact solution is encoded in the multiscale approximation space. The basis functions of the adv-MsFEM-lin may provide an even better approximation of the boundary layer, because the boundary condition is enforced in a strong sense, like in the continuous problem (9.3). However, as a result of the incomplete stabilization of the adv-MsFEM-lin(-B), the resulting approximation does not capture the boundary layer of u^ε properly due to a large overshoot in this region.

12.1.5. Non-intrusive variants. We now compare the MsFEM variants studied above with the variants introduced in Section 11.4 for a non-intrusive implementation of the MsFEM. In Figure 12.7, we compare the Galerkin variants of the adv-MsFEM-CR-B (defined by (11.5)) and the adv-MsFEM-CR-β (defined by (11.11)) with the Petrov-Galerkin variants where each multiscale test function $\phi_e^{\varepsilon,\mathsf{adv}}$ is replaced by the piecewise affine test function $\phi_e^{\mathbb{P}_1} \in V_H^w$ ($e \in \mathscr{E}_H^{in}$). See (11.19) for the explicit formulation in the case of the adv-MsFEM-CR-β. We recall that the PG adv-MsFEM-CR-β can be implemented in a non-intrusive way by computing effective coefficients in the offline stage, see (11.21b). Similarly, one can define a Petrov-Galerkin variant of the MsFEM-lin SUPG (10.3), the test space being replaced by V_H in this case.

For the adv-MsFEM ('lin' or 'CR', with and without bubbles) the above change of test functions does not affect the matrix of the linear system associated to the MsFEM.

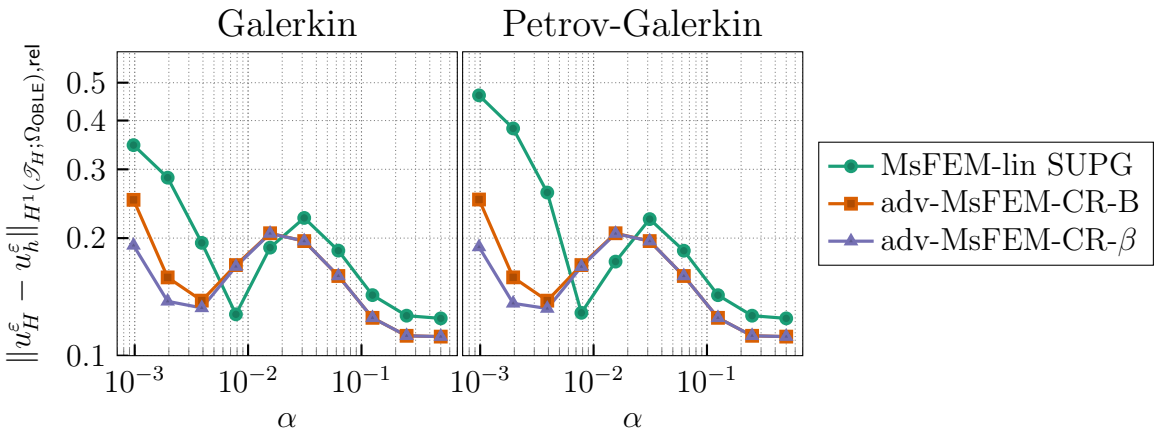

Figure 12.7: *Comparison of some MsFEM variants in Galerkin and in Petrov-Galerkin formulation (with $\mathbb{P}_1$ tests functions). The test case is (12.1) with $\varepsilon = 2^{-7}$, $H = 2^{-4}$, and varying α.*

(We recall Theorem 11.6 for the adv-MsFEM-CR, and a similar property holds for the adv-MsFEM-lin.) The results of Figure 12.7 show that the accuracy of the related MsFEM variants also remains unaffected when changing to a Petrov-Galerkin method. The accuracy of the MsFEM-lin SUPG (for which there is no analogue of Theorem 11.6), on the other hand, deteriorates in the advection-dominated regime when the test functions are changed to $\mathbb{P}_1$ basis functions.

12.2. Second test case

We consider a second test case with a larger contrast of the diffusion coefficient. This way, the difference between multiscale and standard finite element approaches is expected to be more pronounced, at least in the diffusion-dominated regime. More precisely, we consider here

$$A^\varepsilon(x,y) = \mu^\varepsilon(x,y)\,\mathrm{Id}, \quad \mu^\varepsilon(x,y) = \alpha\left(1 + 100\cos^2(\pi x/\varepsilon)\sin^2(\pi y/\varepsilon)\right), \tag{12.4a}$$

$$b(x,y) = \begin{pmatrix} 50\cos(0.3\pi) \\ 50\sin(0.3\pi) \end{pmatrix}, \tag{12.4b}$$

$$f(x,y) = 2 + \sin(2\pi x) + x\cos(2\pi y), \tag{12.4c}$$

where we use $\varepsilon = \pi/150 \approx 0.02$. The error of various numerical approaches as α takes the values $\alpha = 2^k$ for $k = 2, \ldots, -6$ is shown in Figure 12.8. We show the tests for two different values of the coarse mesh size H. The fine mesh size is $h = 2^{-11}$ except for the smallest value of α, which again required a fine mesh size of $h = 2^{-12}$ in order to compute the adv-MsFEM-CR basis functions correctly.

The stabilization parameter of the MsFEM-lin SUPG is again given by (12.2), where we still define the element Péclet number Pe_K based on the minimum and maximum values of μ^ε. We observed numerically that the accuracy of the MsFEM SUPG depends, both in the advection and diffusion dominated regimes, strongly on the value of the diffusion that is used in the definition of Pe_K. Especially in the high-contrast case, one risks taking a value that is either too small or too large, and even more so when μ^ε has a more complicated, non-periodic structure. Too small a value for the diffusion results

in too large a value for Pe_K and thus leads to an overly diffusive scheme in the diffusion dominated regime. On the other hand, too large a value for the diffusion in the element Péclet number may decrease the stabilization of the method and deteriorate its accuracy in the advection-dominated regime. It is thus not obvious to find the correct expression for τ in strongly heterogeneous media, and we consider it useful to introduce an alternative method, namely the adv-MsFEM-CR-B (or -β), that is free from such a parameter, yet is robust with respect to the diffusion strength.

Remark 12.2. We mention a new option to choose the stabilization parameter for the MsFEM-lin SUPG that bypasses the ambiguity due to the heterogeneous character of μ^ε. We can compute the effective coefficients for the MsFEM-lin defined in (12.3). Recall that these coefficients define an effective $\mathbb{P}_1$ FEM on the coarse mesh that is equivalent to the MsFEM-lin. Hence it suffices to find a suitable stabilization parameter for the effective scheme based on the effective coefficients, which are piecewise constant. This strategy has not been investigated during the preparation of this thesis.

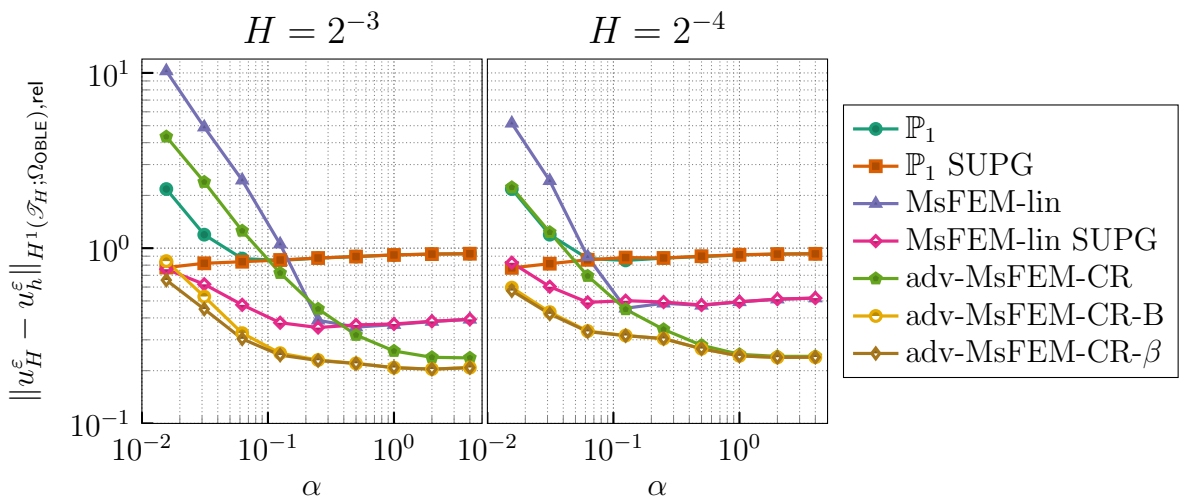

Figure 12.8: *Errors outside the boundary layer element between the reference solution u_h^ε and various numerical approximations u_H^ε, for the test case (12.4) with $\varepsilon \approx 0.02$, two different values of H and varying α.*

In Figure 12.8, we see that the results for the two values of H are qualitatively the same, with the difference that advection-dominating effects are smaller at the same value of α when H is smaller. This is to be expected, since the element Péclet number decreases when H decreases. We observe that the error of the multiscale methods increases slightly if H decreases from $H = 2^{-3}$ to $H = 2^{-4}$. This is in line with the so-called resonance effect that is also observed in the literature, which prevents convergence of MsFEMs if the discretization size H is close to the typical length scale of the microstructure.

As expected, the bad performance of the $\mathbb{P}_1$ FEM due to the unresolved microstructure is more pronounced than in Figure 12.5. One can see again in Figure 12.8 that the $\mathbb{P}_1$ FEM, the MsFEM-lin and the adv-MFEM-CR lose their accuracy in the advection-dominated regime. The MsFEM-lin SUPG, adv-MsFEM-CR-B and the adv-MsFEM-CR-β are the only methods that show a competitive performance in both the regimes where advection dominates and where diffusion dominates. We underline that the adv-MsFEM-CR variants with additional bubble functions are the only such methods that do not depend on the choice of an additional (stabilization) parameter.

Part III

Novel Convergence Analysis for Multiscale Finite Element Methods

Chapter 13

A convergence theorem under minimal regularity hypotheses

In Section 2.3.3 we reviewed the error estimate (2.21) that has been established for multiple MsFEM variants in the literature. We also indicated why an improved error estimate under less stringent regularity hypotheses on the diffusion coefficient and the homogenized solution seemed possible based on a more careful study of the boundary layer of the error around the mesh interfaces. To establish the convergence proof rigorously under those assumptions is the aim of the present chapter, which constitutes part III of this thesis. Let us remind the reader that for the one-dimensional case, the resonance effect disappears, and we have the error estimate (2.20) for which no additional regularity assumptions on the diffusion coefficient are needed (and not even the assumption of periodicity).

The structure of this chapter is as follows. First we give in Section 13.1 a precise definition of the MsFEMs that we consider, following the general framework of Chapter 5 (but without oversampling). We state the improved convergence result, Theorem 13.1, in Section 13.2. In Section 13.3, we recall various notions of periodic homogenization and numerical analysis that can be considered classical. These results are included in this thesis for completeness, because they will be used for the proof of Theorem 13.1. Then we provide the key lemmas of our convergence analysis in Section 13.4, which consist of a homogenization and an interpolation estimate for the multiscale approximation space as well as a bound for the non-conforming error. Finally, the proof of Theorem 13.1 is given in Section 13.5. Besides the improved regularity hypotheses, another new element of the analysis of this chapter is that it unifies the analysis of the MsFEM-lin and the MsFEM-CR.

Notation. Throughout this chapter, we will use the following shorthand notation for standard norms and seminorms on Sobolev spaces. For any $u \in H^k(\Omega)$, where $\Omega \subset \mathbb{R}^d$,

$$\|u\|_{k,\Omega} = \|u\|_{H^k(\Omega)},$$

for Sobolev norms, and

$$|u|^2_{k,\Omega} = \sum_{\alpha \in \mathbb{Z}^d, |\alpha|=k} \|\partial_\alpha u\|^2_{0,\Omega}$$

for seminorms. For non-H^1-conforming functions, we use broken (semi-)norms, denoted by

$$\|u\|_{k,\mathscr{T}}^2 = \sum_{K\in\mathscr{T}} \|u\|_{k,K}^2,$$

where $\mathscr{T}$ is a collection of sets such that $u|_K \in H^1(K)$ for all $K \in \mathscr{T}$. Typically, $\mathscr{T}$ will be a mesh, or a collection of mesh elements. We further recall that, due to the Poincaré inequality [73, Lemma B.61], the H^1-seminorm $|\cdot|_{1,\Omega}$ is in fact a norm on the space $H_0^1(\Omega)$ when Ω is bounded.

13.1. Definition of the MsFEM framework

We consider MsFEMs for the approximation of $u^\varepsilon \in H^1(\Omega)$, which is the solution to the following partial differential equation (PDE) on a bounded polytope (a polygon in dimension 2, a polyhedron in dimension 3) $\Omega \subset \mathbb{R}^d$:

$$-\operatorname{div}(A^\varepsilon \nabla u^\varepsilon) = f, \tag{13.1}$$

and satisfying homogeneous Dirichlet conditions on $\partial\Omega$, i.e., $u^\varepsilon \in H_0^1(\Omega)$. Here, A^ε is a highly oscillatory, uniformly bounded and elliptic $d \times d$ matrix, and $f \in L^2(\Omega)$. The superscript ε refers to the microscopic size of variations of the coefficient, much smaller than the size of the global domain Ω. The dimension $d \geq 2$ is arbitrary.

Problem (13.1) is equivalent to finding $u^\varepsilon \in H_0^1(\Omega)$ such that

$$\forall\, v \in H_0^1(\Omega), \quad a^\varepsilon(u^\varepsilon, v) = F(v), \tag{13.2}$$

where, for any $u, v \in H^1(\Omega)$, the bilinear form a^ε and the linear form F are defined by

$$a^\varepsilon(u,v) = \int_\Omega \nabla v \cdot A^\varepsilon \nabla u, \quad F(v) = \int_\Omega f v.$$

We assume that there exist $m, M > 0$ (independent of ε) such that

$$\begin{aligned} &\forall\, \xi \in \mathbb{R}^d, \quad m\|\xi\|^2 \leq \xi \cdot A^\varepsilon(x)\,\xi \quad \text{a.e. in } \Omega, \\ \text{and} \quad &\forall\, \xi, \eta \in \mathbb{R}^d, \quad \|\eta \cdot A^\varepsilon(x)\xi\| \leq M\,\|\xi\|\,\|\eta\| \quad \text{a.e. in } \Omega, \end{aligned} \tag{13.3}$$

Then (13.2) (and (13.1)) are well-posed due to the classical Lax-Milgram Theorem.

We consider two MsFEM variants here in the common framework of Chapter 5. The precise definitions are recalled here to make the present chapter self-contained. It covers the original MsFEM of [98] where the basis functions are defined with affine boundary conditions, henceforth abbreviated as MsFEM-lin, and the variant of [112] where the basis functions are defined with Crouzeix-Raviart type boundary conditions, abbreviated as MsFEM-CR.

Let $(\mathscr{T}_H)_H$ be a family of simplicial conformal meshes of the domain Ω and with elements of a typical size H that is larger than ε. We suppose that the family of meshes is regular in the sense recalled in Section 13.3.3. It is also supposed in many results that the family of meshes is quasi-uniform (see (13.21)). We shall explicitly mention throughout when this property is needed on top of the supposed regularity.

The notation V_H shall be used for one of two standard finite element spaces of piecewise

affine functions. This space is called the underlying $\mathbb{P}_1$ space of the MsFEM. In the case of the MsFEM-lin, V_H is the $\mathbb{P}_1$ Lagrange space V_H^{lin} and in the case of the MsFEM-CR, V_H is the $\mathbb{P}_1$ Crouzeix-Raviart space V_H^{CR}. Denoting $\mathbb{P}_1(\mathscr{T}_H)$ the space of all piecewise affine functions on $\mathscr{T}_H$, these spaces are defined as

$$V_H^{\mathsf{lin}} = \{v_H \in \mathbb{P}_1(\mathscr{T}_H) \mid v_H \text{ is continuous on } \Omega,\, v_H|_{\partial\Omega} = 0\} \quad \text{(MsFEM-lin)}, \tag{13.4a}$$

and

$$V_H^{\mathsf{CR}} = \left\{ v_H \in \mathbb{P}_1(\mathscr{T}_H) \,\middle|\, \forall\, K \in \mathscr{T}_H, \forall\, e \in \mathscr{F}(K) : \int_e [\![v]\!] = 0 \right\} \quad \text{(MsFEM-CR)}, \tag{13.4b}$$

where $\mathscr{F}(K)$ is the set of faces of K and $[\![v]\!]$ denotes the jump of v_H over the face e, or the restriction of v to e if e lies on $\partial\Omega$.

The standard finite element space is adapted to the multiscale properties of A^ε through the use of numerical correctors defined on each mesh element. They are defined independently on the mesh elements $K \in \mathscr{T}_H$ in a sampling space V_K. This space depends on the underlying $\mathbb{P}_1$ space used, and is either defined as

$$V_K = H_0^1(K) \quad \text{(MsFEM-lin)}, \tag{13.5a}$$

for the MsFEM-lin, or as

$$V_K = \left\{ v \in H^1(K) \,\middle|\, \forall\, e \in \mathscr{F}(K) : \int_e v = 0 \right\} \quad \text{(MsFEM-CR)}, \tag{13.5b}$$

for the MsFEM-CR. (We warn the reader that the notation V_K differs from the notation adopted in Part I, where the same space was denoted by $V_{K,0}$. See Definition 5.10.) We define the bilinear forms, for all $K \in \mathscr{T}_H$,

$$a_K^\varepsilon(u, v) = \int_K \nabla v \cdot A^\varepsilon \nabla u, \quad \text{for all } u, v \in H^1(K).$$

Then for each $\alpha = 1, \ldots, d$, we define the numerical corrector $\chi_K^{\varepsilon,\alpha} \in V_K$ as the unique solution in V_K to

$$\forall\, v \in V_K, \quad a_K^\varepsilon(\chi_K^{\varepsilon,\alpha}, v) = -a^\varepsilon(x^\alpha, v), \tag{13.6}$$

where x^α denotes the α-th coordinate of x. We extend the numerical correctors by 0 outside K.

We can now associate a multiscale function v_H^ε to each $v_H \in V_H$ by

$$v_H^\varepsilon = v_H + \sum_{K \in \mathscr{T}_H} \sum_{\alpha=1}^{d} \partial_\alpha (v_H|_K) \chi_K^{\varepsilon,\alpha}, \tag{13.7}$$

and we define the multiscale approximation space V_H^ε (which depends on the choice made for V_H) as

$$V_H^\varepsilon = \{v_H^\varepsilon \,|\, v_H \in V_H\}\,. \tag{13.8}$$

Combining (13.6) and (13.7) shows that the multiscale finite element functions satisfy

$$\forall\, K \in \mathscr{T}_H,\, \forall\, v \in V_K, \qquad a_K^\varepsilon(v_H^\varepsilon, v) = 0. \tag{13.9}$$

The MsFEM approximation of u^ε is then defined as $u_H^\varepsilon \in V_H^\varepsilon$, the unique solution to the finite-dimensional problem

$$\forall\, v_H^\varepsilon \in V_H^\varepsilon, \quad \sum_{K\in\mathscr{T}_H} a_K^\varepsilon(u_H^\varepsilon, v_H^\varepsilon) = F(v_H^\varepsilon). \tag{13.10}$$

For a non-intrusive implementation of the MsFEM, a Petrov-Galerkin variant of the MsFEM was proposed in Definition 6.1 that defines the approximation $u_H^\varepsilon \in V_H^\varepsilon$ as the unique solution to

$$\forall\, v_H \in V_H, \quad \sum_{K\in\mathscr{T}_H} a_K^\varepsilon(u_H^\varepsilon, v_H) = F(v_H). \tag{13.11}$$

The MsFEM (13.10) is well-posed because (13.3) ensures coercivity of the bilinear form $\sum_{K\in\mathscr{T}_H} a_K^\varepsilon$ on the space V_H^ε. It was shown in Lemma 6.4 that the Petrov-Galerkin MsFEM (13.11) is also well-posed.

The next chapters focus on the convergence analysis of the MsFEMs (13.10) and (13.11). We explained in the Introduction that all error estimates known for the MsFEM are obtained under a periodicity assumption, even though this assumption is not required for the use of the method. We shall adopt this assumption from now on. More precisely, we assume that A^ε is of the form

$$A^\varepsilon(x) = A^{\mathsf{per}}\left(\frac{x}{\varepsilon}\right) \quad \text{a.e. in } \Omega,$$

where $A^{\mathsf{per}} \in L^\infty(\mathbb{R}^d)^{d\times d}$ satisfies (13.3) and is Q-periodic, with Q the unit cube of $\mathbb{R}^d$. We recall some homogenization results for the periodic setting in Section 13.3.1, and in particular the definition of the homogenized limit $u^\star$ of u^ε that only depends on A^{per} and f and that is used in the statements of Theorem 13.1 and Corollary 13.2 below.

13.2. Statement of the convergence results

The main contribution of Part III of this thesis is the following. Here and in the sequel, C denotes a generic constant that is independent of H, f and ε, but that may depend on the dimension d, on Ω, on A^{per} and on the regularity constants of the mesh, and that may take a different value from one occurrence to the other.

Theorem 13.1. *Let $u_H^\varepsilon \in V_H^\varepsilon$ be the solution to (13.10). Suppose that $(\mathscr{T}_H)_H$ is a regular family of simplicial meshes and that it is quasi-uniform, that $\varepsilon \le H$, and that $u^\star \in H^2(\Omega)$. Then*

$$|u^\varepsilon - u_H^\varepsilon|_{1,\mathscr{T}_H} \le C\left(H|u^\star|_{2,\Omega} + \sqrt{\frac{\varepsilon}{H}}\,|u^\star|_{1,\Omega}\right).$$

As an immediate consequence of Theorem 7.10, which estimates the difference of the MsFEM approximations from (13.10) and (13.11), we then also have the following result.

Corollary 13.2. *Let $u_H^\varepsilon \in V_H^\varepsilon$ be the solution to (13.11). Suppose that $(\mathscr{T}_H)_H$ is a regular family of simplicial meshes and that it is quasi-uniform, that $\varepsilon \le H$, and that*

$u^\star \in H^2(\Omega)$. *Then*

$$|u^\varepsilon - u_H^\varepsilon|_{1,\mathscr{T}_H} \leq C\left(H\|f\|_{0,\Omega} + H|u^\star|_{2,\Omega} + \sqrt{\frac{\varepsilon}{H}}\,|u^\star|_{1,\Omega}\right).$$

The only hypotheses on the periodic coefficient A^{per} are those in (13.3) that are used to establish well-posedness of (13.1). We would like to underline that the commonly used smoothness hypothesis of A^ε is *extremely restrictive* from a modelling point of view, because real multiscale materials such as composite materials are typically characterized by discontinuous coefficients. The additional assumption that u^* be in $H^2(\Omega)$ is not very restrictive, and in particular, much less restrictive than the usual hypothesis that $u^\star \in W^{2,\infty}(\Omega)$. For instance, $u^\star \in H^2(\Omega)$ whenever the domain Ω is convex. We refer to [85, Theorem 3.2.1.2] for this result. Moreover, this assumption is unavoidable since even the standard $\mathbb{P}_1$ FEM requires the same regularity for the solution in order to establish convergence at the rate H. Hence, our convergence analysis for the MsFEM is carried out under minimal regularity hypotheses.

13.3. Auxiliary notions and results

In this section, we recall a number of classical results from periodic homogenization and the theory of finite elements that we use to prove Theorem 13.1. One non-classical result is Lemma 13.8, which extends a classical trace estimate to the multiscale space V_H^ε. We also construct a cut-off function that vanishes around the interfaces of the mesh, and that will allow us to estimate boundary layers in Section 13.4. The reader that is familiar with these notions may move on to Section 13.4 and use the present section mainly as a reference for the proofs in the sequel. For completeness, we provide full proofs of most results, including some results that may be considered elementary.

13.3.1. Elements of periodic homogenization theory. Homogenization theory studies the limit of u^ε as $\varepsilon \to 0$. This limit always exists in the periodic setting we consider, and we recall some elements here. See, for instance, [28, 134] or [7, Chapter 1] for details on periodic homogenization. Although this topic was also briefly reviewed in Sections 2.2.1 and 4.7, we recall and complement it here to make the present chapter self-contained.

We recall the definition of the spaces

$$L^2_{per}(Q) = \left\{u \in L^2_{loc}(\mathbb{R}^d) \,\middle|\, \forall\, k \in \mathbb{Z}^d,\ u(x+k) = u(x) \text{ almost everywhere}\right\}$$

and

$$H^1_{per}(Q) = \left\{u \in L^2_{per}(Q) \,\middle|\, \forall\, 1 \leq \alpha \leq d,\ \partial_\alpha u \in L^2_{per}(Q)\right\}.$$

Let Q denote the unit cube of $\mathbb{R}^d$. We introduce the corrector functions $w_1, \ldots, w_d \in H^1_{per}(Q)$ solution to

$$-\mathrm{div}(A^{\mathsf{per}}\nabla w_\alpha) = \mathrm{div}(A^{\mathsf{per}} e_\alpha) \quad \text{in } \mathbb{R}^d, \tag{13.12}$$

which uniquely defines w_α up to an irrelevant additive constant. The corrector functions define the (constant) homogenized matrix $A^\star \in \mathbb{R}^{d\times d}$ by

$$A^\star e_\alpha = \int_Q A^{\mathsf{per}}(e_\alpha + \nabla w_\alpha), \qquad 1 \leq \alpha \leq d, \tag{13.13}$$

where e_α is the unit vector of $\mathbb{R}^d$ in the direction of x^α. Like A^{per}, the homogenized matrix $A^\star$ satisfies the ellipticity property in (13.3).

The homogenized limit $u^\star$ of u^ε is the unique solution in $H^1_0(\Omega)$ to the boundary value problem

$$\begin{cases} -\mathrm{div}(A^\star \nabla u^\star) = f & \text{in } \Omega \\ u^\star = 0 & \text{on } \Omega. \end{cases} \tag{13.14}$$

The sequence of functions u^ε converges to $u^\star$ as $\varepsilon \to 0$ weakly in $H^1(\Omega)$ and strongly in $L^2(\Omega)$. The corrector functions can be used to build a reconstruction of $u^\star$ (called first-order two-scale expansion) as

$$u^{\varepsilon,1}(x) = u^\star(x) + \varepsilon \sum_{\alpha=1}^{d} \partial_\alpha u^\star(x)\, w_\alpha\left(\frac{x}{\varepsilon}\right). \tag{13.15}$$

Now the gradient $\nabla\left(u^\varepsilon - u^{\varepsilon,1}\right)$ converges to 0 strongly in $L^1_{loc}(\Omega)$ as $\varepsilon \to 0$.

This strong convergence, away from the boundary $\partial\Omega$ where non-oscillatory conditions are imposed, is in fact the topic of our Lemma 13.5 below, inside each element of the mesh $\mathscr{T}_H$. In order to obtain this strong convergence of the gradient of $u^{\varepsilon,1} - u^\varepsilon$, we will use the following property of the corrector functions. Note that for each $\alpha = 1, \ldots, d$, the function $A^{\mathsf{per}} e_\alpha + A^{\mathsf{per}} \nabla w_\alpha - A^\star e_\alpha$ is periodic, divergence-free (thanks to (13.12)) and has zero mean (due to (13.13)). Consequently, there exists a skew-symmetric matrix $Z_\alpha \in H^1_{per}(Q)^{d\times d}$ such that

$$[A^{\mathsf{per}} e_\alpha + A^{\mathsf{per}} \nabla w_\alpha - A^\star e_\alpha]_j = \sum_{i=1}^{d} \partial_i [Z_\alpha]_{i,j}. \tag{13.16}$$

This is shown in [134, pp. 6-7] using the Fourier transform. In the special case of dimension 3, for instance, this can be reformulated as $A^{\mathsf{per}} e_\alpha + A^{\mathsf{per}} \nabla w_\alpha - A^\star e_\alpha = \mathrm{curl}(\tilde{Z}_\alpha)$ for a suitable vector $\tilde{Z}_\alpha \in H^1_{per}(Q)^3$.

13.3.2. Classical abstract error estimates. We will use the classical Céa Lemma [73, Lemma 2.28] in our analysis of the MsFEM-lin, and the Second Strang Lemma [73, Lemma 2.25] for the analysis of the non-conforming MsFEM-CR. For the convience of the reader, we recall these general results here in our setting.

Lemma 13.3. *Let u^ε be the solution to (13.1) and u^ε_H to (13.10) for the MsFEM-lin (i.e., with the choice (13.4a) for V_H and (13.5a) for V_K). Then the following estimate holds:*

$$|u^\varepsilon - u^\varepsilon_H|_{1,\Omega} \le \frac{M}{m} \inf_{v^\varepsilon_H \in V^\varepsilon_H} |u^\varepsilon - v^\varepsilon_H|_{1,\Omega}.$$

Lemma 13.4. *Let u^ε be the solution to (13.1) and u^ε_H to (13.10) for the MsFEM-CR (i.e., with the choice (13.4b) for V_H and (13.5b) for V_K). Then the following estimate holds:*

$$|u^\varepsilon - u^\varepsilon_H|_{1,\mathscr{T}_H} \le \frac{M}{m} \inf_{v^\varepsilon_H \in V^\varepsilon_H} |u^\varepsilon - v^\varepsilon_H|_{1,\mathscr{T}_H} + \frac{1}{m} \sup_{v^\varepsilon_H \in V^\varepsilon_H \setminus \{0\}} \frac{\left|\sum_{K\in\mathscr{T}_H} a^\varepsilon_K(u^\varepsilon - u^\varepsilon_H, v^\varepsilon_H)\right|}{|v^\varepsilon_H|_{1,\mathscr{T}_H}}.$$

13.3.3. A cut-off function on individual mesh elements. To analyse the fine-scale structure of u_H^ε, we introduce in this section a cut-off function that vanishes near the interfaces of the mesh. This will allow us to study homogenization properties of u_H^ε outside a thin layer around the mesh interfaces, where the oscillatory behaviour of u_H^ε is perturbed by affine boundary conditions. To this end, we first recall some notions related to the mesh regularity.

The family of meshes $(\mathscr{T}_H)_H$ is supposed to be regular throughout this chapter. We recall that a regular mesh (also referred to as a shape-regular or non-degenerate mesh) satisfies the following properties:

$$\max_{K\in\mathscr{T}_H} \operatorname{diam}(K) \le CH, \tag{13.17a}$$

and

$$\max_{K\in\mathscr{T}_H} \frac{\operatorname{diam}(K)}{\rho(K)} \le C, \tag{13.17b}$$

for some constant C independent of H, and where $\rho(K)$ is the diameter of the largest ball that can be inscribed in K. Roughly speaking, this ensures that all mesh elements are of the same size.

Since we work with a simplicial mesh, for any H, every mesh element $K \in \mathscr{T}_H$ can be obtained as the affine transformation $\Phi_K : \hat{K} \to K$ of a fixed reference simplex $\hat{K} \subset \mathbb{R}^d$. This transformation takes the form $\Phi_K(\hat{x}) = \mathfrak{A}_K\hat{x} + \mathfrak{B}_K$ for some $\mathfrak{A}_K \in \mathbb{R}^{d\times d}$ and $\mathfrak{B}_K \in \mathbb{R}^d$. The Jacobian $\mathfrak{A}_K$ of Φ_K satisfies (see [73, Lemma 1.100])

$$|\det(\mathfrak{A}_K)| = \frac{|K|}{|\hat{K}|} \quad \|\mathfrak{A}_K\| \le \frac{\operatorname{diam}(K)}{\rho(\hat{K})}, \quad \|\mathfrak{A}_K^{-1}\| \le \frac{\operatorname{diam}(\hat{K})}{\rho(K)}, \tag{13.18}$$

where $\|\cdot\|$ denotes the matrix norm induced by the Euclidean norm on $\mathbb{R}^d$.

Let us now introduce the set

$$K_{in}^\varepsilon = \{x \in K \mid \operatorname{dist}(x, \partial K) > \varepsilon\}$$

of points in K lying at least a distance ε away from the boundary. The cut-off function we will use is identically equal to 1 on K_{in}^ε. It is constructed in the following lemma.

Lemma 13.5. *For all H, there exists a cut-off function $\tau_H : \Omega \to \mathbb{R}$ such that, for all $K \in \mathscr{T}_H$,*

1. *It holds $\tau_H|_K \in \mathscr{C}_c^0(K)$, $\|\tau_H\|_{L^\infty(K)} = 1$ and $\tau_H = 1$ on K_{in}^ε.*
2. *We have $\|\nabla\tau_H\|_{L^\infty(K)} \le \dfrac{C}{\varepsilon}$ with a constant C that is independent of K, H and ε.*

Proof. Let $\tau : [0,\infty) \to \mathbb{R}$ be any smooth ($\mathscr{C}^\infty$) function that vanishes in a neighbourhood of 0 and that equals 1 on $[1,\infty)$. We set

$$\tau_H(x) = \tau\left(\frac{\operatorname{dist}\left(\Phi_K^{-1}(x), \partial\hat{K}\right)}{\varepsilon\|\mathfrak{A}_K^{-1}\|/r}\right), \quad x \in K,$$

where $r = C\,\mathrm{diam}(\hat{K})/\rho(\hat{K})$ with C the constant in (13.17b). We note that the distance function $\mathrm{dist}(\cdot, \partial\hat{K})$ is Lipschitz on $\hat{K}$.

Suppose that $x \in K$ is such that $\tau_H(x) < 1$. Then, by definition of τ, we must have

$$\frac{\mathrm{dist}\left(\Phi_K^{-1}(x), \partial\hat{K}\right)}{\varepsilon\|\mathfrak{A}_K^{-1}\|/r} < 1. \tag{13.19}$$

Let $\hat{x}_0 \in \partial\hat{K}$ be a point satisfying

$$\mathrm{dist}\left(\Phi_K^{-1}(x), \partial\hat{K}\right) = \|\Phi_K^{-1}(x) - \hat{x}_0\|. \tag{13.20}$$

Since Φ_K is affine, we have $\Phi_K(\hat{x}_0) \in \partial K$. Therefore,

$$\begin{aligned}
\mathrm{dist}(x, \partial K) &\leq \|x - \Phi_K(\hat{x}_0)\| = \|x - \mathfrak{A}_K\hat{x}_0 - \mathfrak{B}_K\|, \\
&\leq \|\mathfrak{A}_K\|\,\|\mathfrak{A}_K^{-1}(x - \mathfrak{B}_K) - \hat{x}_0\| = \|\mathfrak{A}_K\|\,\|\Phi_K^{-1}(x) - \hat{x}_0\| \quad \text{(by (13.20))}, \\
&= \|\mathfrak{A}_K\| \cdot \mathrm{dist}\left(\Phi_K^{-1}(x), \partial\hat{K}\right) \leq \varepsilon\|\mathfrak{A}_K\|\,\|\mathfrak{A}_K^{-1}\|/r \qquad \text{(by (13.19))}.
\end{aligned}$$

Now inserting (13.18), (13.17b) and the definition of r, we obtain $\mathrm{dist}(x, \partial K) \leq \varepsilon$. Thus, $\tau_H(x) = 1$ when $\mathrm{dist}(x, \partial K) \geq \varepsilon$, and we have the first part of the lemma.

Regarding the gradient of τ_H on K, a direct computation using the chain rule yields

$$\begin{aligned}
\|\nabla\tau_H\|_{L^\infty(K)} &\leq \frac{r}{\varepsilon\,\|\mathfrak{A}_K^{-1}\|}\|\tau'\|_{L^\infty(\mathbb{R})}\,\|\nabla\,\mathrm{dist}(\cdot, \partial\hat{K})\|_{L^\infty(\hat{K})}\,\|\mathfrak{A}_K^{-1}\|, \\
&= \frac{r}{\varepsilon}\|\tau'\|_{L^\infty(\mathbb{R})}\,\|\nabla\,\mathrm{dist}(\cdot, \partial\hat{K})\|_{L^\infty(\hat{K})}
\end{aligned}$$

This is indeed the desired bound. ■

The next result requires an additional regularity property, namely that the mesh be quasi-uniform. This means that there exists a constant $C > 0$ independent of H such that

$$\rho(K) \geq CH. \tag{13.21}$$

We can now state a useful estimate of the number of periodic cells of size ε that may intersect the region $K_b^\varepsilon = K \setminus K_{in}^\varepsilon$. The exact statement is contained in the next lemma.

Lemma 13.6. *Suppose that the mesh $\mathscr{T}_H$ is quasi-uniform. For any $K \in \mathscr{T}_H$, define*

$$\mathscr{I}_K^\varepsilon = \left\{ i \in \mathbb{Z}^d \;\middle|\; \varepsilon(i + \overline{Q}) \cap \overline{K_b^\varepsilon} \neq \varnothing \right\},$$

and cover K_b^ε by

$$K_{band}^\varepsilon = \bigcup_{i \in \mathscr{I}_K^\varepsilon} \varepsilon(i + Q).$$

Finally, suppose that $H \geq \varepsilon$. Then there exists $C > 0$ independent of K, H and ε such that

$$|K_{band}^\varepsilon| = \varepsilon^d\,\#\mathscr{I}_K^\varepsilon \leq C|K|\frac{\varepsilon}{H},$$

where $|T|$ denotes the d-dimensional volume of a set $T \subset \mathbb{R}^d$.

Proof. First note that any point $x \in K^{\varepsilon}_{band}$ that does not lie in K is at a distance of at most $\varepsilon\sqrt{d}$ from ∂K. We introduce the set $\mathscr{K} = \{x \in \mathbb{R}^d \,|\, \mathrm{dist}(x, \partial K) \leq \varepsilon\sqrt{d}\}$ such that $K^{\varepsilon}_{band} \subset \mathscr{K}$.

Furthermore, since all faces of K are $(d-1)$-dimensional hyperplanes, it is easy to see that

$$\begin{aligned} |\mathscr{K}| &\leq \sum_{e \in \mathscr{F}(K)} 2\varepsilon\sqrt{d}\left(2\varepsilon\sqrt{d} + \mathrm{diam}(e)\right)^{d-1}, \\ &\leq C\varepsilon\left(\varepsilon + \mathrm{diam}(K)\right)^{d-1} \leq C\varepsilon H^{d-1}, \end{aligned}$$

using (13.17a) and using that $H \geq \varepsilon$. Now by (13.21), it follows that $|K| \geq CH^d$, and we obtain

$$|K^{\varepsilon}_{band}| \leq |\mathscr{K}| \leq C|K|\,\varepsilon/H,$$

which concludes the proof. ■

13.3.4. Trace estimates. Another classical ingredient for the analysis of discontinuous finite element spaces concerns bounds on the traces and jumps of functions. We first present a well-known estimate for H^1-conforming functions that can also be found e.g. in [112, Lemma 4.4]

Lemma 13.7. *Let $K \in \mathscr{T}_H$ and let e be any face of K. Then there is a constant $C > 0$ independent of e, K and H such that, for any $v \in H^1(K)$ with $\int_e v = 0$, it holds,*

$$\|v\|_{0,e} \leq CH^{1/2}|v|_{1,K}.$$

Proof. Let $v \in H^1(K)$ satisfy the hypotheses of the Lemma. We first recall that the trace of v on e is indeed well-defined by the classical trace theorem, and that the trace operator is continuous from $H^1(K)$ to $L^2(e)$ (and in fact even for the stronger norm $H^{1/2}(e)$ on the target space). See, for instance, [85, Theorem 1.5.1.3].

As is standard, we shall use the affine transformation $\Phi_K : \hat{K} \to K$ from the reference element $\hat{K}$ to K. We denote the linear part of this transformation by $\mathfrak{A}_K$. Let $\hat{e} = \Phi_K^{-1}(e)$ and set $A_e = |e|/|\hat{e}|$. Then a change of variable yields

$$\int_e |v|^2 = A_e \int_{\hat{e}} |v \circ \Phi_K|^2.$$

By continuity of the trace operator on $\hat{K}$, there exists $C > 0$ depending only on $\hat{K}$ such that

$$\int_{\hat{e}} |v \circ \Phi_K|^2 \leq C\,\|v \circ \Phi_K\|^2_{1,\hat{K}}\,.$$

Using that $\int_{\hat{e}} v \circ \Phi_k = 0$ (because $\int_e v = 0$), the Poincaré-Friedrichs inequality (see [73, Lemma B.63]) yields

$$\|v \circ \Phi_K\|_{1,\hat{K}} \leq C\,|v \circ \Phi_K|_{1,\hat{K}}\,,$$

and thus

$$\int_e |v|^2 \leq CA_e \int_{\hat{K}} \left(\|\mathfrak{A}_K\|^2 \|\nabla v \circ \Phi_K\|^2\right).$$

Another change of variables back to the element K gives

$$A_e \int_{\hat{K}} \left(\|\mathfrak{A}_K\|^2 \|\nabla v \circ \Phi_K\|^2\right) = A_e \int_K \|\mathfrak{A}_K\|^2 \|\nabla v\|^2 \, |\det(\mathfrak{A}_K^{-1})|.$$

Finally, inserting the estimates in (13.18) and using mesh regularity (13.17b), we obtain

$$\|v\|_{0,e} \leq C H_K \sqrt{\frac{|e|}{|K|}} |v|_{1,K},$$

setting $H_K = \operatorname{diam}(K)$. We use that $|e| \leq H_K^{d-1}$ and that, by (13.17b), K satisfies $|K| \geq C H_K^d$, to obtain

$$\|v\|_{0,e} \leq C \sqrt{H_K} |v|_{1,K},$$

The proof is completed by applying the mesh regularity property (13.17a). ■

Now let us introduce some additional notation. The set of all faces of the mesh $\mathscr{T}_H$ is denoted by $\mathscr{E}_H$. For any $e \in \mathscr{E}_H$ that is the common face of the mesh elements K_1 and K_2, and for any function $v \in H^1(\mathscr{T}_H)$, the traces of $v_1 = v|_{K_1}$ and $v_2 = v|_{K_2}$ on e are well-defined. The jump of v over e is defined (up to a sign convention that has no importance here) as

$$[\![v]\!] = v_1|_e - v_2|_e \quad \text{on } e.$$

Also recall the notation for broken H^1-norms introduced on page 178. The next lemma provides an estimate for the jump of discontinuous functions belonging to the multiscale space V_H^ε.

Lemma 13.8. *Let V_H^{CR} be the Crouzeix-Raviart underlying $\mathbb{P}_1$ space defined in (13.4b). For any $v_H \in V_H^{\mathsf{CR}}$ and any face $e \in \mathscr{E}_H$, it holds*

$$\|[\![v_H^\varepsilon]\!]\|_{0,e} \leq C H^{1/2} |v_H|_{1,\{K_1,K_2\}},$$

where v_H^ε is defined through (13.7), and where K_1 and K_2 are the mesh elements that share the face e. If e lies on $\partial\Omega$, the same estimate holds with $K_2 = \varnothing$.

Proof. Let $v_H \in V_H$. We first consider the oscillatory part v_H^{osc} of v_H^ε that we define as

$$v_H^{\mathsf{osc}} = v_H^\varepsilon - v_H = \sum_{\alpha=1}^{d} \partial_\alpha (v_H|_K) \chi_K^{\varepsilon,\alpha}.$$

Note that, by definition of the numerical correctors, v_H^{osc} vanishes on average on all interfaces of the mesh.

Let K_1 and K_2 be the two mesh elements sharing the face e. The analysis is analogous when e lies on $\partial\Omega$ and $K_2 = \varnothing$. The application of Lemma 13.7 to v_H^{osc} on both mesh elements shows that

$$2\,\|[\![v_H^{\mathsf{osc}}]\!]\|_{0,e} \leq \left\| v_H^{\mathsf{osc}}|_{K_1} \right\|_{0,e} + \left\| v_H^{\mathsf{osc}}|_{K_2} \right\|_{0,e} \leq C H^{1/2} \left| v_H^{\mathsf{osc}} \right|_{1,\{K_1,K_2\}}. \tag{13.22}$$

We now bound the seminorms $|v_H^{\mathsf{osc}}|_{1,K_i}$ in terms of $|v_H|_{1,K_i}$ $(i = 1, 2)$ following some steps of the proof of Lemma 7.9. Using the fact that ∇v_H is constant in K_i and using linearity

of the identity (13.6), we find that

$$\forall\, w \in V_K, \quad a_K^\varepsilon(v_H^{\mathsf{osc}}, w) = -a_K^\varepsilon(v_H, w).$$

Taking $w = v_H^{\mathsf{osc}}$ in the above, and using (13.3), we deduce

$$|v_H^{\mathsf{osc}}|_{1,K_i} \leq C\, |v_H|_{1,K_i}\,.$$

Then inserting this inequality in (13.22), it holds

$$\|[\![v_H^{\mathsf{osc}}]\!]\|_{0,e} \leq CH^{1/2}\, |v_H|_{1,\{K_1,K_2\}}\,. \tag{13.23}$$

It now remains to treat the jump of v_H. This is a classical element of the convergence analysis of the Crouzeix-Raviart finite element method (see, e.g., [37, p. 282]) and we recall it here for completeness.

For $i = 1, 2$, we set $v_{H,i} = v_H|_{K_i}$. By definition of the space V_H, the jump of v_H vanishes at the centroid of e (denoted e_c), and it holds,

$$(v_{H,1} - v_{H,2})\,(x) = \nabla\,(v_{H,1}|_e - v_{H,2}|_e)\cdot(x - e_c) \quad \text{on } e,$$

Note that $\nabla\,(v_{H,1}|_e) = \nabla v_{H,1}$, respectively $\nabla\,(v_{H,2}|_e) = \nabla v_{H,2}$, and that both gradients are constant in K_1, resp. K_2. Set $H_{K_i} = \mathrm{diam}(K_i)$. Then we obtain by the Cauchy-Schwarz inequality,

$$\begin{aligned}\int_e [\![v_H]\!]^2 &= \int_e (v_{H,1} - v_{H,2})^2 \\ &\leq C(\|\nabla v_{H,1}\| + \|\nabla v_{H,2}\|)^2 \cdot \int_e \|x - e_c\|^2 \\ &\leq CH_{K_i}^{d+1}\left(\|\nabla v_{H,1}\|^2 + \|\nabla v_{H,2}\|^2\right),\end{aligned}$$

where the second inequality uses that $|e| \leq H_{K_i}^{d-1}$ and that $\|x - e_c\| \leq H_{K_i}$ for all $x \in e$. Then we use that $|K_i| \geq CH_{K_i}^d$ $(i = 1, 2)$ due to (13.17b), so that

$$\|[\![v_H]\!]\|_{0,e}^2 \leq CH_{K_i}\left(|v_H|_{1,K_1}^2 + |v_H|_{1,K_2}^2\right),$$

and upon taking the square root and using (13.17a), we have

$$\|[\![v_H]\!]\|_{0,e} \leq CH^{1/2}|v_H|_{1,\{K_1,K_2\}}.$$

The proof is completed upon combining the preceding inequality with (13.23) and a triangle inequality. ■

13.3.5. Interpolation results. We recall now the construction of the Scott-Zhang interpolator defined in [132], which we will denote by $\mathscr{I}_H^C$. In fact, it is a class of projections from $W^{l,p}(\Omega)$ onto the continuous $\mathbb{P}_1$ space on $\mathscr{T}_H$

$$V_H^b = \{v_H \in \mathbb{P}_1(\mathscr{T}_H) \mid v_H \text{ is continuous on } \Omega\}\,,$$

(defined as in (13.4a), but without the restriction of a vanishing trace on $\partial\Omega$). The interpolator preserves continuous piecewise $\mathbb{P}_1$ boundary conditions on $\partial\Omega$. The only

restriction for its definition is that $l > 1/p$, or $l \geq 1$ if $p = 1$, so that traces on $(d-1)$-dimensional interfaces are well-defined. The interpolator enjoys the same useful stability and approximation properties as more elementary interpolators. We provide here in fact an extension of the definition in [132] to obtain a well-defined interpolator for functions that are only in $W^{l,p}(\mathscr{T}_H)$, i.e., having the $W^{l,p}$ regularity only piecewise.

Let $x_1, \ldots, x_N$ be an enumeration of the vertices of the mesh $\mathscr{T}_H$, and let $\phi_1, \ldots, \phi_N$ be the standard basis of V_H^b defined by the property $\phi_i(x_j) = \delta_{i,j}$. For each vertex x_i of the mesh, we choose a mesh element $K_i \in \mathscr{T}_H$ and a face σ_i of K_i satisfying

$$x_i \in \overline{\sigma_i}, \text{ and } \sigma_i \subset \partial\Omega \text{ when } x_i \in \partial\Omega.$$

The second condition ensures that polynomial boundary conditions are preserved. Finally, we associate to each σ_i a basis $\psi_{i,1}, \ldots, \psi_{i,d}$ of $\mathbb{P}_1(\sigma_i)$ as follows. Let $\phi_{i,1}, \ldots, \phi_{i,d}$ be the d non-trivial basis functions on σ_i among $(\phi_i)_{1 \leq i \leq N}$, ordered in such a way that $\phi_{i,1} = \phi_i|_{\sigma_i}$. Then the $\psi_{i,j}$ are the $L^2(\sigma_i)$-dual basis to the former functions:

$$\int_{\sigma_i} \phi_{i,j}\, \psi_{i,k} = \delta_{j,k}.$$

This ensures that the Scott-Zhang interpolator is a projection.

With the above definitions, we define the Scott-Zhang interpolant of any $v \in H^1(\mathscr{T}_H)$ as

$$\mathscr{I}_H^C(v) = \sum_{i=1}^{N} \left(\int_{\sigma_i} \psi_{i,1}\, v|_{K_i} \right) \phi_i.$$

Since the $\psi_{i,1}$ are bounded, and the trace of any function in $H^1(K)$ belongs to $H^{1/2}(\partial K)$ for all $K \in \mathscr{T}_H$, the interpolator is indeed well-defined on $\mathbb{P}_1(\mathscr{T}_H)$ once the mesh elements K_i and the interfaces σ_i are chosen for all $1 \leq i \leq N$.

In the next lemma, we study the approximation and stability properties of the Scott-Zhang interpolator. We specifically consider the application of the interpolator to the $\mathbb{P}_1$ Crouzeix-Raviart space. Finally, we consider the seminorm $|\cdot|_{\frac{1}{2},\mathscr{E}_H}$ defined by

$$|v_H|_{\frac{1}{2},\mathscr{E}_H} = \left(\sum_{e \in \mathscr{E}_H} \frac{1}{H} \|[\![v_H]\!]\|_{0,e}^2 \right)^{1/2}, \tag{13.24}$$

for any v_H that belongs to the $\mathbb{P}_1$ Crouzeix-Raviart space.

Lemma 13.9. *For all $v \in H^2(\Omega)$, it holds*

$$|v - \mathscr{I}_H^C(v)|_{1,\mathscr{T}_H} \leq CH|v|_{2,\Omega}.$$

Let V_H^{CR} be the Crouzeix-Raviart underlying $\mathbb{P}_1$ space defined in (13.4b), and let $v_H \in V_H^{\mathsf{CR}}$. Then it holds

$$|\mathscr{I}_H^C(v_H)|_{1,\Omega} \leq C|v_H|_{1,\mathscr{T}_H}.$$

If, moreover, the family of meshes $(\mathscr{T}_H)_H$ is quasi-uniform, we also have

$$|v_H - \mathscr{I}_H^C(v_H)|_{1,\mathscr{T}_H} \leq C|v_H|_{\frac{1}{2},\mathscr{E}_H}.$$

Proof. The first inequality of the lemma is easily obtained from Equation (4.3) in [132] in the same way as Theorem 4.1 of that reference.

Similarly, the second inequality of the lemma is obtained from the same Equation (4.3) in [132]. (See also Corollary 4.1 of this reference.) We note that, even though the analysis in [132] assumes globally $W^{l,p}$ functions, the estimates are easily verified to hold for functions in $W^{l,p}(\mathscr{T}_H)$ with broken $W^{l,p}$-norms.

We provide more details for the third estimate of the lemma. The idea is to use that $|v_H|_{\frac{1}{2},\mathscr{E}_H} = 0$ implies that v_H has no jumps and thus belongs to V_H^b. Consequently, $\mathscr{I}_H^C(v_H) = v_H$ (since the interpolator is a projection) and the left-hand side of the desired estimate vanishes as well. Since the space V_H^{CR} is finite-dimensional, it follows that the desired estimate holds true for some number C, and the proof below amounts to showing that this constant does not depend on H. To this end, we will again use a transformation to the reference element. However, the proof is complicated by the need to also take the jumps across the faces of K into account in this transformation.

Let us fix $v_H \in V_H^{\mathsf{CR}}$.

Step 1. Transformation to a patch of reference elements.
Let $\hat{K}^+$ be the collection of simplices that is obtained when we glue a copy of $\hat{K}$ to each of the faces of $\hat{K}$, and let $\mathbb{P}_1(\hat{K}^+)$ be the set of piecewise affine functions on $\hat{K}^+$. The role of $\hat{K}^+$ in this analysis is to capture all jumps that $\hat{v} \in \mathbb{P}_1(\hat{K})$ can have with respect to piecewise affine functions across the faces of $\hat{K}$. This is necessary because we need to include the jumps of $v_H \in V_H^{\mathsf{CR}}$ across the faces of K in our study of the reference element.

Fix an element $K \in \mathscr{T}_H$. We use the usual affine transformation $\Phi_K : \hat{K} \to K$ to map the quantity to be estimated to the reference element. In order to also take into account the jumps accross K, we introduce the patch

$$S_K = \{T \in \mathscr{T}_H \mid T \text{ and } K \text{ share a common face}\}.$$

There exists a continuous piecewise affine mapping $\Psi_K : \hat{K}^+ \to S_K$ such that $\hat{K}$ is mapped to K, and more precisely, such that $\Psi_K|_{\hat{K}} = \Phi_K$. We set $\hat{v}_H = v_H \circ \Psi_K$. This function belongs to $\mathbb{P}_1(\hat{K}^+)$.

Step 2. Transformation of the Scott-Zhang interpolant.
On the reference element $\hat{K}$, we define $\hat{\phi}_i = \phi_i \circ \Phi_K$ for all $1 \le i \le N$. Since, before composition with Φ_K, each ϕ_i is supported around a single vertex x_i, there are only $d+1$ non-trivial functions $\hat{\phi}_i$. These are in fact the $\mathbb{P}_1$ nodal basis functions on $\hat{K}$, and we renumber them as $\hat{\phi}_0, \dots, \hat{\phi}_d$, dropping all functions that vanish after transforming to the mesh element K.

For each $0 \le i \le d$ we recall that σ_i is the face associated to the vertex x_i in the definition of the Scott-Zhang interpolator. We define $\hat{\sigma}_i = \Phi_K^{-1}(\sigma_i)$, $A_i = |\sigma_i|/|\hat{\sigma}_i|$ and $\hat{\psi}_{i,1} = A_i\, \psi_{i,1} \circ \Phi_K$. One can show that $\hat{\psi}_{i,1}$ is, for each i, part of the $L^2(\hat{\sigma}_i)$-dual basis of the functions $\hat{\phi}_0, \dots \hat{\phi}_d$ restricted to $\hat{\sigma}_i$ (see [132, Equation (3.3)]), hence the functions $\hat{\psi}_{i,1}$ only depend on K through the choice of one of the faces σ_i in the definition of the Scott-Zhang interpolator. In view of the regularity of the mesh, there is a bounded number of possible choices for this for each i and for all H. For simplicity, we treat here the situation where, for each vertex x_i of the fixed mesh element K under consideration, σ_i is a face of K for each i. The general situation can be treated by a modification of our argument.

With all the above notation, the Scott-Zhang interpolant $\mathscr{I}_H^C(v_H)$ after transformation

to $\hat{K}$ reads

$$\begin{aligned}\mathscr{I}_H^C(v_H)\circ\Phi_K &= \sum_{i=0}^{d}\left(\int_{\hat{\sigma}_i} A_i\,(\psi_{i,1}\,v_H|_{K_i})\circ\Phi_K\right)\hat{\phi}_i\\ &= \sum_{i=0}^{d}\left(\int_{\hat{\sigma}_i} \hat{\psi}_{i,1}\,v_H|_{K_i}\circ\Phi_K\right)\hat{\phi}_i,\end{aligned} \tag{13.25}$$

where we recall that K_i is the mesh element associated to the vertex x_i in the definition of the Scott-Zhang interpolator. Since we treat the situation where each σ_i is a face of K, the identity $\overline{\sigma_i}=\overline{K}\cap\overline{K_i}$ holds.

For any $\hat{v}\in\mathbb{P}_1(\hat{K}^+)$, we now define a function $\hat{\mathscr{I}}_H^C(\hat{v})\in\mathbb{P}_1(\hat{K})$ as

$$\hat{\mathscr{I}}_H^C(\hat{v}) = \sum_{i=0}^{d}\left(\int_{\hat{\sigma}_i}\hat{\psi}_{i,1}\,\hat{v}_i\right)\hat{\phi}_i,$$

with

$$\hat{v}_i = \begin{cases}\hat{v}|_{\hat{K}} & \text{if } K_i \text{ in (13.25) equals the mesh element } K,\\ \hat{v}|_{\hat{K}_i} & \text{otherwise,}\end{cases} \tag{13.26}$$

where $\hat{K}_i$ the unique element of $K^+\setminus\{\hat{K}\}$ that shares the face $\hat{\sigma}_i$ with $\hat{K}$. Note that this definition depends on the mesh element K through the definition of the Scott-Zhang interpolator. The definition of $\hat{\mathscr{I}}_H^C$ is such that one may verify, upon comparing with (13.25), that $\mathscr{I}_H^C(v_H)\circ\Phi_K=\hat{\mathscr{I}}_H^C(\hat{v}_H)$.

Step 3. The desired bound on the reference element.
We denote the set of faces of $\hat{K}$ by $\mathscr{F}(\hat{K})$ and define

$$|\hat{v}|^2_{\frac{1}{2},\partial\hat{K}} = \sum_{\hat{e}\in\mathscr{F}(\hat{K})}\int_{\hat{e}}[\![\hat{v}]\!]^2.$$

Note that $|\hat{v}|_{\frac{1}{2},\partial\hat{K}}=0$ implies that $\hat{v}$ has no jumps. Then $\hat{\mathscr{I}}_H^C(\hat{v})=\hat{v}$, because the Scott-Zhang interpolator is a projection on the space of continuous piecewise affine functions. In other words,

$$|\hat{v}|_{\frac{1}{2},\partial\hat{K}}=0 \text{ implies that } \hat{\mathscr{I}}_H^C(\hat{v})-\hat{v}=0. \tag{13.27}$$

Let us next denote by $\mathbb{P}_1(\hat{K}^+)^\star$ the quotient space of $\mathbb{P}_1(\hat{K}^+)$ by its subspace of continuous functions. One may verify that $|\cdot|^2_{\frac{1}{2},\partial\hat{K}}$ is a norm on $\mathbb{P}_1(\hat{K}^+)^\star$ in view of the preceeding remarks. Then we have

$$\sup_{\substack{\hat{v}\in\mathbb{P}_1(\hat{K}^+)^\star,\\ |\hat{v}|_{\frac{1}{2},\partial\hat{K}}=1}}\left|\hat{\mathscr{I}}_H^C(\hat{v})-\hat{v}\right|_{1,\hat{K}}\le C, \tag{13.28}$$

which is indeed bounded, since the supremum is taken over a compact set. (The set is closed and bounded, and the dimension of $\mathbb{P}_1(\hat{K}^+)^\star$ is finite.) The constant C in principle depends on the mesh element K, since the definition of $\hat{\mathscr{I}}_H^C$ depends on K through (13.26). Since the number of possibile choices in this definition is bounded independently of K and H, the constant C can be chosen as the maximum of the constants for all possible

choices so that (13.28) holds for all $K \in \mathscr{T}_H$ and for all H.

It follows from (13.27) and (13.28) that $\left|\hat{\mathscr{I}}_H^C(\hat{v}) - \hat{v}\right|_{1,\hat{K}} \le C|\hat{v}|_{\frac{1}{2},\partial\hat{K}}$ for all $\hat{v} \in \mathbb{P}_1(\hat{K}^+)$. Since $\hat{v}_H = v_H \circ \Phi_K$ on $\hat{K}$ and $\hat{\mathscr{I}}_H^C(\hat{v}_H) = \mathscr{I}_H^C(v_H) \circ \Phi_K$, we obtain

$$\left|\left(\mathscr{I}_H^C(v_H) - v_H\right) \circ \Phi_K\right|_{1,\hat{K}} \le C|\hat{v}_H|_{\frac{1}{2},\partial\hat{K}}, \tag{13.29}$$

with a constant C that does not depend on K, v_H and H.

Step 4. Application to the mesh element K.
Let us now return to the mesh element K. Denoting by $\mathfrak{A}_K$ the linear part of Φ_K, a change of variables yields

$$\begin{aligned}|\mathscr{I}_H^C(v_H) - v_H|_{1,K}^2 &= \int_K \left|\nabla\left[\mathscr{I}_H^C(v_H) - v_H\right]\right|^2 \\ &= \int_{\hat{K}} \left|\left(\nabla\left[\mathscr{I}_H^C(v_H) - v_H\right]\right) \circ \Phi_K\right|^2 |\det(\mathfrak{A}_K)|.\end{aligned}$$

Since $\nabla\left(\left[\mathscr{I}_H^C(v_H) - v_H\right] \circ \Phi_K\right) = \mathfrak{A}_K\left(\nabla\left[\mathscr{I}_H^C(v_H) - v_H\right]\right) \circ \Phi_K$, and in view of (13.18) and (13.17b), this yields

$$|\mathscr{I}_H^C(v_H) - v_H|_{1,K}^2 \le C H_K^{d-2} \int_{\hat{K}} \left|\nabla\left(\left[\mathscr{I}_H^C(v_H) - v_H\right] \circ \Phi_K\right)\right|^2,$$

where $H_K = \operatorname{diam}(K)$. Inserting (13.29), we have

$$|\mathscr{I}_H^C(v_H) - v_H|_{1,K}^2 \le C H_K^{d-2} |\hat{v}_H|_{\frac{1}{2},\partial\hat{K}}^2 = C H_K^{d-2} \sum_{\hat{e}\in\mathscr{F}(\hat{K})} \int_{\hat{e}} [\![\hat{v}_H]\!]^2. \tag{13.30}$$

It remains to transform the integrals in the latter sum to integrals over the faces of the original mesh element K. For any face e of K, let $\hat{e} = \Phi_K^{-1}(e)$ and set $A_e = |e|/|\hat{e}|$. Then, by a change of variables,

$$\int_{\hat{e}} [\![\hat{v}_H]\!]^2 = A_e^{-1} \int_e [\![v_H]\!]^2 \le \frac{C}{H_K^{d-1}} \int_e [\![v_H]\!]^2, \tag{13.31}$$

using (13.17b) for the inequality. Upon combing (13.30) and (13.31),

$$|\mathscr{I}_H^C(v_H) - v_H|_{1,K}^2 \le \frac{C}{H_K} \sum_{e\in\mathscr{F}(K)} \int_e [\![v_H]\!]^2 \le \frac{C}{H} \sum_{e\in\mathscr{F}(K)} \int_e [\![v_H]\!]^2$$

the second inequality using quasi-uniformity (13.21). Finally summing over all mesh elements K, we obtain

$$|\mathscr{I}_H^C(v_H) - v_H|_{1,\mathscr{T}_H}^2 \le \frac{C}{H} \sum_{e\in\mathscr{E}_H} \int_e [\![v_H]\!]^2.$$

This completes the proof in view of the definition of $|v_H|_{\frac{1}{2},\mathscr{E}_H}$. ■

The two final classical properties that we will need are an approximation and a stability property for the interpolation operator on the Crouzeix-Raviart $\mathbb{P}_1$ space V_H^{CR}. We denote

it by $\mathscr{I}_H^{NC}$. For any $v \in H^1(\Omega)$ we define $\mathscr{I}_H^{NC}$ by

$$\forall\, e \in \mathscr{E}_H, \quad \int_e \mathscr{I}_H^{NC}(v) = \int_e v. \tag{13.32}$$

Then, under the mesh regularity assumptions (13.17), we have the following classical interpolation result (see [73, Theorem 1.103]): there exists $C > 0$ such that, for all $K \in \mathscr{T}_H$, and all $v \in H^2(K)$, we have

$$|v - \mathscr{I}_H^{NC}(v)|_{1,K} \leq CH|v|_{2,K}. \tag{13.33}$$

This property allows us to establish the following lemma.

Lemma 13.10. *For all $u \in H^2(\Omega)$, for all $H > 0$, it holds*

$$|v - \mathscr{I}_H^{NC}(v)|_{1,\mathscr{T}_H} \leq CH|v|_{2,\Omega}$$

and, for the seminorm $|\cdot|_{\frac{1}{2},\mathscr{E}_H}$ defined in (13.24), it holds

$$|\mathscr{I}_H^{NC}(v)|_{\frac{1}{2},\mathscr{E}_H} \leq CH|v|_{2,\Omega}.$$

Proof. The first inequality is a direct consequence of (13.33). For the second inequality, we temporarily fix $e \in \mathscr{E}_H$. Let K_1 and K_2 be the two mesh elements sharing the face e. The analysis is analogous when $e \subset \partial\Omega$ and $K_2 = \varnothing$. The seminorm $|\mathscr{I}_H^{NC}(v)|_{\frac{1}{2},\mathscr{E}_H}$ comprises a sum over the jump norms $\left\|[\![\mathscr{I}_H^{NC}(v)]\!]\right\|_{0,e}^2$. Since $v \in H^2(\Omega)$, its jump across e is zero, so that we have

$$\begin{aligned}\left\|[\![\mathscr{I}_H^{NC}(v)]\!]\right\|_{0,e}^2 &= \left\|[\![v - \mathscr{I}_H^{NC}(v)]\!]\right\|_{0,e}^2, \\ &\leq 2\left\|\left(v - \mathscr{I}_H^{NC}(v)\right)\big|_{K_1}\right\|_{0,e}^2 + 2\left\|\left(v - \mathscr{I}_H^{NC}(v)\right)\big|_{K_2}\right\|_{0,e}^2,\end{aligned}$$

the inequality resulting from a triangle inequality and Young's inequality. By (13.32), $\int_e v - \mathscr{I}_H^{NC}(v) = 0$, so we can apply Lemma 13.7, followed by (13.33), which yields

$$\left\|[\![\mathscr{I}_H^{NC}(v)]\!]\right\|_{0,e}^2 \leq CH\left(\left|\left(v - \mathscr{I}_H^{NC}(v)\right)\right|_{1,\{K_1,K_2\}}^2\right) \leq CH^3|v|_{2,K_1\cup K_2}.$$

Inserting this inequality in the definition of $|\mathscr{I}_H^{NC}(v)|_{\frac{1}{2},\mathscr{E}_H}$ shows the desired result. ■

13.4. Three central estimates

The proof of Theorem 13.1 essentially relies on an interpolation estimate for the multiscale space V_H^ε that is given in Corollary 13.14 and a bound on the non-conforming error for the MsFEM-CR provided in Lemma 13.15. In order to make the dependence on ε explicit in these estimates, we frequently use a homogenization result related to functions of the multiscale space V_H^ε that is stated as the first result of this section in Lemma 13.11.

Throughout this section, for any function ϕ, we use the notation ϕ_ε (with a subscript ε) to define the rescaled function $\phi_\varepsilon(\cdot) = \phi(\cdot/\varepsilon)$.

13.4.1. First-order reconstruction for the multiscale finite element space. It is essential for the convergence analysis of the MsFEM to study the behaviour of the multiscale finite element functions defined in (13.7) as $\varepsilon \to 0$. We recall that any MsFEM function $v_H^\varepsilon \in V_H^\varepsilon$ satisfies (13.9). Since either of the two possible choices for V_K contains the space of compactly supported test functions $\mathscr{C}_c^\infty(K)$, we obtain, for any $K \in \mathscr{T}_H$,

$$-\operatorname{div}(A^\varepsilon \nabla v_H^\varepsilon) = 0 \quad \text{in } K.$$

The homogenized limit of v_H^ε is v_H because $A^\star$ (see (13.13)) is constant and the boundary conditions of v_H^ε are preserved when we pass to the limit. It can thus be expected that v_H^ε is, at least when ε is small, close to its first-order two-scale reconstruction defined analogously to $u^{\varepsilon,1}$ in (13.15).

Rather than exactly following (13.15), we introduce a truncation close to the boundary of the mesh elements in order to obtain a homogenization estimate for the flux $A^\varepsilon \nabla v_H^\varepsilon$ in Lemma 13.11. The truncation is necessary, because the expansion (13.15) is highly oscillatory near the boundary, whereas v_H is not, resulting in a highly oscillatory boundary layer. The exact definition of this truncated first-order expansion is, for any $v_H \in V_H$, the function $v_H^{\varepsilon,1}$ given by

$$v_H^{\varepsilon,1}\big|_K = v_H + \varepsilon \sum_{\alpha=1}^d \tau_H\, \partial_\alpha(v_H|_K)(w_\alpha)_\varepsilon \quad \text{for all } K \in \mathscr{T}_H, \tag{13.34}$$

where τ_H is the cut-off function from Lemma 13.5, which vanishes around the interfaces of the mesh.

A homogenization estimate for the convergence of $A^\varepsilon \nabla v_H^{\varepsilon,1}$ towards $A^\star \nabla v_H$ is given in the following lemma. The difference between $v_H^{\varepsilon,1}$ and the actual MsFEM function v_H^ε defined by (13.7) will be studied below in Lemma 13.13.

Lemma 13.11. *Let $v_H \in V_H$ and introduce $v_H^{\varepsilon,1}$ by (13.34). Suppose that the family of meshes $(\mathscr{T}_H)_H$ is quasi-uniform and that $\varepsilon \le H$. Then*

$$A^\varepsilon \nabla v_H^{\varepsilon,1} = A^\star \nabla v_H + R(v_H), \tag{13.35}$$

where $R(v_H)$ satisfies, for any $K \in \mathscr{T}_H$ and any $q \in H^1(K)$,

$$\left| \int_K R(v_H) \cdot \nabla q \right| \le C \sqrt{\frac{\varepsilon}{H}} |v_H|_{1,K} |q|_{1,K}.$$

Proof. Fix any $K \in \mathscr{T}_H$. The combination of (13.34) and (13.16) shows that (13.35) holds for

$$R(v_H) = (1-\tau_H)(A^\varepsilon - A^\star)\nabla v_H + A^\varepsilon \left(\sum_{\alpha=1}^d \varepsilon \nabla \tau_H\, \partial_\alpha(v_H|_K)(w_\alpha)_\varepsilon \right) + \tau_H \left[\sum_{\alpha=1}^d \sum_{i=1}^d \partial_\alpha\left(v_H|_K\right)\left(\partial_i [Z_\alpha]_{i,j}\right)_\varepsilon \right]_{1\le j\le d},$$

with a skew-symmetric matrix $Z_\alpha \in H^1_{per}(Q)^{d\times d}$. Upon multiplication by ∇q and integra-

tion over K, the third term becomes

$$\sum_{\alpha,i,j=1}^{d} \int_K \tau_H \, \partial_\alpha v_H \, (\partial_i [Z_\alpha]_{i,j})_\varepsilon \, \partial_j q = \sum_{\alpha,i,j=1}^{d} \varepsilon \int_K \partial_i \tau_H \, \partial_\alpha v_H \, ([Z_\alpha]_{i,j})_\varepsilon \, \partial_j q,$$

by an integration by parts over the derivative with index i, using that $(\partial_i \phi)_\varepsilon = \varepsilon \partial_i (\phi_\varepsilon)$ for any function ϕ. The boundary term vanishes because $\tau_H = 0$ on ∂K. The terms with a second derivative on q, i.e., $\tau_H \, \partial_\alpha v_H \, ([Z_\alpha]_{i,j})_\varepsilon \, \partial_{j,i} q$ vanish under the sum over i and j, because Z_α is skew-symmetric. Also note that $\partial_{\alpha,i} v_H = 0$ because v_H is affine on K. It thus holds,

$$\left| \int_K R(v_H) \cdot \nabla q \right| \leq \int_{K_b^\varepsilon} \|A^\varepsilon - A^\star\| \cdot \|\nabla v_H\| \cdot \|\nabla q\| + \sum_{\alpha=1}^{d} \int_{K_b^\varepsilon} \|A^\varepsilon\| \cdot \|\nabla q\| \cdot |\partial_\alpha v_H (w_\alpha)_\varepsilon| + \sum_{\alpha,i,j=1}^{d} \int_{K_b^\varepsilon} |\partial_\alpha v_H| \cdot \left| ([Z_\alpha]_{i,j})_\varepsilon \right| \cdot |\partial_j q|,$$

recalling the properties of τ_H stated in Lemma 13.5 and recalling that $K_b^\varepsilon = K \setminus K_{in}^\varepsilon$. Note in particular that $\nabla \tau_H$ vanishes on K_{in}^ε.

To bound these terms, we use the fact that A^ε and $A^\star$ are uniformly bounded ($A^\star$ is even constant) on Ω, and that $w_\alpha \in L^2_{per}(Q)$ and $Z_\alpha \in L^2_{per}(Q)^{d \times d}$. The Cauchy-Schwarz inequality thus yields

$$\left| \int_K R(v_H) \cdot \nabla q \right| \leq C \|\nabla q\|_{0,K} \left(\|\nabla v_H\|_{0,K_b^\varepsilon} + \sum_{\alpha=1}^{d} \|\partial_\alpha v_H \, (w_\alpha)_\varepsilon\|_{0,K_b^\varepsilon} + \|\partial_\alpha v_H \, (Z_\alpha)_\varepsilon\|_{0,K_b^\varepsilon} \right). \tag{13.36}$$

Let ϕ be any function in $L^2_{per}(Q)$. Since ∇v_H is constant in K, we have

$$\begin{aligned} \|(\partial_\alpha v_H) \; \phi_\varepsilon\|^2_{0,K_b^\varepsilon} &= |\partial_\alpha (v_H|_K)|^2 \, \|\phi_\varepsilon\|^2_{0,K_b^\varepsilon} \\ &\leq |\partial_\alpha (v_H|_K)|^2 \, \|\phi_\varepsilon\|^2_{0,K_{band}^\varepsilon} \\ &= \sum_{i \in \mathscr{I}_K^\varepsilon} |\partial_\alpha (v_H|_K)|^2 \, \|\phi_\varepsilon\|^2_{0,\varepsilon(i+Q)}, \end{aligned}$$

where K_{band}^ε and $\mathscr{I}_K^\varepsilon$ are as defined in Lemma 13.6. Applying the results of this lemma, we further obtain

$$\begin{aligned} \sum_{i \in \mathscr{I}_K^\varepsilon} |\partial_\alpha (v_H|_K)|^2 \, \|\phi_\varepsilon\|^2_{0,\varepsilon(i+Q)} &= \varepsilon^d \, (\# \mathscr{I}_K^\varepsilon) \, |\partial_\alpha (v_H|_K)|^2 \, \|\phi\|^2_{0,Q} \\ &\leq C \frac{\varepsilon}{H} |K| \, |\partial_\alpha (v_H|_K)|^2 \, \|\phi\|^2_{0,Q} = C \frac{\varepsilon}{H} \|\partial_\alpha v_H\|^2_{0,K} \, \|\phi\|^2_{0,Q}. \end{aligned}$$

Since the functions w_α and the entries of Z_α belong to $L^2_{per}(Q)$, the above argument

can be applied in (13.36) and leads to the estimate

$$\|\nabla v_H\|_{0,K_b^\varepsilon} + \sum_{\alpha=1}^{d} \|\partial_\alpha v_H\,(w_\alpha)_\varepsilon\|_{0,K_b^\varepsilon} + \|\partial_\alpha v_H (Z_\alpha)_\varepsilon\|_{0,K_b^\varepsilon} \le C\sqrt{\frac{\varepsilon}{H}}\|\nabla v_H\|_{0,K}.$$

Inserting this inequality in (13.36) completes the proof. ■

13.4.2. Interpolation estimate. Here we show the following interpolation result for our multiscale finite element space V_H^ε. More precisely, the interpolation quality of V_H^ε is expressed in terms of approximation properties of the underlying $\mathbb{P}_1$ space V_H. We start with an interpolation result for the (truncated) first-order two-scale reconstruction of (13.34) in Lemma 13.12. The interpolation property for the space V_H^ε will follow below in Corollary 13.14.

Lemma 13.12. *Let u^ε and $u^\star$ be the solutions to (13.1) and (13.14), respectively, and suppose that the family of meshes $(\mathscr{T}_H)_H$ is quasi-uniform and that $\varepsilon \le H$. Let $v_H \in V_H$ be arbitrary and define $v_H^{\varepsilon,1}$ in each $K \in \mathscr{T}_H$ by (13.34). Then*

$$|u^\varepsilon - v_H^{\varepsilon,1}|_{1,\mathscr{T}_H} \le C\left(|u^\star - v_H|_{1,\mathscr{T}_H} + |v_H|_{\frac{1}{2},\mathscr{E}_H} + \sqrt{\frac{\varepsilon}{H}}|v_H|_{1,\mathscr{T}_H}\right).$$

We recall that $\mathscr{E}_H$ denotes the set of faces of the mesh and that $|v_H|_{\frac{1}{2},\mathscr{E}_H}$ is defined in (13.24).

Proof. Fix $v_H \in V_H$ and set $v_{H,C} = \mathscr{I}_H^C(v_H)$. We recall that $\mathscr{I}_H^C$ denotes the Scott-Zhang interpolation operator from Section 13.3.5. Note that $v_{H,C} = v_H$ when v_H is continuous, but that the interpolant is in general different from v_H itself. Defining the truncated first-order expansions $v_{H,C}^{\varepsilon,1}$ and $v_H^{\varepsilon,1}$ as in (13.34), we have, by the triangle inequality,

$$|u^\varepsilon - v_H^{\varepsilon,1}|_{1,\mathscr{T}_H} \le |u^\varepsilon - v_{H,C}^{\varepsilon,1}|_{1,\Omega} + |v_{H,C}^{\varepsilon,1} - v_H^{\varepsilon,1}|_{1,\mathscr{T}_H}. \tag{13.37}$$

To treat the first term in (13.37), we set $q = u^\varepsilon - v_{H,C}^{\varepsilon,1}$. Then we apply Lemma 13.11 to $v_{H,C}$ and we use (13.3) to obtain

$$\begin{aligned}|u^\varepsilon - v_{H,C}^{\varepsilon,1}|_{1,\Omega}^2 &\le C\int_\Omega \nabla q \cdot A^\varepsilon \nabla(u^\varepsilon - v_{H,C}^{\varepsilon,1}) \\ &= C\int_\Omega \nabla q \cdot (A^\varepsilon \nabla u^\varepsilon - A^\star \nabla v_{H,C} - R(v_{H,C}))\,.\end{aligned}$$

Since $q \in H_0^1(\Omega)$, we deduce from (13.2) and (13.14) that

$$\int_\Omega \nabla q \cdot A^\varepsilon \nabla u^\varepsilon = \int_\Omega fq = \int_\Omega \nabla q \cdot A^\star \nabla u^\star.$$

Therefore,

$$|u^\varepsilon - v_{H,C}^{\varepsilon,1}|_{1,\Omega}^2 \le C\int_\Omega |\nabla q \cdot A^\star \nabla(u^\star - v_{H,C})| + |\nabla q \cdot R(v_{H,C})|.$$

Applying the Cauchy-Schwarz inequality, (13.3) and Lemma 13.11 and cancelling by

$|q|_{1,\Omega} = |u^\varepsilon - v^{\varepsilon,1}_{H,C}|_{1,\Omega}$ yields

$$|u^\varepsilon - v^{\varepsilon,1}_{H,C}|_{1,\Omega} \leq C \left(|u^\star - v_{H,C}|_{1,\Omega} + \sqrt{\frac{\varepsilon}{H}} |v_{H,C}|_{1,\Omega} \right).$$

Then we apply Lemma 13.9 to obtain

$$|u^\varepsilon - v^{\varepsilon,1}_{H,C}|_{1,\Omega} \leq C \left(|u^\star - v_H|_{1,\mathscr{T}_H} + |v_H|_{\frac{1}{2},\mathscr{E}_H} + \sqrt{\frac{\varepsilon}{H}} |v_H|_{1,\mathscr{T}_H} \right). \tag{13.38}$$

For the second term in (13.37) (which in fact vanishes if $V_H = V_H^{\mathsf{lin}}$ defined in (13.4a)), we apply Lemma 13.11 to the function $w_H = v_{H,C} - v_H$ on each $K \in \mathscr{T}_H$. This yields (using again the bounds in (13.3), and the Cauchy-Schwarz inequality in the last line)

$$\begin{aligned} |w_H^{\varepsilon,1}|^2_{1,\mathscr{T}_H} &\leq C \sum_{K \in \mathscr{T}_H} \int_K \nabla w_H^{\varepsilon,1} \cdot A^\varepsilon \nabla w_H^{\varepsilon,1} \\ &= C \sum_{K \in \mathscr{T}_H} \int_K \nabla w_H^{\varepsilon,1} \cdot A^\star \nabla w_H + \int_K R(w_H) \cdot \nabla w_H^{\varepsilon,1} \\ &\leq C |w_H^{\varepsilon,1}|_{1,\mathscr{T}_H} \left(|w_H|_{1,\mathscr{T}_H} + \sqrt{\frac{\varepsilon}{H}} |w_H|_{1,\mathscr{T}_H} \right). \end{aligned}$$

Simplifying by $|w_H^{\varepsilon,1}|_{1,\mathscr{T}_H}$ and applying Lemma 13.9 to $w_H = v_{H,C} - v_H$, we obtain

$$|v^{\varepsilon,1}_{H,C} - v^{\varepsilon,1}_H|_{1,\mathscr{T}_H} \leq C \left(1 + \sqrt{\frac{\varepsilon}{H}} \right) |v_H|_{\frac{1}{2},\mathscr{E}_H} \leq C |v_H|_{\frac{1}{2},\mathscr{E}_H}, \tag{13.39}$$

the last inequality being true because $\varepsilon \leq H$.

The lemma is now shown upon inserting (13.38) and (13.39) in (13.37). ■

We now provide a bound on the difference between the truncated reconstruction $v_H^{\varepsilon,1}$ and the multiscale function v_H^ε.

Lemma 13.13. *Suppose that the family of meshes $(\mathscr{T}_H)_H$ is quasi-uniform. Let $v_H \in V_H$ be arbitrary and define v_H^ε by (13.7) and $v_H^{\varepsilon,1}$ by (13.34) for all $K \in \mathscr{T}_H$. It holds*

$$|v_H^\varepsilon - v_H^{\varepsilon,1}|_{1,\mathscr{T}_H} \leq C \sqrt{\frac{\varepsilon}{H}} |v_H|_{1,\mathscr{T}_H}.$$

Proof. We temporarily fix a mesh element $K \in \mathscr{T}_H$ and set $r = v_H^{\varepsilon,1} - v_H^\varepsilon$ on K. By (13.3) and Lemma 13.11 applied to v_H, we have

$$|v_H^{\varepsilon,1} - v_H^\varepsilon|^2_{1,K} \leq C \int_K \nabla r \cdot A^\varepsilon \nabla (v_H^{\varepsilon,1} - v_H^\varepsilon) = \int_K \nabla r \cdot (A^\star \nabla v_H - A^\varepsilon \nabla v_H^\varepsilon + R(v_H)). \tag{13.40}$$

Note that (13.7) and (13.34) imply that $r \in V_K$. In particular, r vanishes on average on the faces of K for either of the two choices of V_K that we consider; see (13.5). Since, moreover, $A^\star$ and ∇v_H are constant on K, an integration by parts shows that

$$\int_K \nabla r \cdot A^\star \nabla v_H = A^\star \nabla v_H \cdot \int_{\partial K} r \, \vec{n} = 0. \tag{13.41}$$

Since $r \in V_K$, it can be used as a test function in (13.9). Therefore,

$$\int_K \nabla r \cdot A^\varepsilon \nabla v_H^\varepsilon = a_K^\varepsilon(v_H^\varepsilon, r) = 0. \tag{13.42}$$

Combining (13.40), (13.41) and (13.42), and applying Lemma 13.11 to bound the term containing $R(v_H)$, we obtain

$$|v_H^{\varepsilon,1} - v_H^\varepsilon|_{1,K} \leq C\sqrt{\frac{\varepsilon}{H}}|v_H|_{1,K},$$

after simplification on both sides by $|r|_{1,K}$. Squaring and summing this inequality over all mesh elements yields the desired result. ■

As an immediate corollary to Lemmas 13.12 and 13.13, we obtain the following interpolation result for the multiscale space V_H^ε.

Corollary 13.14. *Let u^ε and $u^\star$ be the solutions to (13.1) and (13.14), respectively, and suppose that the family of meshes $(\mathscr{T}_H)_H$ is quasi-uniform and that $\varepsilon \leq H$. Let $v_H \in V_H$ be arbitrary and define v_H^ε by (13.7). Then*

$$|u^\varepsilon - v_H^\varepsilon|_{1,\mathscr{T}_H} \leq C\left(|u^\star - v_H|_{1,\mathscr{T}_H} + |v_H|_{\frac{1}{2},\mathscr{E}_H} + \sqrt{\frac{\varepsilon}{H}}|v_H|_{1,\mathscr{T}_H}\right).$$

13.4.3. Non-conforming error. The analysis of the MsFEM-CR requires one additional ingredient with respect to the analysis of the MsFEM-lin. Due to the fact that the approximation space is not a subspace of $H^1(\Omega)$, the non-conforming error in Lemma 13.4 is nonzero. A useful estimate for the non-conforming error is given by the following lemma.

Lemma 13.15. *Let u^ε, u_H^ε and $u^\star$ be the solutions to (13.1), (13.10) and (13.14), respectively, and suppose that $u^\star \in H^2(\Omega)$. Let V_H^{CR} be the $\mathbb{P}_1$ Crouzeix-Raviart space defined in (13.4b) and V_H^ε the associated MsFEM space defined by (13.8). Also suppose that the family of meshes $(\mathscr{T}_H)_H$ is quasi-uniform and that $\varepsilon \leq H$. Then, for any $v_H \in V_H$, it holds*

$$\sup_{w_H^\varepsilon \in V_H^\varepsilon \setminus \{0\}} \frac{\left|\sum_{K\in\mathscr{T}_H} a_K^\varepsilon(u^\varepsilon - u_H^\varepsilon, w_H^\varepsilon)\right|}{|w_H^\varepsilon|_{1,\mathscr{T}_H}} \leq C\left(H|u^\star|_{2,\Omega} + |u^\star - v_H|_{1,\mathscr{T}_H} + |v_H|_{\frac{1}{2},\mathscr{E}_H} + \sqrt{\frac{\varepsilon}{H}}|v_H|_{1,\mathscr{T}_H}\right).$$

Proof. Let $w_H^\varepsilon \in V_H^\varepsilon$ be arbitrary. For any $v_H \in V_H$, associating to it $v_H^{\varepsilon,1}$ by (13.34), we have

$$\sum_{K\in\mathscr{T}_H} a_K^\varepsilon(u^\varepsilon - u_H^\varepsilon, w_H^\varepsilon) = \sum_{K\in\mathscr{T}_H} a_K^\varepsilon(u^\varepsilon - v_H^{\varepsilon,1}, w_H^\varepsilon) + \sum_{K\in\mathscr{T}_H} a_K^\varepsilon(v_H^{\varepsilon,1} - u_H^\varepsilon, w_H^\varepsilon). \tag{13.43}$$

We can apply Lemma 13.12 to the terms in the first sum, which yields

$$\begin{aligned}\left|\sum_{K\in\mathscr{T}_H} a_K^\varepsilon\big(u^\varepsilon - v_H^{\varepsilon,1}, w_H^\varepsilon\big)\right| &\le C|u^\varepsilon - v_H^{\varepsilon,1}|_{1,\Omega}|w_H^\varepsilon|_{1,\mathscr{T}_H}\\ &\le C\left(|u^\star - v_H|_{1,\mathscr{T}_H} + |v_H|_{\frac{1}{2},\mathscr{E}_H} + \sqrt{\frac{\varepsilon}{H}}|v_H|_{1,\mathscr{T}_H}\right)|w_H^\varepsilon|_{1,\mathscr{T}_H}.\end{aligned} \tag{13.44}$$

Regarding the second sum in (13.43), since u_H^ε solves (13.10), it holds

$$\sum_{K\in\mathscr{T}_H} a_K^\varepsilon(u_H^\varepsilon, w_H^\varepsilon) = \int_\Omega f\, w_H^\varepsilon = \sum_{K\in\mathscr{T}_H}\int_K \nabla w_H^\varepsilon\cdot A^\star\nabla u^\star - \int_{\partial K} w_H^\varepsilon\,\vec{n}\cdot A^\star\nabla u^\star, \tag{13.45}$$

where we introduce the homogenized limit $u^\star$ of u^ε by using (13.14) and an integration by parts in the second equality. Next, applying Lemma 13.11 to v_H, we have

$$\sum_{K\in\mathscr{T}_H} a_K^\varepsilon\big(v_H^{\varepsilon,1}, w_H^\varepsilon\big) = \sum_{K\in\mathscr{T}_H}\int_K \nabla w_H^\varepsilon\cdot A^\star\nabla v_H + \int_K \nabla w_H^\varepsilon\cdot R(v_H) \tag{13.46}$$

Combining (13.45) and (13.46), we can thus write

$$\begin{aligned}\sum_{K\in\mathscr{T}_H} a_K^\varepsilon\big(v_H^{\varepsilon,1} - u_H^\varepsilon, w_H^\varepsilon\big) = \sum_{K\in\mathscr{T}_H}\int_K \nabla w_H^\varepsilon\cdot A^\star\nabla(v_H - u^\star) + \int_K \nabla w_H^\varepsilon\cdot R(v_H) +\\ \int_{\partial K} w_H^\varepsilon\,\vec{n}\cdot A^\star\nabla u^\star.\end{aligned}$$

Using the Cauchy-Schwarz inequality for the first term on the right-hand side and inserting the estimate of Lemma 13.11 for the second term, it follows

$$\begin{aligned}\left|\sum_{K\in\mathscr{T}_H} a_K^\varepsilon\big(v_H^{\varepsilon,1} - u_H^\varepsilon, w_H^\varepsilon\big)\right| \le C\Bigg(&|u^\star - v_H|_{1,\mathscr{T}_H}\,|w_H^\varepsilon|_{1,\mathscr{T}_H} + \sqrt{\frac{\varepsilon}{H}}|v_H|_{1,K}\,|w_H^\varepsilon|_{1,K}\\ &+\left|\sum_{e\in\mathscr{E}_H}\int_e [\![w_H^\varepsilon]\!]\,\vec{n}_e\cdot A^\star\nabla u^\star\right|\Bigg),\end{aligned} \tag{13.47}$$

where we choose for every face e of $\mathscr{T}_H$ an orientation of the unit normal vector $\vec{n}_e$ on e, and where $[\![w_H^\varepsilon]\!]$ is defined as follows: let $K_1(e)$ and $K_2(e)$ be the two mesh elements sharing the face e, and, for definiteness, let $\vec{n}_e$ be the unit outward normal to $K_1(e)$ on e, and let $(w_H^\varepsilon)_1 = w_H^\varepsilon|_{K_1(e)}$, and $(w_H^\varepsilon)_2 = w_H^\varepsilon|_{K_2(e)}$, then $[\![w_H^\varepsilon]\!] = (w_H^\varepsilon)_1|_e - (w_H^\varepsilon)_2|_e$; when e lies on $\partial\Omega$ (and $K_2(e) = \varnothing$), we simply set $[\![w_H^\varepsilon]\!] = (w_H^\varepsilon)_1|_e$. It remains to bound the terms involving the jumps of w_H^ε.

Note that, by definition of the multiscale space V_H^ε, it holds for all $e \in \mathscr{E}_H$ that $\int_e [\![w_H^\varepsilon]\!] = 0$. Therefore, setting $c_e = \int_e \vec{n}_e\cdot A^\varepsilon\nabla u^\star$, it holds

$$\sum_{e\in\mathscr{E}_H}\int_e [\![w_H^\varepsilon]\!]\,\vec{n}_e\cdot A^\star\nabla u^\star = \sum_{e\in\mathscr{E}_H}\int_e [\![w_H^\varepsilon]\!]\,\left(\vec{n}_e\cdot A^\star\nabla u^\star - c_e\right),$$

and, by the Cauchy-Schwarz inequality, we obtain

$$\left|\sum_{e\in\mathscr{E}_H}\int_e [\![w_H^\varepsilon]\!]\,\vec{n}_e\cdot A^\star\nabla u^\star\right| \leq \sum_{e\in\mathscr{E}_H}\|[\![w_H^\varepsilon]\!]\|_{0,e}\,\|\vec{n}_e\cdot A^\star\nabla u^\star - c_e\|_{0,e}.$$

For any $e\in\mathscr{E}_H$, we can now apply Lemma 13.7 to the function $\vec{n}_e\cdot A^\star\nabla u^\star - c_e$, which has zero average on e (by definition of c_e). We can also apply Lemma 13.8 to w_H^ε. Then it follows,

$$\begin{aligned}\left|\sum_{e\in\mathscr{E}_H}\int_e [\![w_H^\varepsilon]\!]\,\vec{n}_e\cdot A^\star\nabla u^\star\right| &\leq CH\sum_{e\in\mathscr{E}_H}|w_H^\varepsilon|_{1,\{K_1(e),K_2(e)\}}\,|u^\star|_{2,K_1(e)}\\ &\leq CH|w_H^\varepsilon|_{1,\mathscr{T}_H}\,|u^\star|_{2,\Omega},\end{aligned}\tag{13.48}$$

where the second inequality is obtained by a discrete Cauchy-Schwarz inequality.

We now insert (13.48) in (13.47) and use the resulting inequality and (13.44) to bound the two sums in (13.43) after applying a triangle inequality. The lemma is then proved upon division by $|w_H^\varepsilon|_{1,\mathscr{T}_H}$. ■

13.5. Proof of Theorem 13.1

We can now prove the main result of part III of the thesis.

Proof of Theorem 13.1. Let $v_H\in V_H$ be the following interpolant of the homogenized limit $u^\star$ of u^ε in the underlying $\mathbb{P}_1$ space: for the MsFEM-lin, we set $v_H=\mathscr{I}_H^C(u^\star)$, the Scott-Zhang interpolant in the Lagrange $\mathbb{P}_1$ space, and for the MsFEM-CR we set $v_H=\mathscr{I}_H^{NC}(u^\star)$ the interpolant in the Crouzeix-Raviart $\mathbb{P}_1$ space defined in (13.32). Using Lemma 13.3 in the case of the MsFEM-lin or Lemma 13.4 for the MsFEM-CR, we find that

$$|u^\varepsilon-u_H^\varepsilon|_{1,\mathscr{T}_H}\leq C|u^\varepsilon-v_H^\varepsilon|_{1,\mathscr{T}_H}+E_{nc},$$

where $v_H^\varepsilon\in V_H^\varepsilon$ is defined in terms of v_H by (13.7) and the non-conforming error E_{nc} is zero for the MsFEM-lin and given by the second term on the right-hand side in Lemma 13.4 for the MsFEM-CR.

We estimate the interpolation error $|u^\varepsilon-v_H^\varepsilon|_{1,\mathscr{T}_H}$ by means of Corollary 13.14, and E_{nc} by Lemma 13.15, to obtain

$$|u^\varepsilon-u_H^\varepsilon|_{1,\mathscr{T}_H}\leq C\left(H|u^\star|_{2,\Omega}+|u^\star-v_H|_{1,\mathscr{T}_H}+|v_H|_{\frac12,\mathscr{E}_H}+\sqrt{\frac{\varepsilon}{H}}|v_H|_{1,\mathscr{T}_H}\right).$$

In the case of the MsFEM-lin, we note that $|v_H|_{\frac12,\mathscr{E}_H}=0$ and we use Lemma 13.9 to estimate $|u^\star-v_H|_{1,\mathscr{T}_H}$. We employ Lemma 13.10 in the case of the MsFEM-CR. In both cases, we conclude that

$$|u^\varepsilon-u_H^\varepsilon|_{1,\mathscr{T}_H}\leq C\left(H|u^\star|_{2,\Omega}+\sqrt{\frac{\varepsilon}{H}}|v_H|_{1,\mathscr{T}_H}\right).$$

Finally, we note that $|v_H|_{1,\mathscr{T}_H}\leq|v_H-u^\star|_{1,\mathscr{T}_H}+|u^\star|_{1,\Omega}$, and we apply Lemma 13.9 or 13.10

to obtain

$$\sqrt{\frac{\varepsilon}{H}}|v_H|_{1,\mathscr{T}_H} \leq \sqrt{\varepsilon H}|u^\star|_{2,\Omega} + \sqrt{\frac{\varepsilon}{H}}|u^\star|_{1,\Omega}.$$

Since $\varepsilon \leq H$, combining the last two inequalities leads to

$$|u^\varepsilon - u_H^\varepsilon|_{1,\mathscr{T}_H} \leq C\left(H|u^\star|_{2,\Omega} + \sqrt{\frac{\varepsilon}{H}}|u^\star|_{1,\Omega}\right),$$

and the proof is complete. ■

Bibliography

[1] J. Aarnes and T. Y. Hou. Multiscale Domain Decomposition Methods for Elliptic Problems with High Aspect Ratios. *Acta Mathematicae Applicatae Sinica, English Series*, 18(1):63–76, 2002.

[2] A. Abdulle. The Finite Element Heterogeneous Multiscale Method: a computational strategy for multiscale PDEs. *GAKUTO International Series - Mathematical Sciences and Applications*, 31:133–181, 2009.

[3] A. Abdulle, D. Arjmand, and E. Paganoni. A parabolic local problem with exponential decay of the resonance error for numerical homogenization. *Mathematical Models and Methods in Applied Sciences*, 31(13):2733–2772, 2021.

[4] A. Abdulle, D. Arjmand, and E. Paganoni. An Elliptic Local Problem with Exponential Decay of the Resonance Error for Numerical Homogenization. *Multiscale Modeling & Simulation*, 21(2):513–541, 2023.

[5] A. Abdulle, W. E, B. Engquist, and E. Vanden-Eijnden. The heterogeneous multiscale method. *Acta Numerica*, 21:1–87, 2012.

[6] A. Abdulle and M. E. Huber. Discontinuous Galerkin finite element heterogeneous multiscale method for advection–diffusion problems with multiple scales. *Numerische Mathematik*, 126(4):589–633, 2014.

[7] G. Allaire. *Shape Optimization by the Homogenization Method*. S. S. Antman, J. E. Marsden, and L. Sirovich, editors, volume 146 of *Applied Mathematical Sciences*. Springer New York, New York, NY, 2002.

[8] G. Allaire. *Analyse Numérique et Optimisation*. Éditions de l'École Polytechnique, Palaiseau, 2012.

[9] G. Allaire and R. Brizzi. A Multiscale Finite Element Method for Numerical Homogenization. *Multiscale Modeling & Simulation*, 4(3):790–812, 2005.

[10] G. Allaire, S. Desroziers, G. Enchéry, and F. Ouaki. A Multiscale Finite Element Method for Transport Modeling. In *Proceedings of the 6th European Congress on Computational Methods in Applied Sciences and Engineering*, pages 3052–3069, Vienna, Austria, 2012.

[11] D. N. G. Allen and R. V. Southwell. Relaxation methods applied to determine the motion in two dimensions of a viscous fluid past a fixed cylinder. *The Quarterly Journal of Mechanics and Applied Mathematics*, 8(2):129–145, 1955.

[12] R. Altmann, P. Henning, and D. Peterseim. Numerical homogenization beyond scale separation. *Acta Numerica*, 30:1–86, 2021.

[13] J.-B. Apoung Kamga and O. Pironneau. Numerical zoom for multiscale problems with an application to nuclear waste disposal. *Journal of Computational Physics*, 224(1):403–413, 2007.

[14] T. Arbogast. Implementation of a Locally Conservative Numerical Subgrid Upscaling Scheme for Two-Phase Darcy Flow. *Computational Geosciences*, 6:453–481, 2002.

[15] T. Arbogast. Mixed Multiscale Methods for Heterogeneous Elliptic Problems. In I. G. Graham, T. Y. Hou, O. Lakkis, and R. Scheichl, editors, *Numerical Analysis of Multiscale Problems*. Volume 83, pages 243–283. Springer Berlin Heidelberg, Berlin, Heidelberg, 2012.

[16] T. Arbogast, G. Pencheva, M. F. Wheeler, and I. Yotov. A Multiscale Mortar Mixed Finite Element Method. *Multiscale Modeling & Simulation*, 6(1):319–346, 2007.

[17] B. Ayuso and L. D. Marini. Discontinuous Galerkin Methods for Advection-Diffusion-Reaction Problems. *SIAM Journal on Numerical Analysis*, 47(2):1391–1420, 2009.

[18] I. Babuška, G. Caloz, and J. E. Osborn. Special Finite Element Methods for a Class of Second Order Elliptic Problems with Rough Coefficients. *SIAM Journal on Numerical Analysis*, 31(4):945–981, 1994.

[19] I. Babuška and R. Lipton. Optimal Local Approximation Spaces for Generalized Finite Element Methods with Application to Multiscale Problems. *Multiscale Modeling & Simulation*, 9(1):373–406, 2011.

[20] I. Babuška and J. E. Osborn. Generalized Finite Element Methods: Their Performance and Their Relation to Mixed Methods. *SIAM Journal on Numerical Analysis*, 20(3):510–536, 1983.

[21] I. Babuška and J. E. Osborn. Can a finite element method perform arbitrarily badly? *Mathematics of Computation*, 69(230):443–463, 1999.

[22] C. Baiocchi and F. Brezzi. Virtual bubbles and Galerkin-least-squares type methods (Ga.L.S.) *Computer Methods in Applied Mechanics and Engineering*, 105:125–141, 1993.

[23] P. Bastian, M. Blatt, A. Dedner, C. Engwer, R. Klöfkorn, R. Kornhuber, M. Ohlberger, and O. Sander. A generic grid interface for parallel and adaptive scientific computing. Part II: implementation and tests in DUNE. *Computing*, 82(2-3):121–138, 2008.

[24] P. Bastian, M. Blatt, A. Dedner, C. Engwer, R. Klöfkorn, M. Ohlberger, and O. Sander. A generic grid interface for parallel and adaptive scientific computing. Part I: abstract framework. *Computing*, 82(2-3):103–119, 2008.

[25] P. Bastian, C. Engwer, J. Fahlke, M. Geveler, D. Göddeke, O. Iliev, O. Ippisch, R. Milk, J. Mohring, S. Müthing, M. Ohlberger, D. Ribbrock, and S. Turek. Advances Concerning Multiscale Methods and Uncertainty Quantification in EXA-DUNE. In H.-J. Bungartz, P. Neumann, and W. E. Nagel, editors, *Software for Exascale Computing - SPPEXA 2013-2015*. Volume 113, Lecture Notes in Computational Science and Engineering, pages 25–43. Springer International Publishing, Cham, 2016.

[26] P. Bastian, C. Engwer, D. Göddeke, O. Iliev, O. Ippisch, M. Ohlberger, S. Turek, J. Fahlke, S. Kaulmann, S. Müthing, and D. Ribbrock. EXA-DUNE: Flexible PDE Solvers, Numerical Methods and Applications. In *Euro-Par 2014: Parallel Processing Workshops*. Volume 8806, Lecture Notes in Computer Science, pages 530–541. Springer, Cham, 2014.

[27] P. Benner, M. Ohlberger, A. Cohen, and K. Willcox, editors. *Model Reduction and Approximation: Theory and Algorithms*. Society for Industrial and Applied Mathematics, Philadelphia, PA, 2017.

[28] A. Bensoussan, J.-L. Lions, and G. Papanicolaou. *Asymptotic Analysis for Periodic Structures*, volume 5 of *Studies in Mathematics and Its Applications*. North-Holland Publishing Company, Amsterdam New York, 1978.

[29] R. A. Biezemans. MsFEM in FreeFEM: Release version 2.0.0, 2023. DOI: 10.5281/zenodo.8312014.

[30] R. A. Biezemans, C. Le Bris, F. Legoll, and A. Lozinski. Multiscale Finite Element Methods and Bubble Functions for the Stable Approximation of Advection-Dominated Problems in Heterogeneous Media. In preparation.

[31] R. A. Biezemans, C. Le Bris, F. Legoll, and A. Lozinski. Non-intrusive implementation of a wide variety of Multiscale Finite Element Methods. *Comptes Rendus. Mécanique, Online first*, 2023.

[32] R. A. Biezemans, C. Le Bris, F. Legoll, and A. Lozinski. Non-intrusive implementation of Multiscale Finite Element Methods: An illustrative example. *Journal of Computational Physics*, 477:111914, 2023.

[33] X. Blanc and C. Le Bris. *Homogenization Theory for Multiscale Problems: An Introduction*, volume 21 of *MS&A*. Springer Nature Switzerland, Cham, 2023.

[34] F. Bonizzoni, P. Freese, and D. Peterseim. Super-localized orthogonal decomposition for convection-dominated diffusion problems, 2022. arXiv: 2206.01975.

[35] F. Bonizzoni, M. Hauck, and D. Peterseim. A reduced basis super-localized orthogonal decomposition for reaction-convection-diffusion problems, 2022. arXiv: 2211.15221.

[36] M. Boutilier, K. Brenner, and V. Dolean. A Trefftz-like coarse space for the two-level Schwarz method on perforated domains, 2023. arXiv: 2211.05880.

[37] S. C. Brenner and L. R. Scott. *The Mathematical Theory of Finite Element Methods*. J. E. Marsden, L. Sirovich, and S. S. Antman, editors, volume 15 of *Texts in Applied Mathematics*. Springer New York, New York, NY, 2008.

[38] F. Brezzi, L. P. Franca, T. J. R. Hughes, and A. Russo. $b = \int g$. *Computer Methods in Applied Mechanics and Engineering*, 145:329–339, 1997.

[39] F. Brezzi, J.-L. Lions, and O. Pironneau. The Chimera method for a model problem. In F. Brezzi, A. Buffa, S. Corsaro, and A. Murli, editors, *Numerical Mathematics and Advanced Applications*, pages 817–825. Springer Milan, Milano, 2003.

[40] F. Brezzi, D. Marini, and E. Suli. Residual-free bubbles for advection-diffusion problems: the general error analysis. *Numerische Mathematik*, 85(1):31–47, 2000.

[41] F. Brezzi and A. Russo. Choosing bubbles for advection-diffusion problems. *Mathematical Models and Methods in Applied Sciences*, 4(4):571–587, 1994.

[42] W. L. Briggs, V. E. Henson, and S. F. McCormick. *A Multigrid Tutorial*. Society for Industrial and Applied Mathematics, second edition, 2000.

[43] A. N. Brooks and T. J. R. Hughes. Streamline Upwind/Petrov-Galerkin Formulations for Convection Dominated Flow with Particular Emphasis on the Incompressible Navier-Stokes Equation. *Computer Methods in Applied Mechanics and Engineering*, 32:199–259, 1982.

[44] A. Buhr, L. Iapichino, M. Ohlberger, S. Rave, F. Schindler, and K. Smetana. Localized model reduction for parameterized problems. In P. Benner, S. Grivet-Talocia, A. Quarteroni, G. Rozza, W. Schilders, and L. Miguel Silveira, editors, *Model Order Reduction*. Volume 2: Snapshot-Based Methods and Algorithms. De Gruyter, 2021.

[45] A. Buhr and K. Smetana. Randomized Local Model Order Reduction. *SIAM Journal on Scientific Computing*, 40(4):A2120–A2151, 2018.

[46] V. M. Calo, E. T. Chung, Y. Efendiev, and W. T. Leung. Multiscale stabilization for convection-dominated diffusion in heterogeneous media. *Computer Methods in Applied Mechanics and Engineering*, 304:359–377, 2016.

[47] V. M. Calo, Y. Efendiev, J. Galvis, and G. Li. Randomized Oversampling for Generalized Multiscale Finite Element Methods. *Multiscale Modeling & Simulation*, 14(1):482–501, 2016.

[48] R. Chakir and Y. Maday. A two-grid finite-element/reduced basis scheme for the approximation of the solution of parameter dependent PDE. In *9e Colloque National En Calcul Des Structures*, Giens, France, 2009.

[49] R. Chakir, Y. Maday, and P. Parnaudeau. A non-intrusive reduced basis approach for parametrized heat transfer problems. *Journal of Computational Physics*, 376:617–633, 2019.

[50] Z. Chen and T. Y. Hou. A mixed multiscale finite element method for elliptic problems with oscillating coefficients. *Mathematics of Computation*, 72(242):541–576, 2002.

[51] I. Christie, D. F. Griffiths, and A. R. Mitchell. Finite Element Methods for Second Order Differential Equations with Significant First Derivatives. *International Journal for Numerical Methods in Engineering*, 10:1389–1396, 1976.

[52] P. G. Ciarlet. *The Finite Element Method for Elliptic Problems*, number 4 in Studies in Mathematics and Its Applications. North-Holland Publishing Company, Amsterdam New York, 1978.

[53] M. Cicuttin, A. Ern, and S. Lemaire. A Hybrid High-Order Method for Highly Oscillatory Elliptic Problems. *Computational Methods in Applied Mathematics*, 19(4):723–748, 2019.

[54] R. Codina, E. Oñate, and M. Cervera. The intrinsic time for the streamline upwind/Petrov-Galerkin formulation using quadratic elements. *Computer Methods in Applied Mechanics and Engineering*, 94(2):239–262, 1992.

[55] A. Cohen and R. DeVore. Approximation of high-dimensional parametric PDEs. *Acta Numerica*, 24:1–159, 2015.

[56] M. Crouzeix and P.-A. Raviart. Conforming and nonconforming finite element methods for solving the stationary Stokes equations I. *Revue française d'automatique informatique recherche opérationnelle. Mathématique*, 7(R3):33–75, 1973.

[57] P. Degond, A. Lozinski, B. P. Muljadi, and J. Narski. Crouzeix-Raviart MsFEM with Bubble Functions for Diffusion and Advection-Diffusion in Perforated Media. *Communications in Computational Physics*, 17(4):887–907, 2015.

[58] L. Demkowicz and J. Gopalakrishnan. A class of discontinuous Petrov–Galerkin methods. Part I: The transport equation. *Computer Methods in Applied Mechanics and Engineering*, 199(23-24):1558–1572, 2010.

[59] L. Demkowicz and J. Gopalakrishnan. A class of discontinuous Petrov-Galerkin methods. II. Optimal test functions: DPG Method. *Numerical Methods for Partial Differential Equations*, 27(1):70–105, 2011.

[60] L. Demkowicz, J. Gopalakrishnan, and A. H. Niemi. A class of discontinuous Petrov–Galerkin methods. Part III: Adaptivity. *Applied Numerical Mathematics*, 62(4):396–427, 2012.

[61] D. A. Di Pietro and A. Ern. *Mathematical Aspects of Discontinuous Galerkin Methods*, volume 69 of *Mathématiques et Applications*. Springer Berlin Heidelberg, Berlin, Heidelberg, 2012.

[62] P. Diercks, K. Veroy, A. Robens-Radermacher, and J. F. Unger. Multiscale modeling of linear elastic heterogeneous structures via localized model order reduction. *International Journal for Numerical Methods in Engineering*, 124(20):4580–4602, 2023.

[63] V. Dolean, P. Jolivet, and F. Nataf. *An Introduction to Domain Decomposition Methods: Algorithms, Theory, and Parallel Implementation*. Society for Industrial and Applied Mathematics, Philadelphia, PA, 2015.

[64] A. K. Dond and T. Gudi. Patch-wise local projection stabilized finite element methods for convection-diffusion-reaction problems. *Numerical Methods for Partial Differential Equations*, 35(2):638–663, 2019.

[65] J. Douglas and J. Wang. An Absolutely Stabilized Finite Element Method for the Stokes Problem. *Mathematics of Computation*, 52(186):495–508, 1989.

[66] M. Duval, J.-C. Passieux, M. Salaün, and S. Guinard. Non-intrusive Coupling: Recent Advances and Scalable Nonlinear Domain Decomposition. *Archives of Computational Methods in Engineering*, 23(1):17–38, 2016.

[67] W. E and B. Engquist. The Heterogeneous Multiscale Methods. *Communications in Mathematical Sciences*, 1(1):87–132, 2003.

[68] Y. Efendiev, J. Galvis, and T. Y. Hou. Generalized multiscale finite element methods (GMsFEM). *Journal of Computational Physics*, 251:116–135, 2013.

[69] Y. Efendiev and T. Y. Hou. *Multiscale Finite Element Methods*, volume 4 of *Surveys and Tutorials in the Applied Mathematical Sciences*. Springer New York, New York, NY, 2009.

[70] Y. Efendiev, T. Y. Hou, and X.-H. Wu. Convergence of a nonconforming multiscale finite element method. *SIAM Journal on Numerical Analysis*, 37(3):888–910, 2000.

[71] D. Elfverson, V. Ginting, and P. Henning. On multiscale methods in Petrov–Galerkin formulation. *Numerische Mathematik*, 131(4):643–682, 2015.

[72] B. Engquist and P. E. Souganidis. Asymptotic and numerical homogenization. *Acta Numerica*, 17:147–190, 2008.

[73] A. Ern and J.-L. Guermond. *Theory and Practice of Finite Elements*. S. S. Antman, J. E. Marsden, and L. Sirovich, editors, volume 159 of *Applied Mathematical Sciences*. Springer New York, New York, NY, 2004.

[74] Q. Feng, G. Allaire, and P. Omnes. Enriched Nonconforming Multiscale Finite Element Method for Stokes Flows in Heterogeneous Media Based on High-order Weighting Functions. *Multiscale Modeling & Simulation*, 20(1):462–492, 2022.

[75] L. P. Franca, S. L. Frey, and T. J. R. Hughes. Stabilized finite element methods: I. Application to the advective-diffusive model. *Computer Methods in Applied Mechanics and Engineering*, 95(2):253–276, 1992.

[76] L. P. Franca and A. Russo. Deriving upwinding, mass lumping and selective reduced integration by residual-free bubbles. *Applied Mathematics Letters*, 9(5):83–88, 1996.

[77] L. P. Franca and A. Russo. Recovering SUPG using Petrov–Galerkin formulations enriched with adjoint residual-free bubbles. *Computer Methods in Applied Mechanics and Engineering*, 182(3-4):333–339, 2000.

[78] A. Galeão, R. Almeida, S. Malta, and A. Loula. Finite element analysis of convection dominated reaction–diffusion problems. *Applied Numerical Mathematics*, 48(2):205–222, 2004.

[79] D. Gallistl and D. Peterseim. Computation of Quasi-Local Effective Diffusion Tensors and Connections to the Mathematical Theory of Homogenization. *Multiscale Modeling & Simulation*, 15(4):1530–1552, 2017.

[80] M. J. Gander and G. Wanner. From Euler, Ritz, and Galerkin to Modern Computing. *SIAM Review*, 54(4):627–666, 2012.

[81] D. Gilbarg and N. S. Trudinger. *Elliptic Partial Differential Equations of Second Order*. Classics in Mathematics. Springer New York, 3rd edition, 2001.

[82] R. Glowinski, J. He, A. Lozinski, J. Rappaz, and J. Wagner. Finite element approximation of multi-scale elliptic problems using patches of elements. *Numerische Mathematik*, 101(4):663–687, 2005.

[83] R. Goudey. *Problèmes d'homogénéisation Elliptique En Présence de Défauts*. PhD thesis, École des Ponts ParisTech, Champs-sur-Marne, France, 2022.

[84] I. G. Graham, P. O. Lechner, and R. Scheichl. Domain decomposition for multiscale PDEs. *Numerische Mathematik*, 106(4):589–626, 2007.

[85] P. Grisvard. *Elliptic Problems in Nonsmooth Domains*. Pitman Publishing, 1985.

[86] E. Grosjean and Y. Maday. Error estimate of the non-intrusive reduced basis method with finite volume schemes. *ESAIM: Mathematical Modelling and Numerical Analysis*, 55(5):1941–1961, 2021.

[87] P. Gupta, J. Pereira, D.-J. Kim, C. Duarte, and T. Eason. Analysis of three-dimensional fracture mechanics problems: A non-intrusive approach using a generalized finite element method. *Engineering Fracture Mechanics*, 90:41–64, 2012.

[88] H. Hajibeygi, G. Bonfigli, M. A. Hesse, and P. Jenny. Iterative multiscale finite-volume method. *Journal of Computational Physics*, 227(19):8604–8621, 2008.

[89] N. Halko, P. G. Martinsson, and J. A. Tropp. Finding Structure with Randomness: Probabilistic Algorithms for Constructing Approximate Matrix Decompositions. *SIAM Review*, 53(2):217–288, 2011.

[90] M. Hauck and D. Peterseim. Super-localization of elliptic multiscale problems. *Mathematics of Computation*, 92(341):981–1003, 2023.

[91] F. Hecht. New development in FreeFem++. *Journal of Numerical Mathematics*, 20(3-4):251–265, 2012.

[92] P. Henning and M. Ohlberger. The heterogeneous multiscale finite element method for advection-diffusion problems with rapidly oscillating coefficients and large expected drift. *Networks & Heterogeneous Media*, 5(4):711–744, 2010.

[93] P. Henning and D. Peterseim. Oversampling for the Multiscale Finite Element Method. *Multiscale Modeling & Simulation*, 11(4):1149–1175, 2013.

[94] J. S. Hesthaven, S. Zhang, and X. Zhu. High-Order Multiscale Finite Element Method for Elliptic Problems. *Multiscale Modeling & Simulation*, 12(2):650–666, 2014.

[95] U. Hetmaniuk and A. Klawonn. Error Estimates for a Two-Dimensional Special Finite Element Method Based on Component Mode Synthesis. *Electronic Transactions on Numerical Analysis*, 41:109–132, 2014.

[96] U. L. Hetmaniuk and R. B. Lehoucq. A special finite element method based on component mode synthesis. *ESAIM: Mathematical Modelling and Numerical Analysis*, 44(3):401–420, 2010.

[97] T. Y. Hou and P. Liu. Optimal local multi-scale basis functions for linear elliptic equations with rough coefficients. *Discrete and Continuous Dynamical Systems*, 36(8):4451–4476, 2016.

[98] T. Y. Hou and X.-H. Wu. A Multiscale Finite Element Method for Elliptic Problems in Composite Materials and Porous Media. *Journal of Computational Physics*, 134(1):169–189, 1997.

[99] T. Y. Hou, X.-H. Wu, and Z. Cai. Convergence of a multiscale finite element method for elliptic problems with rapidly oscillating coefficients. *Mathematics of Computation*, 68(227):913–944, 1999.

[100] T. Y. Hou, X.-H. Wu, and Y. Zhang. Removing the Cell Resonance Error in the Multiscale Finite Element Method via a Petrov-Galerkin Formulation. *Communications in Mathematical Sciences*, 2(2):185–205, 2004.

[101] T. J. R. Hughes. Multiscale phenomena: Green's functions, the Dirichlet-to-Neumann formulation, subgrid scale models, bubbles and the origins of stabilized methods. *Computer Methods in Applied Mechanics and Engineering*, 127(1-4):387–401, 1995.

[102] T. J. R. Hughes, G. R. Feijóo, L. Mazzei, and J.-B. Quincy. The variational multiscale method—a paradigm for computational mechanics. *Computer Methods in Applied Mechanics and Engineering*, 166(1-2):3–24, 1998.

[103] T. J. R. Hughes, L. P. Franca, and G. M. Hulbert. A New Finite Element Method Formulation for Computational Fluid Dynamics: VIII. The Galerkin/Least-Squares Method for Advective-Diffusive Equations. *Computer Methods in Applied Mechanics and Engineering*, 50:181–193, 1985.

[104] T. J. R. Hughes, M. Mallet, and M. Akira. A new finite element formulation for computational fluid dynamics: II. Beyond SUPG. *Computer Methods in Applied Mechanics and Engineering*, 54(3):341–355, 1986.

[105] G. Jankowiak and A. Lozinski. Non-Conforming Multiscale Finite Element Method for Stokes Flows in Heterogeneous Media. Part II: error estimates for periodic microstructure, 2018. arXiv: 1802.04389.

[106] P. Jenny, S. H. Lee, and H. A. Tchelepi. Multi-scale finite-volume method for elliptic problems in subsurface flow simulation. *Journal of Computational Physics*, 187(1):47–67, 2003.

[107] V. John and P. Knobloch. On spurious oscillations at layers diminishing (SOLD) methods for convection–diffusion equations: Part I – A review. *Computer Methods in Applied Mechanics and Engineering*, 196(17-20):2197–2215, 2007.

[108] V. John, J. Maubach, and L. Tobiska. Nonconforming streamline-diffusion-finite-element-methods for convection-diffusion problems. *Numerische Mathematik*, 78(2):165–188, 1997.

[109] C. Johnson, U. Nävert, and J. Pitkäranta. Finite element methods for linear hyperbolic problems. *Computer Methods in Applied Mechanics and Engineering*, 45:285–312, 1984.

[110] P. Knobloch and L. Tobiska. The P_1^{mod} Element: A New Nonconforming Finite Element for Convection-Diffusion Problems. *SIAM Journal on Numerical Analysis*, 41(2):436–456, 2003.

[111] C. Le Bris and F. Legoll. Examples of computational approaches for elliptic, possibly multiscale PDEs with random inputs. *Journal of Computational Physics*, 328:455–473, 2017.

[112] C. Le Bris, F. Legoll, and A. Lozinski. MsFEM à la Crouzeix-Raviart for Highly Oscillatory Elliptic Problems. *Chinese Annals of Mathematics, Series B*, 34(1):113–138, 2013.

[113] C. Le Bris, F. Legoll, and A. Lozinski. An MsFEM type approach for perforated domains. *Multiscale Modeling & Simulation*, 12(3):1046–1077, 2014.

[114] C. Le Bris, F. Legoll, and F. Madiot. A numerical comparison of some Multiscale Finite Element approaches for advection-dominated problems in heterogeneous media. *ESAIM: Mathematical Modelling and Numerical Analysis*, 51(3):851–888, 2017.

[115] C. Le Bris, F. Legoll, and F. Madiot. Multiscale Finite Element Methods for Advection-Dominated Problems in Perforated Domains. *Multiscale Modeling & Simulation*, 17(2):773–825, 2019.

[116] C. Le Bris, F. Legoll, and F. Thomines. Multiscale Finite Element approach for "weakly" random problems and related issues. *ESAIM: Mathematical Modelling and Numerical Analysis*, 48(3):815–858, 2014.

[117] F. Legoll, P.-L. Rothé, C. Le Bris, and U. Hetmaniuk. An MsFEM Approach Enriched Using Legendre Polynomials. *Multiscale Modeling & Simulation*, 20(2):798–834, 2022.

[118] G. Li, D. Peterseim, and M. Schedensack. Error analysis of a variational multiscale stabilization for convection-dominated diffusion equations in two dimensions. *IMA Journal of Numerical Analysis*, 38(3):1229–1253, 2018.

[119] F. Madiot. *Multiscale finite element methods for advection-diffusion problems*. PhD thesis, Université Paris-Est, 2016.

[120] A. Målqvist and D. Peterseim. Localization of elliptic multiscale problems. *Mathematics of Computation*, 83(290):2583–2603, 2014.

[121] A. Målqvist and D. Peterseim. *Numerical Homogenization by Localized Orthogonal Decomposition*, number 5 in SIAM Spotlights. Society for Industrial and Applied Mathematics, Philadelphia, PA, 2021.

[122] A. Mizukami and T. J. R. Hughes. A Petrov-Galerkin finite element method for convection-dominated flows: An accurate upwinding technique for satisfying the maximum principle. *Computer Methods in Applied Mechanics and Engineering*, 50(2):181–193, 1985.

[123] B. P. Muljadi, J. Narski, A. Lozinski, and P. Degond. Nonconforming Multiscale Finite Element Method for Stokes Flows in Heterogeneous Media. Part I: Methodologies and Numerical Experiments. *Multiscale Modeling & Simulation*, 13(4):1146–1172, 2015.

[124] F. Murat and L. Tartar. H-Convergence. In A. Cherkaev and R. Kohn, editors, *Topics in the Mathematical Modelling of Composite Materials*, pages 21–43. Birkhäuser, Boston, MA, 1997.

[125] L. H. Nguyen and D. Schillinger. A residual-driven local iterative corrector scheme for the multiscale finite element method. *Journal of Computational Physics*, 377:60–88, 2019.

[126] J. T. Oden. Historical comments on finite elements. In S. G. Nash, editor, *A History of Scientific Computing*, pages 152–166. ACM, New York, NY, 1990.

[127] P. J. Park. *Multiscale Numerical Methods for the Singularly Perturbed Convection-Diffusion Equation*. PhD thesis, California Institute of Technology, Pasadena, CA, 2000.

[128] P. J. Park and T. Y. Hou. Multiscale Numerical Methods for Singularly Perturbed Convection-Diffusion Equations. *International Journal of Computational Methods*, 01(01):17–65, 2004.

[129] A. Quarteroni. *Numerical Models for Differential Problems*, volume 16 of *MS&A*. Springer International Publishing, Cham, 3rd edition, 2017.

[130] A. Quarteroni, A. Manzoni, and F. Negri. *Reduced Basis Methods for Partial Differential Equations*, volume 92 of *UNITEXT*. Springer International Publishing, Cham, 2016.

[131] H.-G. Roos, M. Stynes, and L. Tobiska. *Robust Numerical Methods for Singularly Perturbed Differential Equations*, volume 24 of *Springer Series in Computational Mathematics*. Springer Berlin Heidelberg, Berlin, Heidelberg, 2008.

[132] L. R. Scott and S. Zhang. Finite Element Interpolation of Nonsmooth Functions Satisfying Boundary Conditions. *Mathematics of Computation*, 54(190):483–493, 1990.

[133] L. Tartar. *The General Theory of Homogenization: A Personalized Introduction*, volume 7 of *Lecture Notes of the Unione Matematica Italiana*. Springer Berlin Heidelberg, Berlin, Heidelberg, 2010.

[134] V. V. Zhikov, S. M. Kozlov, and O. A. Oleinik. *Homogenization of Differential Operators and Integral Functionals*. Springer Berlin, Heidelberg, 1994.

[135] J. Zitelli, I. Muga, L. Demkowicz, J. Gopalakrishnan, D. Pardo, and V. Calo. A class of discontinuous Petrov–Galerkin methods. Part IV: The optimal test norm and time-harmonic wave propagation in 1D. *Journal of Computational Physics*, 230(7):2406–2432, 2011.

Detailed Table of Contents

List of Tables xx

List of Figures xxi

Publications based on the work in this thesis xxiii

Talks in conferences and seminars xxiv

1 Résumé étendu en français 1

1.1 Motivation . . . 1

1.2 Contexte . . . 2

1.3 Contributions de la thèse . . . 4

1.3.1 Approches MsFEM non-intrusives . . . 4

1.3.2 Méthodes MsFEM pour les problèmes avec advection dominante . . . 8

1.3.3 Analyse de convergence de la MsFEM sous des hypothèses de régularité minimales . . . 10

2 Introduction 11

2.1 Motivation . . . 11

2.1.1 The finite element method . . . 13

2.1.2 The finite element method applied to multiscale problems . . . 15

2.2 Introduction to multiscale methods . . . 19

2.2.1 Homogenization theory . . . 19

2.2.2 Multiscale computational methods; numerical homogenization . . . 22

2.2.3 The multiscale finite element method . . . 25

2.3 Contributions of the thesis . . . 31

2.3.1 Non-intrusive implementation of the MsFEM . . . 31

2.3.2 MsFEMs for the stabilization of advection-dominated problems . . . 36

2.3.3 Convergence analysis of the MsFEM under minimal regularity hypothes . . . 40

I Non-intrusive Implementation of Multiscale Finite Element Methods

3 An illustrative example 47

3.1 Introduction . . . 47

3.2 Non-intrusive implementation of MsFEM: a simple case . . . 48

3.2.1 The Multiscale Finite Element Method . . . 49

3.2.2 Equivalent problem on the macroscopic scale . . . 51

3.3 Comparison of Galerkin and Petrov-Galerkin MsFEM . . . 55

3.3.1 Theoretical results . . . 55

3.3.2 Numerical results . . . 57

3.4 Concluding remarks on possible extensions . . . 58

4 The intrusive nature of the MsFEM 61

4.1 Discrete variational formulation . . . 62
4.2 A simple multiscale finite element method . . . 63
4.3 Intrusive workflow . . . 65
4.4 Effective problem on the macroscopic scale . . . 66
4.5 Non-intrusive workflow . . . 68
4.6 Interpretation of the non-intrusive MsFEM . . . 70
4.7 Relation to homogenization theory . . . 70

5 A general framework for multiscale finite element methods 73

5.1 Why develop a general framework? . . . 73
5.1.1 Local boundary conditions . . . 73
5.1.2 The non-intrusive approach . . . 74
5.1.3 Other motivations for the general framework . . . 75
5.2 The continuous problem . . . 75
5.3 Piecewise affine structure . . . 77
5.4 Local problems . . . 79
5.4.1 Oversampling patches . . . 79
5.4.2 Degrees of freedom on oversampling patches . . . 79
5.4.3 Numerical correctors: first oversampling strategy . . . 81
5.4.4 Numerical correctors: second oversampling strategy . . . 84
5.4.5 Well-posedness of DOF-continuous numerical correctors . . . 85
5.5 The multiscale basis functions . . . 87
5.6 The global problem . . . 89

6 Non-intrusive MsFEM for the general framework 91

6.1 The Petrov-Galerkin MsFEM . . . 91
6.2 The non-intrusive Galerkin MsFEM . . . 94
6.3 Further extensions of the non-intrusive MsFEM . . . 96
6.4 Intrusiveness of other multiscale methods . . . 97
6.4.1 The heterogeneous multiscale method . . . 97
6.4.2 The localized orthogonal decomposition . . . 98
6.4.3 Non-intrusive methods in other fields of computing . . . 100

7 Comparison of the classical and non-intrusive MsFEM for diffusion problems 101

7.1 The general framework for diffusion problems . . . 101
7.2 Convergence results . . . 102
7.3 Convergence results in the periodic setting . . . 107
7.4 Numerical study of non-intrusive MsFEMs . . . 110
7.4.1 Description of the numerical experiments . . . 110
7.4.2 Results . . . 111

8 Some further considerations 115

8.1 Different oversampling techniques for the MsFEM-CR . . . 115
8.2 Non-intrusive implementation of a $\mathbb{P}_2$ MsFEM . . . 118
8.2.1 Definition of a high-order MsFEM . . . 119

8.2.2 Exact quadrature for quadratic functions . . . 120
8.2.3 Effective formulation of the $\mathbb{P}_2$ MsFEM . . . 122

II Multiscale Finite Element Methods for Advection-Dominated Problems

9 Introduction and classical stabilization methods 129
9.1 Advection-dominated problems . . . 130
9.2 The multiscale setting . . . 131
9.3 Strongly consistent stabilization methods . . . 133
9.4 Variational stabilization methods . . . 134
9.4.1 The variational multiscale framework . . . 134
9.4.2 The residual-free bubble method . . . 135
9.4.3 Deriving the SUPG method from the RFB method . . . 136

10 Multiscale finite element methods for advection-diffusion problems 139
10.1 The multiscale finite element method . . . 139
10.2 A residual-free bubble point of view . . . 141
10.3 Enrichment by additional residual-free bubble functions . . . 144
10.4 Numerical experiment in 1D . . . 146
10.5 On the generalization to higher dimension . . . 148

11 An MsFEM with weak bubbles 151
11.1 The coarse scales . . . 152
11.2 Additional bubbles for the adv-MsFEM-CR . . . 154
11.3 A closer look at the bubbles . . . 155
11.4 Non-intrusive implementation . . . 158
11.4.1 The adv-MsFEM without bubbles . . . 159
11.4.2 Extension to MsFEMs with bubbles . . . 161

12 Numerical results 165
12.1 First test case . . . 165
12.1.1 Stability . . . 166
12.1.2 Error measurement outside the boundary layer . . . 166
12.1.3 Delineating the advection-dominated regime . . . 169
12.1.4 Errors including the boundary layer . . . 170
12.1.5 Non-intrusive variants . . . 171
12.2 Second test case . . . 172

III Novel Convergence Analysis for Multiscale Finite Element Methods

13 A convergence theorem under minimal regularity hypotheses 177
13.1 Definition of the MsFEM framework . . . 178
13.2 Statement of the convergence results . . . 180
13.3 Auxiliary notions and results . . . 181
13.3.1 Elements of periodic homogenization theory . . . 181
13.3.2 Classical abstract error estimates . . . 182
13.3.3 A cut-off function on individual mesh elements . . . 183
13.3.4 Trace estimates . . . 185

13.3.5 Interpolation results 187
13.4 Three central estimates 192
13.4.1 First-order reconstruction for the multiscale finite element space . . 193
13.4.2 Interpolation estimate 195
13.4.3 Non-conforming error 197
13.5 Proof of Theorem 13.1 199

Bibliography **203**

Detailed Table of Contents **213**